Studies on DNA Binding and Photocleavage Activities of Some New Metallointercalators

A Thesis

Submitted for the Degree of

DOCTOR OF PHILOSOPHY

By

M. Mariappan

School of Chemistry
University of Hyderabad
Hyderabad - 500 046
India

March 2005

Dedicated To

My beloved Parents.....

School of Chemistry
University of Hyderabad
Central University P.O.
Hyderabad 500 046
India

Statement

I hereby declare that the matter embodied in this thesis is the result of investigations carried out by me in the School of Chemistry, University of Hyderabad, Hyderabad, India under the supervision of **Late Prof. Bhaskar G. Maiya**.

In keeping with the general practice of reporting scientific observations, due acknowledgements have been made wherever the work described is based on the findings of other investigators.

M. Mariappan

School of Chemistry
University of Hyderabad
Central University P.O.
Hyderabad 500 046
India

Certificate

Certified that the work contained in this thesis entitled **"Studies on DNA Binding and Photocleavage Activities of Some New Metallointercalators"** has been carried out by **M. Mariappan** under the supervision of **Late Prof. Bhaskar G. Maiya** and that the same has not been submitted elsewhere for a degree.

Dean
School of Chemistry

Prof. Samudranil Pal
Thesis Co-Supervisor

Acknowledgements

It gives me immense pleasure to express my deep sense of gratitude and profound respect to my supervisor **Late Prof. Bhaskar G. Maiya** for his constant guidance, encouragement and above all for the freedom he gave me in carrying out my research. His commitment to the work with a great sense of discipline and patience are highly admirable and truly inspiring. My association with him throughout my research tenure in this lab was a rewarding experience, which I never wish to forget.

I express my sincere thanks to Prof. Samudranil Pal, for the discussions, suggestions and corrections of the papers as well as my thesis. His co-operation and help towards the last stages of my work cannot be expressed in words.

I thank Prof. M. Periasamy, Dean, School of Chemistry, former Deans and all the faculty members of School of Chemistry especially Prof. M. J. Swamy, Prof. K. C. Kumara Swamy and Prof. T. P. Radhakrishnan for their help during the course of my study.

I owe a lot to Prof. D. K. Palit (BARC, Mumbai) for his sprit of collaboration and fruitful discussions in fluorescence studies. Prof. P. Sambasiva Rao and Prof. H. Surya Prakash Rao, of Pondicherry University are remembered for their wonderful teaching, encouragement and affection.

I thank my lab seniors Dr. L. Giribabu, Dr. C. V. Sastri, Dr. A. Ashok Kumar, Dr. D. Raghunath Reddy, Dr. P. Prashanth Kumar, and my present labmates G. Premaladha, Tamal Ghosh, A. Narahari and S. Prathap Chandran for the unending discussions and above all for creating a pleasant atmosphere in this laboratory.

I thank DST for the National Single Crystal X-ray Diffractometer Facility at our School and CSIR for the financial support. I also thank the authorities of

Centre for Modelling, Simulation and Design (CMSD) and also the Universities with Potential for Excellence (UPE) programme of the University of Hyderabad. Central Drug Research Institute, Lucknow for the FAB mass spectral data and Central Salt and Marine Chemicals Research Institute, Bhavnagar for analytical data are highly acknowledged.

I thank all the non-teaching staff of the school. I thank Mr. Shetty for the timely supply of chemicals, Mr. Vara Prasad for his art of glass blowing, Mr. Satyanarayana and Mr. Bhaskar Rao for their excellent job with NMR machine, Ms. Asia for her tireless effort in collecting IR spectra and Mr. Raghavaiah for mounting our crystals. The assistance of Mr. Suresh for EPR spectra is also gratefully appreciated.

I am extremely thankful to Dr. Ramanathan, Dr. Muthiah, Dr. Doss, Dr. V. S. Senthil Kumar and Dr. Kamaraj for their timely help and encouragement. I also thank Dr. SivaKumar, Dr. Jothilingam, Dr. Mariappan and Dr. Mahalakshmi, for their support and affection.

I thank all my friends and well wishers for making my stay in the campus a memorable one.

Last, but not the least, I am deeply grateful to my parents, sisters, Selvi and Shanthi, brother Murugan and brother-in-law who made growing up fun and for being there in good and bad times to offer support, without which this task would have been highly impossible. I thank Chellamma periyamma, Sampath anna and Poongudi anni for showering lots of love, making me laugh and keeping my momentum always up which is something I will always cherish.

Synopsis

This thesis entitled **"Studies on DNA Binding and Photocleavage Activities of Some New Metallointercalators"** deals with the design, synthesis, characterization as well as DNA binding and photonuclease activities of some new ruthenium(II), copper(II), nickel(II) and zinc(II) complexes that incorporate pyrene, anthracene, acridine and salen photo-active ligands. The major interest in the DNA interactions of these metallointercalators stems from their potential use as structural/spectroscopic probes and photocleaving agents for DNA. The strategy adopted in the design of all the new chromophores investigated in this study largely relies on means of enhancing their DNA intercalation. To understand their modes of DNA binding and mechanisms of DNA photocleavage, various physicochemical and biochemical techniques have been used during the course of this work.

Studies with simple tris-complexes of the type $[M(phen^*)_3]^{n+}$ (where phen* is either 1,10-phenanthroline or a modified phen ligand and n is an integer) and mixed-ligand complexes of the type $[M(phen)_2L]^{n+}$ (where L is a polypyridyl ligand other than phen, e.g. dppz - dipyrido[3,2-*a*:2',3'-*c*]phenazine) have provided a basis for conceptualizing how octahedral complexes might interact noncovalently with DNA. An added advantage of this class of DNA binding species is that both the ligand and the metal ion can be varied in such a way that complexes having wide range properties can be generated to facilitate an individual application. Square planar complexes including cis-platin have attracted much attention in the cancer therapy. Since then, much effort has been devoted to investigate the interactions of square planar compounds incorporating an aromatic heterocyclic ligand with improved pharmacological properties.

Mixed-ligand ruthenium(II) complexes of the type $[Ru(phen)_2L]^{2+}$, where L is a photoactive ligand (*viz*: N-[1,10]phenanthrolin-5-yl-pyrenylmethanimine (ppym), 2-(9-anthryl)-1H-imidazo[4,5-f][1,10]phenanthroline (aip), 2-(1-pyrenyl)-1H-imidazo[4,5-f][1,10]phenanthroline (pyip), 11-(9-acridinyl)dipyrido[3,2-a:2',3'-c]phenazine (acdppz)) and neutral complexes of general formula [M(daasal)] (M = Cu(II), Ni(II) and Zn(II)) where H_2daasal is an acridine tethered Schiff base have been prepared and their interactions with DNA have been investigated in detail. The DNA binding and photocleavage proclivities of the new complexes are observed to be dependent on not only the structural intricacies of the intercalating ligand L, but also the metal ion present in the corresponding complexes. The work embodied in this thesis has been divided into seven chapters. A brief, chapter-wise account of the results is presented below.

Chapter 1. Introduction

In this chapter, recent literature related to DNA binding and photocleavage by organic molecules and metallointercalators including donor – acceptor (D – A) type systems has been reviewed in light of their applicability as spectroscopic and structural probes, site-specific agents, molecular light switches *etc*.

Chapter 2. Materials and Methods

A general description of the synthesis of various precursor compounds as well as the structural, spectroscopic, electrochemical, magnetic resonance and biochemical techniques employed during the research work is presented in this chapter.

Chapter 3. A Ruthenium(II) Complex That Incorporates a Pyrene Bearing Polypyridine Ligand: Synthesis, Characterization, Photochemistry and DNA Interactions

This chapter deals with the synthesis, characterization and DNA binding studies of a mixed-ligand Ru(II) complex, $[Ru(phen)_2(ppym)]^{2+}$, containing a ligand (N-[1,10]phenanthrolin-5-yl-pyrenylmethanimine (ppym)) which has pyrene fluorophore in its architecture. The novel pyrene-linked ppym was synthesized upon condensation of 1-pyrenecarboxaldehyde and 5-amino-1,10-phenanthroline. The corresponding mixed-ligand ruthenium(II) complex (Fig. 1) was prepared by reacting $[Ru(phen)_2Cl_2]\cdot 2H_2O$ with ppym. Both the ligand and complex is characterized by spectroscopic (UV-visible, infra-red, ^1H (1D and ^1H-^1H COSY), ^{13}C NMR and FAB-MS), electrochemical and X-ray crystallographic methods.

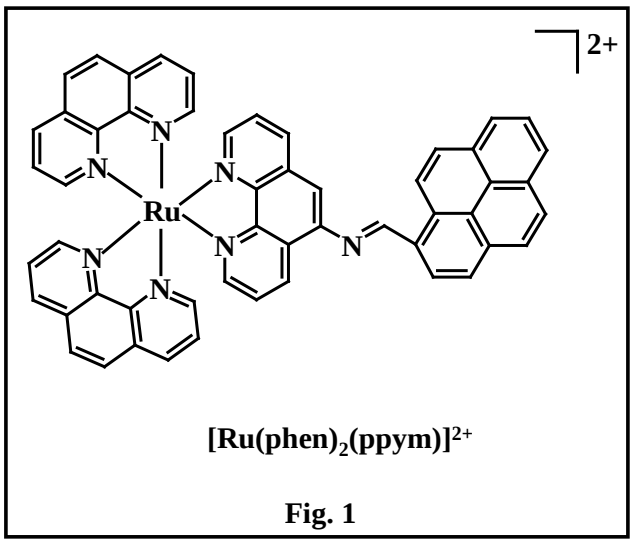

$[Ru(phen)_2(ppym)]^{2+}$

Fig. 1

UV-visible spectrum of ppym is characterized by prominent low energy, structured absorption bands in the 380 – 401 nm region which is ascribed to the $\pi\rightarrow\pi^*$ transition of pyrene chromophore. The high-energy bands (231 and 278 nm) are attributed to the $\pi\rightarrow\pi^*$ transitions corresponding to the phenanthroline moiety of the ligand. The MLCT transition characteristic for the ruthenium(II) complex is observed at 453 nm.

The presence of two different sets of clearly distinguishable peak in the fluorescence spectrum for ppym (λ_{ex} = 340 nm in CH_3CN) is reminiscent of dual emission seen earlier for various fluorophores. In order to elucidate the dual emission, we have carried out various concentration, solvent dependent and metal ion titration experiments. The results suggest in region II (centered at 482 nm) for ppym is due to its excimer (excited state dimer) and that in region I (centered at 387) is due to the monomer. $[Ru(phen)_2(ppym)]^{2+}$ shows only one emission band centered at 604 nm (λ_{ex} = 450 nm, ϕ = 0.029 in CH_3CN) which corresponds to the ^{3}MLCT state.

Absorption, fluorescence, thermal denaturation and viscometric titration studies have revealed that $[Ru(phen)_2(ppym)]^{2+}$ is an avid binder of the calf-thymus (CT) DNA. The apparent binding constant (K_b) value evaluated for $[Ru(phen)_2(ppym)]^{2+}$ is 1.20 x 10^5 M^{-1}. Based on the results obtained, an intercalative mode of DNA binding has been suggested. Fluorescence studies have revealed that $[Ru(phen)_2(ppym)]^{2+}$ shows moderate "molecular light switch" effect with DNA.

Results of DNA photocleavage experiments carried out with $[Ru(phen)_2(ppym)]^{2+}$ are compared with those obtained for $[Ru(phen)_3]^{2+}$. No cleavage activity was observed for both the complexes in dark whereas the cleavage activity under light (λ_{ex} = 450 nm, 30 min.) is higher for $[Ru(phen)_2(ppym)]Cl_2$ than $[Ru(phen)_3]Cl_2$ under similar experimental conditions. To unravel the probable DNA photocleavage mechanism of $[Ru(phen)_2(ppym)]^{2+}$, a few control experiments have been conducted in the presence of 'inhibitors' and it suggest that DMSO and mannitol ($OH^{\cdot}$ quencher) are inhibiting the photocleavage.

Chapter 4. DNA Binding and Photonuclease Activities of New Metallointercalators Containing Imidazo-phenanthroline Ligands

This chapter deals with the synthesis, spectral, electrochemical characterization, DNA binding and the photocleavage properties of mixed-ligand ruthenium(II) complexes, $[Ru(phen)_2L]^{2+}$(where L = aip or pyip, Fig. 2). The ligands aip and pyip were prepared by the condensation of 1,10-phenanthroline-5,6-dione with 9-anthraldehyde or 1-pyrenecarboxaldehyde in the presence of ammonium acetate and glacial acetic acid. The corresponding ruthenium(II) complexes were synthesized by reacting $[Ru(phen)_2Cl_2]\cdot 2H_2O$ with either aip or pyip. These compounds have been characterized by CHN, IR, UV-visible, mass and ^1H NMR spectroscopic and electrochemical methods.

The NMR spectra of both aip and pyip showed a characteristic singlet at 14.20 and 13.73 ppm respectively, which can be assigned to the N-H peak of the imidazole ring.

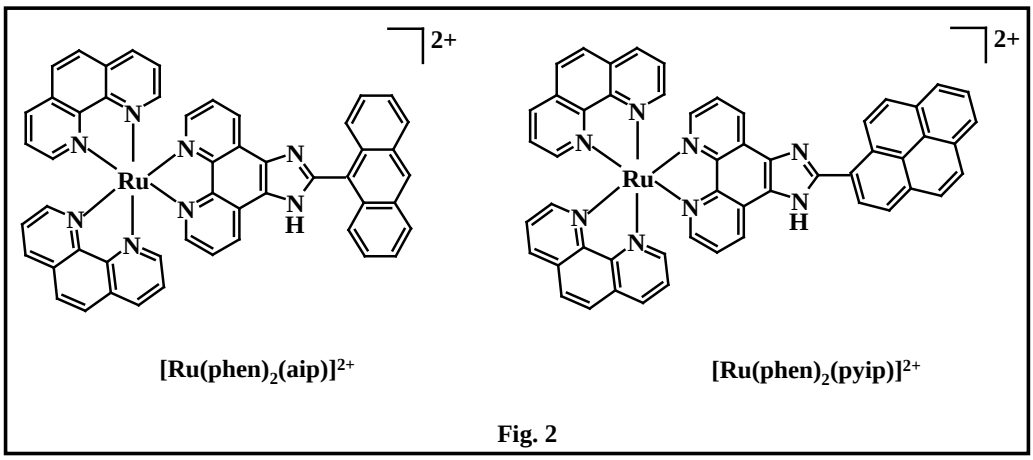

$[Ru(phen)_2(aip)]^{2+}$ **$[Ru(phen)_2(pyip)]^{2+}$**

Fig. 2

Due to the fast proton exchange between the two imidazole nitrogen atoms, this proton was not observed in the spectrum of either of the two complexes. The electronic spectra of aip and pyip showed low intensity, structured absorption bands (at 383 and 366 nm for aip and at 368 nm for pyip)

due to the $\pi \rightarrow \pi^*$ transitions corresponding to the anthracene and pyrene chromophores attached to the phenanthroline moiety. The low energy band at 452 nm (ε = 19670 $M^{-1}cm^{-1}$) and 457 nm (ε = 24070 $M^{-1}cm^{-1}$) is assigned as MLCT Ru(dπ) $\rightarrow$ aip/pyip(π^*) transition for $[Ru(phen)_2(aip)]^{2+}$ and $[Ru(phen)_2(pyip)]^{2+}$, respectively. When aip is excited at 360 nm, the emission maxima appeared at 535 nm (ϕ = 0.81 in CH_3CN). In the case of pyip (excited at 330 nm) the emission maxima appeared at 494 nm (ϕ = 0.63 in CH_3CN). Complexes $[Ru(phen)_2(aip)]^{2+}$ and $[Ru(phen)_2(pyip)]^{2+}$ showed an emission band due to the ^{3}MLCT state centered at 604 and 601 nm with quantum yields of 0.005 and 0.0006, respectively in CH_3CN (λ_{exc} = 450 nm).

Absorption, fluorescence, thermal denaturation and viscometric titration studies reveal that both the complexes bind to DNA *via* the intercalative mode. The K_b values evaluated from the absorption titration data are 1.01 x 10^6 and 1.57 x 10^6 M^{-1} for $[Ru(phen)_2(aip)]^{2+}$and $[Ru(phen)_2(pyip)]^{2+}$, respectively. The binding ability of $[Ru(phen)_2(pyip)]^{2+}$ is slightly higher than that of $[Ru(phen)_2(aip)]^{2+}$ and its parent reference complex, *viz*: $[Ru(phen)_3]^{2+}$. This observation suggests that increase in the surface area available for stacking of a complex within the duplex leads to a substantial increase in its intercalative binding affinity. $[Ru(phen)_2(pyip)]^{2+}$ is found to be a better "molecular light switch" for DNA than $[Ru(phen)_2(aip)]^{2+}$. While $[Ru(phen)_2(aip)]^{2+}$ is moderately emitive, the emission of $[Ru(phen)_2(pyip)]^{2+}$ is quenched in aqueous buffer solution. Successive addition of CT DNA to the buffer solutions containing these complexes results in an enhancement of the emission in each case, with the enhancement factors at the saturation point being 5 and 9 for $[Ru(phen)_2(aip)]^{2+}$ and $[Ru(phen)_2(pyip)]^{2+}$, respectively. Thus the intercalative strength follows the order, $[Ru(phen)_2(dppz)]^{2+} \approx [Ru(ip)_2(dppz)]^{2+} \geq$

$[Ru(phen)_2(pyip)]^{2+}$ > $[Ru(phen)_2(aip)]^{2+}$ > $[Ru(phen)_3]^{2+}$ where ip = imidazo[4,5-f][1,10]phenanthroline.

Upon 60 min. irradiation, single strand nicking of pBR 322 DNA was observed followed by the conversions from form I (super coiled) to form II (open circular) in the gel electrophoresis. Based on the % of conversion for these complexes, DNA nicking efficiencies were seen to follow the trend: $[Ru(phen)_2(pyip)]Cl_2$ > $[Ru(phen)_2(aip)]Cl_2$ > $[Ru(phen)_3]Cl_2$. This trend can be attributed to the extended π aromatic nature of the ligands aip/pyip in the complexes. The photocleavage efficiency of these complexes are also comparable with that of $[Ru(bpy)_2(ip)]^{2+}$ and $[Ru(bpy)_2(pip)]^{2+}$ (where pip = 2-phenylimidazo[4,5-f][1,10]phenanthroline) reported in the literature. An attempt was made to identify the reactive species responsible for the DNA cleavage using various inhibitors. The results suggest that the hydroxyl radical ($^{\bullet}OH$) and singlet oxygen ($^1O_2$, to a lesser extent) may play a signify
cant role in the cleavage mechanism for $[Ru(phen)_2(pyip)]Cl_2$ whereas for $[Ru(phen)_2(aip)]Cl_2$ hydroxyl radical ($^{\bullet}OH$) alone is responsible for the photocleavage.

Chapter 5. A New Metallointercalator Containing Dipyridophenazine Ligand Endowed with an Acridine Subunit

This chapter presents synthesis, crystal structure, characterization, DNA binding and DNA photocleavage properties of a novel mixed-ligand ruthenium(II) complex, $[Ru(phen)_2(acdppz)]^{2+}$ (Fig. 3) where acdppz is 11-(9-acridinyl)dipyrido[3,2-a:2,3-c]phenazine - a dppz based ligand that incorporates an acridine chromophore in its architecture. The ligand acdppz was prepared by the condensation of 1,10-phenanthroline-5,6-dione with 9-(3,4-diaminophenyl)acridine. $[Ru(phen)_2(acdppz)]^{2+}$ was synthesized by refluxing the

precursor $[Ru(phen)_2Cl_2]\cdot 2H_2O$ with acdppz. Acdppz and its Ru(II) complex have been characterized by X-ray diffraction, CHN, IR, UV-visible, fluorescence, FAB-MS, ^1H NMR spectroscopic and electrochemical methods.

In acdppz, the intramolecular bond lengths and bond angles are found to be comparable to other structurally characterized similar molecules reported in the literature. In the crystal lattice, acdppz forms a one-dimensional array through intermolecular C-H···N and π-π interactions. The C-H···N and π-π interactions are roughly orthogonal to each other. In the complex $[Ru(phen)_2(acdppz)]^{2+}$, the metal center is in distorted octahedral N_6 coordination sphere. The acridine moiety of one cation is involved in π-π interaction with the dppz plane of the adjacent cation with an interplanar distance of 3.365 Å and forms a discrete dimer. This value is similar to the base-pair stacking distance in DNA and to the intercalator-base pair stacking distance in oligonucleotide intercalator complexes.

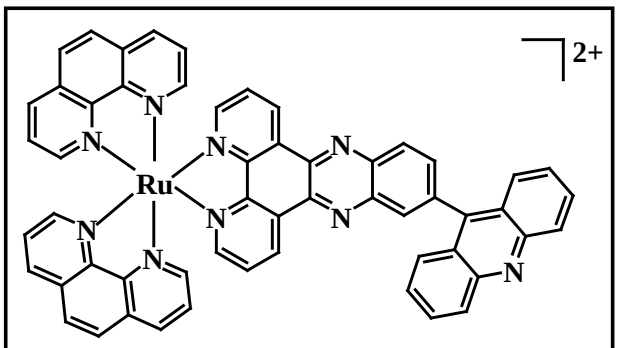

$[Ru(phen)_2(acdppz)]^{2+}$

Fig. 3

The absorption spectrum of acdppz in acetonitrile displays low energy bands at 362 and 386 nm which are assigned to π→π* transitions of dppz and acridine chromophores. The low energy shoulder type band at 450 nm (ε = 19670 $M^{-1}cm^{-1}$) is assigned as MLCT (Ru(dπ) → acdppz(π*)) transition for $[Ru(phen)_2(acdppz)]^{2+}$. When acdppz is excited at 330 nm in acetonitrile, the emission maxima appeared at 562 nm (ϕ = 0.83 in CH_3CN). It is intensively fluorescent in CH_3CN at 667nm (ϕ = 0.002), but weakly fluorescent in H_2O at

610 nm (ϕ = 0.0003). The intensity in the former solvent is about 2 times larger than that in the latter solvent. The quenching of fluorescent in water can be interpreted by the mechanism of both the polarity and the proton-donating ability of the solvent. Interaction of $[Ru(phen)_2(acdppz)]^{2+}$ with CT DNA has been monitored using absorption, fluorescence, thermal denaturation and viscometric titration methods. The absorption spectra of $[Ru(phen)_2(acdppz)]^{2+}$ with increasing concentration of DNA show hypochromicity and the K_b has been evaluated to be 2.65 x 10^6 M^{-1}. Eventhough acdppz is a modified dppz ligand from a structural point of view, its binding ability with the DNA falls short of that observed for $[Ru(phen)_2(dppz)]^{2+}$. The new complex is weakly emitive in aqueous buffer solutions. It also shows a five-fold enhancement in its emission intensity and bathochromic shift of about 4 nm in the presence of excess CT DNA suggesting moderate “molecular light switch” behaviour.

When pBR 322 DNA is treated with $[Ru(phen)_2(acdppz)]^{2+}$, no nicking has been observed in the absence of light. Irradiation of the complex at 450 ± 5 nm with the plasmid causes very low photocleaving efficiency (41% of form II) when compared to $[Ru(phen)_3]^{2+}$ (52% of form II). The same observation has been noted over various bp/Ru molar ratio. There is an enhancement in the photocleavage activity (59% of form II) when the irradiation is carried out in D_2O instead of buffer. In order to establish the reactive species responsible for the photoinduced cleavage of the plasmid, inhibition experiments have been carried out in the presence of various inhibitors. Degassing of the solution with purified nitrogen for 30 min., decreased the efficiency of the breakage by a factor of 2. However, it was largely inhibited by DABCO ($^1O_2$ quencher). Thus the singlet oxygen is likely to be the reactive species for the cleavage mechanism as is the case with $[Ru(phen)_3]^{2+}$. This is also supported by the enhanced cleavage activity in D_2O. The lifetime of singlet oxygen is higher in D_2O than in H_2O. A

possible reason for the lower photocleavage activity of $[Ru(phen)_2(acdppz)]^{2+}$ is that when the complex is intercalated, it is well protected from oxygen and so the yield of singlet oxygen and subsequently the cleavage efficiency of the complex becomes lower when compared with $[Ru(phen)_3]^{2+}$.

Chapter 6. DNA Binding and Photonuclease Activity of a Series of Metallointercalators with an Acridine Tethered Schiff Base

In this chapter, synthesis, structure, DNA binding and photocleavage properties of a Schiff base H_2daasal and its Ni(II), Cu(II) and Zn(II) complexes (Fig. 4) have been described. H_2daasal was prepared by the reaction of 9-(3,4-diaminophenyl)acridine and salicylaldehyde. The tetradentate N_2O_2 donar deprotonated Schiff bases are capable of coordinating various metal ions. The complexes were prepared by reacting the appropriate precursor ($CuCl_2 \cdot 2H_2O$, $NiCl_2 \cdot 6H_2O$ and $Zn(CH_3COO)_2 \cdot 2H_2O$) with H_2daasal. X-ray diffraction, elemental analysis, UV-visible, IR, ^{1}H NMR, FAB-MS and cyclic voltammetry methods were used for the characterization of the compounds. The crystal structures of H_2daasal and it's Ni(II) complex [Ni(daasal)] have been determined. In the absorption spectra, low energy bands (355-390 nm) are characterized by low intensity structured $\pi \rightarrow \pi^*$ transition due to the acridine chromophore. In [Ni(daasal)], the prominent feature is the MLCT band at 482 nm typical of Ni-salen complexes.

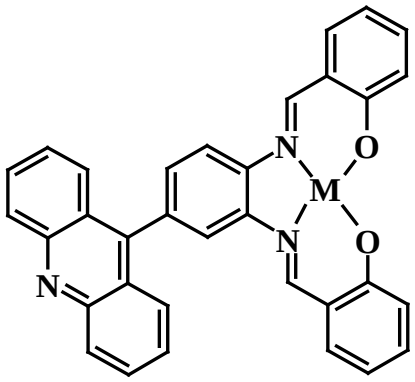

M = 2H, H_2daasal
Ni, [Ni(daasal)]
Cu, [Cu(daasal)]
Zn, [Zn(daasal)]

Fig. 4

The dissymmetric nature of this band may suggest the presence of $\pi \rightarrow \pi^*$ intraligand transition which undergoes a bathochromic shift relative to that of the free Schiff base. The presence of metal ion has little effect on the emission spectra of [Ni(daasal)] and [Cu(daasal)] when compared to the emission spectrum of H_2daasal. But in the case of [Zn(daasal)], there is a large red shift (60 nm) of the emission band when compared to that of free H_2daasal.

Solvent dependent absorption and emission spectra have been recorded for all these compounds and the results indicate that specific interactions of the compounds (such as ion-dipole, dipole-dipole, H-bonding *etc*) with the solvent might be operative. The EPR spectral data for the complex [Cu(daasal)] are consistent with that of the reported typical monomeric square planar or square pyramidal Cu(II) complexes. Binding of all these compounds with CT DNA has been monitored by absorption, fluorescence, thermal denaturation as well as viscometric titrations. The results suggest the possibility of intercalative mode of interactions for all the compounds with CT DNA.

Based on these similarities, it is proposed that acridine is involved in the intercalation with DNA in the present set of compounds and moreover, the K_b values of all the compounds are higher than that of the free acridine ($k_b = 8.9x10^4$). From this observation, we conclude that metal ion and the extended conjugation with the salen moiety are also contributing to a significant extent for the enhancement in the binding affinity with CT DNA. Overall the binding is in the order [Cu(daasal)] > [Ni(daasal)] > H_2daasal > [Zn(daasal)] ~ acridine.

All the compounds except H_2daasal are needed to be activated in presence of light by some oxidizing/reducing agent for effective DNA photocleavage. For [Cu(daasal)], 3-mercaptopropionic acid(MPA) was used as a reducing agent and it results effective cleaving of DNA (72% form II). The cleavage mechanism for this complex involves $OH^{\cdot}$ mediated cleavage which is proved by inhibition

experiments (with DMSO and mannitol). For [Ni(daasal)], the active species for DNA scission is probably a Ni(III) which is generated by the oxidizing agent oxone in the presence of light. In the case of [Zn(daasal)], ascorbic acid was used and very likely DNA cleaving occurs *via* a process that is similar to that in the case of [Cu(daasal)].

Chapter 7. Conclusion

This chapter presents general conclusions based on the investigations carried out in this work.

Contents

CHAPTER 1

Introduction

Studies leading to the design of artificial nucleases (molecules that cleave DNA) remains to be of much current interest because these molecules may be developed as probes for DNA structure and conformation, as DNA foot printing agents and as anti-tumor drugs. For applications that require specificity of the cleavage such as in the development of drugs or structural probes, the reagents should have high binding affinity for the site of interest and cleave with high specificity. Among the reagents studied over the past decade are numerous molecules that can be activated by photoirradiation. These DNA photonucleases are inactive in the dark but can be activated by irradiation at a particular wavelength - a property that gives specific advantages over other DNA cleaving agents.

The DNA photocleaving agents developed so far may be classified as those that are based on derivatives of organic molecules and those that are based on metal complexes. Especially, transition metal complexes are being used at the forefront of many of these efforts. Stable, inert and water-soluble complexes containing spectroscopically active metal centers are extremely valuable as probes of various biological systems. Most of these molecules cause DNA strand-breaks through mechanisms that involve the formation of intermediates, which participate in oxidation processes involving the base or the sugar of the DNA. This study deals with the design, DNA binding and DNA photocleavage of new, rationally designed photonucleases, based mainly on metallo-polypyridyl complexes.

1.1 Structure of DNA

DNA is composed of a series of polymerized nucleotides, joined by phosphodiester bonds between the 5' and 3' carbons of deoxyribose units. A double helix is formed between the two strands, running in opposite directions.[1] The nucleotide bases form hydrogen bonds to maintain the structure, with two bonds between adenine and thymine bases (A=T) and three between cytosine and guanine (C≡G) residues. These bases are in the center of the double helix, with the deoxyribose and phosphate groups on the outside.

The most common form of the DNA double helix is referred to as B-DNA. The B-DNA helix contains two grooves; the major groove and the minor groove. The major groove is wider and deeper. There is a greater opportunity for the molecules to interact in the major groove due to its larger size. In addition, there is a potential for hydrogen bonding with the base pairs in these grooves, as there is access to both sides of DNA. A-DNA, is a helical form that is generated when the duplex is dehydrated. This helix is wider and shorter than B-DNA, and has a narrower major groove and almost no minor groove. A third DNA species is the Z-DNA - a form which consists of a left handed helix (A- and B-DNA are right handed). Z-DNA has only a single groove, and this form is present in oligonucleotides with alternating pyrimidine and purine bases. Most physiological DNA is present in the B-form.

The drugs (DNA binding species/‘ligands’) can interact with DNA, primarily, in the following ways (Fig. 1.1)

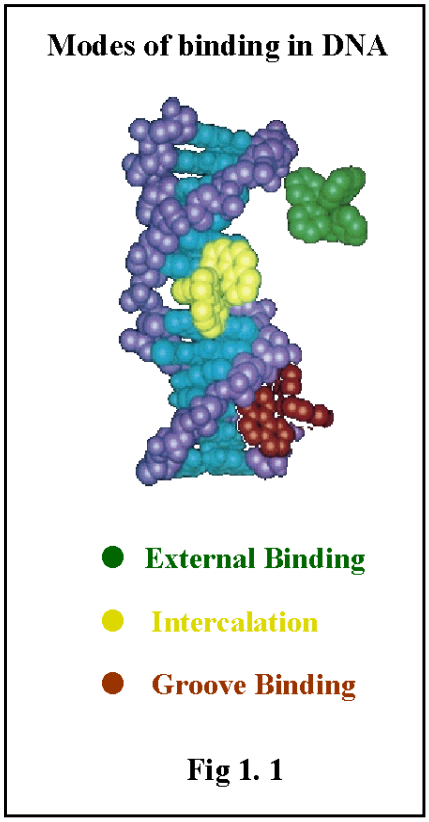

Fig 1. 1

(i) Surface binding by inter-ionic interactions with the positively charged species.

(ii) Intercalation of the polycyclic aromatic rings in between the base stacks.

(iii) Specific recognition in major and minor grooves *via* hydrophobic and hydrogen bonding interactions.

Among the three basic components of DNA– sugars, phosphate and heterocyclic bases – the sugar and phosphate provide centers for non-specific hydrophobic and electrostatic interactions, respectively. The heterocyclic bases are responsible for the specific hydrogen bonding interactions in the major and minor grooves. Many molecules use combination of the above modes to generate high sequence specificity in DNA binding.

If the ligand has an extended aromatic portion, it can position itself between the base pairs, in a sandwich like complex. This phenomenon, called intercalation,[2-4] was first described by Lerman to explain the binding of aminoacridines to DNA.[5] Intercalation is generally brought out by π-π interaction between the molecule and the aromatic heterocyclic bases of DNA. Intercalation increases the separation of adjacent base pairs and the resulting helix distortions are compensated by adjustments in the sugar phosphate backbone, generally by

an unwinding of the duplex. Ethidium bromide (EtBr) is the classical example of a DNA intercalator.[3,4]

1.2 Methods to study drug – DNA interactions

The drug-DNA interactions can be conveniently monitored by the spectroscopic, electrochemical and other physical methods and also by various biochemical methods.[6-15] These techniques which are of relevance to the study of metal complex-DNA interactions are briefly discussed here.

Absorption and fluorescence titrations are the methods of choice to monitor the DNA-metal complex interactions. The hypochromism and bathochromic shift in the absorption maxima, appearance of isosbestic point/s in the UV-visible spectra and fluorescence enhancement for the drug in the presence of DNA are all characteristic features of DNA-metal complex interactions. The different modes of interaction of Δ and Λ isomers of a given metal complex with DNA can be studied not only by the above techniques but also by the circular dichroism (CD) spectroscopy. The CD spectroscopy is also useful in monitoring the conformational changes occurring in DNA upon binding with the metal complexes. DNA exhibits chiral properties, and its ellipticity generally changes upon binding with the metal complex. The transition between single and double stranded DNA can also be monitored effectively by this method.

Study of emission lifetimes of the drug in the presence of DNA has the potential to provide comprehensible details of binding. An increase in the emission lifetime of the drug is generally observed in its DNA-bound state. Competitive binding studies using EtBr can be done for evaluating the DNA binding by non- fluorescent complexes. On the other hand, better understanding of the mode of binding, *viz*: intercalation/surface binding can be achieved by

monitoring the lifetime quenching of the DNA-bound metal complex in the presence of various external quenchers.

High resolution NMR (usually, ^{1}H and or sometimes, ^{31}P) is an important tool for the investigation of DNA-metal complex conjugates in both intercalating and non-intercalating situations. NMR characteristics of the protons on free DNA and the complex-bound DNA (or those on free complex and the DNA-bound complex) can be used to derive structure of the DNA-complex conjugate and to provide evidence for the mode and the site of binding by the complex. The model that is generally employed assumes that the chemical shift changes for the various protons on the DNA molecule are caused exclusively by binding the metal complex in the immediate vicinity of the proton being monitored. This model is best suited for 1:1 binding of the complex and DNA. More elaborate models are used where the complex/DNA binding ratio is more than unity.

Electrochemistry is a powerful technique for the study of drug-DNA interactions. Results of cyclic/differential-pulse voltammetric experiments (for example, change in the current and/or shift in the redox potential of the drug in the presence of DNA) can be utilized to estimate the affinity constant for binding and the number of drug molecules bound per nucleotide. This method has an additional advantage that it can be used to evaluate the DNA binding constants of both the oxidized and the reduced species of a given metal complex.[16]

Equilibrium dialysis is a specific application of the general phenomenon of dialysis that is important for the study of the binding of small molecules and ions by proteins or DNA. The objective of an equilibrium dialysis experiment is usually to measure the amount of complex bound to DNA. However, this is typically done through an indirect method, for e.g., in absorption/fluorescence titration *etc*. As discussed before, it is difficult to distinguish between bound and free complex in any mixture of the complex and DNA in these latter methods. If,

however, the free complex can be dialyzed through a membrane, until its concentration across the membrane is same at equilibrium, one can easily quantify the bound and the unbound species and determine binding constants and the number of binding sites. One can also directly examine the enantioselectivity in complexes binding to DNA by this method.

Sedimentation technique is based on the behaviour of particles in an applied centrifugal field and can be used effectively for monitoring the drug-DNA interactions. The technique is useful especially when the optical and photophysical probes provide insufficient clues to support one binding mode or the other. Sedimentation technique can also be applied to the detection of conformational changes in DNA upon binding by the drug. The more compact the molecule, the lower will be its frictional resistance to the solvent. The more disorganized the molecule becomes, greater is the frictional resistance, and sedimentation occurs more slowly.

Thermal denaturation method is based on the stabilization of DNA in the presence of the drug. Thermal melting of DNA is conversion of the double stranded DNA into the single strand at elevated temperatures. This conversion results in the increase in the absorbance of DNA, which can be conveniently monitored at 260 nm. The mode of binding of the drug to DNA can be interpreted based on the thermal melting data.

Intercalation of a ligand to DNA is known to cause a significant increase in the viscosity of DNA solution due to an increase in the separation of the base pairs at the intercalation site and hence, an increase in the overall DNA molecular length. In contrast, a ligand that binds in the DNA grooves causes either a less pronounced change (positive or negative) or no change in the viscosity of a DNA solution. A partial, non-classical intercalation could bend (or kink) the DNA helix and reduce its effective length and, hence, its viscosity.

Electrophoresis is the standard method used to separate, identify or purify DNA fragments. The technique is simple, rapid to perform and capable of resolving fragments of DNA that cannot be separated by other procedures. In general, electrophoretic separation is carried out on agarose gels for DNA samples.

Separation in agarose gels is assisted by resistance to the movement caused by the gel matrix. Closed circular (Form I), nicked circular (Form II) and linear (Form III) DNA of the same molecular weight migrate through agarose gels at different rates.[14,15] Form I of DNA (super coiled) is seen to have maximum mobility due to its shape while, form II of DNA (open circular) has the least mobility. The mobility of form III (linear) is in between the other two forms, Fig. 1.2.

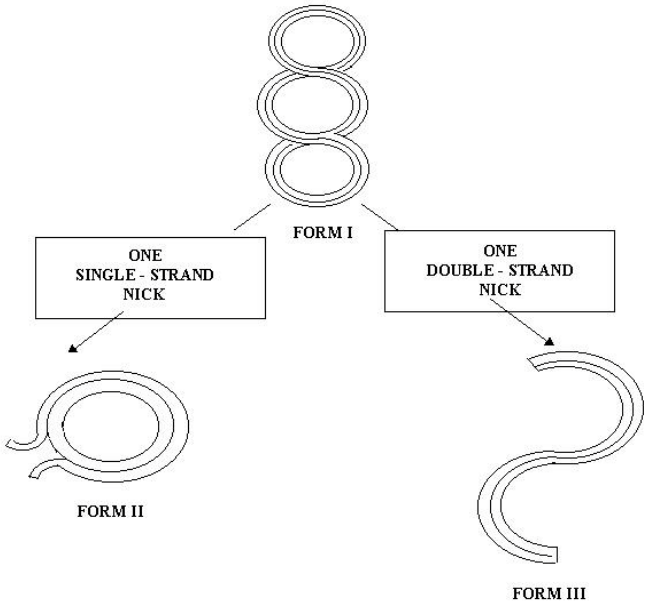

Fig. 1.2 Pictorial representation of the three forms of DNA: Form I (supercoiled), Form II (open circular) and Form III (linear).

In the present study, absorption, fluorescence, thermal denaturation, viscometric titrations and agarose gel electrophoretic techniques have been employed to monitor the drug-DNA interactions.

1.3 DNA interactions by various compounds

1.3.1 Organic molecules

Several organic molecules are known to interact with DNA through different modes; the one of a kind that is of relevance to the present study is briefly alluded here. Owing to the planar structure and excellent photoactivities of anthracene and pyrene, host of anthracene or pyrene appended molecules have been designed and their interactions with DNA have been studied in detail.[17-27] For e.g., an anthryl moiety that is capable of intercalation has been attached to a hydrophilic cationic function through an appropriate linker to form cationic anthryl probes shown in Fig. 1.3.[17-19] In these molecules, while the planar anthryl moiety was shown to intercalate into the helix, the cationic function provides favorable electrostatic interactions. Geometry permits the cationic ammonium group of the side chain to be positioned on the helix to form hydrogen bond and to serve as a recognition element.

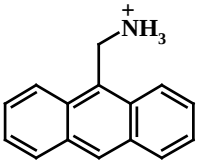

AMAC

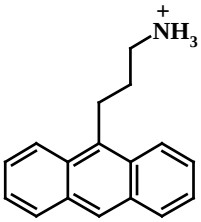

APAC

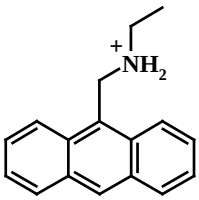

N-Et-AMAC

Fig. 1.3

The length and flexibility of the linker connecting the hydrophobic and cationic functions has a determining role in controlling the binding properties of these ligands.

DNA binding properties of piperazinecarbonyloxy-2-propyl derivatives of anthracene, pyrene and phenylanthracene (Fig. 1.4) have also been investigated.[28,29] An intercalative binding mode was found for 2-propyl derivatives of anthracene and pyrene ((**a**) and (**b**) in Fig. 1.4), whereas the phenyl group of phenylanthracene ((**c**) in Fig. 1.4) prevents intercalation and leads to external electrostatic binding. Preferential binding of the (*S*)-enantiomers were found for both anthracene and pyrene propyl derivatives shown in Fig. 1.4. Affinities of the anthracene and pyrene derivatives for poly(dA-dT)$_2$ are 10^4 M^{-1} and 10^5 M^{-1}, respectively.

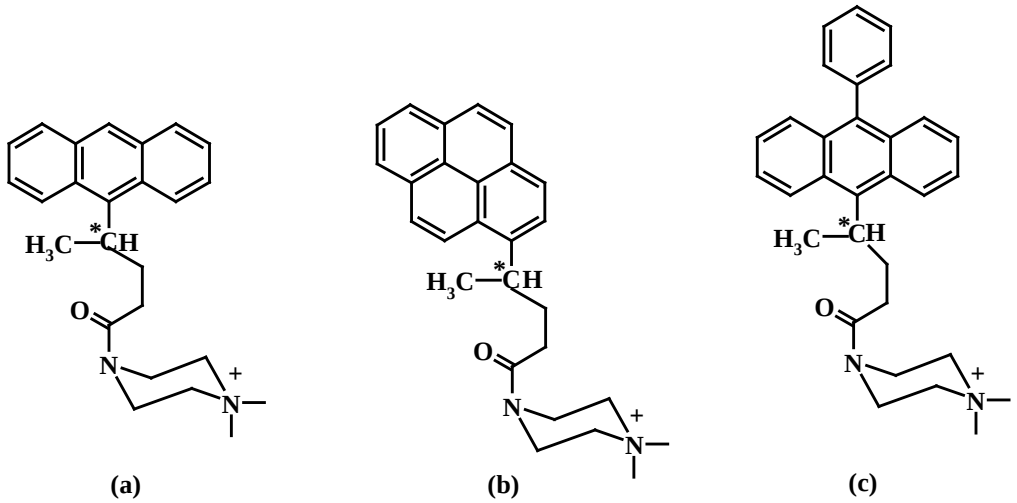

Fig. 1.4

The affinities for poly(dG-dC)$_2$ were an order of magnitude lower than those for poly(dA-dT)$_2$. This can be explained by invoking steric interference of the piperazinium tail with the exocyclic amino groups of guanine in the minor groove of GC, leading to a weak intercalation in GC than in AT.

Porphyrins and related compounds possess most qualities that are expected in an ideal photosensitizer for photodynamic therapy (PDT).[30-35] Simple water soluble porphyrins, like 5,10,15,20-tetrakis(*N*-methylpyridinium-4-yl)porphyrin ((TMPyP)H_2) are known to bind DNA by intercalation.[36-39] Such cationic porphyrins interact with DNA *via* groove binding and groove binding with self-stacking.[40] (TMPyP)H_2 photosensitizes singlet oxygen ($^1O_2$) production with high quantum yield.[41] Moreover, it directly photosensitizes DNA damage by electron transfer from guanosine bases.[40,42] The porphyrin-chlorambucil dyads[43] and also the triads composed of porphyrin, cholic acid and chlorambucil moieties are shown to exhibit significant photoinduced nuclease activities.[44] Several other porphyrin-intercalator hybrids are also known to be effective photonucleases.[45-48] The stereoisomers *trans-RR*, *trans-SS* and *cis*- forms of N,N^1-bis-(phenanthrolin-2-yl)-1,2-cyclohexanediamine conjugates composed from phenanthroline and stereo isomer of 1,2-diaminocyclohexane and their Cu(II) complexes (Fig. 1.5) show stereoselectivity in binding with the DNA.

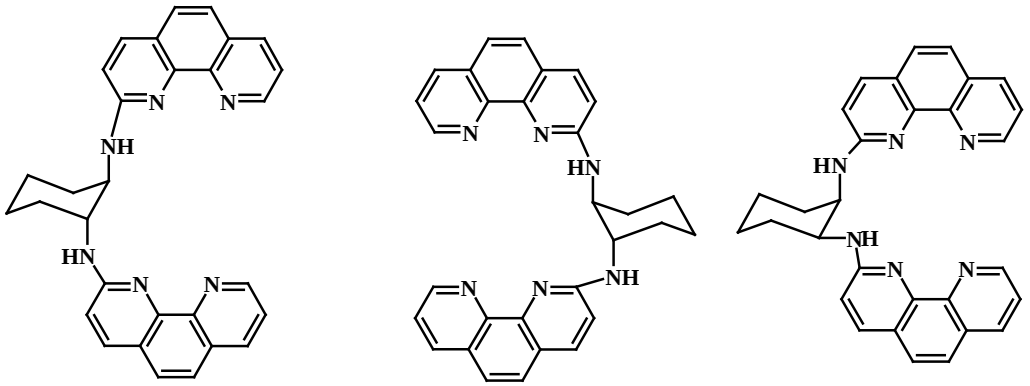

***trans-RR*, (1)** ***trans-SS*, (2)** ***cis*- (3)**

Fig. 1.5

The binding constants are 1.2 x 10^5 M^{-1}, 3.5 x 10^4 and 8.3 x 10^4 M^{-1} for compounds **1**, **2** and **3**, respectively. The binding order follows *trans-RR*> *cis*-> *trans-SS*. These compounds photocleave pBR 322 (ligand:Cu(II) = 1:1 and 1:2) in the same order.[49]

Wenders *et al.* synthesized a novel family of activatable radical based DNA cleaving agents represented by triazoles **1-4** (Fig. 1.6).[50,51] These agents are shown to serve as readily available, versatile and activatable precursors of Ph radicals. These compounds **1-3** generates a azoimine type singlet intermediate which can react directly or undergo Inter System Crossing (ISC) to the triplet state which is capable of hydrogen abstraction and thereby of serving as a potential agent for DNA cleavage. The DNA cleavage efficiency and selectivity of benzimidazole photonucleases were expected to be enhanced by covalent attachment to specific DNA recognition elements. A series of novel benzotriazoles conjugated to DNA minor groove binders (**4**) incorporating one to

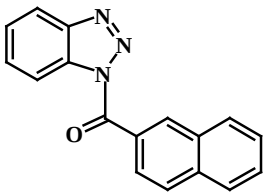

1

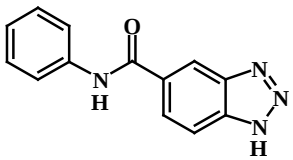

2

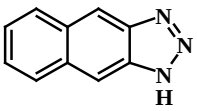

3

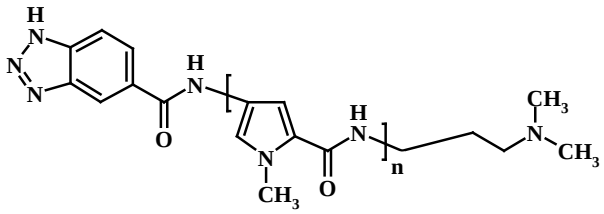

4

Fig. 1.6

three pyrrole units related to the DNA binders netropsin and distamycin bind DNA at specific AT sites, in agreement with the binding preference of netropsin and distamycin. This series of benzotriazoles conjugated to DNA minor groove binders is atleast 10-fold more effective in cleaving DNA than the earlier reported compounds **1-3** by Wenders *et al.*

1.3.2 Acridine based DNA intercalating molecules

Acridine and its derivatives have been a well established class of DNA and RNA binding compounds.[52] These compounds have held the interest of biochemists and chemists for some years due to the possibilities of their clinical use. The binding mode of acridine molecules involve intercalation of the acridine tricyclic ring between adjacent base pairs in the DNA duplex.[15,53] The acridine moieties are held in place by van der Waals forces supplemented by stronger ionic bonds to the phosphate ions of the DNA backbone. Considerable synthetic attention has also been paid to the substituted aminoacridines.[54]

Most interesting case is that of *m*-AMSA (4'-(9-acridiny-amino)methanesulfon-*m*-anisidide) and its structural conformer, *o*-AMSA (4'-(9-acridinyamino)methanesulfon-*o*-anisidide) whose structures are shown in Fig. 1.7.

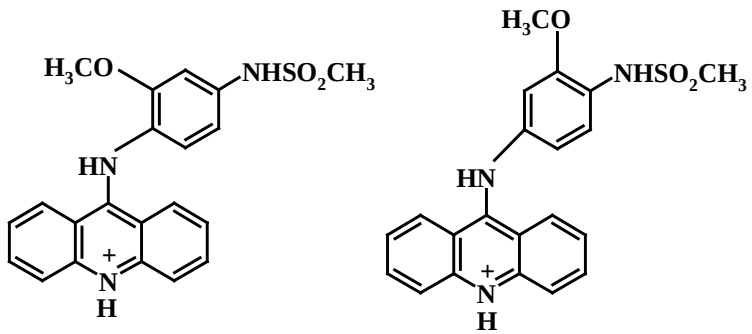

***m*-AMSA** ***o*-AMSA**

Fig. 1.7

Both the ligands bind to the DNA by intercalation. In fact, the binding affinity of *o*-AMSA is approximately 4 times higher than that of *m*-AMSA. In contrast to the biophysical properties associated with complex formation, *m*-AMSA is shown to stimulate single and double-strand topoisomerase II mediated DNA cleavage, while *o*-AMSA is ineffective in eliciting such an effect.

For *m*-AMSA, the value of K_b (1.8×10^4 M^{-1}) was comparatively less than the value of K_b (5.4×10^4 M^{-1}) for *o*-AMSA. Hydrophobicity of the drug plays an important role in bringing the drug to the intercalation site.[55-58] Thermodynamic properties associated with the interaction of the experimental antitumor agents N-[2-(dimethylamino)ethyl]-9-aminoacridine-4- carboxamide (AAC) and N-[2-(dimethylamino)ethyl]acridine-4-carboxamide (DACA) with nucleic acids were studied using absorption techniques and these have been compared with the 9-amino acridine (9AA) and a dicationic amino acridine derivative 9-[[2-methoxy-4-(methylsulfonylamino)phenyl]amino]-N-[2-(dimethylamino)ethyl]acridine-4- carboxamide (AMSAAC), respectively (Fig. 1.8).[59]

These studies show that placement of the amino moiety at C9 results in 6 times greater DNA binding affinity as compared to the deamino analog (DACA). Groove selectivity of these acridine analogs were probed by examining the binding profiles to native and groove-modified DNAs which included glycosylated T4 DNA and the distamycin-DNA complex. These studies are indicative of minor groove interactions for both compounds DACA and AAC with DNA. In AMSAAC, bulky substituents protruding into both major and minor groove and cationic charges over the molecules also play a role for higher binding. The binding order follows AAC > AMSAAC > DACA > 9AA. Some N-oxide derivative intercalators (Fig. 1.9) are selectively toxic under hypoxic conditions. The selectivity and binding of these compounds with DNA are due to

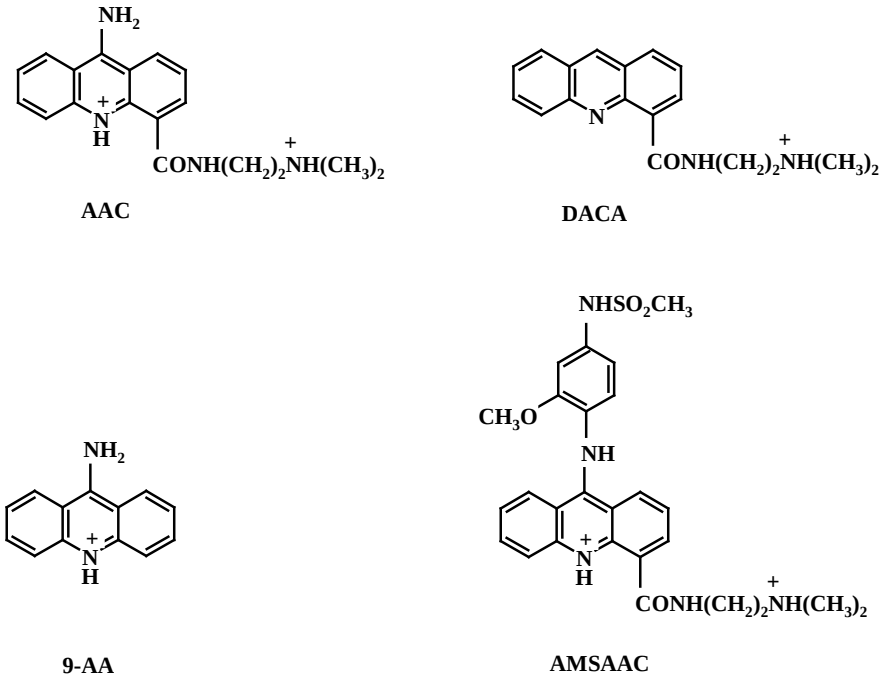

Fig. 1.8

the reduction of N-oxide moiety. DNA binding measurements by equilibrium dialysis process demonstrated that binding affinity is lowered more by aromatic than tertiary amine (side-chain) N-oxides.

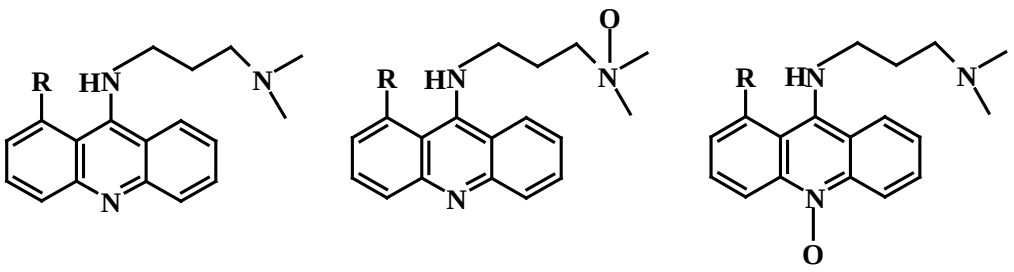

Fig. 1.9

Reduction of the aromatic N-oxide would result in an increase in binding affinity of 100-fold for DAPA-ao and *ca*. 50 for the corresponding nitroacridine NC-ao. Reduction of the tertiary amine N-oxides would result in a similar increase in DNA binding affinity by 16 and 8 fold for DAPA-to and NC-to, respectively. In general, the N-oxide on the acridine molecule shows more affinity with DNA than the other molecules where it resides on the side chains.[60]

A series of bifunctional ligands has been developed as prototype DNA binding combilexins[61] using a DNA template-directed approach. These novel agents contain a 1,3-diaryltriazene linker moiety, which is present in the established DNA minor groove-binder berenil [1,3-bis(4'-amidinophenyl)-triazene], is attached to an intercalating acridine chromophore by a functionalized thiazole residue (Fig. 1.10). This 9-arylacridine is predicted to confer rotational freedom to the hybrid molecule and thus facilitate bifunctional interaction with double-stranded DNA through a combination of 'classical' intercalation and minor groove binding processes. In addition, the binding behaviours of these acridine compounds are compared to those of proflavine (3,6-diaminoacridine) and its 9-phenyl derivative.

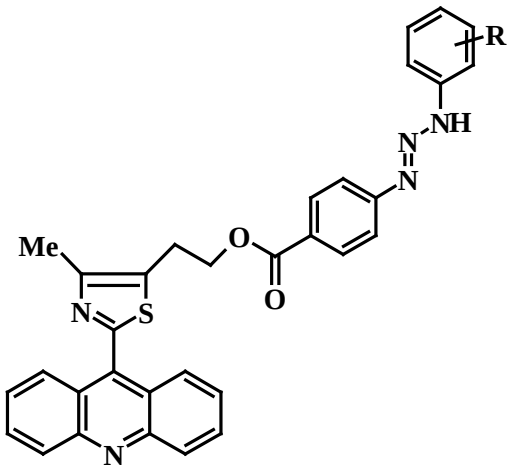

R = **4-C(NH)NH$_2$**
4-CO$_2$(CH$_2$)$_2$N(4-morpholine)
4-CO$_2$(CH$_2$)$_2$N(1-piperidine)
4-CO$_2$(CH$_2$)$_2$N(1-pyrrolidine)
4-CO$_2$(CH$_2$)$_2$NMe$_2$
3-CO$_2$(CH$_2$)$_2$NMe$_2$

Fig. 1.10

These suggest that the prototype combilexins can bind in a bimodal manner that induces little distortion of the host DNA duplex. The binding constants (K_b) evaluated for these compounds are in the range 2.1–10.5x10^6 M^{-1}. As the length of side chain increases at 9th position of acridine, binding strength increases. Unless a bulky aromatic side chain is involved, acridine derivatives having an amino ester or amino alcohol substituent[62] (Fig. 1.11) bind to calf thymus DNA *via* intercalation. Here the intercalation of the acridine moiety of compounds **1** and **2** (Fig. 1.11) leaves the amino ester or amino alcohol substituent in a chiral environment.

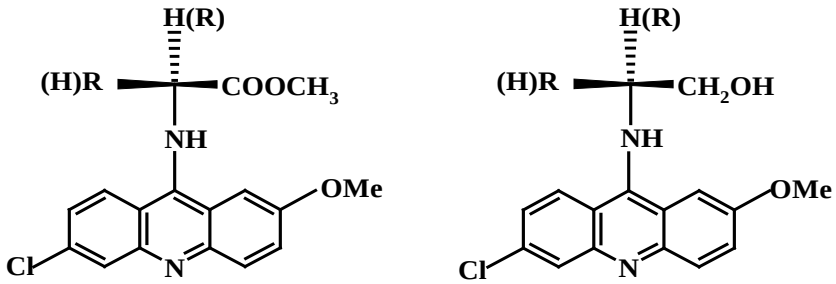

L-1 (D-1)
1

L-2 (D-2)
2

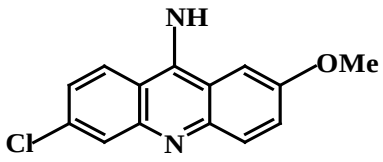

3

Fig. 1.11

The substituents introduced are rather inhibitory of the binding and L-enantiomers are preferred binder over the D-enantiomers by a factor of K_L/K_D = 1.1-1.4, which is similar to that observed in the case of $[Ru(phen)_3]^{2+}$,[63] except for the case of aspartic and glutamic esters where the optical selectivity is very

low or even reversed. The present enantioselectivity is discussed in terms of a local C2 chirality at the interaction site, steric effects of the amino ester or amino alcohol substituents, and a possible conformation-controlling effect of the $COOCH_3$ or CH_2OH group.

In the case of compounds **1a** and **1b** (Fig. 1.12), photophysical and DNA binding studies have revealed that the *p*-isomer (**1a**) exists in the extended conformation and binds to DNA by partial intercalation whereas the *o*-isomer (**1b**) exists both in folded and extended conformations and fails to interact with DNA.[64]

Novel water-soluble viologen and pyridinium linked tolylacridines (**1(a, b)**, **2(a, b)** and **3(a, b)**, Fig. 1.12) were synthesized and its photophysical and DNA binding properties including the photoinduced electron transfer reactions were studied by Ramaiah *et al*.[65] It suggests that the viologen moiety quenches the fluorescence of the acridine chromophore efficiently when compared to the case of the pyridinium moiety from the intramolecular quenching rate constants (k_{ET}) calculated in H_2O. It was observed that the singlet and triplet excited states of the acridine chromophore are capable of donating an electron to the viologen moiety and more over tolyl spacer controls the electron transfer properties of the molecules.

In the case of an acridine moiety covalently linked to viologen by an alkylidene spacer[66] (**4a-c** and **5a-c**, Fig. 1.12) changes in free energy for the electron transfer reactions were found to be favourable and the fluorescence quenching observed in these systems are explained by an electron transfer mechanism. Here the rate decreases with increase in the spacer length. Nano-second laser flash photolysis of these systems in aqueous solutions showed no transient absorption. But in the presence of guanosine or calf thymus DNA, transient absorption due to the reduced viologen radical cation was observed.

Studies on DNA binding demonstrated that the viologen linked acridines bind effectively to DNA in both intercalative and electrostatic modes. Results of PM2 DNA cleavage studies indicate that, on photoexcitation, these molecules induce DNA damage, which is sensitive to the formamido pyrimidine DNA glycosylase.

A new synthetic bis-9-acridinyl derivative (**6**, Fig. 1.12)[67,68] containing a viologen linker chain binds strongly to DNA *via* intercalation and was found to cleave the double chain DNA strand effectively under irradiation by visible light.

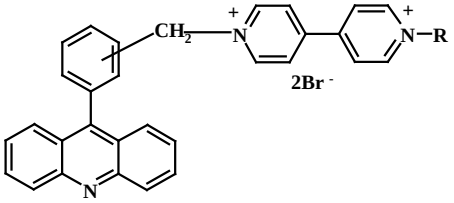

1a, b

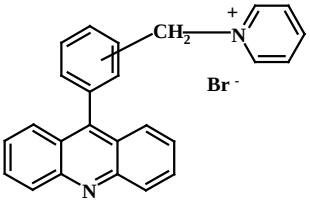

2a, b

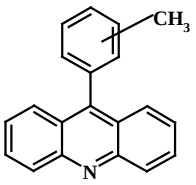

3a, b

a, b = *o*, *p* - isomer, R = -$(CH_2)_3$-CH_3

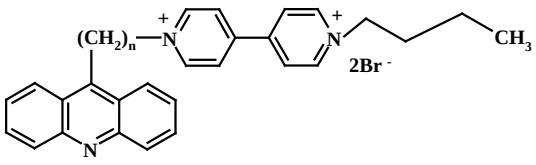

4a-c

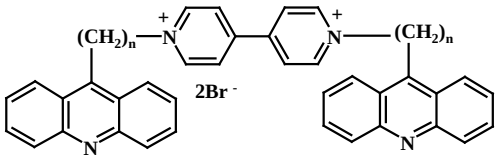

5a-c

n = 1, (a): 3, (b): 11, (c)

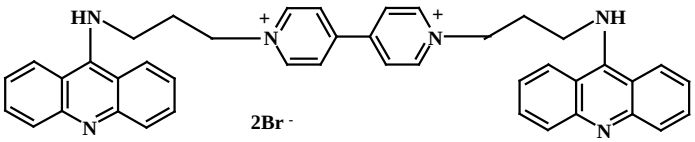

6

Fig. 1.12

This is due to the photosensitized intramolecular electron transfer from the acridine to the viologen moieties within the derivatives. Moreover, it shows a typical cyclic voltammogram, indicating a potential for use as a reversible electrochemical labeling agent for DNA.

A schematic representation for the design of photoactivated DNA oxidizing reagents given in Fig. 1.13 is shown below.

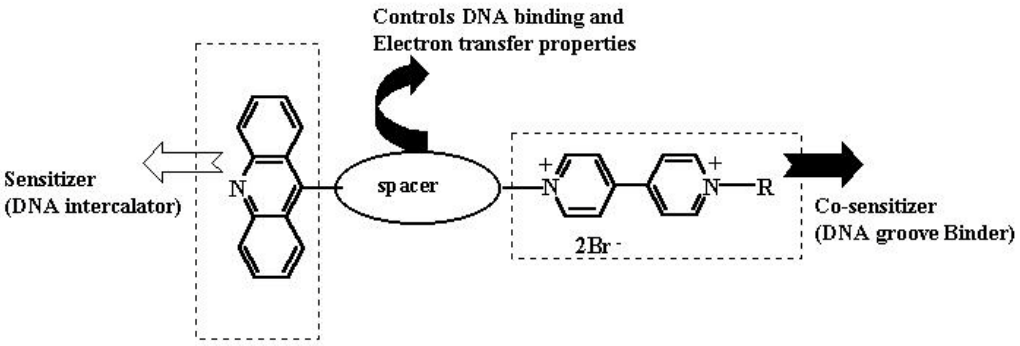

Fig. 1.13

1.4 Transition metal complexes

First major breakthrough in the use of transition metal complexes in bioinorganic/biomedicinal chemistry came from the discovery of "cisplatin" in 1969 by Rosenberg and co-workers.[69] Keck and Lippard have established that square planar platinum(II) complexes containing an aromatic heterocyclic ligand could bind to DNA by intercalation.[70] Ever since, much effort has been devoted to investigate the interactions of platinum compounds with DNA in order to develop more potent "cisplatin" analogues with improved pharmacological properties.[71]

The possible advantages in using transition metal ions other than platinum, may involve (i) availability of additional coordination sites, (ii) changes in oxidation state, (iii) alterations in ligand affinity and substitution kinetics and (iv) photodynamic approaches to therapy.[72-74] In this regard, the use of 1,10-phenanthroline (phen)[75], 2,2'-bipyridine (bpy)[76] and salen[77-79] ligands has been found to be of immense utility in designing efficient nucleases along with the metal ions other than platinum. The phen-copper complex, $[Cu(phen)_2]^+$, is the first synthetic coordination complex demonstrated to have an efficient nucleolytic activity.[80,81] Encouraged by this discovery, detailed chemical and biochemical studies were undertaken to understand the properties of various square planar copper(II) complexes.[82,83] This metallointercalation was later extended to three dimension using octahedral complexes. The application of octahedral metallointercalators has permitted the targeting of specific DNA sites by matching the shape, symmetry and functionalities of the metal complexes to that of the DNA target. Moreover, taking advantage of the photophysical and redox properties of metallointercalators, sensitive spectroscopic and reactive probes of DNA have been developed.[72,78,79,84-93]

Recent literature concerning DNA interactions of ruthenium, cobalt, iron, nickel and zinc complexes, as relevant to the present investigation, are described below.

1.4.1 Ruthenium complexes

Barton and co-workers pioneered in the application of polypyridyl transition metal complexes as tools to probe recognition of double helical DNA by matching their shapes, symmetries and functionalities to sites along the strand.[94-98] Studies with these simple complexes provided a basis for conceptualizing how octahedral complexes might interact noncovalently with

DNA and for exploring how the properties of metal complexes, most notably their photophysical and redox characteristics, might be utilized in developing novel probes for DNA. Early experiments indicated a preference for the right handed Δ-isomer intercalate into the right handed DNA.[99] The enantiomeric discrimination in binding was seen for ruthenium(II) complex of 4,7-diphenyl-1,10-phenanthroline (dip), $[Ru(dip)_3]^{2+}$ (Fig. 1.14). While Δ-$[Ru(dip)_3]^{2+}$ was seen to preferentially bind the B form of DNA.

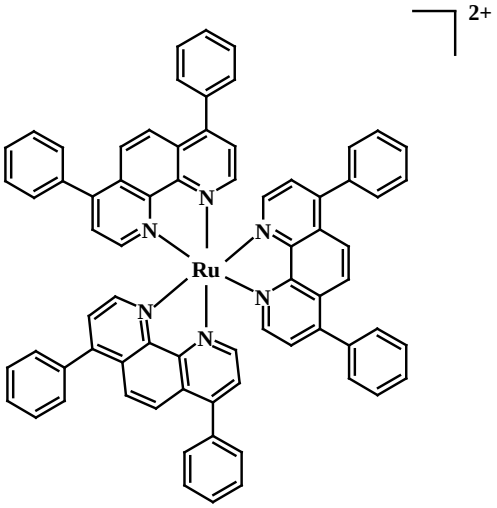

Fig. 1.14

Λ-$[Ru(dip)_3]^{2+}$, the left handed isomer, did not bind intercalatively to the right handed helix. Quite different results were obtained with Z-DNA; both Δ- and Λ-$[Ru(dip)_3]^{2+}$ bind essentially with equal binding strengths.[98] While the binding interactions of these Δ and Λ-isomers are still being debated, the enantiomeric preferences were seen quite consistently in many of such complexes.[100-102]

Increasing the surface area for intercalative stacking by a complex leads to a substantial increase in intercalative binding affinity. As a result,

metallointercalators that contain an extended aromatic heterocyclic ligand can provide immensely powerful tools to probe nucleic acids.[89,90,93,103-107] In an elegant experiment, Barton and co-workers have shown that $[Ru(bpy)_2(dppz)]^{2+}$ (dppz = dipyrido[3,2-a:2',3'-c]phenazine) works as a "molecular light switch" for DNA.[108] $[Ru(bpy)_2(dppz)]^{2+}$ is non-fluorescence in aqueous buffer solution but the fluorescence increases to > 10^4 times in the presence of CT DNA or Z-form of DNA to which the complex binds avidly ($K_b = 10^6\ M^{-1}$). Similar light switch effect was noticed for $[Ru(phen)_2(dppz)]^{2+}$ in the presence of DNA.[109] This has been attributed to the protection of phenazine nitrogen atoms by interacting with water, whereas, in the free complex, the excited state is quenched by water. Examples of such ruthenium(II) complexes bearing planar ligands and behaving

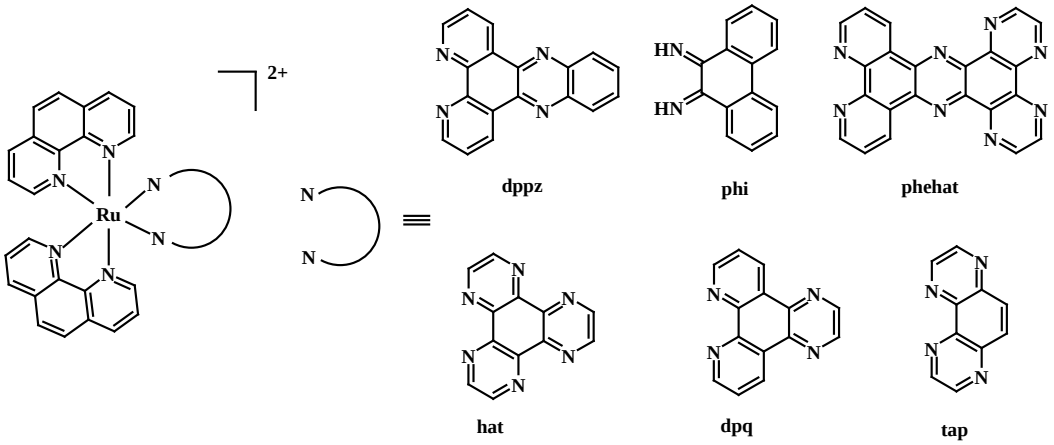

Fig. 1.15

as molecular light switches are provided in Fig. 1.15. In their efforts to develop novel DNA diagnostics, Hartshorn and Barton have synthesized a series of mixed-ligand ruthenium(II) complexes with modified dppz as a ligand.[109] All these new complexes were found to be fluorescent to some degree in aqueous solution in the absence of DNA. However, for a few complexes 20-300 times emission enhancement was observed upon binding with DNA.

$[Ru(phen)_2(qdppz)]^{2+}$ (qdppz = naptho[2,3-*a*]dipyrido[3,2-*h*:2',3'-*f*]phenazine-5,18-dione) endowed with a novel, quinone fused dipyridophenazine ligand, is not only an avid binder of DNA but also an efficient photocleaver of the plasmid. The corresponding reduced species, $[Ru(phen)_2(hqdppz)]^{2+}$, also binds and photocleaves DNA, albeit with less efficiency.[110,111] It has also been demonstrated that the redox couple $[Ru(phen)_2(qdppz)]^{2+}/[Ru(phen)_2(hqdppz)]^{2+}$ represents an "electro-photo switch".

A series of ruthenium(II) complexes containing another modified dipyridophenazine ligand, *viz*: 6,7-dicyanodipyridoquinoxaline (dicnq) was reported to bind DNA with moderate strengths.[110,112] $[Ru(phen)_2(dicnq)]^{2+}$ has been shown to be an efficient "molecular light switch" for DNA.[110] Thus, these results testify the importance of the architectural intricacies and electronic structures of the new dppz-based ligands in dictating the useful photochemical/electrochemical functions of their complexes.

Strekas and co-workers have designed two ruthenium(II) complexes with 'out of plane' ligands; $[Ru(bpy)_2(qpy)]^{2+}$ (qpy = quaterpyridyl) and $[Ru(bpy)_2(dpp)]^{2+}$ (dpp = 2,3-di-2-pyridylpyrazine).[113,114] While the former complex can intercalate DNA, the latter cannot. Ji and co-workers have reported a series of imidazole fused phen ligands wherein the imidazole ring is out of the plane from the phen moiety (Fig. 1.16) and also biphenyl derivatives of phen/dppz, all of which exhibit the effect of ligand planarity on the DNA binding strength of the ip (Imidazo[4,5-f][1,10]phenanthroline)complexes.[85,87,115-123] The DNA binding affinity for $[Ru(bpy)_2(pip)]^{2+}$ (pip=2-phenylimidazo[4,5-f][1,10]phenanthroline) is higher than that of $[Ru(bpy)_2(ip)]^{2+}$ and this has been attributed to the extended conjugation provided by the phenyl ring in pip, Fig. 1.16.[118] DNA binding affinities of the corresponding modified pip ligands present in the complexes ($[Ru(bpy)_2(hpip)]^{2+}$ (hpip = 2-(2-hydroxyphenyl)imidazo[4,5-

f][1,10]phenanthroline), $[Ru(bpy)_2(cip)]^{2+}$ (cip = 2-(2-chlorophenyl)imidazo[4,5-f][1,10]phenanthroline) and $[Ru(bpy)_2(nip)]^{2+}$ (nip=2-(2-nitrophenyl)imidazo[4,5-f][1,10]phenanthroline)) are quite varied.[116,117] In the case of $[Ru(bpy)_2(hpip)]^{2+}$, the *o*-phenolic group of hpip would be nearly coplanar with the imidazole ring due to the formation of an intramolecular hydrogen bond with the nitrogen atom of imidazole ring, leading to some additional affinity.[116] On the other hand, intramolecular hydrogen bond is non-existent for $[Ru(bpy)_2(cip)]^{2+}$ and $[Ru(bpy)_2(nip)]^{2+}$ and hence, phenyl group is out of plane leading to lower DNA binding affinity in each case.[116] Because of the inherent chirality of DNA, its interaction with metal bound chiral ligands give rise to distinguishable diastereomers of complexes. Such a chiral discrimination is interesting, as it could provide insight about mechanisms of interactions and stereoselective effects that might be exploited for nucleic acid target recognitions.

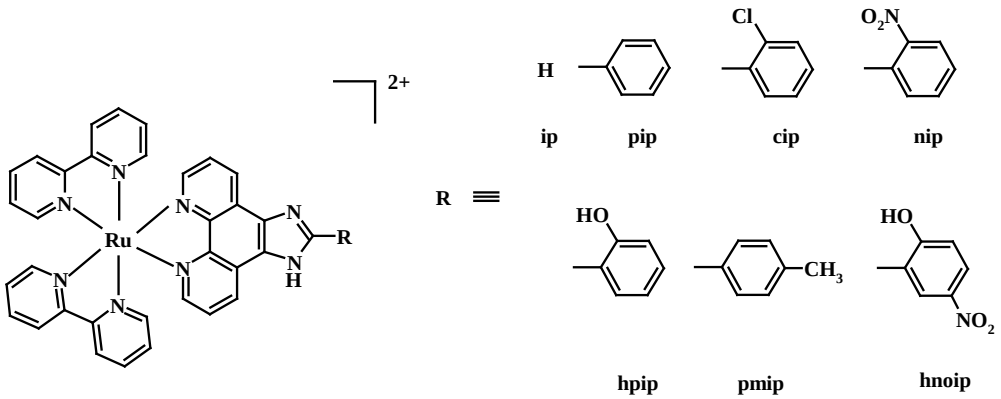

Fig. 1.16

It has been reported that racemic Tröger base containing phen subunits can bind to nucleic acids and cleave DNA in the presence of copper(II) ions Fig. 1.17a).[124] Bailly and co-workers have recently reported the synthesis of asymmetric Tröger base containing the two well characterized DNA binding chromophores - proflavine and phen (Fig. 1.17b).[125]

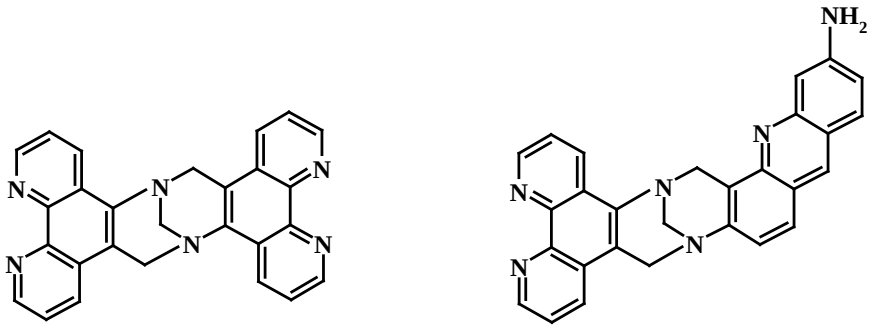

(a) **(b)**

Fig. 1.17

The DNA binding experiments of the ruthenium(II) complex with this ligand have shown that the proflavine moiety intercalates between DNA base pairs and the phen ring occupies the DNA groove. The DNA cleavage experiments were also carried out to investigate the sequence preference of this hybrid ligand and a well resolved footprint was detected at a site encompassing two adjacent 5'-GTC·5-GAC triplets.

1.4.2 Rhodium, manganese, cobalt, nickel, copper and zinc complexes

Brewer and co-workers have reported trimetallic complexes of the type $\{[(bpy)_2Ru(BL)]_2MCl_2\}^{5+}$ incorporating the bridging ligands (BL), 2,2'-bipyrimidine (bpm), 2,3-bis(2-pyridyl)pyrazine (dpp), 2,3-bis(2-pyridyl)quinoxaline (dpq) or 2,3-bis(2-pyridyl) benzoquinoxaline (dpb) and the central metal (M) as iridium(III) or rhodium(III).[126-131] When dpp was used as a bridging ligand with rhodium(III) as the central metal, orbital inversion takes place for Rh(σ^*) orbitals, allowing the rhodium to function as an electron acceptor giving a low lying Ru $\rightarrow$ Rh metal to metal charge transfer (MMCT) excited state in this complex. The DNA photocleavage results have demonstrated that mixed-metal supramolecular complex, $[\{(bpy)_2Ru(dpp)\}_2RhCl_2]^{5+}$ (Fig.

1.18) is capable of inducing single-strand nick in DNA and that similar systems without a Rh(σ*) based LUMO do not display this behaviour.[131] Compared to the wealth of literature available on the DNA interactions of ruthenium(II) and rhodium(III) complexes, little attention seems to have been paid to the corresponding studies on the cobalt(III) complexes. With a redox active metal ion present in them, cobalt(III) complexes have the potential to provide a valuable chance to probe the DNA interactions of both the +2 and +3 oxidation states by electrochemical means and hence, can find application in site specific DNA cleavage.[88,132-141]

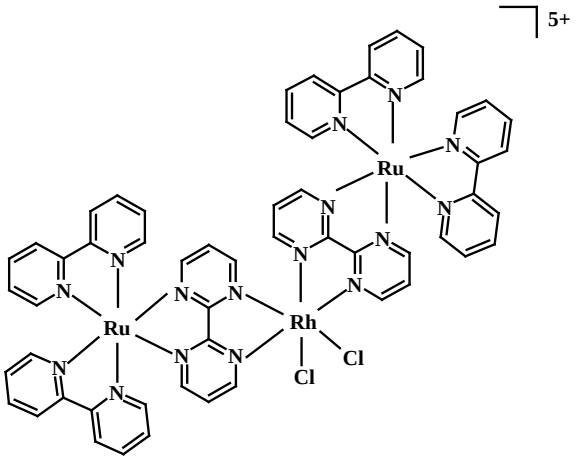

Fig. 1.18

Also, the ability of cobalt(III) complexes to generate active oxygen radicals in aqueous phase upon photolysis by UV-visible light renders them suitable candidates for exploring the DNA photocleavage activity.[142-147]

Several polypyridyl cobalt(III) complexes have been reported which bind DNA through intercalation and are effective photonucleases. For example, Ji and co-workers have published several reports on the DNA binding and photonuclease activities of cobalt(III) complexes.[87,133-136] They have shown that

these complexes are avid intercalators of DNA. They have also investigated the effect of ligand planarity and hydrogen bonding ability on the DNA binding by cobalt(III) complexes containing cip, nip, hpip and hnoip (2-(2-hydroxy-5-nitro-phenyl)imidazo[4,5-f][1,10]phenanthroline) and the structure for all these ligands are given in Fig. 1.16.[134,135] These complexes were shown to effectively cleave DNA and involve $^1O_2$ or $^{\bullet}OH$ as the reactive species in the cleavage mechanisms. The overall DNA binding and photocleavage results obtained for these cobalt(III) complexes were in parallel with those obtained for their parent ruthenium(II) complexes.[116,148]

Nickel(II) complexes of tetradentate macrocycles have been used for recognition of the guanine structures in nucleic acids.[91] Very little attention has been paid to the DNA interactions of nickel(II) octahedral complexes.[139-141] Except for $[Ni(phen)_2(qdppz)]^{2+}$, most other investigated nickel(II) octahedral complexes are found to be quite ineffective DNA cleaving agents.[139-141] The ability of $[Ni(phen)_2(qdppz)]^{2+}$ to photocleave DNA underscores the importance of the quinone functionality in the qdppz structure in the photochemical cleavage process.[141]

Reports on the ability of $[Cu(phen)_2]^+$ to act as an efficient chemical nuclease,[80,81] seem to have attracted studies on the DNA interactions of copper complexes. Recently, Mahadevan *et al.* have reported a series of copper(II/I) complexes of substituted phen and have evaluated their DNA binding characteristics.[149,150] The results indicated that substitution of methyl groups at different sites on the phen ring alters the affinity of the complex towards the intercalative site to different extents. In addition, they have shown that the copper(II) complex of 5,6-dimethyl substituted phen induces conformational changes in DNA (B to Z form).[150] More recently, Chakravarty and co-workers have reported that copper(II) complexes are capable of photoinduced DNA

nicking.[151-154] It was shown that mixed-ligand copper(II) complexes containing either L-methionine[151] or 2-(methylthio)ethylsalicylaldimine[152] bind to the double stranded DNA at the minor groove and interestingly they exhibit photonuclease activity when irradiated with 312 or 532 nm light in the absence of any externally added reducing agent or H_2O_2 through a mechanistic pathway involving singlet oxygen. They have also reported that while dipyrido[3,2-d:2',3'-f]quinoxaline showed significant photonuclease activity on exposure to UV light, it was inactive under red light irradiation.[153] On the other hand, the copper(II) complex of this ligand showed enhanced DNA cleavage activity on photoirradiation at UV as well as visible red light in the absence of any additive. A dual mechanistic pathway involving hydroxyl radical under red light exposure and singlet oxygen ($^1O_2$) for UV irradiation has been proposed for this complex. These results are of significance as they provide examples of copper-based photosensitizers capable of showing visible light induced DNA damage.

The effect of a conjugated acridine moiety on the binding and reactivity of Cu(II)[9-acridinylmethyl-1,4,7-triacyclononane] with DNA was studied (Fig. 1.19) by introducing intercalator acridine to [9]aneN_3, (**1**).[155]

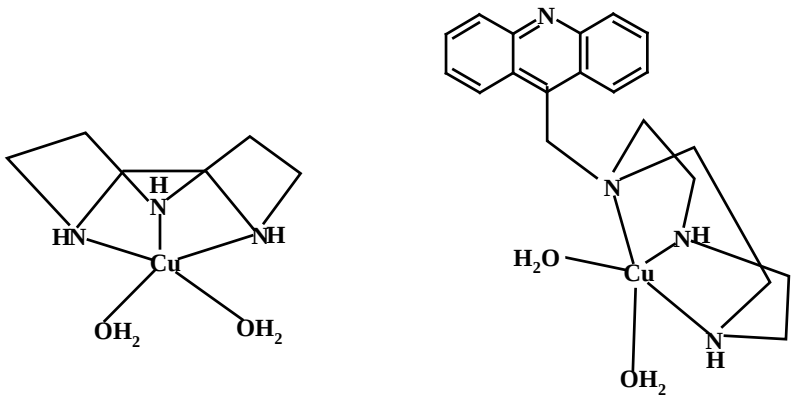

1 **2**

Fig. 1.19

The free rotational motion of $[Cu([9]aneN_3]^{2+}$ moiety in **2** on DNA was limited and the orientation of the reactive center was also fixed stereospecifically relative to the DNA double helical axis and the same is not the case with **1**. Thus $[Cu([9]aneN_3]^{2+}$-acridine (**2**) is more effective in both oxidative and hydrolytic cleavage reactions with DNA than **1**.

In a series of elegant studies, Karlin, Rokita and their co-workers have shown that multinuclear copper(II) complexes are efficient chemical nucleases.[156-159] Interestingly, one of the binuclear copper complexes reported by this group was shown to mediate efficient oxidative cleavage of pBR322 under reducing conditions.[156,157] The necessary presence of both a reductant and dioxygen indicated that the intermediate responsible for DNA cleavage is produced by the activation of dioxygen by the copper(I) form of the complex. The lack of sensitivity to radical quenching agents and the high level of site selectivity in scission suggested a mechanism that does not involve a diffusible radical species. This complex is capable of even mediating efficient specific strand scission at much lower concentrations compared to $[Cu(phen)_2]^{2+}$. The same group has also reported a trinuclear copper(II) complex that exhibits a remarkable ability to promote specific strand scission at junctions between single and double stranded DNA.[158,159]

1.4.2.1 Cationic and neutral metallo-salen complexes

Griffin *et al.* reported that $[SalenMn^{III}]^+$ (**1**) (Fig. 1.20) mediates the cleavage of right handed DNA in the presence of terminal oxidants.[160] Moreover, the nature of the constituents (electron donating, electron withdrawing and bulky aryl groups) on the salen ligand also changes the steric and electronic effects of the metal salen compounds considerably. Chiral derivatives of **1**, also have been studied and the cleavage efficiency of **3** (*R*,*R*) is 5 times higher than that of **4**

(*S*,*S*).[161] The effect of the central metal ion in the DNA binding was studied by Yu *et al*.[162]

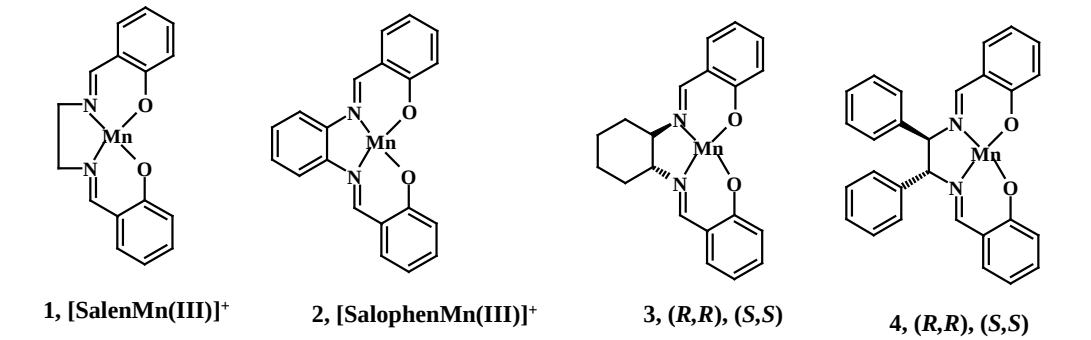

1, [SalenMn(III)]$^+$ **2, [SalophenMn(III)]$^+$** **3, (*R*,*R*), (*S*,*S*)** **4, (*R*,*R*), (*S*,*S*)**

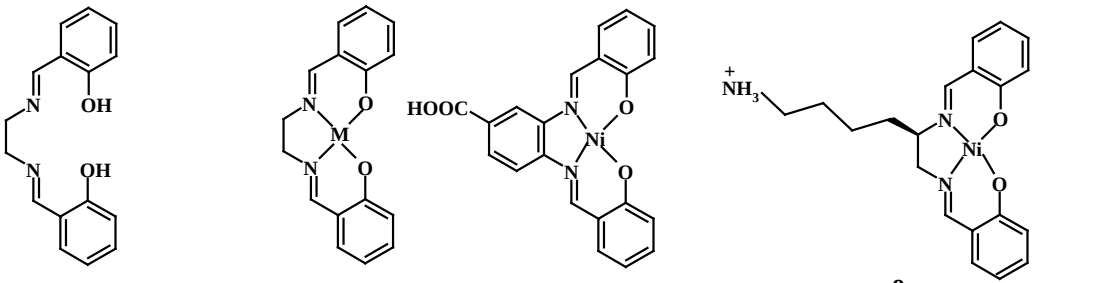

5 **6** **7** **8**

M=Cu(II), Ni(II), Mn(III) and Co(II)

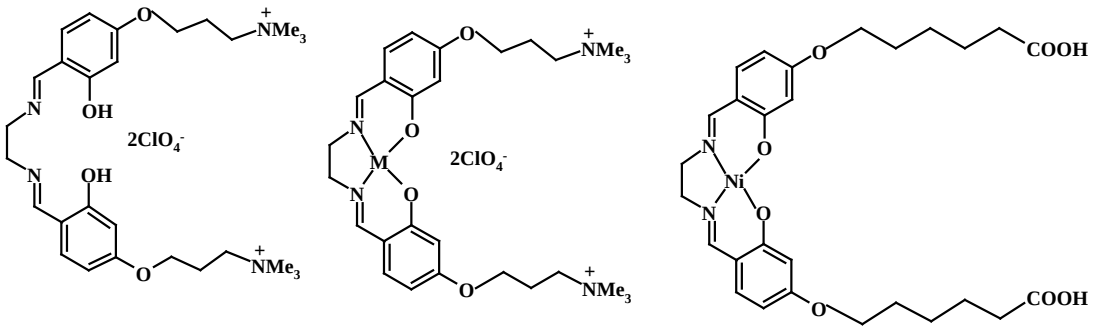

9 **10** **11**

M=Ni(II), Cu(II), Co(II)

Fig. 1.20

All the metal complexes (Cu(II), Ni(II), Mn(II) and Co(II), Fig. 1.20) are interacting with DNA through intercalative mode and the binding constants are of the order of 10^6 M^{-1}. Among this, Co-salen complex shows better binding with K_b = 5.76 x 10^6 M^{-1} and the binding site size in base-pair is 0.058. The neutral molecules reported so far are less soluble in water/buffer and 5-10% of DMF/C_2H_5OH/DMSO are used to avoid precipitation during the progress of the experiments. Highly water soluble ionic salen compounds also have been synthesized. Bhattacharya *et al*[163,164] reported some cationic salen compounds and studied the role of the central metal ion in DNA binding and photocleavage process.[165]

Here probably a combination of both the electrostatic and intercalative/groove binding modes operate (compounds **9**, **10**, **11**, Fig. 1.20). The anionic salen complex (**7**, Fig. 1.20) neither bind DNA nor induce strand scission irrespective of the metal ion selected. Large number of nickel(II)-salen (salen = ethylenediamine-N,N'-bis(salicylaldimine)) type complexes are found to be well suited for covalent modification of DNA, since the $Ni^{III/II}$ couple often lies near the redox potential of the ligand. In such cases, the coordinated metal ion serves to trigger redox chemistry that is ligand based, generating a reactive intermediate which couples with a nucleobase to form a new covalent bond.[78]

1.4.3 Polyintercalators

Natural antibiotics that bind to DNA by bisintercalation have stimulated an approach to achieve high affinity for DNA by linking two or more subunits of known DNA mono-intercalators to form polyintercalating compounds.[166-168]

Efforts to extend the interaction beyond bisintercalation, however, have met with relatively few successes.[169-172] Most of the known trisintercalators bind DNA with association constants within an order of magnitude higher than the

corresponding bisintercalating counterparts. One noteworthy exception to this is a polyamine linked triacridine synthesized by Roques and co-workers that exhibited an unusually high binding affinity for double stranded DNA ($K_b = 10^{14}$ M^{-1}).[173] More recently, tris-, tetra- and even hexamers of intercalating drugs have been synthesized, some of which exhibit high DNA binding affinity and extremely slow dissociation rates.[174,175] [μ-(11,11'-bidppz)$(phen)_4Ru_2]^{4+}$ - the bisintercalating ruthenium(II) complex reported by Lincoln and Norden is a dinuclear ruthenium(II) complex connected by two dppz ligands together.[176] This complex is non-fluorescent both in aqueous solution and in the presence of DNA, but it effectively quenches the fluorescence of DNA bound Δ-$[Ru(phen)_2(dppz)]^{2+}$ by displacing the latter monomeric complex from the DNA groove. Both the ΔΔ and ΛΛ enantiomers of this complex bind DNA with extremely high affinities and the estimated binding constants are in the range of 10^{12} M^{-1}.

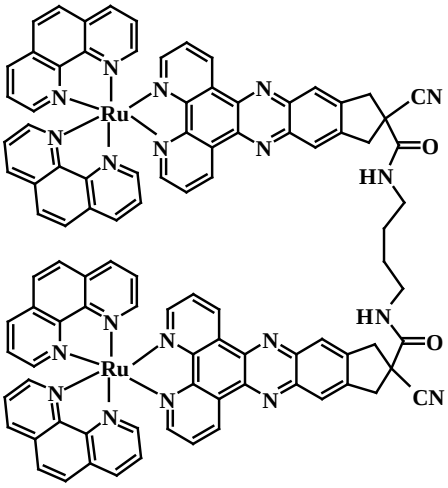

Fig. 1.21

More recently, the same group has also reported the photophysical[177] and DNA binding[178] properties of a novel type of chiral bisintercalating ruthenium complex $[\mu\text{-C4(cpdppz)}_2(\text{phen})_4\text{Ru}_2]^{4+}$ (Fig. 1.21).[179]

An overall scheme for photosensitized DNA modification is discussed by Meunier *et al*[180] and an expanded view is shown in Fig. 1.22.

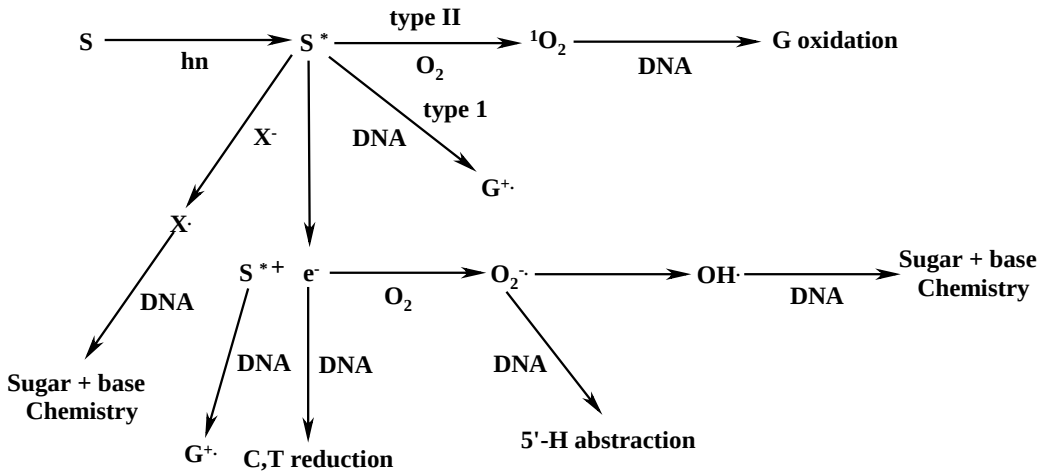

Fig. 1.22 Chemistry resulting from photosensitized irradiation of DNA.

1.5 References

1. Watson, J. D.; Crick, F. H. *Nature* **1953,** *171*, 737.
2. Neidle, S.; Abraham, Z. *CRC Crit. Rev. Biochem.* **1984,** *17*, 73.
3. Wang, J. C. *J. Mol. Biol.* **1974**, *89*, 783.
4. Wang, A. H-J. *Current Opinion in Structrural Biology* **1992,** *2*, 361.
5. Lerman, L. S. *J. Mol. Biol.* **1961**, *3*, 18.
6. *Practical Biochemistry*; Wilson, K., Walker, J., Eds.; Cambridge University Press: Cambridge, 2000.

7. *Nucleic Acid – Metal Ion Interactions*; Spiro, T. G., Ed.; John Wiley & Sons: New York, 1980.
8. Sambrook, J.; Russell, D. W. *Molecular Cloning A Laboratory Manual;* 3rd Ed. Cold Spring Harbor Laboratory Press: New York, 2001.
9. Long, E. C.; Barton, J. K. *Acc. Chem. Res.* **1990,** *23*, 271.
10. Kelly, J. M.; Tossi, A. B.; McConnell, D. J.; OhUigin, C. *Nucl. Acid. Res.* **1985**, *13*, 6017.
11. Marmur, J.; Doty, P. *J. Mol. Biol*. **1962**, *5*, 109.
12. Cohen, G.; Eisenberg, H. *Biopolymers* **1969,** *8*, 45.
13. Thorne, H. V. *J. Mol. Biol*. **1967**, *24*, 203.
14. Wang, J. *J. Mol. Biol*. **1974**, *89*, 783.
15. Waring, M. J. *J. Mol. Biol*. **1970**, *54*, 247.
16. Carter, M. T.; Rodrigues, M.; Bard, A. J. *J. Am. Chem. Soc.* **1989,** *111*, 8901.
17. Kumar, C. V.; Punzalan, E. H. A.; Tan, W. B. *Tetrahedron* **2000**, *56*, 7027.
18. Kumar, C. V.; Asuncion, E. H. *J. Chem. Soc., Chem. Commun*. **1992**, 470.
19. Kumar, C. V.; Asuncion, E. H. *J. Am. Chem. Soc*. **1993**, *115*, 8547.
20. Rodger, A.; Taylor, S.; Adlam, G.; Blagbrough, I, S.; Haworth, I. S. *Bioorg. Med. Chem*. **1995**, *3*, 961.
21. Urano, S.; Price, H. L.; Fetzer, S. M.; Briedis, A. V.; Milliman, A.; LeBreton, P. R. *J. Am. Chem. Soc.* **1991,** *113*, 3881.
22. Sharifian, H. A.; Pyun, C. H.; Jiang, F. B.; Park, S. M. *Jour. Photochem*. **1985**, *30*, 229.
23. Blacker, J.; Jazwinski, J.; Lehn, J-M. *Helv. Chim. Acta* **1987**, *70*, 1.
24. Slama-Schwok, A.; Jazwinski, J.; Bere, A.; Montenay-Garestier, T.; Rougee, M.; Helene, C.; Lehn, J-M. *Biochemistry* **1989**, *28*, 3227.

25. Piantanida, I.; Tomisic, V.; Zinic, M. *J. Chem. Soc., Perkin Trans. 2* **2000**, 375.
26. Palm, B, S.; Piantanida, I.; Zinic, M.; Schneider, H, J. *J. Chem. Soc., Perkin Trans. 2* **2000**, 385.
27. Piantanida, I.; Palm, B, S.; Zinic, M.; Schneider, H, J. *J. Chem. Soc., Perkin Trans. 2* **2001**, 1801.
28. Becker, H-C.; Norden, B. *J. Am. Chem. Soc.* **2000**, *122*, 8344.
29. Becker, H-C.; Norden, B. *J. Am. Chem. Soc.* **1999**, *121*, 11947.
30. *Photodynamic Therapy: Basic Principles and Clinical Application;* Henderson, B. W., Dougherty, T. J., Eds.; Marcel Dekker: New York, 1992**.**
31. Dougherty, T. J. *Photochem. Photobiol.* **1993**, *58*, 895.
32. Gomer, C. J.; Doiron, D. R.; Dunn, S.; Rucker, N.; Razum, N.; Fountain, S. *Photochem. Photobiol.* **1983,** *37S*, S91.
33. Girotti, A. W. *Photochem. Photobiol.* **1983,** *38*, 745.
34. Dolphin, D. *Can. J. Chem.* **1994,** *72*, 1005.
35. Bonnet, R. *Chem. Soc. Rev.* **1995,** 19.
36. Fiel, R. J.; Howard, J. C.; Mark, E. H.; Gupta, N. D. *Nucleic Acids Res.* **1979**, *6*, 3093.
37. Fiel, R. J.; Munson, B. R. *Nucleic Acids Res.* **1980**, *8*, 2835.
38. Carvlin, M. J.; Fiel, R. J. *Nucleic Acids Res.* **1983**, *11*, 6121.
39. Kelly, J. M.; Murphy, M. J.; McConnell, D. J.; OhUigin, C. *Nucleic Acids Res.* **1985**, *13*, 167.
40. Fiel, R. J. *J. Biomol. Struct. Dyn.* **1989**, *6*, 1259.
41. Verlhac, J. B.; Gaudemer, A.; Kraljic, I. *Nouv. J. Chim.* **1983**, *8*, 401.
42. Pasternack, R. F.; Gibbs, E. J. *Metal Ions in Biological Systems;* Sigel, A., Sigel, H., Eds.; Marcel Dekker: New York, 1996, *33*, 367.

43. Mehta, G.; Sambaiah, T.; Maiya, B. G.; Sirish, M.; Dattagupta, A. *Tetrahedron Lett*. **1994**, *35*, 4201.
44. Mehta, G.; Muthusamy, S.; Maiya, B. G.; Mallena, S. *J. Chem. Soc., Perkin Trans. 1* **1996**, 2421.
45. Mehta, G.; Sambaiah, T.; Maiya, B. G.; Sirish, M.; Chatterjee, D. *J. Chem. Soc., Perkin Trans. 1* **1993,** 2667.
46. Mehta, G.; Thota, S.; Maiya, B. G.; Mallena, S. Dattagupta, A. *J. Chem. Soc., Perkin Trans. 1* **1995**, 295.
47. Mehta, G.; Muthusamy, S.; Maiya, B. G.; Arounaguiri, S. *Tetrahedron Lett*. **1997**, *38*, 7125.
48. Mehta, G.; Muthusamy, S.; Maiya, B. G.; Arounaguiri, S. *J. Chem. Soc., Perkin Trans.1* **1999**, 2177.
49. Hayashi, K.; Nakajima, R.; Kiyosawa, I.; Ozaki, H.; Sawai, H. *Chem. Lett.* **2004**, *33*, 684.
50. Wender, P. A.; Touami, S. M.; Alayrac, C.; Philipp, U. C. *J. Am. Chem. Soc*. **1996**, *118*, 6522.
51. Touami, S. M.; Poon, C. C.; Wender, P. A. *J. Am. Chem. Soc.* **1997**, *119*, 7611.
52. Blake, A.; Peacocke, A. R. *Biopolymers* **1961**, *6*, 1225.
53. Sakore, T. D.; Jain, S. C.; Tsai, C.; Sobell, H. M. *Proc. Natl. Acad. Sci. U.S.A.* **1962**, *74*, 188.
54. Martin, R. F.; Kelly, D. P. *Aust. J. Chem.* **1979**, *32*, 2637.
55. Cain, B. F.; Atwell, G. J.; Denny, W. A. *J. Med. Chem.* **1975**, *18*, 1110.
56. Wilson, W. R.; Baugley, B. C.; Wakelin, L. P. G.; Waring, M. J. *Mol. Pharmacology* **1981**, *20*, 404.
57. Wadkins, R. M.; Graves, D. E. *Biochemistry* **1991**, *30*, 4277.
58. Wadkins, R. M.; Graves, D. E. *Nucleic Acid. Res*. **1989**, *17*, 9933.

59. Crenshaw, J. M.; Graves, D. E.; Denny, W. A. *Biochemistry* **1995**, *34*, 13682.
60. Siim, B. G.; Hicks, K. O.; Pullen, S. M.; van Zijl, P. L.; Denny, W. A.; Wilson, W. R. *Biochemical Pharmacology* **2000**, *60*, 969.
61. McConnaughie, A W.; Jenkins, T. C. *J. Med. Chem.* **1995**, *38*, 3488.
62. Asakawa, M.; Endo, K.; Kobayashi, K.; Toi, H.; Aoyama, Y. *Bull. Chem. Soc. Jpn.* **1992**, *65*, 2050.
63. Barton, J. K.; Danishefsky, A. T.; Goldberg, J. M. *J. Am. Chem. Soc.* **1984**, *106*, 2172.
64. Eldho, N. V.; Joseph, J.; Ramaiah, D. *Chem. Lett*. **2001**, *5*, 438.
65. Joseph, J.; Eldho, N. V.; Ramaiah, D. *J. Phys. Chem. B* **2003,** *107*, 4444.
66. Joseph, J.; Eldho, N. V.; Ramaiah, D. *Chem. Eur. J.* **2003**, *9*, 5926.
67. Takenaka, S.; Ihara, T.; Takagi, M. *J. Chem. Soc., Chem. Commun*. **1990**, *21*, 1485.
68. Takenaka, S.; Ihara, T.; Takagi, M. *Chem. Lett*. **1992**, 1.
69. Rosenberg, B.; van Camp, L.; Trosko, J. E. *Nature* **1969**, *222*, 385.
70. Keck, M. V.; Lippard, S. J. *J. Am. Chem. Soc.* **1992,** *114*, 3386.
71. Jamieson, E. R.; Lippard, S. J. *Chem. Rev.* **1999**, *99*, 2467.
72. Clarke, M, J.; Zhu, F.; Frasca, D. R. *Chem. Rev.* **1999**, *99*, 2511.
73. Ali, H.; Van Lier, J. E. *Chem. Rev.* **1999**, *99*, 2379.
74. Clarke, M. J.; Stubbs, M. *Metal Ions in Biological Systems;* Sigel, A., Sigel, H., Eds.; Marcel Dekker: New York 1996, *32*, 727.
75. Sammes, P. G.; Yahioglu, G. *Chem. Soc. Rev*. **1994**, 327.
76. Kaes, C.; Katz, A.; Hosseini, M. W. *Chem. Rev.* **2000**, *100*, 3553.
77. Routier, S.; Bernier, J-L.; Waring, M. J.; Colson, P.; Houssier, C.; Bailly, C. *J. Org. Chem.* **1996,** *61*, 2326.
78. Yam, V. W-W.; Lo, K. K-W. *Coord. Chem. Rev*. **1998**, *184*, 157.

79. Muller, J. G.; Kayser, L. A.; Paikoff, S. J.; Duarte, V.; Tang, N.; Perez, R. J.; Rokita, S. E.; Burrows, C. J. *Coord. Chem. Rev*. **1999**, *185-186*, 761.
80. Sigman, D. S.; Graham, D. R.; D'Aurora, V.; Stern, A. M. *J. Biol. Chem.* **1979,** *254*, 12269.
81. Sigman, D. S. *Acc. Chem. Res*. **1986**, *19*, 180.
82. Sigman, D. S.; Bruice, T. W.; Mazumder, A.; Sutton, C. L. *Acc. Chem. Res*. **1993**, *26*, 98.
83. McMillin, D. R.; McNett, K. M. *Chem. Rev.* **1998**, *98*, 1201.
84. Armitage, B. *Chem. Rev*. **1998**, *98*, 1171
85. Xiong, Y.; Ji, L-N. *Coord. Chem. Rev*. **1999**, *185-186*, 711.
86. Clarke, M. J. *Coord. Chem. Rev*. **2002**, *232*, 69.
87. Ji, L-N.; Zou, X-H.; Liu, J-G. *Coord. Chem. Rev*. **2001**, *216-217*, 513.
88. Ortmans, I.; Moucheron, C.; Mesmaeker, A. K-D. *Coord. Chem. Rev*. **1998**, *168*, 233.
89. Erkkila, K. E.; Odom, D. T.; Barton, J. K. *Chem. Rev*. **1999**, *99*, 2777.
90. Mesmaeker, A. K.; Lecomte, J-P.; Kelly, J-M. *Topics in Current Chem*. **1996,** *177*, 25.
91. Burrows, C. J.; Rokita, S. E. *Acc. Chem. Res.* **1994**, *27*, 295.
92. Johnston, D. H.; Welch, T. W.; Thorp, H. H. *Metal Ions in Biological Systems;* Sigel, A., Sigel, H., Eds.; Marcel Dekker: New York, 1996, *33*, 297.
93. Norden, B.; Lincoln, P.; Akerman, B.; Tuite, E. *DNA Interactions with Substitution-Inert Transition Metal Ion Complexes*; Sigel, A., Sigel, H., Eds.; Marcel Dekker: New York, 1996, *33*, 177.
94. Barton, J. K.; Dannenberg, J. J.; Raphael, A. L. *J. Am. Chem. Soc.* **1982**, *104*, 4967.

95. Barton, J. K.; Basile, L. A.; Danishefsky, A.; Alexandrescu, A. *Proc. Nat. Acad. Sci. U S A* **1984**, *81*, 1961.

96. Barton, J. K.; Danishefsky, A. T.; Goldberg, J. M. *J. Am. Chem. Soc.* **1984**, *106*, 2172.

97. Barton, J. K.; Raphael, A. L. *Proc. Natl. Acad. Sci. U. S. A.* **1985**, *82*, 6460.

98. Kumar, C. V.; Barton, J. K.; Turro, N. J. *J. Am. Chem. Soc.* **1985**, *107*, 5518.

99. Barton, J. K. *Science* **1986**, *233*, 727.

100. Satyanarayana, S.; Dabrowiak, J. C.; Chaires, J. B. *Biochemistry* **1992**, *31*, 9319.

101. Satyanarayana, S.; Dabrowiak, J. C.; Chaires, J. B. *Biochemistry* **1993**, *32*, 2573.

102. Eriksson, M.; Leijon, M.; Hiort, C.; Norden, B.; Graslund, A. *Biochemistry* **1994**, *33*, 5031.

103. Pyle, A. M.; Barton, J. K. *Progress in Inorganic Chemistry: Bioinorganic Chemistry*; Lippard, S. J., Ed.; John Wiley & Sons: New York, 1990, *38*, 413.

104. Chow, C. S.; Barton, J. K. *Methods Enzymol.* **1992**, *212*, 219.

105. Murphy, C. J.; Barton, J. K. *Methods Enzymol.* **1993**, *226*, 576.

106. Kane-Maguire, N. A. P.; Wheeler, J. F. *Coord. Chem. Rev*. **2001**, *211*, 145.

107. Kelly, S. O.; Barton, J. K. *Metal Ions in Biological Systems;* Sigel, A., Sigel, H., Eds.; Marcel Dekker: New York, 1999, *39*, 211.

108. Friedman, A. E.; Kumar, C. V.; Turro, N. J.; Barton, J. K. *Nucleic Acid. Res*. **1991**, *19*, 2595.

109. Hartshorn, R. M.; Barton, J. K. *J. Am. Chem. Soc*. **1992**, *114*, 5919.

110. Arounaguiri, S.; Maiya, B. G. *Inorg. Chem.* **1999**, *38*, 842.
111. Ambroise, A.; Maiya, B. G. *Inorg. Chem.* **2000**, *39*, 4256.
112. Ambroise, A.; Maiya, B. G. *Inorg. Chem.* **2000**, *39*, 4264.
113. Morgan, R. J.; Chatterjee, S.; Baker, A. D.; Strekas, T. C. *Inorg. Chem.* **1991**, *30*, 2687.
114. Tysoe, S. A.; Morgan, R. J.; Baker, A. D.; Strekas, T. C. *J. Phys. Chem*. **1993**, *97*, 1707.
115. Zhen, Q-Z.; Ye, B-H.; Zhang, Q-L.; Liu, J-G.; Li, H.; Ji, L-N.; Wang, L. *J. Inorg. Biochem*. **1999**, *76*, 47.
116. Liu, J-G.; Ye, B-H.; Li, H.; Zhen, Q-H.; Ji, L-N.; Fu, Y-H. *J. Inorg. Biochem*. **1999**, *76*, 265.
117. Xiong, Y.; He, X-F.; Zou, X-Z.; Wu, J-H.; Chen, X-M.; Ji, L-N.; Li, R-H.; Zhou, J-Y.; Yu, K-B. *J. Chem. Soc*., *Dalton Trans*. **1999**, 19
118. Wu, J-Z.; Ye, B-H.; Wang, L.; Ji, L-N.; Zhou, J-Y.; Li, R-H.; Zhou, Z-Y. *J. Chem. Soc*., *Dalton Trans*. **1997**, 1395.
119. Zhen, Q-X.; Zhang, Q-L.; Liu, J-G.; Ye, B-H.; Ji, L-N.; Wang, L. *J. Inorg. Biochem*. **2000**, *78*, 293.
120. Garoufis, A.; Liu, J-G.; Ji, L-N.; Hadjiliadis, N. *J. Inorg. Biochem*. **2003**, *93*, 221.
121. Xu, H.; Zheng, K-C.; Chen, Y.; Li, Y-Z.; Lin, L-J.; Li, H.; Zhang, P-X.; Ji, L-N. *J. Chem. Soc., Dalton Trans.* **2003**, 2260.
122. Zhen, Q-Z.; Ye, B-H.; Liu, J-G.; Zhang, Q-L.; Ji, L-N.; Wang, L. *Inorg. Chim. Acta*. **2003**, *303*, 141.
123. Xu, H.; Zheng, K-C.; Deng, H.; Lin, L-J.; Zhang, Q-L.; Ji, L-N. *New J. Chem*. **2003**, *27*, 1255.
124. Yashima, E.; Akasi, M.; Miyauchi, N. *Chem. Lett*. **1991**, 1017.

125. Baldeyrou, B.; Tardy, C.; Bailly, C.; Colson, P.; Houssier, C.; Charmantray, F.; Demeunynck, M. *Eur. J. Med. Chem*. **2002**, *37*, 315.
126. Bridgewater, J. S.; Vogler, L. S.; Molnar, S. M.; Brewer, K. J. *Inorg. Chim. Acta* **1993**, *208*, 179.
127. Molnar, S. M.; Jensen, G. E.; Vogler, L. M.; Jones, S. W.; Laverman, L.; Bridgewater, J. S.; Richter, M. M.; Brewer, K. J. *J. Photochem. Photobiol. A: Chem*. **1994**, *80*, 315.
128. Richter, M. M.; Brewer, K. J. *Inorg. Chem*. **1992**, *31*, 1594.
129. Molnar, S. M.; Nallas, G. N.; Bridgewater, J. S.; Brewer, K. J. *J. Am. Chem. Soc*. **1994**, *116*, 5206.
130. Nallas, G. N. A.; Jones, S. W.; Brewer, K. J. *Inorg. Chem.* **1996,** *35*, 6974.
131. Swavey, S.; Brewer, K. J. *Inorg. Chem.* **2002,** *41*, 6196.
132. Selvi, P. T.; Palaniandavar, M. *Inorg. Chim. Acta **2002**, 337*, 420.
133. Zhang, Q-L.; Liu, J-G.; Chao, H.; Xue, G-Q.; Ji, L-N. *J. Inorg. Biochem*. **2001**, *83*, 49.
134. Zhang, Q-L.; Liu, J-G.; Liu, J.; Xue, G-Q.; Li, H.; Liu, J-Z.; Zhou, H.; Qu, L-H.; Ji, L-N. *J. Inorg. Biochem*. **2001**, *85*, 291.
135. Zhang, Q-L.; Liu, J-G.; Xu, H.; Li, H.; Liu, J-Z.; Zhou, H.; Qu, L-H.; Ji, L-N. *Polyhedron* **2001**, *20, 3049.*
136. Zhang, Q-L.; Liu, J-H.; Ren, X-Z.; Xu, H.; Huang, Y.; Liu, J-Z.; Ji, L-N. *J. Inorg. Biochem*. **2003**, *95*, 194.
137. Kumar, C. V.; Tan, W. B.; Betts, P. W. *J. Inorg. Biochem*. **1997**, *68*, 177.
138. Sargeson, A. M. *Coord. Chem. Rev*. **1996**, *151*, 89.
139. Arounaguiri, S.; Maiya, B. G. *Inorg. Chem*. **1996**, *35*, 4267.
140. Arounaguiri, S.; Easwaramoorthy, D.; Kumar, A. A.; Dattagupta, A.; Maiya, B. G. *Proc. Indian Acad. Sci.* (*Chem. Sci.*) **2000**, *112*, 1.

141. Sastri, C. V.; Eswaramoorthy, D.; Giribabu, L.; Maiya, B. G. *J. Inorg. Biochem*. **2003**, *94*, 138.
142. Adamson, A. W. *Coord. Chem. Rev*. **1968**, *3*, 169.
143. *Concepts of Inorganic Photochemistry;* Adamson, A. W., Fleischauer, P. D., Eds.; Wiley-Interscience: New York, 1975.
144. Prakash, H.; Natarajan, P. *Res. Chem. Intermediates* **2003**, *29*, 349.
145. Arunachalam, S.; Natarajan, P. *Chem. Commun*. **1983**, 472.
146. Natarajan, P.; Raghavan, N. V. *J. Phys. Chem*. **1981**, *85*, 188.
147. Natarajan, P. *J. Chem. Soc*., *Dalton Trans*. **1977**, 1400.
148. Xiong, Y.; He, X-F.; Zou, X-Z.; Wu, J-H.; Chen, X-M.; Ji, L-N.; Li, R-H.; Zhou, J-Y.; Yu, K-B. *J. Chem. Soc*., *Dalton Trans*. **1999**, 19
149. Mahadevan, S.; Palaniandavar, M. *Inorg. Chem*. **1998**, *37*, 693.
150. Mahadevan, S.; Palaniandavar, M. *Inorg. Chem*. **1998**, *37*, 3927.
151. Dhar, S.; Chakravarty, A. R. *Inorg. Chem*. **2003**, *42*, 2483.
152. Patra, A. K.; Dhar, S.; Nethaji, M.; Chakravarty, A. R. *Chem. Commun*. **2003**, 1562.
153. Dhar, S.; Senapati, D.; Reddy, P. A. N.; Das, P. K.; Chakravarty, A. R. *Chem. Commun*. **2003**, 2452.
154. Dhar, S.; Senapati, D.; Das, P. K.; Chattopadhyay, P.; Nethaji, M.; Chakravarty, A. R. *J. Am. Chem. Soc*. **2003**, *125*, 12118.
155. Hirohama, T.; Arii, H.; Chikira, M. *J. Inorg. Biochem*. **2004**, *98*, 1778.
156. Humphreys, K. J.; Johnson, A. E.; Karlin, K. D.; Rokita, S. E. *J. Biol. Inorg. Chem*. **2002**, *7*, 835.
157. Humphreys, K. J.; Karlin, K. D.; Rokita, S. E. *J. Am. Chem. Soc*. **2002**, *124*, 6009.
158. Humphreys, K. J.; Karlin, K. D.; Rokita, S. E. *J. Am. Chem. Soc*. **2002**, *124*, 8055.

159. Humphreys, K. J.; Karlin, K. D.; Rokita, S. E. *J. Am. Chem. Soc*. **2001**, *123*, 5588.
160. Gravert, D. J.; Griffin, J. H. *J. Org. Chem.* **1993**, *58*, 820.
161. Gravert, D. J.; Griffin, J. H. *Inorg. Chem.* **1996**, *35*, 4837.
162. Liu, G-D.; Yang, X.; Chen, Z-P.; Shen, G-L.; Yu, R-Q. *Anal. Sci*. **2000,** *16*, 1255.
163. Mandal, S. S.; Vinaykumar, N.; Varshney, U.; Bhattacharya, S. *J. Inorg. Biochem*. **1996,** *63*, 265.
164. Mandal, S. S.; Renuka, K.; Guru Row, T. N.; Bhattacharya, S. *J. Chem. Soc., Chem. Commun*. **1996,** 2725.
165. Mandal, S. S.; Varshney, U.; Bhattacharya, S. *Bioconjugate Chem*. **1997,** *8*, 798.
166. Muller, W.; Crothers, D. M. *J. Mol. Biol.* **1968**, *35*, 251.
167. Leroy, J. L.; Gao, X. L.; Misra, V.; Gueron, M.; Patel, D. J. *Biochemistry* **1992**, *31*, 1407.
168. Boger, D. L.; Chen, J-H.; Saionz, K. W. *J. Am. Chem. Soc.* **1996**, *118*, 1629.
169. Wirth, M.; Ole, B.; Torben, K.; Nielsen, P.; Norden, B. *J. Am. Chem. Soc*. **1988**, *110*, 932.
170. Gaugain, B.; Markovits, J.; Le Pecq, J-B.; Roques, B. P. *FEBS Lett*. **1984**, *169*, 123.
171. Atwell, G. J.; Baguley, B. G.; Wilmanska, D.; Denny, W. A. *J. Med. Chem*. **1986**, *29*, 69.
172. Hansen, J. B.; Koch, T.; Buchardt, O.; Nielsen, P. E.; Norden, B.; Wirth, M. *Chem. Commun*. **1984**, 509.
173. Laugaa, P.; Markovits, J.; Delbarre, A.; Le Pecq, J-B.; Roques, B. P. *Biochemistry* **1985**, *24*, 5567.

174. Guelev, V.; Cubberley, M.; Murr, M.; Lokey, R. S.; Iverson, B. L. *Methods Enzymol.* **2001**, *340*, 556.
175. Murr, M.; Iverson, B. L. *Bioorg. Med. Chem.* **2001**, *9*, 1141.
176. Lincoln, P.; Norden, B. *Chem. Commun*. **1996**, 2145.
177. Onfelt, B.; Lincoln, P.; Norden, B.; Baskin, J. S.; Zewail, A. H. *Proc. Natl. Acad. Sci. U. S. A.* **2000**, *97*, 5708.
178. Onfelt, B.; Lincoln, P.; Norden, B. *J. Am. Chem. Soc.* **1999**, *121*, 10846.
179. Onfelt, B.; Lincoln, P.; Norden, B. *J. Am. Chem. Soc.* **2001**, *123*, 3630.
180. Meunier, B.; Pratviel, G.; Bernadou, J. *Bull. Soc. Chim. Fr.* **1994**, *13*1, 933.

CHAPTER 2

Materials and Methods

2.1 Introduction

In this chapter, a listing of all the materials employed at different stages of the investigation and procedures for purification of the utilized chemicals and solvents are given. Also given here are preparations of the various precursor materials and a brief description of the physicochemical as well as biochemical techniques employed in this study.

2.2 Materials

2.2.1 Chemicals and biochemicals

Ruthenium(III) chloride trihydrate, ammonium hexaflurophosphate (NH_4PF_6), tetrabutylammonium perchlorate (TBAP), tetrabutylammonium chloride hydrate (TBACl), anthracene and pyrene were all obtained from Aldrich Chemical Co. (USA). 1,10-phenanthroline monohydrate (phen), ammonium acetate, potassium bromide, hydrazine hydrate, palladium on charcoal (Pd/C (10%)), 1,4-diazabicyclo[2.2.2]octane (DABCO) and mannitol were purchased from E. Merck (India). 4-nitro-1,2-diaminobenzene was purchased from Acros Organics (Belgium). 9-anthraldehyde was obtained from Spectrochem (India) and it was recrystallized from glacial acetic acid before use. 1-pyrenecarboxaldehyde and acridine were purchased from Lancaster. The metal perchlorates used were acquired from either Aldrich Chemical Co. (USA) or Acros Organics (Belgium) or were synthesized from their corresponding carbonate salts.

Aluminium oxide (basic and neutral) and silica gel (60 - 200 mesh size) for column chromatography was obtained from Acme Synthetic Chemicals (India). The drying agents employed at various stages of purification procedures *viz*: anhydrous sodium sulphate, calcium chloride, calcium hydride, magnesium turnings and magnesium sulphate and the mineral acids such as hydrochloric acid, sulphuric acid, nitric acid and oleum were all of Analytical Reagent grade obtained from either B.D.H. (India) or Ranbaxy (India). All other common chemicals were purchased from locally available sources. The nitrogen gas utilized in this study was obtained from India Oxygen Limited (India). It was further purified by using pyrogallol and BASF catalyst before use.

Supercoiled DNA pBR 322 (cesium chloride purified) was obtained from Bangalore Genei (India). Agarose (low melt, 65 ^{o}C, Molecular Biology grade for DNA gels) was purchased from Bio-Rad Laboratories Inc. (USA). Highly polymerized calf thymus DNA (CT DNA), ethidium bromide and bromophenol blue were procured from Sigma (USA). These biochemicals were used as received. Tris(hydroxylmethyl)aminomethane (Tris), sucrose, sodium chloride, ethylenediaminetetraacetic acid disodium salt (EDTA-Na_2), disodium hydrogen phosphate (Na_2HPO_4) and sodium dihydrogen phosphate (NaH_2PO_4) were of Molecular Biology grade, obtained from Sisco Research Laboratories (India). Salicylaldehyde is purchased from Ranbaxy and distilled under reduced pressure.

2.2.2 Solvents

Acetonitrile was of spectroscopic grade from E. Merck (India). It was further purified by distilling over phosphorus pentoxide. CH_3OH and 2-isopropanol were of Spectroscopic grade from E. Merck (India). They were further purified by distilling over calcium hydride. Spectroscopic grade

dimethylformamide (DMF) was obtained from E. Merck (India) and was purified using flash distillation over calcium hydride under vacuum.

Methylene chloride used for the spectroscopic and electrochemical studies was purified rigorously. The Laboratory Reagent (LR) grade solvent obtained from B.D.H. (India) was washed twice with sulphuric acid and then with water. This was followed by washing twice with sodium carbonate solution and water again. The solvent was dried over calcium chloride and distilled from calcium hydride before use. Chloroform (LR) was washed 3 - 4 times with water, stored over calcium chloride overnight and distilled from phosphorus pentoxide. It was stored in the dark over basic alumina.

Toluene, 1,4-dioxane, tetrahydrofuran (THF) and pyridine used for spectroscopic studies were of Spectroscopic grade from E. Merck (India). They were further purified by distilling from sodium. Glacial acetic acid and chlorobenzene were purchased from Ranbaxy (India). The other solvents used were acetone, diethyl ether, ethanol, ethylene glycol, ethyl acetate and dimethylsulphoxide. They were purified according to the known procedures before use.[1,2] $CDCl_3$ (99.9%), CD_3OD (99.8%), D_2O (99.2%) and $(CD_3)_2SO$ (99.5%) were obtained from Aldrich Chemical Co. (USA). Water used for the biochemical studies was triply distilled using a quartz distillation setup and then autoclaved before use.

2.3 Preparation of the starting materials

The following precursor molecules that are necessary for the synthesis of new ligands investigated in this study have been prepared by adopting the published procedures.

2.3.1 1,10-phenanthroline-5,6-dione (phen-dione)[3]

A round bottom flask containing phen (5.00 g 25.20 mmol) and KBr (29.75 g, 250.00 mmol) was placed in an ice bath. Concentrated H_2SO_4 (100 mL) was added in small portions, followed by addition of concentrated HNO_3 (50 mL). The resulting solution was heated for 2 h at 80 – 85 ^oC. It was cooled to room temperature and was poured onto ice cool water (1500 mL). The solution was neutralized with $NaHCO_3$ and then extracted with CH_2Cl_2. Evaporation of CH_2Cl_2 gave crude sample of phen-dione. Pure product was obtained by column chromatographic purification of this crude sample using neutral alumina as the stationary phase and CH_2Cl_2 as the eluent. Yield = 4.34 g (75%).

2.3.2 Dipyrido[3,2-a:2',3'-c]phenazine (dppz)[4]

Phen-dione (0.50 g, 2.40 mmol) and 1,2-diaminobenzene (0.50 g, 4.60 mmol) were refluxed together in C_2H_5OH (50 mL) for 10 min. The solution was cooled to room temperature to yield golden yellow needles of dppz, which was suction filtered and recrystallized from aqueous C_2H_5OH. Yield = 0.54 g (80%).

2.3.3 5-nitro-1,10-phenanthroline (5-nitro-phen)[5]

Phen (5.00 g, 25.20 mmol) in 20% oleum (25 mL) was heated to 110 - 115 ^oC and 72% HNO_3 (7 mL) was added. The reaction mixture was then refluxed at 143 ^oC while 72% HNO_3 (14 mL) was being added over 30 min. At the end of the addition, the reaction temperature was reduced and maintained at 115 ^oC. After stirring further for 45 min., it was cooled to room temperature and poured onto ice cold water (1000 mL). Upon neutralization with $NaHCO_3$, the solution turned pale yellow in color and subsequently, a pale yellow precipitate slowly settled down. The precipitate was removed by filtration, thoroughly washed with water and dried under vacuum. Yield = 4.25 g (68%).

2.3.4 5-amino-1,10-phenanthroline (5-amino-phen)

Reduction of 5-nitro-phen to 5-amino-phen was achieved with a slight modification of the reported procedure.[5] A mixture containing 5-nitro-phen (6.00 g, 26.60 mmol) and 0.50 g of Pd/C (10%) was refluxed in C_2H_5OH (200 ml). To this, hydrazine hydrate (6 mL, 103.20 mmol) was added drop wise over a period of 30 min. and the refluxion was continued for another 4 h. The reaction was monitored by TLC (neutral alumina/$CHCl_3$) to ensure complete reduction. The reaction mixture was filtered hot and a solid was obtained upon concentrating the filtrate to one third of its initial volume. Cooling the filtrate to 0 ^oC yielded a yellow solid, which was recrystallized from aqueous C_2H_5OH to yield yellow needles of 5-amino-phen. Yield = 3.28 g (63%).

2.3.5 Imidazo[4,5-f][1,10]phenanthroline (ip)[6]

A mixture of formaldehyde (0.26 cm^3 of 38% solution, 3.5 mmol), phen-dione (0.525 g, 2.5 mmol), ammonium acetate (3.88 g, 50 mmol) and acetic acid (7mL) was refluxed for 2 h then cooled to room temperature and diluted with H_2O. Dropwise addition of concentrated aqueous NH_3 to the above solution gave a yellow precipitate, which was filtered, washed with H_2O and dried. It was recrystallized from CH_3OH-H_2O (4:1, v/v). Yield = 0.39 g (79%). The purity of the sample was checked according to the reported procedure.[6]

2.3.6 9-(3,4-diaminophenyl)acridine (daa)[7]

Acridine was dissolved in C_2H_5OH and anhydrous HCl gas was passed through the solution for 5 min. The solution was concentrated and the hydrochloride salt was precipitated by the addition of ether and then dried. A

mixture of the acridine hydrochloride salt (0.57 g, 2.60 mmol) thus obtained, sulphur (0.25 g, 7.80 mmol) and 1,2–diaminobenzene (0.57 g, 5.30 mmol) was heated to 130 ^{o}C with vigorous stirring. The mixture turned black and formed a tar with the evolution of H_2S. Heating was continued for 1 h. The melt was cooled and washed with ether. The black solid was extracted with 10% HCl and the acidified solution was neutralized with aqueous ammonia. A brown solid was precipitated which was dried and recrystallized by using xylene to get the desired product. Yield = 0.42 g (56%).

2.3.7 Bis(1,10-phenanthroline)ruthenium(II)dichloride dihydrate, $[Ru(phen)_2Cl_2]\cdot 2H_2O$[8]

$RuCl_3\cdot 3H_2O$ (2.60 g, 9.93 mmol), phen (4.00 g, 20.00 mmol) and LiCl (2.80 g, 61.00 mmol) were taken in reagent grade DMF (50 mL) and the resulting mixture was refluxed for 8 h. It was then cooled to room temperature afterwhich acetone (250 mL) was added and the resultant solution was kept overnight at 0 ^{o}C. Filtering the mixture yielded a red to red-violet solution and a dark green-black microcrystalline product. The solid was washed thrice with 25 ml portions of H_2O followed by three 25 mL portions of diethyl ether. The crude product obtained was taken in C_2H_5OH –H_2O (1:1, v/v) and refluxed for 2 h. At the end of the refluxing period, small amount of LiCl was added to the reaction mixture and C_2H_5OH was distilled off. The left over solution was poured onto ice cold H_2O and kept at 4 ^{o}C overnight and then filtered. The solid obtained was washed thrice with 25 mL portions of H_2O followed by three 25 mL portions of diethyl ether. It was dried by suction to obtain the pure product. Yield = 3.22 g (57%).

2.3.8 Tris(1,10-phenanthroline)ruthenium(II) dichloride, $[Ru(phen)_3]Cl_2$[9]

$K_2[RuCl_5]\cdot H_2O$ (0.50 g, 1.30 mmol) was dissolved in hot H_2O (50 mL) containing a drop of 6 N HCl and a stoichiometric amount of phen was added slowly with stirring. The mixture was refluxed until a deep green solution resulted (10 - 20 min.). H_3PO_2 (1.2 mL of 30% solution) neutralized with NaOH (~ 3.5 mL of a 2N solution) was added and the mixture was refluxed for 15 - 30 min. until the colour changed to deep orange-red. The mixture was filtered and 6N HCl (10 mL) was added dropwise with stirring to the hot filtered solution. The crude product was recrystallized from hot H_2O. Yield = 0.74 g (70%).

2.3.9 Bis(1,10-phenanthroline)(dipyrido[3,2-a:2,3-c]phenazine) ruthenium(II) hexafluorophosphate dihydrate, $[Ru(phen)_2(dppz)](PF_6)_2\cdot 2H_2O$[10]

A mixture of $[Ru(phen)_2Cl_2]\cdot 2H_2O$ (0.85 g, 1.50 mmol) and dppz (0.47 g, 1.60 mmol) in $CH_3OH–H_2O$ (1:2 v/v; 380 mL) was refluxed for 5 h. The deep red solution obtained was concentrated to 10% of its original volume, diluted with water (140 mL), boiled for 10 min., cooled in an ice bath and filtered. The hexafluorophosphate salt of the complex was precipitated by the addition of 10% NH_4PF_6 (30 mL) to the filtrate. Yield = 1.60 g (75%).

2.4 Physical methods

All the compounds synthesized during this study were characterized by elemental analysis, mass (FAB and MALDI), infrared, electronic absorption, emission, proton nuclear magnetic resonance (^1H and ^1H-^1H COSY NMR) spectroscopies, electron spin resonance, magnetic susceptibility and electrochemical (cyclic and differential-pulse voltammetry) methods. The solid state structures have been determined by X-ray crystallography whenever we

were able to grow X-ray quality single crystals. These methods are briefly alluded below.

Elemental analyses were done on a Flash EA 1112 series CHNS (Thermo Finnigan\Eager 300) analyzer. Acetanilide was used as a reference standard. FAB Mass spectra were recorded on a JEOL SX 102/DA-6000 mass spectrometer/data system. The accelerating voltage was 10 kV and the spectra were recorded using m-nitrobenzyl alcohol (NBA) as the matrix. MALDI-TOF mass spectra were recorded on a Kompact MALDI 4 mass spectrometer (Kratos Analytical Ltd.). The instrument was operated in reflection time-of-flight mode with an accelerating potential of 20 kV and in the negative ion recording mode. The infrared spectra were recorded on a Jasco Model 5300 FT-IR spectrophotometer. The spectra of the solid samples were recorded by dispersing the samples as KBr pelletes. The ^{1}H NMR spectra were recorded on a Bruker NR-200 AF-FT or a Bruker DRX-400 NMR spectrometer using $CDCl_3$, CD_3OD, D_2O or $(CD_3)_2SO$ as the solvent. Tetramethylsilane (TMS) was the internal standard employed while recording these spectra. The electron spin resonance (ESR) spectra were recorded for the Cu(II) system at room temperature and frozen (110K, DMF), on a JEOL JES-FA200 X-band ESR spectrometer. Diphenylpicrylhydrazyl (DPPH) was used as the g-marker.

UV-visible spectra were recorded with either a JASCO model UV 7800 or a Shimadzu model UV-3101PC spectrophotometer. A matched pair of quartz cuvettes (path length = 1 cm) were employed. Steady state fluorescence spectra were recorded on a Spex Fluoromax-3 spectrophotometer using a 1 cm quartz cell. Detection of emission was done at the right angle to the incident beam. The excitation and emission slit widths employed were typically, 3/5 nm. While hexafluorophosphate salts of the complexes were employed for the fluorescence measurements in nonaqueous solvents (rigorously dried CH_2Cl_2, THF, 1,4-

dioxane, CH_3CN and DMF), the corresponding chloride salts were used for measurements in aqueous and aqueous buffer solutions. Optical densities for the samples were adjusted to ≤ 0.2 at the excitation wavelength in each case. Emission quantum yields (ϕ) were estimated by integrating the area under the fluorescence curves and by using the formula[11]

$$\phi_{sample} = \frac{OD_{standard} \times A_{sample}}{OD_{sample} \times A_{standard}} \times \phi_{standard} \qquad (2.1)$$

where, A is the area under the emission spectral curve and OD is optical density of the compound at the excitation wavelength. The standards used for the fluorescence quantum yield measurements were pyrene (ϕ = 0.32 in cyclohexane),[12] 1,6-diphenyl-1,3,5-hexatriene (ϕ = 0.80 in cyclohexane),[12] or $[Ru(phen)_3](PF_6)_2$ (ϕ = 0.028 in CH_3CN).[13] Refractive index corrections have been incorporated while reporting the fluorescence data in various solvents.[14]

The photoactive ligand (ppym) under study (10 – 30 μM) were titrated against the transition metal ions (1 – 20 μM) in CH_3CN and the binding was monitored by the fluorescence method. Cyclic and differential-pulse voltammetric experiments (CH_3CN/DMF/CH_2Cl_2, 0.1 M TBAP) were performed on a CH Instruments model CHI 620A electrochemical analyzer (working and auxiliary electrodes: Pt; reference electrode: SCE). Fc^+/Fc (Fc = ferrocene) couple was used to calibrate the redox potential values.

Room temperature (298 K) solid state magnetic susceptibility was measured by using a Sherwood Scientific magnetic susceptibility balance. $Hg[Co(NCS)_4]$ was used as the standard. Diamagnetic corrections calculated

from Pascal's constants,[15] were used to obtain the molar paramagnetic susceptibilities.

2.5 DNA binding experiments

CT DNA was used for binding with the various metal complexes investigated during this work. The stock solution was made by dissolving CT DNA in appropriate buffers and kept overnight at 4 ^{o}C for complete dissolution. The concentration of CT DNA was measured by using its known extinction coefficient at 260 nm (6600 $M^{-1}cm^{-1}$).[16] Unless otherwise specified, concentration of the DNA is expressed in base pairs (BP) throughout. Buffer A (5 mM Tris, 50 mM NaCl, pH 7.1), buffer B (1 mM NaH_2PO_4, 1 mM Na_2HPO_4, 2 mM NaCl, pH 7.0) and buffer C (1.5 mM Na_2HPO_4, 0.5 mM NaH_2PO_4, 0.25 mM Na_2EDTA, pH 7.0) were used for absorption and fluorescence titration, thermal denaturation and viscometric experiments, respectively. TAE (Tris-acetate-$EDTANa_2$, pH = 8.0) 1X buffer was used for gel electrophoresis cleavage and inhibition experiments.

2.5.1 Absorption titration

Absorption titration experiments were performed by maintaining a constant metal complex concentration and varying the nucleic acid concentration. Typical concentration of the metal complex used was 5 - 15 μM and that of DNA ranged between 0 - 200 μM. After the addition of DNA to the metal complex, the resulting solution was allowed to equilibrate for 10 min. at 25 ^{o}C, after which the absorption readings were noted. The data were then fit to the following equation to obtain the intrinsic binding constant K_b.[17]

$$[DNA]/(\varepsilon_a-\varepsilon_f) = [DNA]/(\varepsilon_b-\varepsilon_f) + 1/K_b\ (\varepsilon_b-\varepsilon_f) \quad (2.2)$$

where ε_a, ε_f, and ε_b are the apparent, free and bound metal complex extinction coefficients, respectively. A plot of $[DNA]/(\varepsilon_a-\varepsilon_f)$ vs [DNA] gave a slope of $1/(\varepsilon_b-\varepsilon_f)$ and a y-intercept equal to $1/K_b(\varepsilon_b-\varepsilon_f)$; K_b is the ratio of slope to y-intercept.

2.5.2 Fluorescence titration

Fluorescence titration experiments were performed by using a fixed metal complex concentration (7 – 20 μM) to which increments of the stock DNA solutions (0 – 300 μM) containing the same concentration of the metal complex were added. After the addition of DNA to the metal complex, the resulting solution was allowed to equilibrate for 10 min. at 25 ^oC in the dark before being excited by 450 ± 5 nm light. The data obtained were analyzed using equn. 2.3.

$$C_F = C_T[(I / I_o) – P] / [1 – P] \quad (2.3)$$

where C_F is the concentration of the free complex, C_T is the concentration of the complex added and I_o and I are the fluorescence intensities in the absence and in the presence of DNA, respectively. P is ratio of the observed fluorescence quantum yield of the bound complex to the free complex. The value of P was obtained from a plot of I / I_o vs 1/ [DNA] such that the limiting fluorescence yield is given by the y-intercept. The amount of bound complex (C_B) at any concentration was equal to $C_T - C_F$. A plot of r/C_F vs r where r is equal to C_B / [DNA], was constructed according to the modified Scatchard equation given by McGhee and Von Hippel.[18]

$$r / C_F = K_b (1\text{-}nr) [(1\text{-}nr) / [1\text{-} (n\text{-}1) r]]^{n-1} \quad (2.4)$$

where, K_b is the intrinsic binding constant and n is the binding site size in base pairs.

2.5.3 Thermal denaturation

DNA melting experiments were carried out by monitoring the absorption (260 nm) of CT DNA (160 μM, nucleotide pairs, NP), using a Shimadzu model UV-160A spectrophotometer coupled with a temperature controller model TCC-240 A or Julabo-F12 circulator, at various temperatures in the absence and in the presence of a given complex. The melting temperature (T_m) and the curve width σ_T (temperature range where 10% - 90% of the absorption increase occurred) were calculated as previously described.[19,20]

2.5.4 Viscometric titration

Viscometric titrations were performed at 25 ± 1 ^oC with a Cannon-Ubblehode viscometer. Titrations were performed for various metal complexes investigated in this study including $[Ru(phen)_3]^{2+}$ and ethidium bromide (EtBr) (3 - 40 μM). Each compound was introduced into the degassed DNA solution (300 μM) present in the viscometer using a Hamilton syringe fitted with a glass extender. Mixing of the drug and DNA was done by bubbling nitrogen. Flow times were measured, using a digital stopwatch, at least three times and were accepted if they agreed within 0.1 s. Reduced specific viscosity was calculated according to Cohen and Eisenberg.[21] Plots of $(\eta/\eta_o)^{1/3}$ (η and η_o are the reduced specific viscosities of DNA in the presence and absence of the drug) vs [drug]/[DNA] were constructed. Plots of $(\eta/\eta_o)^{1/3}$ vs [EtBr]/[DNA] and

[[$Ru(phen)_3$]$^{2+}$]/[DNA] were found to be similar to those reported in the literature.[22]

2.6 DNA photocleavage and agarose gel electrophoresis

Electrophoresis through agarose is the standard method used to separate, identify or purify DNA fragments.[23-26] Using this technique, bands containing as little as 1-10 ng of DNA can be detected by direct examination of the agarose gel (stained with EtBr) in the UV light.[26] When an electric field is applied across the gel, DNA, which is negatively charged at neutral pH, migrate towards the anode. The intact supercoiled (Form I) DNA migrates faster than the single nicked (Form II) in the gel. This technique has been employed to identify the product/s of the DNA photocleavage, which was carried out in this work.

2.6.1 Buffers/Reagents

2.6.1.1 Tris-acetate ethylenediaminetetraacetate (TAE) electrolyte buffer (50 X stock)

Tris base (48.40 g) was dissolved in water (100 mL). EDTA disodium salt (7.44 g) was dissolved in water (50 mL) and the pH was adjusted to 8.0 using NaOH. This pH-adjusted EDTA solution was added to the tris solution followed by the addition of glacial acetic acid (11.42 mL). The volume was made up to 200 ml with H_2O and the resulting buffer was stored at 4 ^oC.

2.6.1.2 Sample buffer (6X)

A 0.25% bromophenol blue in 40% sucrose-H_2O was used as the sample buffer. This buffer was prepared by first dissolving sucrose (2.00 g) in water (3 mL) and then adding bromophenol blue (12.50 g) to this solution. The volume was made up to 5 mL. The resulting buffer was stored at 4 ^oC.

2.6.1.3 Ethidium bromide stock solution (10 mg/ml)

A 0.10 g of EtBr was dissolved in water (10 mL) by stirring in dark for several hours. The resulting solution was stored in a brown bottle at the ambient temperature. Working concentration of 0.5 μg/mL was used for staining the gels after electrophoresis.

2.6.2 Gel configuration and gel casting

A horizontal slab gel electrophoresis chamber (3.5 x 7.5 inches or 6.0 x 7.5 inches) made of polystyrene snaplock box obtained from Broviga Inc. (India) was used to carry out the agarose gel electrophoresis. Platinum wire was used as each of the two electrodes. A platform composed of four lantern slides glued together in a stack is cemented in the center of the box. A gel plate of 7.0 cm x 10.0 cm in size rests on this platform so that the gel is submerged just beneath the surface of the electrophoresis buffer. The details of gel casting are given below.

A 0.40 g of low melt agarose (Molecular Biology grade) was added to TAE buffer (50 mL). The slurry was then heated on a boiling water bath until the agarose dissolved completely. The solution was cooled to 50 ^{o}C. Both ends of the gel mold were closed with a clean autoclaved tape and a small quantity of agarose solution was applied with a pipette along the edges of the gel mold so as to seal it completely. Remaining warm agarose solution was poured onto the gel mold and immediately the comb was clamped into position near one end of the gel. The teeth of the comb formed the sample wells. Care was taken to see that at least 0.5 - 1.0 mm of agarose was left between the bottom of the teeth and the base of the gel, so that the sample wells are completely sealed. After 35 - 40 min.

(by which time the gel was completely set), the comb and the autoclaved tape were removed carefully and the gel was mounted in the electrophoresis tank. Working buffer (200 mL, TAE) was poured into the gel until the gel was covered to a depth of about 1 mm.

2.6.3 Photolysis of pBR 322 DNA and separation of the products

Photolysis experiments were carried out for pre-incubated (1 h) samples of pBR 322 DNA (100 μM nucleotide phosphate, 10 μL) and the appropriate concentration of the drug placed in a quartz tube of 3 mm internal diameter. Tris-HCl buffer (pH 8.0) was the medium in the case of polypyridyl complexes and tris-HCl buffer (pH 8.0) containing not more than 10% dimethylformamide was used in the remaining cases. Irradiation of the samples were done using a Xe arc lamp (150 W, Photon Technology International). The required wavelength for the irradiation was isolated from the source using a PTI Model S/N 1366 (10 nm band pass) monochromator. At times, photolysis was also carried out inside the sample chamber of a Jasco Model FP-777 spectrofluorometer with the slit width 5 nm. The temperature was maintained at 20 ^{o}C throughout irradiation.

After irradiation, 2 μL of sample buffer was added to the quartz tube containing the irradiated sample and the contents were directly loaded onto a 0.8% (w/v) agarose gel. The gel was run with standard TAE buffer pH 8.0 at 40 V for 4 h after which it was stained with 0.5 μg/mL solution of EtBr for 30 min. The data were documented using a UVITEC Gel Documentation center. The percentage of cleavage (C) was calculated using the expression

$$C = \frac{[\text{Form II}] + 2[\text{Form III}]}{[\text{Form I}] + [\text{Form II}] + 2[\text{Form III}]} \qquad (2.5)$$

In order to identify the actual reactive oxygen species responsible for DNA damage, a number of control experiments were carried out using various types of quenchers ('inhibitor studies'). Nitrogen gas was used to flush dioxygen, DABCO (10 mmol) was used as a $^1O_2$ quencher. DMSO (200 mmol) and mannitol (100 mmol) were used as $OH^\bullet$ scavengers. 4,5-dihydroxy-1,3-benzenedisulfonic acid disodium salt (Tiron, 10 mM) was used as a superoxide anion radical quencher. D_2O was used in some cases, where singlet oxygen ($^1O_2$) is involved in the photocleavage mechanism.

2.7 X-ray Crystallography

X-ray diffraction data were collected at 293 K on a Bruker Nonius Smart Apex CCD detector diffractometer equipped with a graphite monochromator and a MoKα fine-focus sealed tube (λ = 0.71073 Å). The detector was placed at a distance of 6.003 cm from the crystal. The frames were collected with a scan width of 0.3º in ω. The frames were integrated with the Bruker SAINT software package using a narrow-frame integration algorithm.[27] Data were corrected for absorption effects using the multi-scan technique (SADABS). All non-hydrogen atoms were found using the direct method analysis in SHELXTL[28] and after several cycles of refinement the positions of the hydrogen atoms were calculated and added to the refinement process. The ORTEX6a[29] and the PLATON[30] packages were used for molecular graphics.

2.8 General considerations

Error estimation of the data, reconstruction of various spectra, calculations of equilibrium constants, various regression analysis *etc*., that appear throughout this dissertation, have been carried out on an IBM compatible PC

Pentium IV computer using the available in-house software/Origin 6.0 software package.

Care was taken to avoid the entry of direct, ambient light into the samples in all the spectroscopic and electrochemical experiments. Care was also taken to avoid the direct human contact of DNA and EtBr solutions. All solutions containing EtBr and other hazardous chemicals were decontaminated before disposal. Protective goggles, gloves and safety mask were used to minimize the exposure to obnoxious chemicals/biochemicals, ultraviolet light etc. Unless otherwise specified, all the experiments were carried out at 293 ± 3 K. Standard error limits involved in various measurements (unless otherwise stated):

^{1}H NMR chemical shift (δ)	± 0.01 ppm
λ_{max}	± 1 nm
log ε	± 10%
$E_{1/2}$	± 0.03 V
λ_{em}	± 1 nm
λ_{exc}	± 1 nm
ϕ	± 10%
K_b	± 10%
T_m	± 1 ^oC
σ_T	± 1 ^{o}
% DNA cleavage (C)	± 8%

2.9 Summary

A brief account on procurement and purification of solvents and chemicals and also the syntheses of various precursor compounds used during

this work are given in this chapter. Also given here is a description of the spectroscopic as well as other physical and biochemical methods employed in this study.

2.10 References

1. *Vogel's Text Book of Practical Organic Chemistry*; (Revised by Furniss, B. S.; Hannaford, A. J.; Smith, P. W. G.; Tatchell, A. R.), 5th Edn.; Longmann (ELBS): Essex (UK.), 1991.
2. Perrin, D. D.; Armarego, W. L. F.; Perrin, D. R. *Purification of laboratory Chemicals*; Pergamon: Oxford, 1986.
3. Yamada, M.; Tanaka, Y.; Yoshimoto, Y.; Kuroda, S.; Shimao, I. *Bull. Chem. Soc. Jpn.* **1992,** *65*, 1006.
4. Dickeson, J. E.; Summers, L. A. *Aust. J. Chem.* **1970,** *23*, 1023.
5. Lecomte, J-P.; Mesmaeker, A. K; Demeunynck, M.; Lhomme, J. *J. Chem. Soc., Faraday Trans.* **1993**, *89*, 3261.
6. Wu, J-Z.; Ye, B-H.; Wang, L.; Ji, L-N.; Zhou, J-Y.; Li, R-H.; Zhou, Z-Y. *J. Chem. Soc*., *Dalton Trans.* **1997**, 1395.
7. Plater, M. J.; Greig, I.; Helfrich, M. H.; Ralston, S. H. *J. Chem. Soc., Perkin Trans. 1* **2001**, 2553.
8. Sullivan, B. P.; Salmon, D. J.; Meyer, T. J. *Inorg. Chem.* **1978**, *17*, 3334.
9. Lin, C.-T.; Bottcher, W.; Chou, M.; Cruetz, C.; Sutin, M. *J. Am. Chem. Soc.* **1976**, *98*, 6536.
10. Amouyal, E.; Homsi, A.; Chambron, J. C.; Sauvage, J. P. *J. Chem. Soc., Dalton Trans.* **1990,** 1841.
11. Austin, E.; Gouterman, M. *Bioinorg. Chem.* **1978,** *9*, 281.
12. Berlman, I. B. *Handbook of Fluorescence Spectra of Aromatic Molecules*; Academic press: New York, 1971**.**

13. Juris, A.; Balzani, V.; Barigelletti, F.; Campagna, S.; Belser, P.; Zelewsky, A. V. *Coord. Chem. Rev.* **1988,** *84*, 85.
14. Lackowicz, J. R. *Principles of Fluorescence Spectroscopy*; Plenum Press: New York, 1983**.**
15. Eranshaw, A. *Introduction to Magnetochemistry*, Academic press, London: 1968
16. Reichmann, M. E.; Rice, S. A.; Thomas, C. A.; Doty, P. *J. Am. Chem. Soc.* **1954,** *76*, 3047.
17. Wolfe, A.; Shimer, G. H.; Meehan, T. *Biochemistry* **1987,** *26*, 6392.
18. McGhee, J. D.; Von Hippel, P. H. *J. Mol. Biol*. **1974**, *86*, 469.
19. Kelly, J. M.; Tossi, A. B.; McConnell, D. J.; OhUigin, C. *Nucl. Acid. Res*. **1985**, *13*, 6017.
20. Marmur, J.; Doty, P. *J. Mol. Biol*. **1962**, *5*, 109.
21. Cohen, G.; Eisenberg, H. *Biopolymers* **1969,** *8*, 45.
22. Satyanarayana, S.; Dabrowiak, J. C.; Chaires, J. B. *Biochemistry* **1992,** *31*, 9319.
23. Sambrook, J.; Russell, D. W. *Molecular Cloning A Laboratory Manual*; 3rd ed. Cold Spring Harbor Laboratory Press: New York, 2001.
24. Fisher, M. P.; Dingman, C. W. *Biochemistry* **1971,** *10*, 895.
25. Ajay, C.; Borst, P. *Biochim. Biophys. Acta* **1972,** *269*, 192.
26. Sugden, P. A. B.; Sambrook, J. *Biochemistry* **1973,** *12*, 3055.
27. *SAINT*. Version 6.2. Bruker AXS Inc., Madison, Wisconsin, USA.
28. (a) *SHELX-97*, Sheldrick, G. M., University of Göttingen, Göttingen, Germany, 1997; (b) *SHELXTL* Version 6.14, Bruker AXS. Inc., Madison, Wisconsin, USA.
29. P. McArdle, *J. Appl. Crystallogr.* **1995**, *28*, 65.

30. Spek, A. L. *PLATON, A Multipurpose Crystallographic Tool*, Utrecht University, Utrecht, The Netherlands, 2002.

CHAPTER 3

A Ruthenium(II) Complex That Incorporates a Pyrene Bearing Polypyridine Ligand: Synthesis, Characterization, Photochemistry and DNA Interactions

3.1 Introduction

As detailed in chapter 1, studies aimed at probing the effect of variation of the ligand architecture on the ability to bind and photocleave DNA by metal complexes incorporating the polypyridyl family of ligands are of current interest in view of their relevance to various biochemical and biomedical applications. In particular, ruthenium(II) complexes containing modified 2,2'-bipyridine (bpy), 1,10-phenanthroline (phen) or dipyridophenazine (dppz) class of ligands are the most widely investigated systems because of their useful structural as well as photo- and electrochemical properties.[1-15] Complexes containing modified polypyridyl ligands featuring donor-acceptor (D - A) type design are also being investigated by a few research groups including ours.[16-25] In this chapter, we describe the synthesis, spectral, photophysical and electrochemical characterization of N-[1,10]phenanthrolin-5-yl-pyrenylmethanimine (ppym) and also its mixed-ligand ruthenium(II) complex $[Ru(phen)_2(ppym)]^{2+}$ (Fig. 3.1) respectively. Results of the experiments carried out to probe the DNA binding and photocleavage proclivities of the new complex is also presented.

3.2 Experimental section

1,10-phenanthroline-5,6-dione (phen-dione), 5-nitro-1,10-phenanthroline, 5-amino-1,10-phenanthroline (5-amino-phen), $[Ru(phen)_2Cl_2]\cdot 2H_2O$ and $[Ru(phen)_3]^{2+}$ were synthesized by the following reported procedures as

described in chapter 2. Syntheses of the new ligand ppym and its mixed-ligand ruthenium(II) complex, $[Ru(phen)_2(ppym)]^{2+}$, are described below.

3.2.1 N-[1,10]phenanthrolin-5-yl-pyrenylmethanimine (ppym)

A mixture of 5-amino-phen (1.00 g, 5.12 mmol), 1-pyrenecarboxaldehyde (1.38 g, 6.00 mmol) and glacial acetic acid (2 mL as a catalyst) were refluxed in CH_3OH (80 mL) for 6 h. The precipitate of ppym obtained was filtered and purified by recrystallization from $CHCl_3$. Yield = 1.16 g (55%)

Analytical data: Found: C, 85.20; H, 4.17; N, 10.32; Calculated for $C_{29}H_{17}N_3$: C, 85.48; H, 4.21; N, 10.31; FAB-MS (m/z): 407 $(M)^+$; IR: ν_{max} (KBr, cm^{-1}): 3426 (N-H), 1602 (C=N). ^1H NMR ($CDCl_3$, 200 MHz, TMS): 9.71 (s, 1H), 9.22 (m, 2H), 8.91 (m, 2H), 8.19 (m, 8H), 7.68 (m, 2H), 7.49 (s, 1H).

3.2.2 Bis(1,10-phenanthroline)(N-[1,10]phenanthrolin-5-yl-pyrenylmethanimine)ruthenium(II) hexafluorophosphate dihydrate, $[Ru(phen)_2(ppym)](PF_6)_2 \cdot 2H_2O$

$[Ru(phen)_2Cl_2]\cdot 2H_2O$ (0.40 g, 0.71 mmol) and ppym (0.33 g, 0.80 mmol) were refluxed in CH_3OH under nitrogen atmosphere for 4 h. The bright orange-red solution was filtered and a saturated solution of NH_4PF_6 was added to the filtrate to precipitate the complex. The crude complex was purified by column chromatography using neutral alumina as the stationary phase and CH_3CN – toluene (70:30, v/v) mixture as the eluent followed by repeated recrystallization from acetone–diethyl ether (1:5, v/v). Yield = 0.39 g (47%).

Analytical data: Found: C, 53.97; H, 3.02; N, 8.14; Calculated for $C_{53}H_{37}N_7O_2F_{12}P_2Ru$: C, 54.87; H, 3.19; N, 8.45; FAB-MS (m/z): 1013 $[M - PF_6^-]^+$; 461 $[M - 2PF_6^{2-} - C_{29}H_{17}N_3]^+$; IR: ν_{max} (KBr, cm^{-1}): 3426 (N-H), 1602 (C=N). ^1H NMR ($(CD_3)_2SO$, 200 MHz, TMS): 10.10 (d, 1H, J = 8.6 Hz), 8.91 (m, 1H),

8.76 (m, 5H), 8.38 (m, 5H), 8.27 (m, 2H), 8.06 (m, 6H), 7.75 (m, 7H), 7.58 (m, 2H), 7.45 (m, 2H), 7.10 (s, 1H), 6.88 (s, 1H).

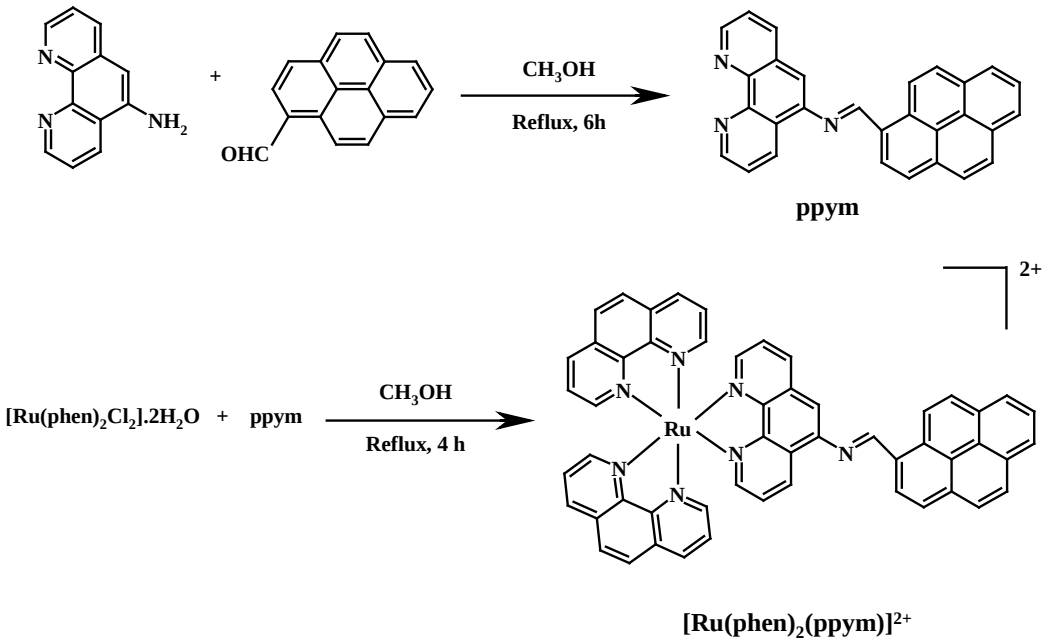

Fig.3.1 Scheme leading to the synthesis of ppym and $[Ru(phen)_2(ppym)]^{2+}$.

The hexafluorophosphate salt of this complex was converted to the water-soluble, chloride salt by treating the former salt solution in acetone with excess TBACl. The chloride salt, being insoluble in acetone, was instantaneously precipitated out of the solution. It was filtered and vacuum dried before use. The yield was ~ 90% of the theoretical value.

All the spectroscopic, electrochemical and biochemical experiments were carried out as described in chapter 2.

3.3 Results and discussion

3.3.1 Synthesis

The scheme leading to the synthesis of ppym and $[Ru(phen)_2(ppym)]^{2+}$ is given in Fig. 3.1. Ligand ppym was synthesized by the Schiff base condensation of 5-amino-phen and 1-pyrenecarboxaldehyde. The mixed-ligand ruthenium(II) complex was synthesized by reacting $[Ru(phen)_2Cl_2]\cdot 2H_2O$ with ppym. Each synthetic step involved here was straightforward and provided good-to-moderate yield of the desired product in pure form.

3.3.2 Crystal structure

A single crystal of ppym was obtained by slow evaporation of the chloroform solution at room temperature. Molecular structure of ppym (including one $CHCl_3$ molecule) with atom-labeling scheme is given in Fig. 3.2.

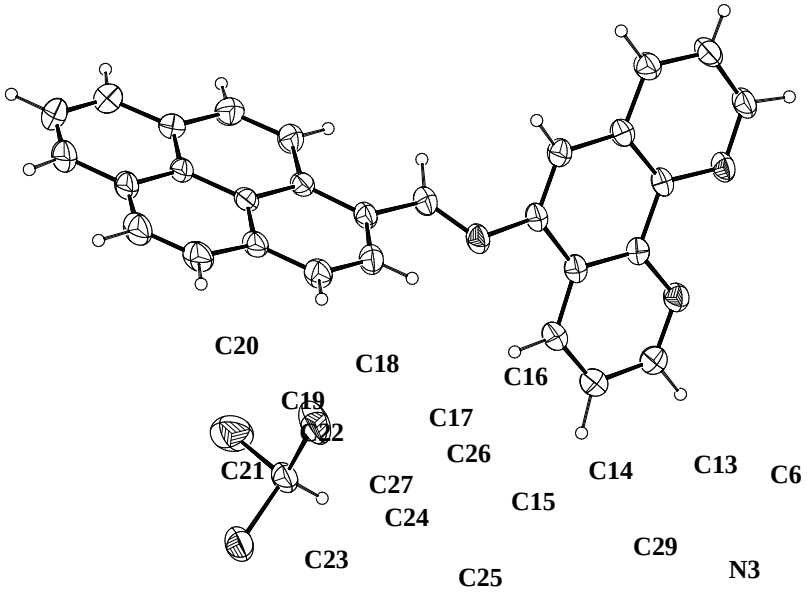

Fig. 3.2 Molecular structure of ppym with atom-labeling scheme. All non-hydrogen atoms are represented by their 30% probability thermal ellipsoids.

Crystal and refinement data for ppym and the selected bond lengths (Å) and bond angles (^{o}) are given in Table 3.1 and Table 3.2, respectively. Atomic coordinates and equivalent isotropic displacement parameters are presented in Appendix I (Table 1). The C13–N3 bond length (1.276(5) Å) is comparable with the typical C=N length (1.269 Å).[26] Phenanthroline and pyrene rings are not coplanar. The dihedral angle between these two planes is 62.44^{o}. The structural features of ppym suggest that it would be less effective to intercalate into the base pairs since an intercalative ligand generally requires not only an extended aromatic surface but also a special geometry that allows effective overlapping between the intercalating ligand and the base pairs of DNA.[27,28] In the crystal lattice, there is no significant intermolecular non-covalent interaction.

3.3.3 Ground state properties

Both the new ligand ppym and the PF_6^- salt of $[Ru(phen)_2(ppym)]^{2+}$ showed expected fragmentation patterns in the FAB-MS spectra. The mass spectrum of ppym showed the base peak at m/z = 407 $[M]^+$. In the case of $[Ru(phen)_2(ppym)]^{2+}$, two peaks were seen at 1013 $[M - PF_6^-]^+$ and 461 $[M - 2PF_6^{2-} - C_{29}H_{17}N_3]^+$ corresponding to the removal of the first PF_6^- counter ion followed by the removal of the second PF_6^- counter ion and the bound-ppym, typical of PF_6^- salts of ruthenium(II) polypyridyl complexes.[21-23,29]

^1H NMR spectrum of ppym has been analyzed with the proton assignments being made on the basis of both integrated intensity data and ^1H - ^1H coupling patterns observed in the 2D (COSY) spectra. The data of all the new compounds are given in Section 3.2. Salient features of the spectra are discussed below. Confirmation that ppym bears a Schiff base ‘spacer’ between phenanthroline and pyrene subunits come from the fact that the –N = C(H) proton

Table 3.1 Crystal data for ppym·$CHCl_3$

	ppym·$CHCl_3$
Chemical formula	C30 H18 Cl3 N3
Formula weight	526.82
Crystal system	Monoclinic
Space group	$P2_1$ / c
a (Å)	19.665(3)
b (Å)	7.1852(9)
c (Å)	19.514(3)
α (°)	90
β (°)	118.715(2)
γ (°)	90
V (Å^3)	2418.1(5)
Z	4
μ (mm^{-1})	0.405
F (000)	1080
Crystal size (mm^3)	0.31 x 0.13 x 0.08
Reflections collected	26991
Reflections unique	5819 [R(int) = 0.0803]
Parameters	397
*R*1, *wR*2 [$I \geq 2\sigma(I)$]	0.0650, 0.1488
*R*1, *wR*2 (all data)	0.1714, 0.2042
Goodness-of-fit on F^2	1.004
Largest peak, hole [*e* Å^{-3}]	0.563, -0.540

Table 3.2 Selected bond lengths [Å] and angles [^{o}] for ppym·$CHCl_3$

Cl(1)-C(30)	1.744(4)	C(10)-N(2)-C(11)	117.8(3)
Cl(2)-C(30)	1.741(4)	N(2)-C(11)-C(7)	122.0(3)
Cl(3)-C(30)	1.755(5)	N(2)-C(11)-C(12)	118.0(3)
C(12)-N(1)	1.353(4)	C(15)-C(14)-C(13)	121.6(3)
N(1)-C(1)	1.333(5)	C(13)-N(3)-C(6)	119.0(3)
N(2)-C(10)	1.319(5)	C(5)-C(6)-N(3)	123.1(3)
N(2)-C(11)	1.358(4)	N(3)-C(6)-C(7)	117.1(3)
C(14)-C(13)	1.464(5)	N(3)-C(13)-C(14)	122.2(4)
N(3)-C(13)	1.276(5)	N(1)-C(1)-C(2)	124.0(4)
N(3)-C(6)	1.411(4)	N(2)-C(10)-C(9)	124.3(4)
N(1)-C(12)-C(4)	122.4(3)	Cl(2)-C(30)-Cl(1)	110.5(3)
N(1)-C(12)-C(11)	118.7(3)	Cl(2)-C(30)-Cl(3)	110.1(3)
C(1)-N(1)-C(12)	117.2(3)	Cl(1)-C(30)-Cl(3)	109.1(2)

resonates as a singlet at 9.71 ppm in the ^{1}H NMR spectrum of this ligand (Fig. 3.3a). In comparison, spectrum of its precursor 1-pyrenecarboxaldehyde has a singlet at 10.74 ppm corresponding to the aldehyde proton. The protons at positions 1, 4 and 3, 6 (phen ring) of ppym also resonate at downfield region when compared to the corresponding protons of 5-amino-phen. Proton H9 of ppym is shifted downfield when compared to pyrene where all protons resonate as multiplet at 8.5-8.3 ppm. ^{1}H NMR resonance due to the spacer –N=C(H) proton of complexed ppym in $[Ru(phen)_2(ppym)]^{2+}$ (Fig. 3.3b) appears as two singlet centered at 10.03 ppm. This may be due to *cis-trans* isomerization along the bond N=C in $(CD_3)_2SO$ medium which could be measurable in the nmr time scale. As expected, the remaining protons of ppym and phen in $[Ru(phen)_2(ppym)]^{2+}$ are also shifted to downfield upon complexation.[22,23]

UV-visible spectrum of ppym is characterized by prominent low energy, structured absorption bands in the 350 – 420 nm region (Fig. 3.4). It also shows high intensity and high energy bands in the UV region (278 and 231 nm).

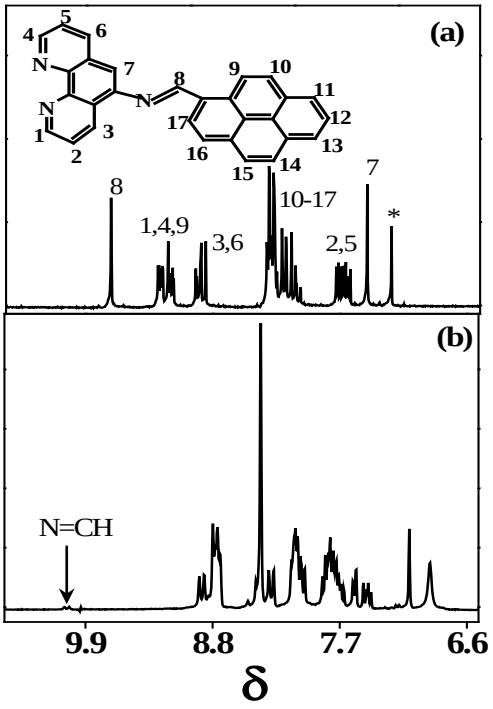

Fig. 3.3 ^{1}H NMR spectra of (a) ppym (in $CDCl_3$) and (b) $[Ru(phen)_2(ppym)](PF_6)_2$ (in $(CD_3)_2SO$)

A comparison of this spectrum with the spectra of 5-amino-phen and 1-pyrenecarboxaldehyde reveals that the structured bands seen for ppym are a composite of both 5-amino-phen and the pyrenyl chromophores, Table 3.3. Considerable shifts in the wavelengths of absorption maxima (λ_{max}) and molar extinction coefficients (ε) have been noticed for these low energy (and also the high energy) bands of ppym in comparison with those obtained from either the physical mixture or the summation spectra involving the corresponding starting materials. This is not surprising if one considers that phen and the pyrenyl chromophore is connected to the phenanthroline through imine spacer in ppym.

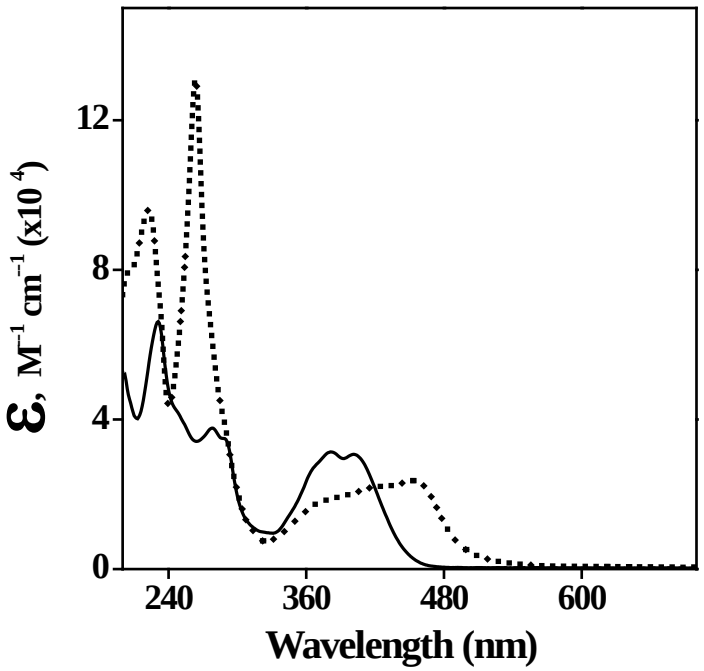

Fig. 3.4 UV-visible spectra of ppym (——) and $[Ru(phen)_2(ppym)]^{2+}$ (·····) in CH_3CN.

In the UV-visible spectrum of $[Ru(phen)_2(ppym)]^{2+}$, intense bands arising from the intra-ligand transitions due to the coordinated phen and ppym are observed below 340 nm (Fig. 3.4). Although, it is partially overlapped with the low energy, low intensity bands of ppym, the MLCT transition characteristic of the ruthenium(II) polypyridyl complexes is observed at 453 nm for this new complex. The UV-visible data for ppym and $[Ru(phen)_2(ppym)]^{2+}$ along with the corresponding reference compounds are listed in Table 3.3.

Table 3.3 UV-visible and fluorescence data in CH_3CN[a]

Compound	Absorbance λ_{max}, nm (log ε)		Emission λ_{em}, nm (ϕ)
	Ligand Transitions	MLCT	
phen	226 (4.71), 264 (4.55)	---	---
pyrene	239 (4.75), 262 (4.38), 272 (4.59), 319 (4.43), 334 (4.60)	---	371, 382, 392 (0.31)
1-pyrenecarboxaldehyde	233 (4.70), 287 (4.57), 362 (4.44), 372 (4.42), 394 (4.33)	---	---
5-amino-phen	217 (4.41), 234 (4.40), 281 (4.35), 333 (3.84), 387 (3.43)	---	490 (0.014)
ppym	231 (4.52), 278 (4.27), 381 (4.19), 401 (4.19)	---	387, 482 (0.01)
$[Ru(phen)_3](PF_6)_2$	223 (4.93), 263 (5.07), 422 (4.25)	446 (4.28)	596 (0.028)
$[Ru(phen)_2(ppym)](PF_6)_2$	263 (5.11), 222 (4.98)	453 (4.37)	604 (0.029)

a) Error limits: λ_{max} and $\lambda_{em,}$ ± 1 nm; log ε, ± 10%; ϕ, ± 10%

Redox potential data are summarized in Table 3.4. During the cathodic scan in the cyclic voltammetric experiments carried out in DMF containing 0.1 M TBAP, uncomplexed ppym showed a reversible (i_{pc}/i_{pa} = 0.9 - 1.0) and diffusion controlled ($i_{pc}/\nu^{1/2}$ = constant in the scan rate (ν) range 50 - 500 mV s^{-1}) one-electron transfer (ΔE_p = 60 - 70 mV; ΔE_p = 65 ± 3 mV for Fc^+/Fc couple)[30]

response at –1.19 V vs SCE. This potential is close to that for the one-electron reduction of 1-pyrenecarboxaldehyde (–1.27 V). The second reduction response (at –1.56 V) of ppym is quasi-reversible.

Table 3.4 Redox potential data[a]

Compound	**Oxidation** $E_{1/2}$ **(V vs SCE)**	**Reduction**[d] $E_{1/2}$ **(V vs SCE)**
phen	---	-1.92
pyrene	+1.49[b]	---
1-pyrenecarboxaldehyde	+1.64[b]	-1.27
ppym	+1.50[b]	-1.19, -1.56
$[Ru(phen)_3](PF_6)_2$	+1.37[c]	-1.19, -1.34, -1.69
$[Ru(phen)_2(ppym)](PF_6)_2$	+1.27, +1.42[c]	-1.25, -1.42, -1.75

a) Error limits: $E_{1/2,} \pm 0.03$ V
b) CH_2Cl_2, 0.1 M TBAP
c) CH_3CN, 0.1 M TBAP
d) DMF, 0.1 M TBAP

The ligand also showed an oxidation peak in CH_2Cl_2 (0.1 M TBAP) at +1.50 V, which is very close to the oxidation potential (+1.49 V) of pyrene. This suggests that phen and pyrene subunits generate an extended aromatic system in ppym connected by an imine spacer, which is easily oxidizable compared to its precursor pyrene. The cyclic (CV) and differential-pulse voltammograms (DPV) of the new complex is compared with those of $[Ru(phen)_3]^{2+}$ (Fig. 3.5). The first one-electron reduction peak of $[Ru(phen)_2(ppym)]^{2+}$ is reversible and observed at –1.25 V. This reduction can be assigned to an electron addition to the ruthenium bound ppym. The next two successive reduction peaks for this complex, seen at –1.42 V and –1.75 V are either quasi-reversible ($i_{pc}/i_{pa} = 0.2 – 0.7$ and $\Delta E_p = 90$

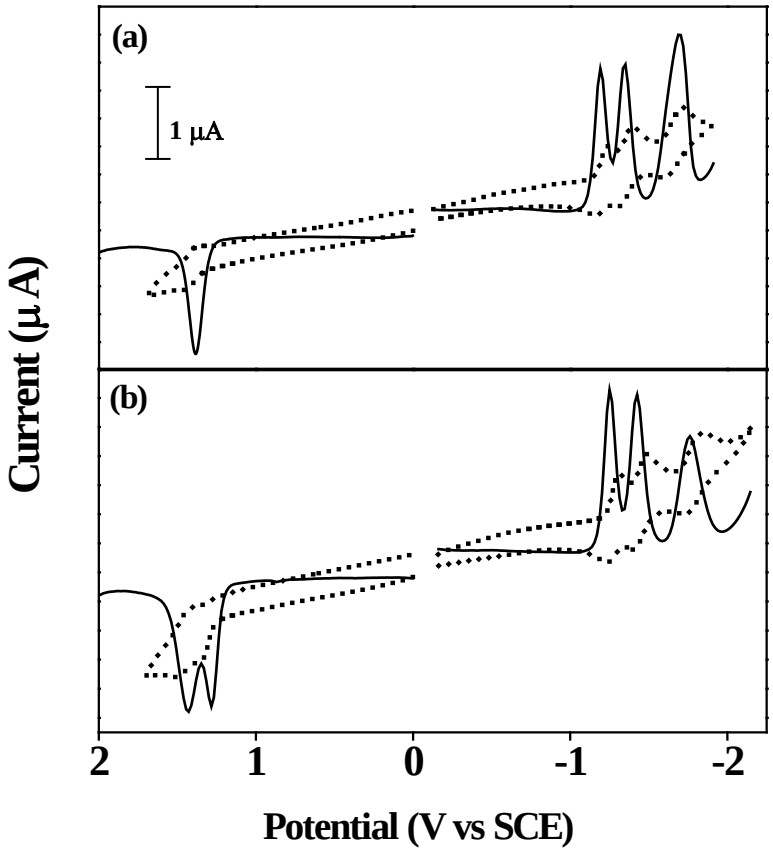

Fig. 3.5 Cyclic and differential-pulse voltammograms of (a) $[Ru(phen)_3]^{2+}$ and (b) $[Ru(phen)_2(ppym)]^{2+}$. CH_3CN and DMF containing 0.1 M TBAP were used as solvents for the anodic and cathodic runs, respectively. Scan rate: CV, 100 mV s^{-1}; DPV, 10 mV s^{-1}.

- 200 mV in the scan rate (ν) over the range of 100 – 500 mV s^{-1}) or totally irreversible, as judged by the wave analysis in the corresponding cyclic voltammetric experiments. Pyrene based anions are known to undergo chemical

reactions[31-33] and this possibility could explain the quasi-reversible/irreversible nature of these peaks.

During the anodic scan, $[Ru(phen)_2(ppym)]^{2+}$ shows two closely spaced oxidation peaks at +1.27 and +1.42 V whereas $[Ru(phen)_3]^{2+}$ shows one oxidation peak at +1.37 V (Fig. 3.5). A comparison of the oxidation potentials of these two complexes and of the ligands present in them suggest that the two peaks seen for $[Ru(phen)_2(ppym)]^{2+}$ correspond to the one-electron oxidations of the coordinated ppym and the ruthenium center (Ru^{III}/Ru^{II}) whereas in the case of $[Ru(phen)_3]^{2+}$, the peak observed at +1.37 V corresponds to the Ru^{III}/Ru^{II} redox couple.

3.3.4 Fluorescence experiments

3.3.4.1 Fluorescence studies with ppym

When excited at 340 nm, fluorescence spectrum of ppym showed two clearly distinguishable sets of peaks in CH_3CN (Fig. 3.6). The spectrum is characterized by sharp structured peaks between 350 and 410 nm (region I) and a broad band between 420 and 590 nm (region II). Pyrene was used as the standard for determining the quantum yield of ppym. The data on emission maxima (λ_{em}) and the quantum yield (ϕ) are summarized in Table 3.3.

The presence of two different sets of clearly distinguishable peaks in the spectrum for ppym is reminiscent of dual emission seen earlier for various fluorophores.[34-39] It is likely that an additional decay pathway (other than the normal radiative and non-radiative processes) is operating in ppym as well. In order to probe this aspect further studies with ppym were carried out under various solution conditions and the results of which are summarized below.

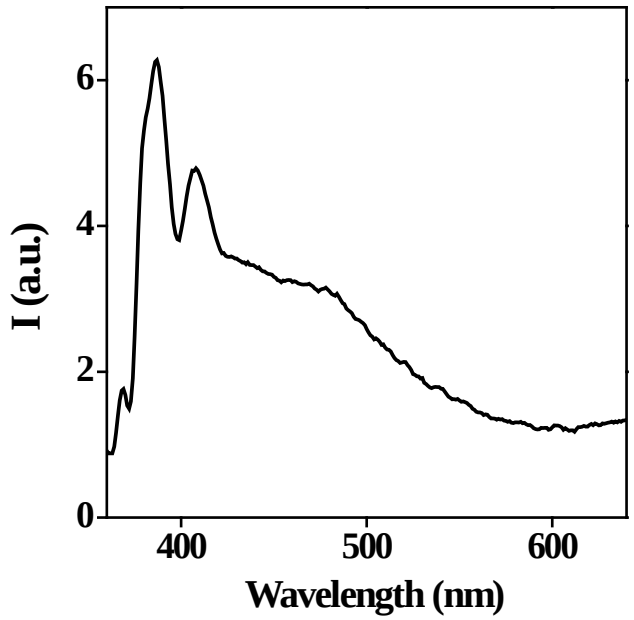

Fig. 3.6 Fluorescence spectrum of ppym (OD = 0.10, CH_3CN, λ_{exc} = 340 nm).

Concentration dependent absorption spectral studies revealed that ppym follows the Beer's law in CH_3CN solution. Variable concentration emission spectrum is also recorded for ppym in CH_3CN (Fig. 3.7) with the emission intensities being monitored in region I (387 nm) and region II (482 nm). Inset figure shows the plot of fluorescence intensity vs concentration and it is found to be curved upwards. With dilution to less than 1.5 μM, the relative intensity of the 482 nm band of ppym decreases in intensity with a concurrent growth of pyrene-monomer-like fluorescence with maxima at 386 and 408 nm. In fact, at higher concentration range (> 8.2 μM), ppym prominently exhibits the so-called 'green' fluorescence due to dominance of the broad emission band centered at 482 nm

and the plot of region II to region I emission intensity ratio vs concentration shows a clear upward curvature in nonpolar solvent such as cyclohexane.

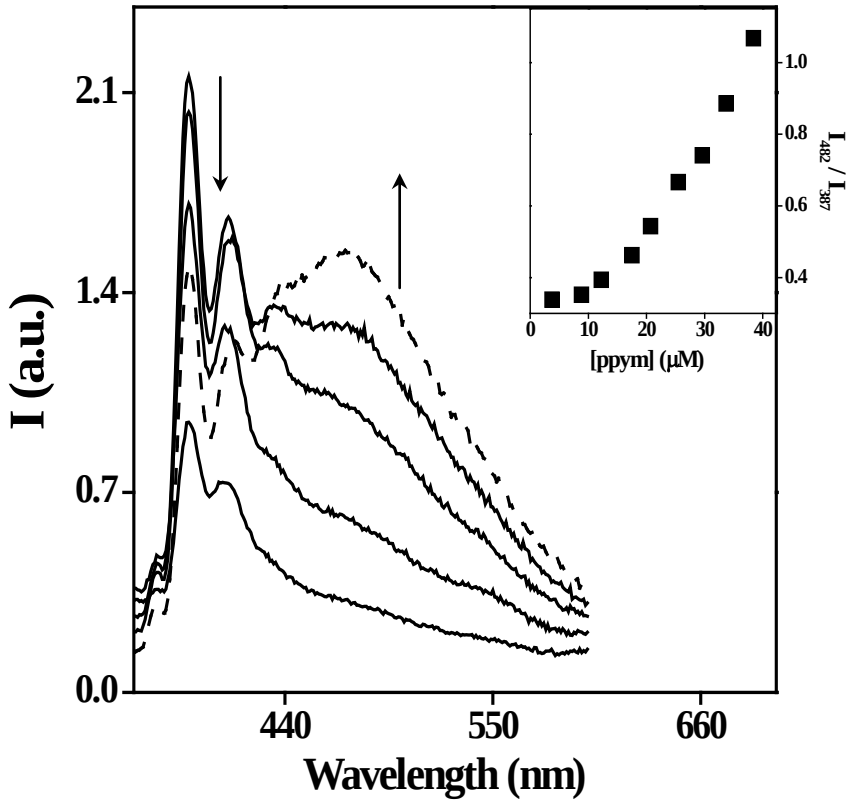

Fig. 3.7 Concentration dependent (4 – 38 μM) emission spectra of ppym (CH_3CN, λ_{exc} = 340 nm). Inset: Concentration dependence of region II to region I emission intensity ratio.

Such features observed for pyrene have been ascribed earlier to the formation of the aggregated fluorophore (excimer).[40-42] The solvatochromic shift observed in region II of the fluorescence spectrum of ppym is also consistent with this proposition. Interestingly, peaks in the absorption spectra and also those in region I of the fluorescence spectra of ppym remained invariant in various investigated solvents having different dielectric constants (1,4-dioxane, CH_2Cl_2,

THF, 2-propanol, CH_3CN and DMF). The modest solvatochromic shifts seen in solvents of low to medium polarity and the presence of emission only in region I in CH_3OH for ppym (OD = 0.10; λ_{exc} = 340) (Fig. 3.8) are quite similar to what was reported earlier for pyrene.[40-42]

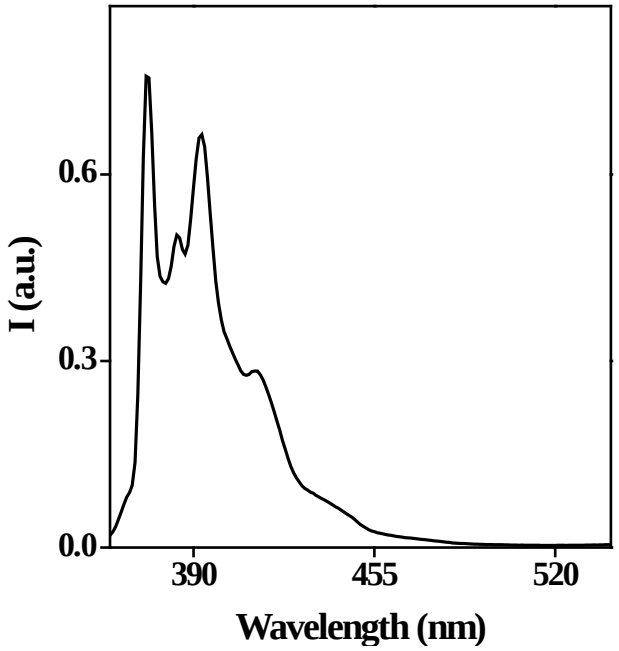

Fig. 3.8 Fluorescence spectrum of ppym (OD = 0.10, CH_3OH) at λ_{exc} = 340 nm.

Thus, we have analyzed that the fluorescence in region II for ppym is due to its excimer and that in region I is due to the monomer. The excimer properties of the fluorophoric ligand can also be confirmed by the metal ion titration experiments.

Fig. 3.9 shows the complexation induced quenching nature of the fluorescence of ppym in the presence of various concentrations of copper(II) perchlorate. This fact is clear from the plots of I/I_o vs $[Cu^{II}]$ shown in the inset of

Fig. 3.9 where, I_o and I are the emission intensities of ppym in the absence and presence of the metal ions, respectively.

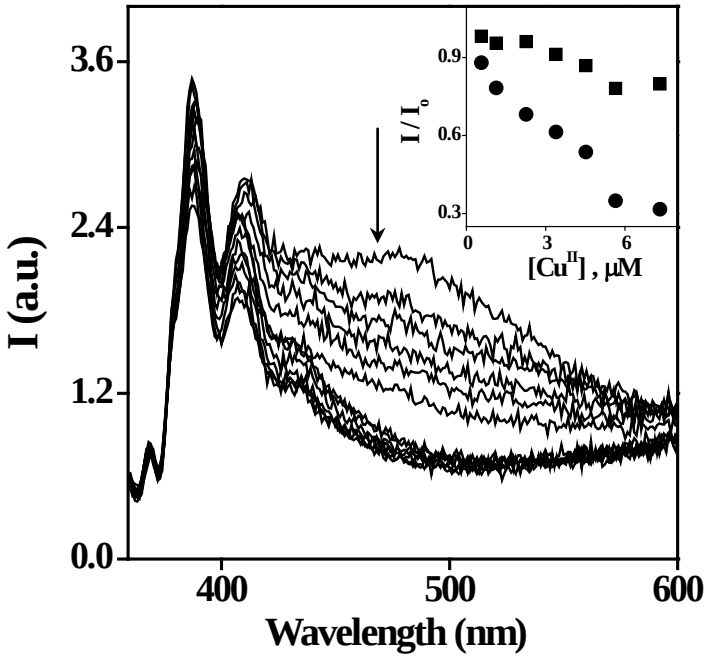

Fig. 3.9 Effect of addition of successive concentrations of Copper(II) perchlorate (0 – 24 μM) on the fluorescence due to ppym (17 μM, CH_3CN, λ_{exc} = 340 nm). Inset graph shows a comparison of the relative decrease in the fluorescence intensity monitored at (region I) 387 nm (■) and (region II) 482 nm (●) with respect to [Cu(II)] ion.

On increasing concentration of Cu(II) ion, the excimer emission centered at 482 nm quenches with the increase in the pyrene monomer emission (387 nm) followed by the saturation at 6 μM. This is evident from the plot of I/I_o vs [Cu^{II}] (using the data obtained at 482 nm), which shows a steep drop followed by flat

saturation. This suggests that the pyrene group in the metal ion bound complex cannot adopt an overlaying geometry. The loss of geometry results in the progressive dissociation of the excimer emission for this ligand. Finally, exciplex pathway can also be conceived for ppym but the presence of emission in region II in both polar (DMF) and nonpolar (1,4-dioxane) media disfavors the exciplex formation.[34]

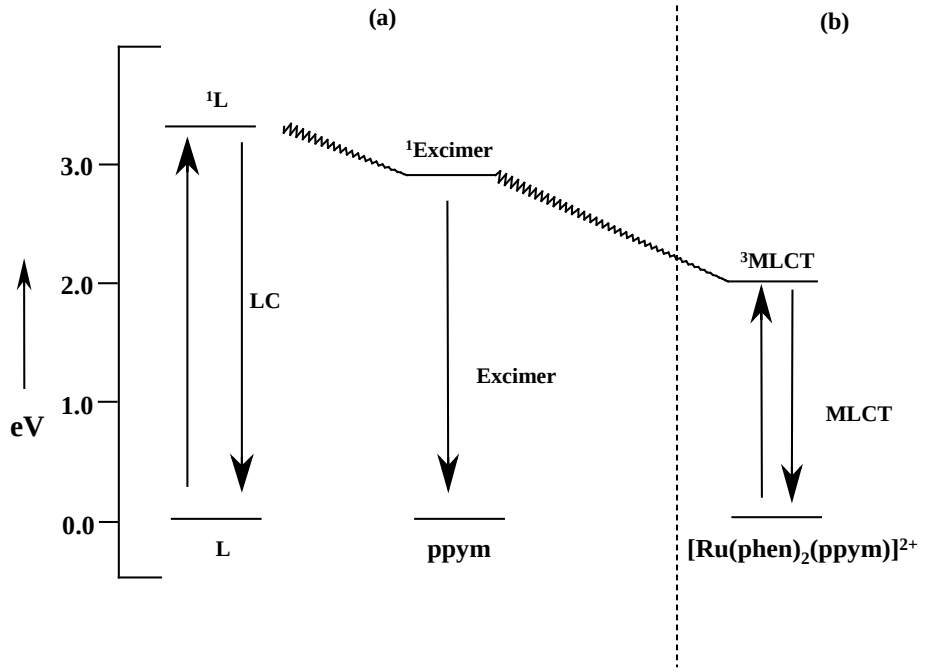

Fig. 3.10 Energy level diagram illustrating various photophysical processes of (a) ppym and (b) $[Ru(phen)_2(ppym)]^{2+}$. Solid lines represent radiative transitions and waved lines represent non-radiative transitions (L = free/bound ppym).

Overall, the energy level scheme shown in Fig. 3.10a that involves the participation of an excimer state can rationalize the excited state decay of ppym.

The metal ion induced quenching experiments conducted for ppym is also consistent with the deactivation mechanism of the singlet state shown in Fig. 3.10a.

3.3.4.2 Fluorescence studies with $[Ru(phen)_2(ppym)]^{2+}$

$[Ru(phen)_2(ppym)]^{2+}$ shows an emission band centered at 604 nm with a quantum yield of 0.029 in CH_3CN (λ_{exc} = 450 nm). The spectral shape and the λ_{em} value are quite similar to those reported for $[Ru(phen)_2(dppz)]^{2+}$, the ^{3}MLCT emission band maximum of which has been reported to be located at 618 nm.[43] Thus, the emission behaviour of this new mixed-ligand complex does not show the complexity that characterized the spectral feature of ppym. Specifically, there is no dual emission seen for this complex and it emits only from the ^{3}MLCT state.

The energy level diagram shown in Fig. 3.10a can thus be modified to that shown in Fig. 3.10b to describe the decay features of $[Ru(phen)_2(ppym)]^{2+}$. The ^{3}MLCT state of $[Ru(phen)_2(ppym)]^{2+}$ lies lower than the excimer state and is the ultimate 'sink' for the photon energy absorbed by the complex. In accordance with this proposition, excitation of CH_3CN solution of $[Ru(phen)_2(ppym)]^{2+}$ at either 300 or 340 nm also resulted in only the ^{3}MLCT band suggesting that the rates of photon migration from the ^{1}L → ^{1}excimer (L = ppym) and ^{1}excimer → ^{3}MLCT states are faster than those of 'vertical' radiative decays from either ^{1}L or ^{1}excimer states (Fig. 3.10).

3.3.5 DNA binding

DNA binding by $[Ru(phen)_2(ppym)]^{2+}$ has been monitored by electronic absorption, fluorescence, thermal denaturation and also by the viscometric titration methods. These results are summarized in this section. We have also

discussed the aspects related to the ability of this complex to act as “molecular light switch” for DNA.

$[Ru(phen)_2(ppym)]^{2+}$ shows the presence of isosbestic points (317 and 476 nm) and hypochromicity (11%) during the absorption titration experiment with CT DNA (Fig. 3.11).

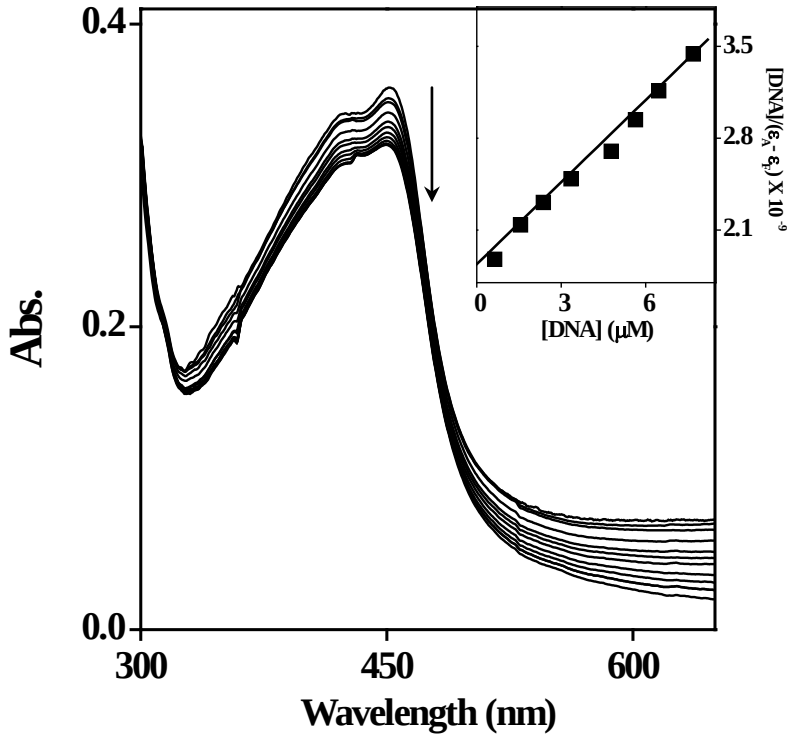

Fig. 3.11 UV-visible spectra of $[Ru(phen)_2(ppym)]^{2+}$ (20 μM) in the absence (top curve) and presence (subsequent curves) of increasing concentrations (0 – 100 μM) of CT DNA in buffer A. The inset graph shows a fit of the absorbance data to equn. 2.2 (Chapter 2).

The value of intrinsic binding constant (K_b) estimated using equn. 2.2 was found to be as high as 1.20 x 10^5 M^{-1}. The extent of hypochromism commonly parallels to the intercalative strength of the ligand and moreover higher planar area, extended π system, hydrophobicity and aromaticity lead to the deep penetration and hence more stacking within the base pairs of DNA.

$[Ru(phen)_2(ppym)]^{2+}$ is a fairly good emitive species in buffer A with the quantum yield of 0.018 in the absence of DNA. Fluorescence intensity of this complex increases initially at low $[DNA_{NP}]/[Ru]$ ratio and reaches a plateau with the apparent enhancement factor of ~ 1.4 at a $[DNA_{NP}]/[Ru]$ ratio of 27, (Fig. 3.12). Concomitant with this fluorescence enhancement, bathochromic shift (~ 2 nm) in the emission maxima is also noticed in the presence of excess DNA. Results of the fluorescence titration experiments are not quite similar to those reported for $[Ru(phen)_2(dppz)]^{2+}$ which is a classical example of "molecular light switch" for DNA. $[Ru(phen)_2(dppz)]^{2+}$ and other dppz based complexes have been reported to cause a $>10^4$ times enhancement in emission in presence of DNA.[7,43-45] The emission enhancement has been ascribed to the protection of the imine nitrogens on ppym from attack by water and a consequent decrease in the non-radiative processes upon intercalation.[7,43-50] Despite the fact that the DNA-induced emission enhancement in $[Ru(phen)_2(ppym)]^{2+}$ is not as dramatic as in the case of $[Ru(phen)_2(dppz)]^{2+}$, it is reasonable to expect that emission enhancement observed for the former complex in the presence of DNA. It is partially a consequence of decrease in the non-radiative deactivation process of the excited state due to the protection of ppym by intercalation. The binding constant obtained utilizing the emission titration data (K_b = 1.05 x 10^5 M^{-1}) is in agreement with that obtained from the absorption titration experiment (*vide supra*).

CT DNA was seen to melt at 61±1 ^{o}C (2 mM NaCl, 1 mM phosphate) in the absence of any added complex. The T_m is increased by 6(±1)^{o} in the presence

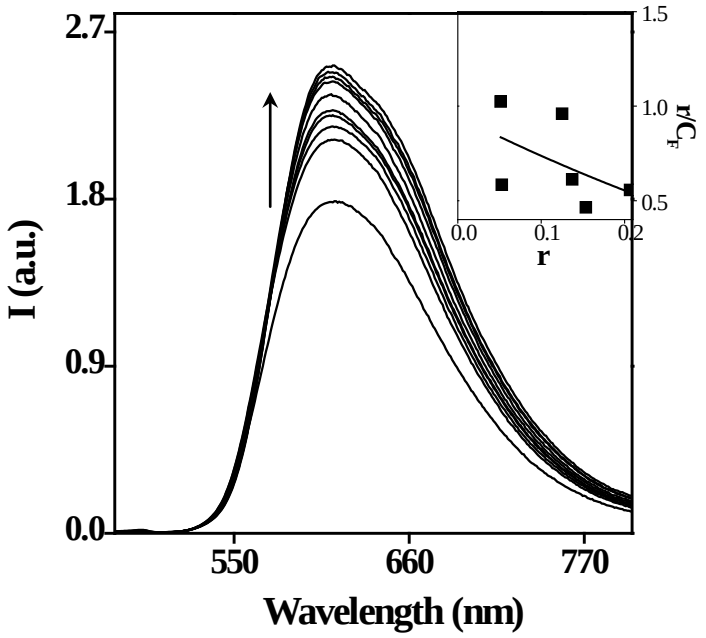

Fig. 3.12 Fluorescence spectra of $[Ru(phen)_2(ppym)]^{2+}$ (10 μM) in the absence (bottom curve) and presence (subsequent curves) of increasing concentrations (0 – 200 μM) of CT DNA in buffer A (λ_{exc} = 450 nm). The inset graph shows a fit of the data to equn. 2.4 (Chapter 2).

of $[Ru(phen)_2(ppym)]^{2+}$ at $[DNA_{NP}]$/[complex] = 25 (Fig. 3.13). This observation indicates the increased stability of the double helix when $[Ru(phen)_2(ppym)]^{2+}$ binds to DNA and the values observed are comparable with the classical intercalator EtBr and lend strong support for the intercalation in to the helix.

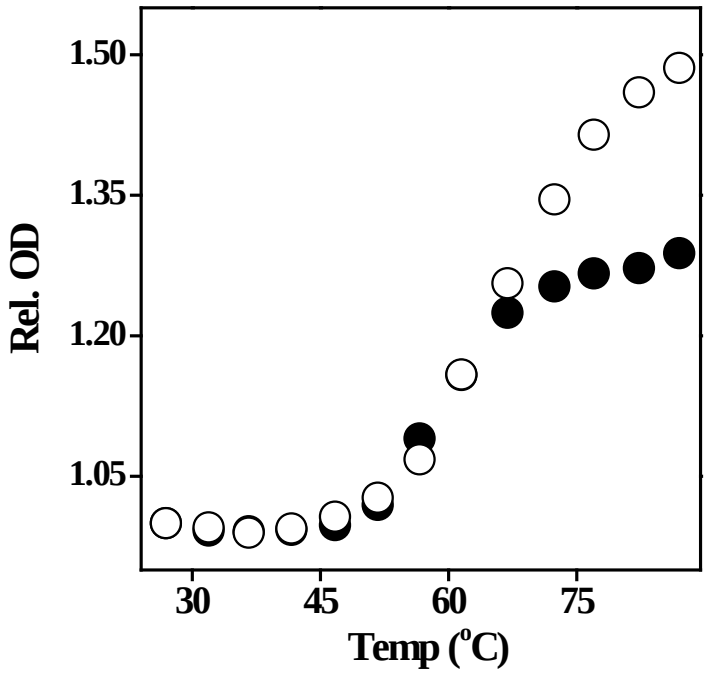

Fig. 3.13 Thermal Melting curves for CT DNA in the absence (●) and in the presence (○) of $[Ru(phen)_2(ppym)]^{2+}$ in buffer B.

The effects of $[Ru(phen)_2(ppym)]^{2+}$, EtBr and $[Ru(phen)_3]^{2+}$ on the viscosity of CT DNA solution have been studied in order to assess the binding mode of these complexes with DNA. Plots of $(\eta/\eta_o)^{1/3}$ vs [Drug]/[DNA] are constructed (Fig.3.14). The viscosity of the DNA bound with $[Ru(phen)_2(ppym)]^{2+}$ and EtBr (classical intercalator) increases dramatically. However, addition of complex $[Ru(phen)_3]^{2+}$ has no effect on the DNA viscosity as previously reported.[51]

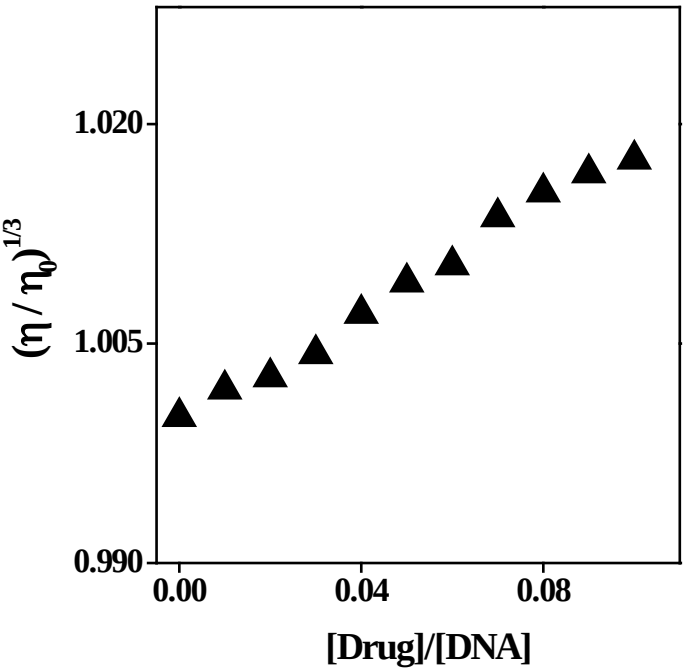

Fig. 3.14 Results of viscometric titrations carried out for CT DNA (300 μM) in the presence of $[Ru(phen)_3]^{2+}$ (■) and $[Ru(phen)_2(ppym)]^{2+}$ (▲) in buffer C.

The above observations are similar to those reported earlier for various metallointercalators[21-25,43-47,52-56] and suggest that $[Ru(phen)_2(ppym)]^{2+}$ strongly binds to DNA *via* an intercalative mode. This observation and the facts that the ruthenium-bound dppz is an avid intercalator of DNA ($K_a > 10^6$ M^{-1})[44] and $[Ru(phen)_3]^{2+}$ is not a classical intercalator[51], suggest that ppym in $[Ru(phen)_2(ppym)]^{2+}$ is intercalating with DNA and the phen ligands act only as spectators. The favorable structural feature of ppym is expected to aid $[Ru(phen)_2(ppym)]^{2+}$ to intercalate deeply into the DNA base pairs.

3.3.6 DNA photocleavage

Results of DNA photocleavage experiments carried out with $[Ru(phen)_2(ppym)]^{2+}$ are compared with those obtained for $[Ru(phen)_3]^{2+}$. Fig. 3.15 summarizes these results. Control experiments have suggested that untreated pBR 322 DNA does not show any cleavage in the dark and even upon irradiation by a 450 ± 5 nm light (compare lanes 1 and 2, Fig. 3.15).

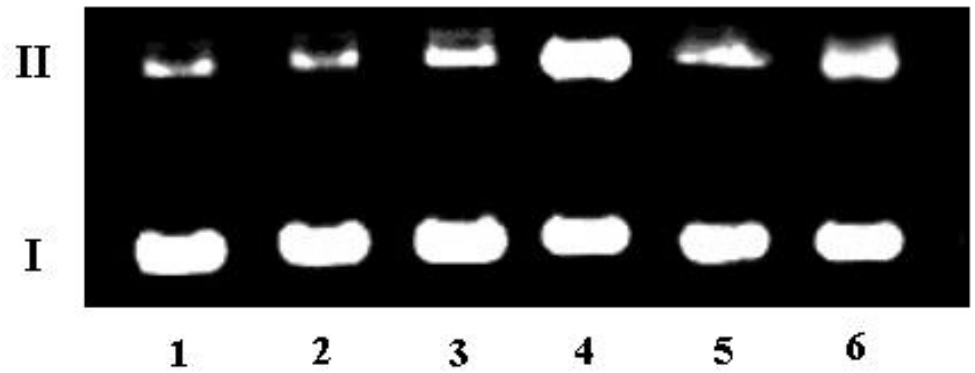

Fig. 3.15 Light-induced nuclease activities of the investigated ruthenium(II) complexes. Dark and Light Experiments: Lanes 1 and 2: Untreated pBR 322 (100 μM) in the dark and upon irradiation. Lanes 3 and 5: pBR 322 + $[Ru(phen)_2(ppym)]^{2+}$ and $[Ru(phen)_3]^{2+}$ respectively (10 μM) in dark. Lanes 4 and 6: pBR 322 + $[Ru(phen)_2(ppym)]^{2+}$ and $[Ru(phen)_3]^{2+}$, respectively upon irradiation. $\lambda_{irrd.}$= 450 ± 5 nm (30 min.) in each case.

Similarly, nicking of DNA could not be observed when pBR 322 is treated with both $[Ru(phen)_2(ppym)]^{2+}$ and $[Ru(phen)_3]^{2+}$ in the dark experiments (Lanes 3 and 5). On the other hand, irradiation of DNA in the presence of $[Ru(phen)_2(ppym)]^{2+}$ is seen to effectively photocleave the DNA (Lane 4).

Under comparable experimental conditions, DNA nicking efficiency of $[Ru(phen)_2(ppym)]Cl_2$ is much greater than that of $[Ru(phen)_3]Cl_2$ (Lane 6). As discussed before, the extended π structure of ppym results in effective intercalation of $[Ru(phen)_2(ppym)]^{2+}$ with the DNA. The inefficient deactivation of its low lying photochemically active MLCT excited state permits an enhanced DNA photocleavage activity when compared to $[Ru(phen)_3]^{2+}$.

In attempts to unravel the probable DNA photocleavage mechanism of $[Ru(phen)_2(ppym)]^{2+}$, a few control experiments have been conducted in the presence of 'inhibitors'. Results are summarized in Fig. 3.16.

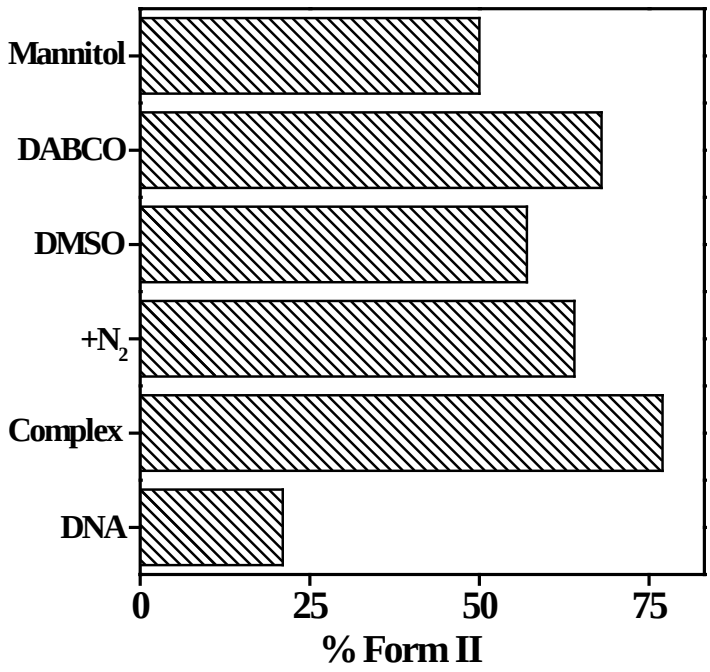

Fig. 3.16 Effects of 'inhibitors' on the light-induced nuclease activity of $[Ru(phen)_2(ppym)]^{2+}$. In each case, the sample was irradiated at 450 ± 5 nm for 30 min.

Inhibitions of photocleavage in the presence of DMSO and mannitol are comparable. However, DABCO was seen to cleave the DNA marginally less. These results suggest that both $^1O_2$ and $^{\bullet}OH$ play role in this photodamage. However, $OH^{\bullet}$ might be the key reactive oxygen species involved in the whole process.

3.4 Summary

New pyrene appended polypyridyl ligand, ppym and the mixed-ligand ruthenium(II) complex $[Ru(phen)_2(ppym)]^{2+}$ have been synthesized and fully characterized by spectroscopic, photophysical and electrochemical methods. Ligand ppym shows dual emission characteristics and this has been interpreted by invoking a excimer mechanism. Studies with DNA have revealed that the complex binds to DNA, mainly, *via* an intercalative mode with moderate strength. While fluorescence studies have revealed that $[Ru(phen)_2(ppym)]^{2+}$ is showing moderate "molecular light switch" behaviour with DNA. Agarose gel electrophoresis experiments have shown that this new complex is an efficient photocleaving agent for the plasmid and hydroxyl radical plays a key role in the photocleavage mechanism.

3.5 References

1. Ji. L-N.; Zou, X-H.; Liu, J-G. *Coord. Chem. Rev*. **2001**, *216-217*, 513.
2. Kane-Maguire, N. A. P.; Wheeler, J. F. *Coord. Chem. Rev*. **2001**, *211*, 145.
3. Erkkila, K. E.; Odom, D. T.; Barton, J. K. *Chem. Rev*. **1999**, *99*, 2777.
4. Kelly, S. O.; Barton, J. K. in *Metal ions in Biological Systems.* Sigel, A.; Sigel, H. Eds.; Marcel Dekker, New York, 1999, *39*, 211.

5. Ortmans, I.; Moucheron, C.; Mesmaeker, A. K-D. *Coord. Chem. Rev*. **1998**, *168*, 233.
6. Norden, B.; Lincoln, P.; Akerman, B.; Tuite, E. *Metal ions in biological systems*. Sigel, A.; Sigel, H. Eds.; Marcel Dekker, New York, 1996, *33*, 177.
7. Murphy, C. J.; Barton, J. K. *Methods Enzymol*. **1993**, *226*, 576.
8. Holder, A. A.; Swavey, S.; Brewer, K. J. *Inorg. Chem.* **2004**, *43*, 303.
9. Liu, F.; Wang, K.; Bai, G.; Zhang, Y.; Gao, L. *Inorg. Chem.* **2004**, *43*, 1799.
10. Ortmans, I.; Elias B.; Kelly, J. M.; Moucheron, C.; Mesmaeker, A. K-D. *J. Chem. Soc., Dalton Trans.* **2004**, 668.
11. Xu, H.; Zheng, K-C.; Deng, H.; Lin, L-J.; Zhang, Q-L.; Ji, L-N. *New J. Chem*. **2003**, *27*, 1255.
12. Delaney, S.; Pascaly, M.; Bhattacharya, P. K.; Han, K.; Barton, J. K. *Inorg. Chem*. **2002**, *41*, 1966.
13. Swavey, S.; Brewer, K. J. *Inorg. Chem.* **2002,** *41*, 6196.
14. Wilhelmsson, L. M.; Westerlund, F.; Lincoln, P.; Norden, B.; *J. Am. Chem. Soc.* **2002**, *124*, 12092.
15. Hergueta-Bravo, A.; Jimenez-Hernandez, E. M.; Montero, F.; Oliveros, E.; Orellana, G. *J. Phys. Chem. B.* **2002**; *106*, 4010.
16. Fu, P, K-L.; Bradley, P. M.; van Loyen, D.; Durr, H.; Bossmann, S. H.; Turro, C. *Inorg. Chem*. **2002**, *41*, 3808.
17. Hurley, D. J.; Tor, Y. *J. Am. Chem. Soc.* **2002**, *124*, 13231.
18. Ossipov, D.; Pradeepkumar, P. I.; Holmer, M.; Chattopadhyaya, J. *J. Am. Chem. Soc.* **2001**, *123*, 3551.
19. Carvalho, I. M. M.; Moreira, I. S.; Gehlen, M. H. *Inorg. Chem.* **2003**, *42*, 1525.

20. Johansson, O.; Borgstrom, M.; Lomoth, R.; Palmblad, M.; Bergquist, J.; Hammarstrom, L.; Sun, L.; Akermark, B. *Inorg. Chem.* **2003**, *42*, 2908.
21. Arounaguiri, S.; Maiya, B. G. *Inorg. Chem.* **1999**, *38*, 842.
22. Ambroise, A.; Maiya, B. G. *Inorg. Chem.* **2000**, *39*, 4256.
23. Ambroise, A.; Maiya, B. G. *Inorg. Chem.* **2000**, *39*, 4264.
24. Murali, S.; Sastri, C. V.; Maiya, B. G. *Proc. Indian Acad. Sci.* (*Chem. Sci.*), **2002**, *114*, 403.
25. Sastri, C. V.; Eswaramoorthy, D.; Giribabu, L.; Maiya, B. G. *J. Inorg. Biochem*. **2003**, *94*, 138.
26. Wozniak, K.; Grech, E.; Chelmieniecka, A. S. *Polish J. Chem.* **2000**, *74*, 717.
27. Yang, G.; Wang, L.; Ji, L-N. *J. Inorg. Biochem*. **1997**, 289.
28. Xiong, Y.; Ji, L-N. *Coord. Chem. Rev*. **1999**, *185-186*, 711
29. Didier, P.; Jacquet, L.; Mesmaeker, A. K-D.; Hueber, R.; van Dorsselaer, A. *Inorg. Chem.* **1992**, *31*, 4803.
30. Nicholson, R. S.; Shain, I. *Anal. Chem*. **1964**, *36*, 706.
31. Adams, R. N. *Electrochemistry at Solid Electrodes*; Marcel Dekker: New York, 1969.
32. Weinberg, N. L.; Weinberg, H. R. *Chem. Rev.* **1968**, *68*, 449.
33. Simon, J. A.; Curry, S. L.; Schmehl, R. H.; Schatz, T. R.; Piotrowiak, P.; Jin, X.; Thummel, R. P. *J. Am. Chem. Soc.* **1997**, *119*, 11012.
34. Chandross, E. A. *The Exciplex*; Gordon, M., Ware, W. R., Eds.; Academic Press: New York, 1975**.**
35. Al-ansari, I. A. Z. *J. Photochem. Photobiol. A: Chem.* **1993**, *72, 15*.
36. Weigel, W.; Rettig, W.; Dekhtyar, M.; Modrakowski, C.; Beinhoff, M.; Schlulter, A. D. *J. Phys. Chem. A* **2003,** *107*, 5941.

37. Yoshihara, T.; Galievsky, V. A.; Druzhinin, S. A.; Saha, S.; Zachariasse, K. A. *Photochem. Photobiol. Sci.* **2003**, *2*, 342.
38. Sankaran, N. B.; Das, A.; Samanta, A. *Chem. Phys. Lett.* **2002**, *351*, 61.
39. Mataga, N. *Molecular Interactions*, Ratajcak, H., Orwell-Thomas, W., Eds.; Wiley: Chichester, 1981.
40. Castanheira, E. M. S.; Martinho, J. M. G. *Chem. Phys. Lett.* **1991**, *185*, 319.
41. Castanheira, E. M. S.; Martinho, J. M. G. *J. Photochem. Photobiol. A: Chemistry* **1994**, *80*, 151.
42. Beens, H.; Knibbe, H.; Weller, A. *J. Chem. Phys*. **1967**, *47*, 1183.
43. Hartshorn, R. M.; Barton, J. K. *J. Am. Chem. Soc.* **1992**, *114*, 5919.
44. Friedman, A. E.; Chambron, J-C.; Sauvage, J-P.; Turro, N. J.; Barton, J. K. *J. Am. Chem. Soc.* **1990**, *112*, 4960.
45. Dupureur, C. M.; Barton, J. K. *J. Am. Chem. Soc*. **1994**, *116*, 10286.
46. Olson, E. J. C.; Hu, D.; Hormann, A.; Jonkman, A. M.; Arkin, M. R.; Stemp, E. D. A.; Barton, J. K.; Barbara, P. F. *J. Am. Chem. Soc.* **1997**, *119*, 11458.
47. Friedman, A. E.; Kumar, C. V.; Turro, N. J.; Barton, J. K. *Nucleic Acids Res.* **1991**, *19*, 2595.
48. Holmlin, R. E.; Barton, J. K. *Inorg. Chem*. **1995**, *34*, 7.
49. Linncoln, B.; Broo, A.; Norden, B. *J. Am. Chem. Soc*. **1996**, *118*, 2644.
50. Schoch, K.; Hubbard, J. L.; Zoch, C. R.; Yi, G-B.; Sorlie, M. *Inorg. Chem.* **1996**, *35*, 4383.
51. Satyanarayana, S.; Dabrowiak, J. C.; Chaires, J. B. *Biochemistry* **1992,** *31*, 9319.
52. Jenkins, Y.; Friedman, A. E.; Turro, N. J.; Barton, J. K. *Biochemistry* **1992**, *31*, 10809.

53. Gupta, N.; Grover, N.; Neyhart, G. A.; Liang, W.; Singh, P.; Thorp, H. H. *Angew. Chem. Int. Ed. Engl*. **1992**, *31*, 1048.

54. Holmlin, R. E.; Yao, J. A.; Barton, J. K. *Inorg. Chem*. **1999**, *38*, 174.

55. Hiort, C. H.; Lincoln, P.; Norden, B. *J. Am. Chem. Soc*. **1993**, *115*, 3448.

56. Chambron, J-C.; Sauvage, J-P. *Chem. Phys. Lett*. **1991**, *182*, 603.

CHAPTER 4

DNA Binding and Photonuclease Activities of New Metallointercalators Containing Imidazo-phenanthroline Ligands

4.1 Introduction

It is a well known fact that the five-membered imidazole ring is a component of the purine bases in the DNA. L-N Ji and co-workers have reported a series of imidazole modified phen/bpy ligands wherein the imidazole ring is out of the plane from the phen moiety. Polypyridyl Ru(II) complexes with such ligands exhibit the effect of ligand planarity on the DNA binding strength.[1-5] The ancillary ligands (phen/bpy) have also shown significant effects on the spectral properties and the DNA binding behaviour of their complexes.[6-8] Thus, we have focused on the construction of novel imidazole fused polypyridyl ligands containing fluorophore such as pyrene and anthracene in their architecture. The present chapter deals with the synthesis, characterization and DNA binding studies of mixed-ligand Ru(II) complexes, $[Ru(phen)_2(aip)]^{2+}$ and $[Ru(phen)_2(pyip)]^{2+}$, containing ligands which have anthracene (*viz*. 2-(9-anthryl)-1H-imidazo[4,5-f][1,10]phenanthroline (aip)) or pyrene (*viz*. (2-(1-pyrenyl)-1H-imidazo[4,5-f][1,10]phenanthroline (pyip)) fluorophore in their architecture.

4.2 Experimental section

The precursor compounds, 1,10-phenanthroline-5,6-dione (phen-dione), $[Ru(phen)_2Cl_2]\cdot 2H_2O$, $[Ru(phen)_3]Cl_2$ and $[Ru(phen)_2(dppz)]Cl_2$ were synthesized by the following reported procedures as described in chapter 2. Synthesis of aip, pyip and the corresponding mixed-ligand ruthenium(II) complexes (Fig. 4.1) are described below.

4.2.1 2-(9-anthryl)-1H-imidazo[4,5-f][1,10]phenanthroline (aip)

A mixture of phen-dione (0.53 g, 2.50 mmol), 9-anthraldehyde (0.72 g, 3.50 mmol), ammonium acetate (3.88 g, 50.00 mmol) and glacial acetic acid (15 mL) was refluxed for 4 h by adopting the Steck and Day method[9] and then cooled to room temperature. It was diluted with water and drop wise addition of concentrated aqueous ammonia gave a yellow precipitate, which was collected, washed with H_2O and dried. The crude product obtained was purified by recrystallization using $CHCl_3$-MeOH (4:1, v/v) mixture and dried. Yield = 0.71 g (72%).

Analytical data: Found: C, 81.63; H, 4.21; N, 14.19; Calculated for $C_{27}H_{16}N_4$: C, 81.70; H, 4.04; N, 14.13; MALDI-TOF (m/z): 396 $(M)^+$; IR: ν_{max} (KBr, cm^{-1}): 3441 (N-H), 1604 (C=N). ^{1}H NMR ($(CD_3)_2SO$, 200 MHz, TMS): 14.20 (s, 1H), 9.09 (dd, 2H), 8.94 (dd, 2H), 8.80 (d, 1H), 8.26 (d, 2H), 7.84 (m, 4H), 7.57 (m, 4H).

4.2.2 2-(1-pyrenyl)-1H-imidazo[4,5-f][1,10]phenanthroline (pyip)

A mixture of phen-dione (0.53 g, 2.50 mmol), 1-pyrenecarboxaldehyde (0.81 g, 3.50 mmol), ammonium acetate (3.88 g, 50.00 mmol) and glacial acetic acid (15 mL) was refluxed for 4 h. The above solution was cooled to the room temperature and diluted with water. Drop wise addition of concentrated aqueous ammonia gave a yellow precipitate which was collected, washed with H_2O and dried. The crude product thus obtained was purified by recrystallization with C_5H_5N-H_2O (9:1, v/v) and dried. Yield = 0.71 g (68%).

Analytical data: Found: C, 82.81; H, 3.74; N, 13.39; Calculated for $C_{29}H_{16}N_4$: C, 82.77; H, 3.81; N, 13.32; MALDI-TOF (m/z): 420 $(M)^+$; IR: ν_{max} (KBr, cm^{-1}): 3426 (N-H), 1602 (C=N). ^{1}H NMR ($CDCl_3$ - $(CD_3)_2SO$, 200 MHz, TMS): 13.73

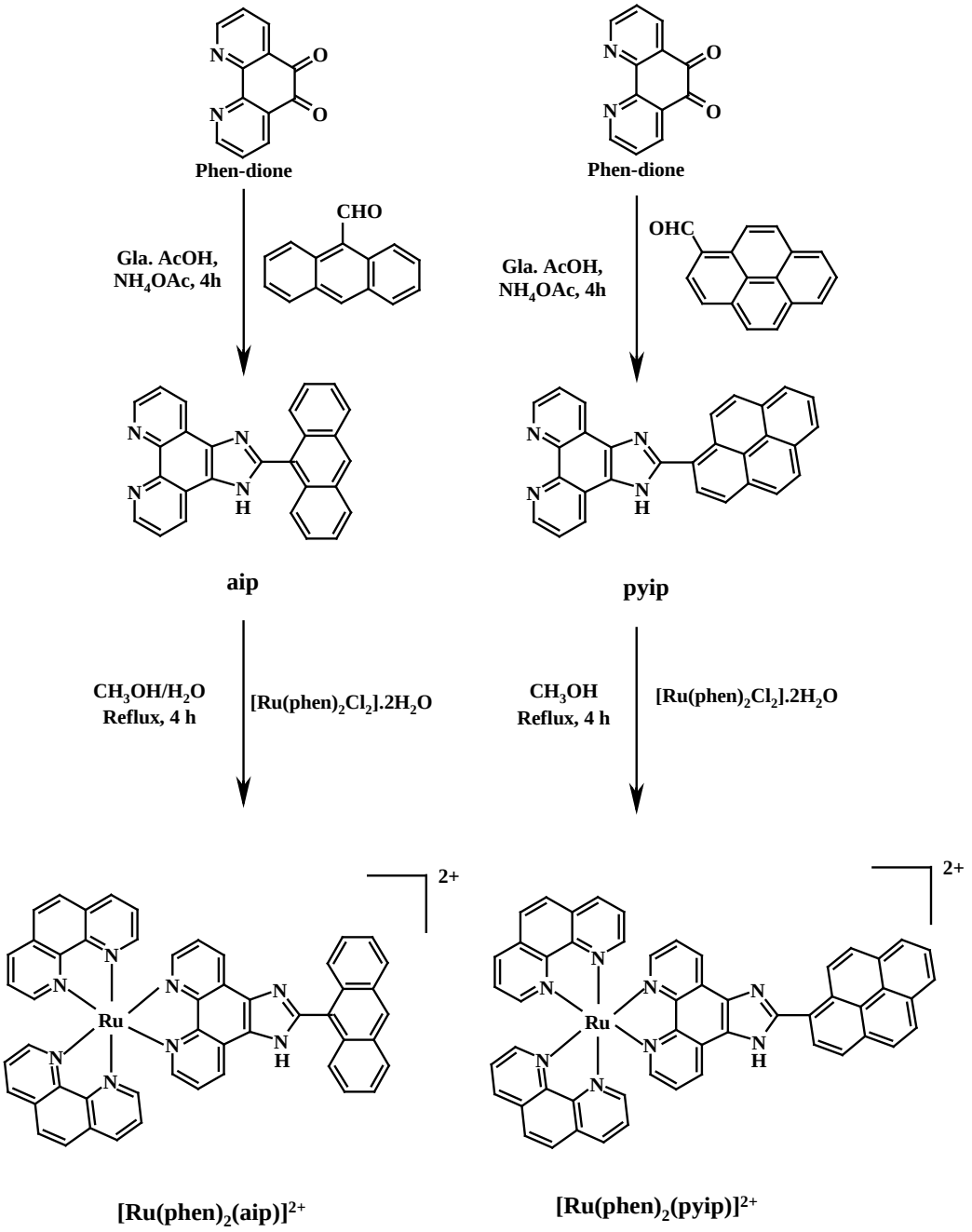

Fig. 4.1 Scheme leading to the synthesis of aip, pyip and their mixed-ligand ruthenium(II) complexes.

(s, 1H), 9.28 (d, 1H), 9.12 (dd, 2H), 8.93 (d, 1H), 8.52 (d, 1H), 8.18 (m, 8H), 7.66 (dd, 2H).

4.2.3 Bis-(1,10-phenanthroline)(2-(9-anthryl)-1H-imidazo[4,5-f][1,10]phenanthroline)ruthenium(II) hexafluorophosphate dihydrate $[Ru(phen)_2(aip)](PF_6)_2 \cdot 2H_2O$

This complex was prepared by refluxing aip (0.30 g, 0.76 mmol) with $[Ru(phen)_2Cl_2]\cdot 2H_2O$ (0.43 g, 0.75 mmol) in CH_3OH-H_2O (1:1, v/v) mixture for 4 h. The resulting solution was cooled to room temperature, followed by the addition of 15 mL of H_2O and filtered. Addition of aqueous saturated solution of NH_4PF_6 to the filtrate precipitated bright orange-red coloured crude $[Ru(phen)_2(aip)](PF_6)_2$, which was purified by column chromatography (alumina and CH_3CN-toluene (3:2, v/v) mixture) and further recrystallized from acetone-ether mixture (1:5, v/v). Yield = 0.48 g (54%).

Analytical data: Found: C, 51.86; H, 2.98; N, 9.53; Calculated for $C_{51}H_{36}N_8O_2F_{12}P_2Ru$: C, 51.71; H, 3.04; N, 9.46; MALDI-TOF (m/z): $[M - PF_6^-]^+$, 1003; $[M - 2PF_6^{2-}]^+$, 858; IR: ν_{max} (KBr, cm^{-1}): 3381 (N-H), 1601 (C=N), 837 (PF_6). ^1H NMR ($(CD_3)_2SO$, 200 MHz, TMS): 8.97 (d, 1H), 8.81 (m, 4H), 8.42 (s, 4H), 8.26 (m, 4H), 8.09 (m, 5H), 7.82 (m, 9H), 7.61 (m, 4H).

4.2.4 Bis-(1,10-phenanthroline)(2-(1-pyrenyl)-1H-imidazo[4,5-f][1,10]phenanthroline)ruthenium(II) hexafluorophosphate dihydrate $[Ru(phen)_2(pyip)](PF_6)_2 \cdot 2H_2O$

This mixed-ligand Ru(II) complex was prepared by refluxing pyip (0.34 g, 0.82 mmol) with $[Ru(phen)_2Cl_2]\cdot 2H_2O$ (0.45 g, 0.80 mmol) in CH_3OH-H_2O (1:1, v/v) mixture for 4 h. The crude bright orange-red coloured $[Ru(phen)_2(pyip)]^{2+}$ was obtained on adding saturated solution of NH_4PF_6. It was

purified by column chromatography (alumina and CH_3CN-toluene (3:2, v/v) mixture) and further recrystallized from acetone-ether mixture (1:5, v/v). Yield = 0.49 g (53%).

Analytical data: Found: C, 52.78; H, 3.13; N, 9.17; Calculated for $C_{53}H_{36}N_8O_2F_{12}P_2Ru$: C, 52.67; H, 2.98; N, 9.28; MALDI-TOF (m/z): $[M - PF_6^-]^+$, 1026 ; $[M - 2PF_6^{2-}]^+$, 883; IR: ν_{max} (KBr, cm^{-1}): 3377 (N-H), 1599 (C=N), 837 (PF_6). ^1H NMR ($(CD_3)_2SO$, 200 MHz, TMS): 9.43 (d, 1H), 9.19 (d, 2H), 8.80 (m, 4H), 8.69 (d, 1H), 8.58 (d, 1H), 8.43 (m, 8H), 8.15 (m, 6H), 7.82 (m, 6H), 7.20 (m, 2H).

The hexafluorophosphate salts of these complexes were converted to the water-soluble, chloride salts by treating the former salt solutions in acetone with excess TBACl. The chloride salts, being insoluble in acetone, were instantaneously precipitated out of the solution. They were filtered and vacuum dried before use. The yield was ~ 90% in each case. All the spectroscopic, electrochemical and biochemical experiments were carried out as described in chapter 2.

4.3 Results and discussion

4.3.1 Synthesis and characterization

The scheme leading to the synthesis of the new ligands and their complexes is given in Fig. 4.1. The ligands aip and pyip were prepared by a method similar to that described by Steck and Day.[9] Condensation of 1,10-phenanthroline-5,6-dione and 9-anthraldehyde or 1-pyrenecarboxaldehyde in the presence of ammonium acetate and glacial acetic acid provided aip or pyip. The corresponding ruthenium(II) complexes were synthesized by reacting $[Ru(phen)_2Cl_2]\cdot 2H_2O$ with either aip or pyip (Fig. 4.1). Each synthetic step

involved here is straightforward and provided good-to-moderate yield of the desired product in pure form.

The ligands aip and pyip and their Ru(II) complexes were characterized by elemental analysis, IR, UV-visible, fluorescence, MALDI-TOF mass and ^{1}H NMR spectroscopic methods. MALDI-TOF spectra showed base-peak at 396 (M^+ for aip) and at 420 (M^+ for pyip). In the case of corresponding mixed-ligand Ru(II) complexes, peaks were seen at 1003 $(M - PF_6^-)^+$ and 858 $(M - 2PF_6^{2-})^+$ for $[Ru(phen)_2(aip)](PF_6)_2$ and at 1026 $(M - PF_6^-)^+$ and 883 $(M - 2PF_6^{2-})^+$ for $[Ru(phen)_2(pyip)](PF_6)_2$ typical of PF_6 salts of ruthenium(II) polypyridyl complexes.[10-13]

^{1}H NMR spectrum of each new compound synthesized during this study was analyzed with the proton assignments being made on the basis of resonance position, integrated intensity data and ^{1}H - ^{1}H coupling patterns observed in the 2D (COSY) spectra. The ^{1}H NMR spectra of aip and pyip are displayed in Fig. 4.2. The ^{1}H NMR values for all the new compounds are given in the experimental section.

^{1}H NMR spectra of both 9-anthraldehyde and 1-pyrenecarboxaldehyde showed a singlet at 11.50 and 10.78 ppm respectively, corresponding to the aldehyde proton. The spectra of both aip and pyip showed a characteristic singlet at 14.20 and 13.73 ppm respectively, which can be assigned to the peak of N-H in the imidazole ring.[4,5] In each of these two complexes, the proton on the nitrogen atom of the imidazole ring was not observed. Metal coordination causes electron deficiency in the ligand. As a result, the imidazole proton becomes active and there is fast proton exchange between the two imidazole nitrogen atoms. Similar observations have been reported earlier.[4,5,14] In both the complexes, $[Ru(phen)_2(aip)]^{2+}$ and $[Ru(phen)_2(pyip)]^{2+}$, the *o*- and *p*- protons of the phenanthroline fragment of the ligands aip/pyip shift to downfield and *m*- protons

experience upfield shift compared to the free ligands (aip/pyip). However, the protons in the anthracene and pyrene fragments of the ligands do not experience much shift compared to the free ligands (aip and pyip). The other protons of both the complexes and the ligands gave well-defined ^{1}H NMR spectra which permits unambiguous identification and assessment of purity.

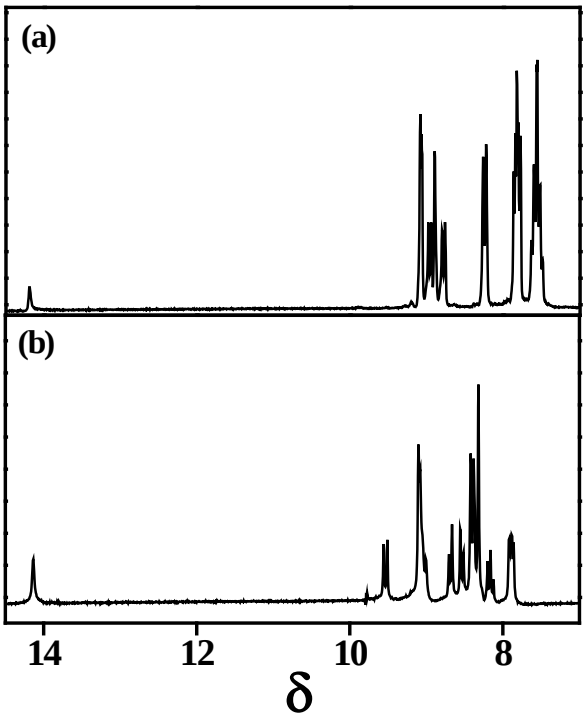

Fig. 4.2 ^{1}H NMR spectra of (a) aip(in $CDCl_3$ + 5% CD_3OD) and (b) pyip (in $(CD_3)_2SO$).

4.3.2 Absorption and emission spectra

UV-vis data of aip, pyip and their ruthenium(II) complexes synthesized during this study along with the corresponding reference compounds are

summarized in Table 4.1. The UV-vis and the fluorescence spectra of both the complexes are given in Fig. 4.3. As seen, the spectra of aip and pyip are characterized by low intensity, low energy structured absorption bands due to $\pi \rightarrow \pi^*$ transitions at 383 and 366 nm for aip and at 368 nm for pyip. These bands are ascribed to the anthracene and pyrene chromophores attached to the phenanthroline moiety.[15,16] The high-energy bands (aip: 251 nm and pyip: 234 and 280 nm) are attributed to the $\pi \rightarrow \pi^*$ transitions corresponding to the phenanthroline moiety of the ligands.

The low energy band at 452 nm (ε = 19670 $M^{-1}cm^{-1}$) and 457 nm (ε = 24070 $M^{-1}cm^{-1}$), are assigned as MLCT Ru(dπ) $\rightarrow$ aip/pyip(π^*) transition for the complexes $[Ru(phen)_2(aip)]^{2+}$ and $[Ru(phen)_2(pyip)]^{2+}$, respectively, typical of any Ru(II) polypyridyl complexes. The λ_{max} values for the MLCT transitions of these new complexes are bathochromically shifted in relation to the MLCT band of $[Ru(phen)_3]^{2+}$ (446 nm). $[Ru(phen)_2(pyip)]^{2+}$ shows a higher red shift by 5 nm compared to $[Ru(phen)_2(aip)]^{2+}$ due to the difference in π delocalization of the chromophore. The band centered at 254 and 264 nm for $[Ru(phen)_2(aip)]^{2+}$ and $[Ru(phen)_2(pyip)]^{2+}$ are attributed to the intra-ligand (IL) $\pi \rightarrow \pi^*$ transitions.

When aip is excited at 360 nm, the emission maxima appeared at 535 nm (ϕ = 0.81 in CH_3CN). In the case of pyip (excited at 330 nm), the emission maxima appeared at 494 nm (ϕ = 0.63 in CH_3CN). Steady-state and time-resolved absorption and fluorescence spectroscopic properties of aip, a bichromophoric molecule, reveals that a rapid and efficient intra-EET process dominates its excited-state relaxation dynamics in solution.[17] $[Ru(phen)_2(aip)]^{2+}$ and $[Ru(phen)_2(pyip)]^{2+}$ show an emission band each centered at 604 and 601nm with quantum yields of 0.005 and 0.0006, respectively in CH_3CN (λ_{exc} = 450 nm) (Fig. 4.3).

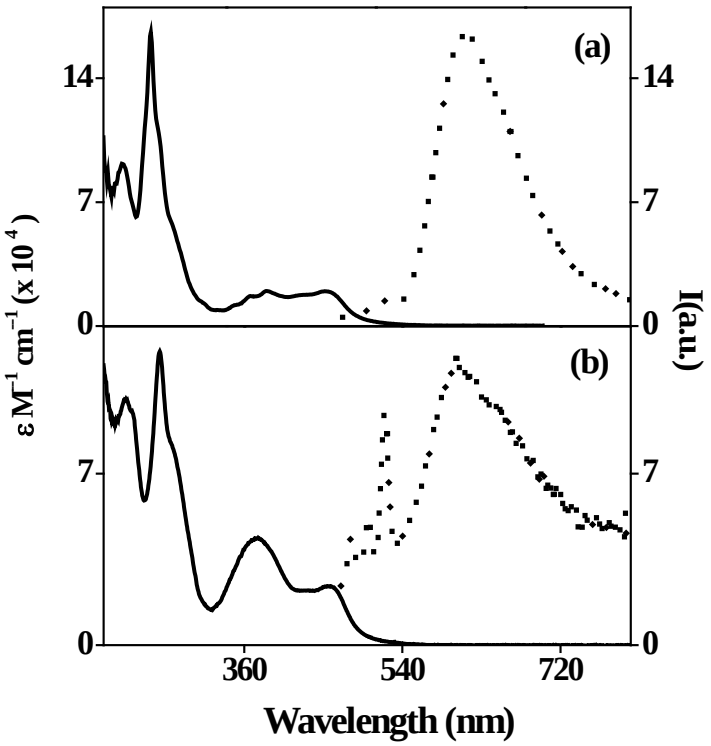

Fig. 4.3 UV-visible (——) and fluorescence (·····) spectra of $[Ru(phen)_2(aip)]^{2+}$ (a) and $[Ru(phen)_2(pyip)]^{2+}$ (b) in CH_3CN.

The origin of the spike at ~ 520 nm in the emission spectrum (Fig. 4.3b) is due to Raman scattering. Since $[Ru(phen)_2(pyip)]^{2+}$ is weakly fluorescent and the gain of the instrument is increased to compensate the low quantum yield (ϕ = 0.0006 in CH_3CN), the Raman scatter becomes visible. For highly fluorescent $[Ru(phen)_2(aip)]^{2+}$ (ϕ = 0.005 in CH_3CN), the emission spectra overwhelms the Raman peak and thus it is not observed. The spectral shape and the λ_{em} values are quite similar to those of $[Ru(phen)_2(dppz)]^{2+}$, the ^{3}MLCT emission band maximum of which has been reported to be located at 618 nm.[18]

Table 4.1 UV-visible and Emission spectral data in CH_3CN[a]

Compound	Absorbance λ_{max}, (logε)		Emission λ_{max}
	Ligand Transitions	MLCT	
phen	226 (4.71), 264 (4.55)	--	--
phen-dione	232 (3.82), 260 (3.81), 304 (3.64)	--	---
9-anthraldehyde	261 (4.29), 371 (3.15), 399 (3.16)	--	---
1-pyrenecarboxaldehyde	233 (4.70), 287 (4.57), 362 (4.44), 372 (4.42), 394 (4.33)	--	---
aip	251(4.94), 366 (3.89), 383 (3.88)	--	447, 535 (0.81)
pyip	234 (4.71), 280 (4.52), 368 (4.44)	--	411, 443, 494 (0.63)
$[Ru(phen)_3](PF_6)_2$	223 (4.93), 263 (5.07), 422 (4.25)	446 (4.28)	596 (0.028)
$[Ru(phen)_2(aip)](PF_6)_2$	221 (4.96), 254 (5.22), 385 (4.30)	452 (4.29)	604 (0.005)
$[Ru(phen)_2(pyip)](PF_6)_2$	376 (4.64), 264 (5.08), 225 (5.00)	457 (4.38)	601(0.0006)

a) Error limits: λ_{max} and $\lambda_{em.}$ ± 1 nm; log ε, ± 10%; ϕ, ± 10%

Emission quantum yields of these complexes (Table 4.1) investigated are lower than that of $[Ru(phen)_3]^{2+}$ (ϕ = 0.028 in CH_3CN)[19] and the order is $[Ru(phen)_3]^{2+}$ > $[Ru(phen)_2(aip)]^{2+}$ >> $[Ru(phen)_2(pyip)]^{2+}$.

4.3.3 Electrochemistry

The redox potential data, as measured by the differential-pulse voltammetric method, are summarized in Table 4.2. During the cathodic scans in the cyclic voltammetric experiments carried out in DMF containing 0.1 M TBAP, ligands aip and pyip showed reversible (i_{pc}/i_{pa} = 0.9 - 1.0) and diffusion controlled ($i_{pc}/\nu^{1/2}$ = constant in the scan rate (ν) range 50 - 500 mV s^{-1}) one-electron transfer (ΔE_p = 60 - 70 mV; ΔE_p = 65 ± 3 mV for Fc^+/Fc couple)[20] responses at -1.48 and –1.46 V (vs SCE), respectively. These potentials are close to those observed for the one-electron reductions of phen-dione (-1.47). The second reduction step appears as either quasi-reversible (i_{pc}/i_{pa} = 0.2 – 0.7 and ΔE_p = 90 - 200 mV in the scan rate (ν) over the range of 100 – 500 mV s^{-1}) or totally irreversible responses for aip and pyip at –1.61 and –1.64 V, respectively.

The oxidation of pyip occurs at +1.42 V where as for the aip, it occurs at +1.38 V. The oxidation potential shifts more positively for pyip when compared to aip due to the expanded π delocalization nature of pyrene moiety in the case of pyip when compared to anthracene in aip. The cyclic and differential-pulse voltammogram of the two new complexes are compared with that of $[Ru(phen)_3]^{2+}$ in Fig. 4.4. Each complex exhibits well shaped oxidation and reduction waves in the sweep range from –2.0 to + 1.6 V vs SCE containing 0.1 M TBAP. The complex $[Ru(phen)_2(aip)]^{2+}$ exhibits well shaped reversible oxidation wave (+1.43 V) in CH_3CN and three reduction waves -1.29, -1.49 and -1.96 V in DMF. The first two reduction waves are reversible and the last one at -1.96 V is of poorly shaped quasi-reversible one. For $[Ru(phen)_2(pyip)]^{2+}$, reversible oxidation wave at +1.47 V in CH_3CN and two reversible reduction waves at -1.21, -1.43 V are observed in DMF.

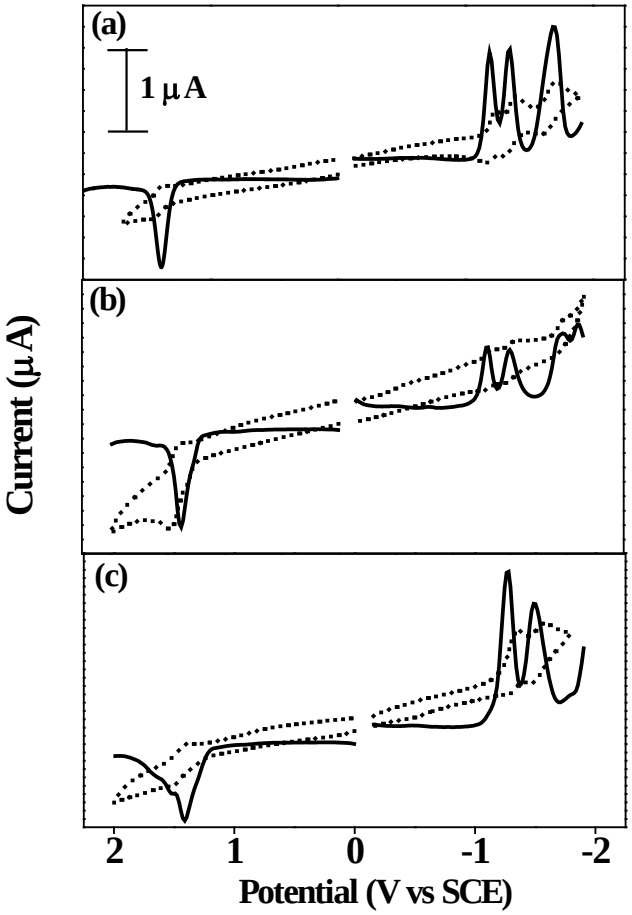

Fig. 4.4 Cyclic (·····) and differential-pulse voltammograms (——) of (a) $[Ru(phen)_3]^{2+}$, (b) $[Ru(phen)_2(aip)]^{2+}$ and (c) $[Ru(phen)_2(pyip)]^{2+}$. CH_3CN and DMF containing 0.1 M TBAP were used as solvents for the anodic and cathodic runs, respectively. Scan rate: 100 mV s^{-1}.

Oxidation of the complexes involves removal of an electron from the dπ orbital of Ru(II), while reduction involves transfer of an electron to the ligand (aip/pyip) centered orbitals.[5] As expected, the oxidation potential of $[Ru(phen)_2(pyip)]^{2+}$ is 40 mV more positive when compared to

$[Ru(phen)_2(aip)]^{2+}$. The attachment of the pyrene ring (extended hydrophobicity/aromaticity) to the ip(Imidazo-phenanthroline) moiety expands the π delocalization and thus decreases the σ donor capacity of pyip which leads to the decrease in the electron density on Ru(II) ion and in turn stabilizes the metal π (t_{2g}) orbital.[21]

Table 4.2 Redox potential data[a]

Compound	**Oxidation, $E_{1/2}$ (V vs SCE)**	**Reduction, $E_{1/2}$ (V vs SCE)**
phen	---	-1.92[d]
phen-dione	---	-0.45, -1.08[c]
9-anthraldehyde	+1.67[b]	-1.12[d]
pyrene	+1.49[c]	---
1-pyrenecarboxaldehyde	+1.64[b]	-1.27[d]
aip	+1.38[b]	-1.48, -1.61[d]
pyip	+1.42[b]	-1.46, -1.64[d]
$[Ru(phen)_3](PF_6)_2$	+1.37[c]	-1.19, -1.34, -1.69[d]
$[Ru(phen)_2(dppz)](PF_6)_2$	+ 1.41[c]	-0.82, -1.25, -1.47[d]
$[Ru(phen)_2(aip)](PF_6)_2$	+1.43[c]	-1.29, -1.49, -1.96[d]
$[Ru(phen)_2(pyip)](PF_6)_2$	+1.47[c]	-1.21, -1.43[d]

a) Obtained from the differential-pulse voltammetric measurements. Error limits: $E_{1/2} \pm 0.03$ V
b) CH_2Cl_2, 0.1 M TBAP
c) CH_3CN, 0.1 M TBAP
d) DMF, 0.1 M TBAP

As a result, oxidation potential shifts positively for $[Ru(phen)_2(pyip)]^{2+}$ when compared to $[Ru(phen)_2(aip)]^{2+}$. The first reduction in both the complexes are expected to be centered at aip/pyip because of the availability of the most

stable LUMO.[22] The other reductions observed for both complexes are characteristics of the ancillary phen ligands.[23] Thus in the case of $[Ru(phen)_2(aip)]^{2+}$, reductions at –1.29, -1.49 and -1.96 V are assigned to aip/aip$^{\cdot-}$, $phen_1$/ $phen_1^{\cdot-}$ and $phen_2$/ $phen_2^{\cdot-}$ couples, respectively. For $[Ru(phen)_2(pyip)]^{2+}$, the reduction at -1.21 and –1.43V are assigned to pyip/pyip$^{\cdot-}$ and $phen_1$/ $phen_1^{\cdot-}$ processes respectively. Here the second reduction associated with $phen_2$ could not be observed.

4.3.4 DNA binding experiments

Binding of the chloride salts of the two Ru(II) complexes synthesized in this study with CT DNA were monitored by absorption, fluorescence, thermal denaturation and viscosity methods and the results are summarized in this section, which also discusses on aspects related to the ability of these complexes to act as “molecular light switches” for DNA.

4.3.4.1 Absorption titration

Both $[Ru(phen)_2(aip)]^{2+}$ and $[Ru(phen)_2(pyip)]^{2+}$ are titrated with CT DNA. The change in the spectral profiles during titration is shown in Fig. 4.5a and Fig. 4.5b. As the DNA concentration is increased, $[Ru(phen)_2(aip)]^{2+}$ and $[Ru(phen)_2(pyip)]^{2+}$ showed hypochromicity (39% and 61%) and isosbestic points (482 and 496 nm) along with the bathochromic shifts of 6 and 9 nm respectively. To compare quantitatively the affinity of the two complexes towards DNA, the intrinsic binding constant values (K_b) were determined by monitoring the absorbance at the MLCT band position and are evaluated as high as 1.01 x 10^6 and 1.57 x 10^6 M^{-1} for $[Ru(phen)_2(aip)]^{2+}$and $[Ru(phen)_2(pyip)]^{2+}$, respectively (Table 4.3).

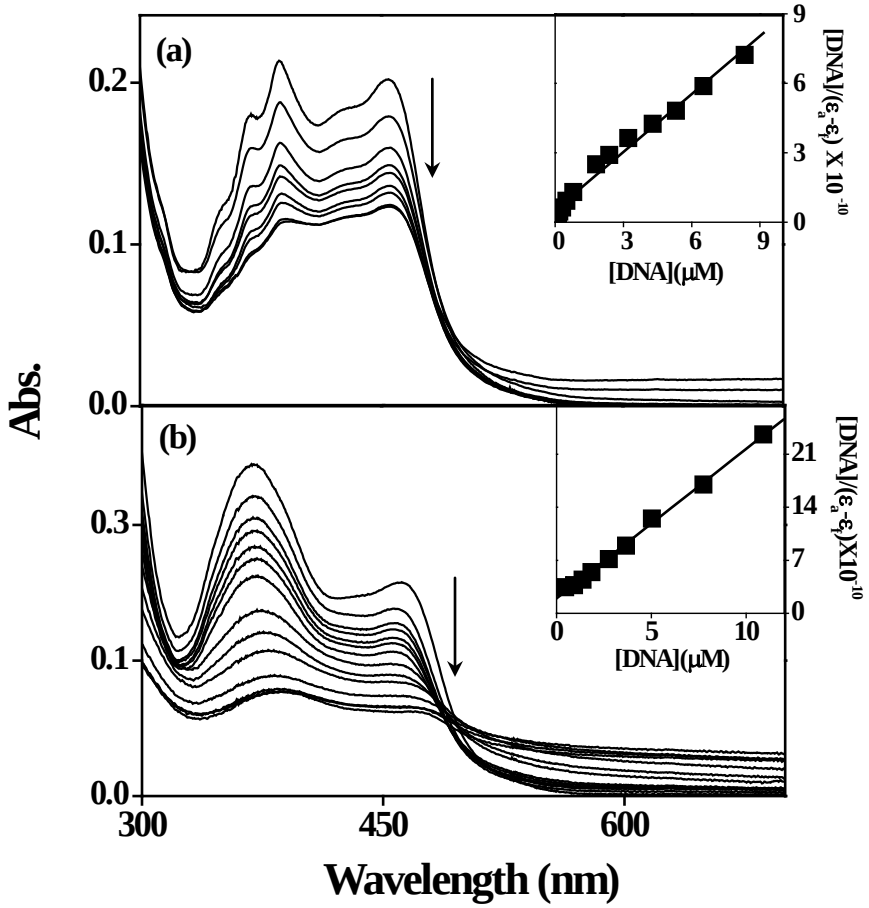

Fig. 4.5 UV-visible spectra of (a) $[Ru(phen)_2(aip)]^{2+}$ (5 μM) and (b) $[Ru(phen)_2(pyip)]^{2+}$ (5 μM) in the absence (top curve) and presence (subsequent curves) of increasing concentrations (0 – 100 μM) of CT DNA in buffer A. The inset graphs show the fits of the absorbance data to obtain the binding constants.

The extent of hypochromism commonly parallels to the intercalative strength of the ligand and moreover higher planar area, extended π system,

hydrophobicity and aromaticity lead to the deep penetration and hence more stacking within the base pairs of DNA. Thus the intercalative strength follows the order, $[Ru(phen)_2(dppz)]^{2+} \approx [Ru(ip)_2(dppz)]^{2+} \geq [Ru(phen)_2(pyip)]^{2+} > [Ru(phen)_2(aip)]^{2+} > [Ru(phen)_3]^{2+}$ where ip = imidazo[4,5-f][1,10]phenanthroline.[6]

4.3.4.2 Fluorescence titration

Steady state emission spectra of 7 μM solutions of $[Ru(phen)_2(aip)]^{2+}$ and $[Ru(phen)_2(pyip)]^{2+}$ in tris buffer (5 mM Tris, 50 mM NaCl, pH 7.1) showed an increase in the emission intensity with successive addition of CT DNA. In the case of $[Ru(phen)_2(aip)]^{2+}$, the emission maxima at 604 nm due to the ^{3}MLCT ($d\pi(Ru)\rightarrow\pi^*(aip)$)[19] state increases initially at low [DNA nucleotide phosphate]/[Ru] ratio but, reaches a plateau with the apparent enhancement factor of ~ 5 at higher [DNA nucleotide phosphate]/[Ru] ratio of 27. The complex had an appreciable emission in the buffer in the absence of DNA and had showed marginal red shift of 2 nm on addition of DNA (Fig. 4.6a). The fluorescence due to $[Ru(phen)_2(pyip)]^{2+}$ at 601 nm is assigned as ^{3}MLCT ($d\pi(Ru)\rightarrow\pi^*(pyip)$) state which increases steadily with increasing addition of CT DNA and reaches a maximum (~ 9 times) at [DNA nucleotide phosphate]/[Ru] ratio of 43 (Fig. 4.6b). The complex has very weak emission in the aqueous medium in the absence of DNA, but on addition of increasing amount of DNA the emission intensity increases with a bathochromic shift of about 4 nm. The emission enhancement of both the complexes in presence of DNA are much smaller than observed for the normal dppz based Ru(II) polypyridyl based intercalators reported by Barton *et al*.[18,24,25] The shielding of the nitrogens on the intercalating ligands especially imidazole nitrogens from protonation in the bulk solvent medium causes

emission enhancement and it has been extensively characterized and described as the “molecular light switch”.[18,24,25]

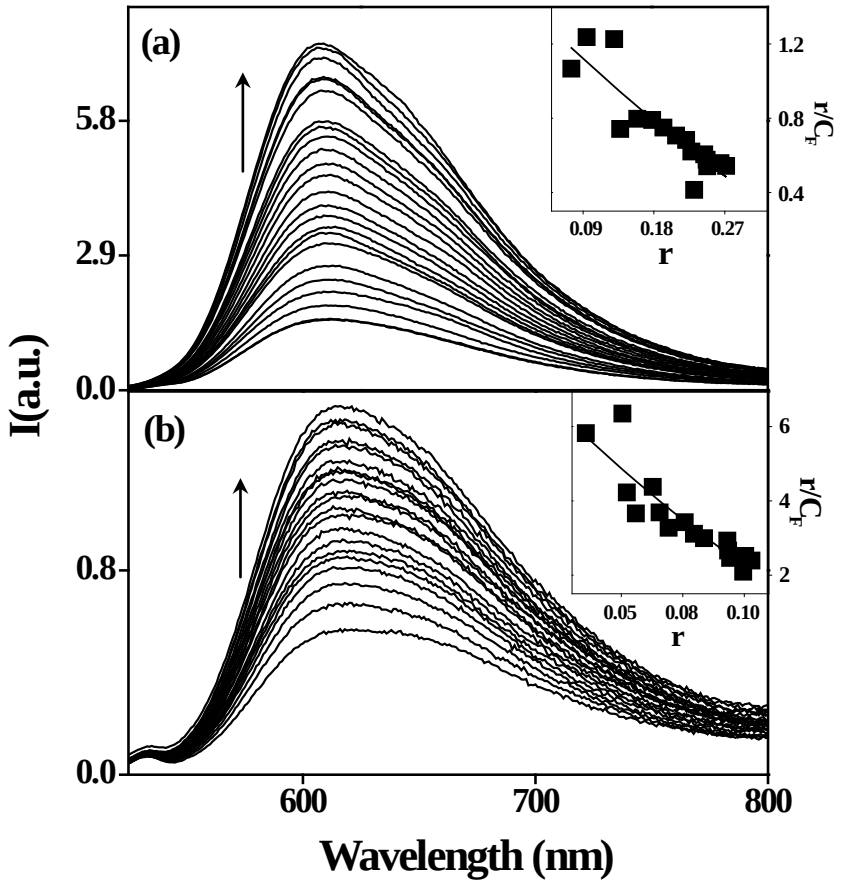

Fig. 4.6 Fluorescence spectra of (a) $[Ru(phen)_2(aip)]^{2+}$ (7 μM) and (b) $[Ru(phen)_2(pyip)]^{2+}$ (7 μM) in the absence (bottom curve) and presence (subsequent curves) of increasing concentrations (0 – 300 μM) of CT DNA in buffer A (λ_{exc} = 450 nm). The inset graphs show the fits of the emission data to equn. 4 (Chapter 2).

The mobility of these complexes is restricted at the binding site and so the vibrational modes of relaxation (collision and discipation) decreases on intercalation.[5] The binding constants obtained are reasonably well in agreement with the values from the absorption titration experiment. The binding site sizes (n) for $[Ru(phen)_2(aip)]^{2+}$ and $Ru(phen)_2(pyip)]^{2+}$ are evaluated as 2 and 3 respectively.

4.3.4.3 DNA melting experiments

Other strong evidence for the intercalation of both the complexes into the helix was obtained from the DNA melting studies. Intercalation of small molecules into the double helix is known to increase the helix melting temperature, the temperature at which the double helix denatures into single-stranded DNA.[26] The extinction coefficient of DNA bases at 260 nm in the double-helical form is much less than in the single-stranded form; hence, melting of the helix leads to an increase in the absorption at this wavelength.[27]

CT DNA was seen to melt at 61 ± 1 ^oC (in buffer B) in the absence of any added complex. The T_m of DNA is increased by 4 and 5 ^oC in the presence of $[Ru(phen)_2(aip)]^{2+}$ and $[Ru(phen)_2(pyip)]^{2+}$ (at [DNA nucleotide phosphate] /[Ru] = 25), respectively. The DNA melting curves in the absence and in the presence of both the complexes are presented in Fig. 4.7. The T_m and the σ_T values of CT DNA in the absence and in the presence of the complexes are tabulated in Table 4.3. These data establish the increased stability of the double helix when $[Ru(phen)_2(aip)]^{2+}$ and $[Ru(phen)_2(pyip)]^{2+}$ bind DNA. These increases in the melting temperatures are comparable to the values observed with the classical intercalator EtBr and lend strong support for the intercalation of the complexes in to the helix.[27,28]

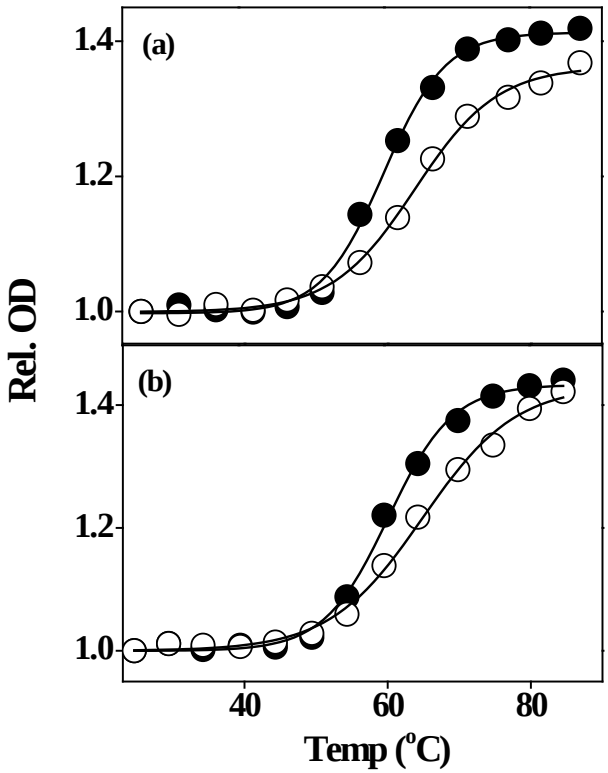

Fig. 4.7 Melting curves for CT DNA in the absence (●) and in the presence (○) of (a) $[Ru(phen)_2(aip)]^{2+}$ and (b) $[Ru(phen)_2(pyip)]^{2+}$ in buffer B.

Table 4.3 Results of absorption titration and thermal melting experiments[a]

Compound	K_b (M^{-1})	T_m °C (σ_T °)
DNA	--	61 (19)
$[Ru(phen)_3]^{2+}$	8.24×10^3	62 (21)
$[Ru(phen)_2(aip)]^{2+}$	1.01×10^6	64 (28)
$[Ru(phen)_2(pyip)]^{2+}$	1.57×10^6	65 (25)
$[Ru(phen)_2(dppz)]^{2+}$	$> 10^7$	65 (26)

a) Error limits: K_b, ± 10%; T_m, ±1 °C; σ_T, ±1 °

4.3.4.4 Viscometric titration

Intercalation of a ligand in to the DNA is known to cause a significant increase in the viscosity of DNA solution due to an increase in the separation of the base pairs at the intercalation site and, hence, an increase in the overall DNA molecular length (contour length). In contrast, a ligand that binds in the DNA grooves causes a less pronounced change (positive or negative) or no change in the viscosity of a DNA solution.[29] The effects of $[Ru(phen)_2(aip)]^{2+}$, $[Ru(phen)_2(pyip)]^{2+}$, EtBr and $[Ru(phen)_3]^{2+}$ on the viscosity of CT DNA solution have been studied in order to assess the binding mode of these complexes with DNA. Plots of $(\eta/\eta_o)^{1/3}$ vs [Drug]/[DNA] ratio are constructed, Fig. 4.8.

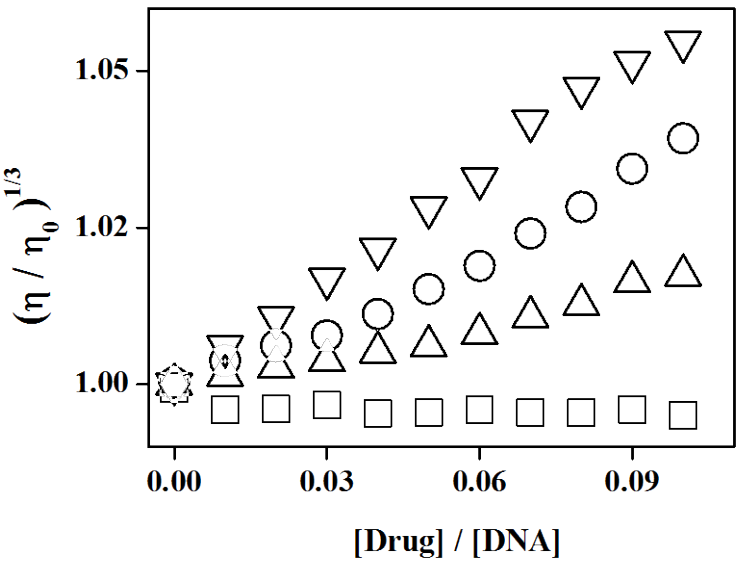

Fig. 4.8 Results of viscometric titrations carried out for CT DNA (300 μM) in the presence of $[Ru(phen)_3]^{2+}$ (□), $[Ru(phen)_2(aip)]^{2+}$ (Δ), $[Ru(phen)_2(pyip)]^{2+}$ (○) and EtBr (∇) in buffer C.

The viscosity of DNA bound with complexes $[Ru(phen)_2(aip)]^{2+}$, $[Ru(phen)_2(pyip)]^{2+}$ and EtBr increases dramatically, indicating that both complexes as well as the classical intercalator EtBr, intercalate between the base pairs of DNA and that $[Ru(phen)_2(pyip)]^{2+}$ has a considerably stronger binding affinity in comparison with that of $[Ru(phen)_2(aip)]^{2+}$. However, addition of complex $[Ru(phen)_3]^{2+}$ has no effect on the DNA viscosity as previously reported.[29]

4.3.5 DNA photocleavage

When circular plasmid DNA is subjected to electrophoresis, relatively fast migration will be observed for the supercoiled form (Form I). If scission occurs on one strand (nicking), the supercoils will relax to generate a slower-moving open circular form (Form II). DNA photocleavage experiments were carried out with both the complexes along with $[Ru(phen)_3]^{2+}$ (for comparison). The Fig. 4.9 summarizes the results. Control runs in the agarose gel electrophoresis experiments suggested that untreated pBR 322 DNA does not show any cleavage in the dark and even upon irradiation by a 450 ± 5 nm light (compare lanes 1 and 2 in Fig. 4.9). Lesser activity is observed for pBR 322 treated with $[Ru(phen)_2(aip)]^{2+}$, $[Ru(phen)_2(pyip)]^{2+}$, and $[Ru(phen)_3]^{2+}$ in the dark experiments (Lanes 3, 5 and 7, Fig. 4 9). Upon 60 min. irradiation (Lanes 4 ,6 and 8, Fig. 4.9), single strand nicking is observed and the percentage of conversions from form I to form II using the equn. 2.5 (Chapter 2) are also calculated. Based on the % of conversion from form I to form II for these complexes, DNA nicking efficiencies is seen to roughly follow the trend: $[Ru(phen)_2(pyip)]Cl_2$ > $[Ru(phen)_2(aip)]Cl_2$ > $[Ru(phen)_3]Cl_2$. These can be explained on the basis of the binding nature of the intercalating ligands in the

complexes due to the extended π aromatic nature in the case of pyip when compared to aip.

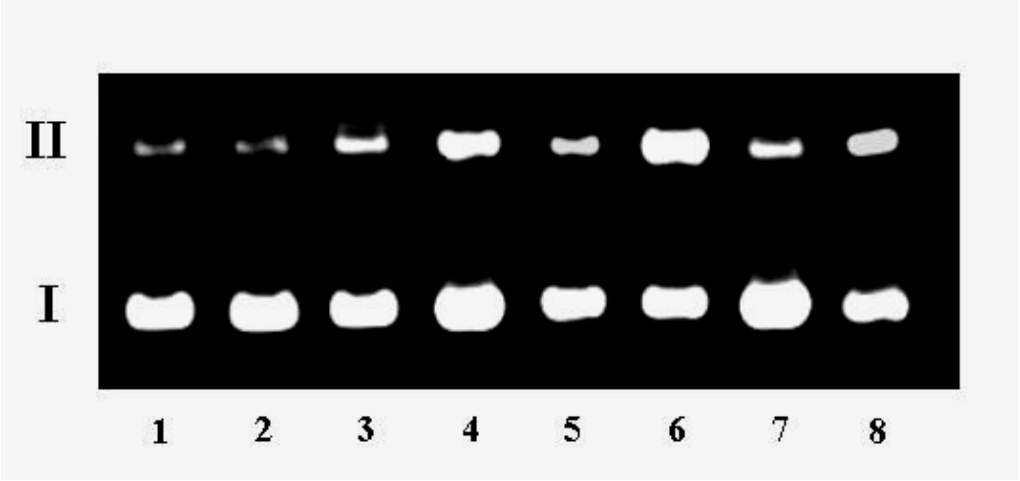

Fig. 4.9 Light-induced nuclease activities of the investigated ruthenium(II) complexes. Dark and Light Experiments: Lanes 1 and 2: Untreated pBR 322 (100 μM) in the dark and upon irradiation. Lanes 3, 5, and 7: pBR 322 + $[Ru(phen)_2(aip)]^{2+}$, $[Ru(phen)_2(pyip)]^{2+}$ and $[Ru(phen)_3]^{2+}$ respectively (10 μM) in dark. Lanes 4, 6 and 8: pBR 322 + $[Ru(phen)_2(aip)]^{2+}$, $[Ru(phen)_2(pyip)]^{2+}$ and $[Ru(phen)_3]^{2+}$ respectively, upon irradiation. $\lambda_{irrd.}$= 450 ± 5 nm (60 min.) in each case.

The photocleavage efficiency of these complexes are also comparable with that of $[Ru(bpy)_2(ip)]^{2+}$ and $[Ru(bpy)_2(pip)]^{2+}$ where (ip = imidazo[4,5-f][1,10]phenanthroline, pip = 2-phenylimidazo[4,5-f][1,10]phenanthroline, bpy = 2,2'-bipyridine) reported in the literature.[5]

In attempts to unravel the probable DNA photocleavage mechanism of these new complexes, a few control experiments have been conducted in the

presence of various 'inhibitors'. Photocleavage by $[Ru(phen)_3]Cl_2$ has been reported[30] to involve $^1O_2$ - based mechanism. In the case of $[Ru(phen)_2(aip)]^{2+}$ (Fig. 4.10) irradiating for 60 min, DABCO (Lane 5) - a $^1O_2$ 'quencher', and tiron (Lane 7) (superoxide anion radical quencher) are not inhibiting the photocleavage mechanism. Purging the reaction mixture with N_2, lane 3 (15 min. to remove O_2) was not found to inhibit the photocleavage mechanism. Inhibition was seen in the presence of DMSO (Lane 4) and mannitol (Lane 6). In fact, mannitol acts as a better inhibitor when compared to DMSO. Both DMSO and mannitol are acting as the scavengers for hydroxyl radicals.

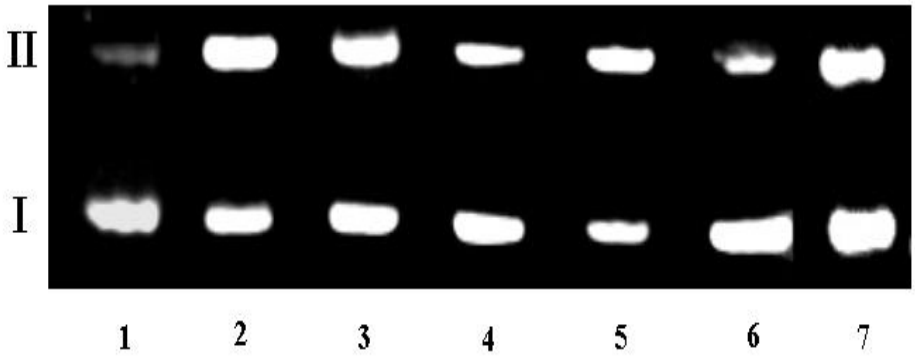

Fig. 4.10 Effects of 'inhibitors' on the light-induced nuclease activity of $[Ru(phen)_2(aip)]^{2+}$. Lane 1: pBR 322, Lane 2: pBR 322 + $[Ru(phen)_2(aip)]^{2+}$. Lanes 3-7: pBR 322 + $[Ru(phen)_2(aip)]^{2+}$ in the presence of N_2, DMSO (200 mM), DABCO (10mM), mannitol (100 mM) and tiron (10 mM) respectively, upon irradiation for 60 min. at 450 ± 5 nm in each case.

In the case of $[Ru(phen)_2(pyip)]^{2+}$ (Bar diagram in Fig. 4.11) irradiation at 60 min, shows moderate activity in presence of N_2, DABCO and in DMSO. No

effect is observed when using N_2 and tiron. It inhibits enormously when mannitol is used as inhibitor. These results suggest that the reactive oxygen species ($OH^{\bullet}$) and singlet oxygen (to a lesser extent) may play a significant role in the cleavage mechanism for $[Ru(phen)_2(pyip)]Cl_2$ whereas for $[Ru(phen)_2(aip)]Cl_2$, only hydroxyl radical ($OH^{\bullet}$) plays a role in the photocleavage mechanism.[31]

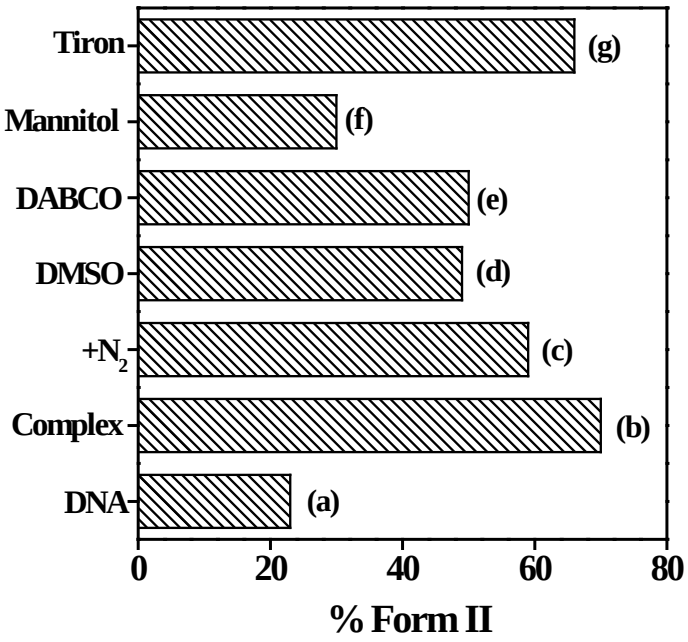

Fig. 4.11 Bar diagram representation of the effects of 'inhibitors' on the light-induced nuclease activity of $[Ru(phen)_2(pyip)]^{2+}$. **(a)** DNA control: **(b)** pBR 322 + $[Ru(phen)_2(pyip)]^{2+}$ (**c-g**): pBR 322 + $[Ru(phen)_2(pyip)]^{2+}$ in the presence of N_2, DMSO (200 mM), DABCO (10mM), mannitol (100 mM) and tiron (10mM) respectively, upon irradiation for 60 min. at 450 ± 5 nm in each case.

4.4 Summary

Two new anthracene/pyrene chromophore appended polypyridyl ligands, aip and pyip and their mixed-ligand ruthenium(II) complexes, $[Ru(phen)_2(aip)]^{2+}$ and $[Ru(phen)_2(pyip)]^{2+}$, have been synthesized and fully characterized by spectroscopic and electrochemical methods. Studies with DNA have revealed that these complexes bind to DNA, mainly, *via* an intercalative mode with moderate strengths. The observation that $[Ru(phen)_2(pyip)]^{2+}$ binds DNA more strongly than $[Ru(phen)_2(aip)]^{2+}$ suggests that increased surface area available for stacking by this complex within the duplex leads to a substantial increase in its intercalative binding affinity. In accordance with this interpretation, $[Ru(phen)_2(pyip)]^{2+}$ is found to be a better "molecular light switch" for DNA than $[Ru(phen)_2(aip)]^{2+}$. The photonuclease activity is also higher for $[Ru(phen)_2(pyip)]^{2+}$ than $[Ru(phen)_2(aip)]^{2+}$ and is comparable to that of $[Ru(bpy)_2(ip)]^{2+}$ and $[Ru(phen)_3)]^{2+}$. Moreover the reactive oxygen species ($OH^{\bullet}$) plays a significant role in the cleavage mechanism of both $[Ru(phen)_2(pyip)]Cl_2$ and $[Ru(phen)_2(aip)]Cl_2$.

4.5 References

1. Xiong Y.; Ji, L-N. *Coord. Chem. Rev*. **1999**, *185-186*, 711.
2. Ji, L-N.; Zou, X-H.; Liu, J-G. *Coord. Chem. Rev*. **2001**, *216-217*, 513.
3. Zhen, Q-Z.; Ye, B-H.; Zhang, Q-L.; Liu, J-G.; Li, H.; Ji, L-N.; Wang, L. *J. Inorg. Biochem*. **1999**, *76*, 47.
4. Wu, J- Z.; Li, L.; Zeng, T-X.; Ji, L- N.; Zhou, J-Y.; Luo T.; Li, R-H. *Polyhedron* **1997**, *16*, 103.
5. Wu, J-Z.; Ye, B-H.; Wang, L.; Ji, L-N.; Zhou, J-Y.; Li, R-H.; Zhou, Z-Y. *J. Chem. Soc., Dalton Trans.* **1997,** 1395.
6. Liu, J-G.; Zhang, Q-L.; Shi, X-F.; Ji, L- N. *Inorg. Chem.* **2001**, *40*, 5045.

7. Xu, H.; Zheng, K-C.; Chen, Y.; Li, L- Y-Z.; Lin, J.; Li, H.; Zhang, P-X.; Ji, L-N. *J. Chem. Soc., Dalton Trans.* **2003**, 2260.
8. Xu, V.; Zheng, K-C.; Deng, H.; Lin, L-J.; Zhang, Q-L.; Ji, L-N. *New J. Chem*. **2003**, *27*, 1255.
9. Steck, E. A.; Day, A. R. *J. Am. Chem. Soc*. **1943**, *65*, 452.
10. Arounaguiri, S.; Maiya, B. G. *Inorg. Chem.* **1999**, *38*, 842.
11. Ambroise, A. ; Maiya, B. G. *Inorg. Chem.* **2000**, *39*, 4256.
12. Ambroise, A. ; Maiya, B. G. *Inorg. Chem.* **2000**, *39*, 4264.
13. Didier, P.; Jacquet, L.; Mesmaeker, A. K-D.; Hueber, R.; Dorsselaer, A. V. *Inorg. Chem.* **1992**, *31*, 4803.
14. (a) wang, R.; Vos, J. G.; Schmehl, R. H.; Hage, R. *J. Am. Chem. Soc*. **1992**, *114*, 1964. (b) Tan, L-F.; Chao, H.; Li, H.; Liu, Y-J.; Sun, B.; Wei, W.; Ji, L-N. *J. Inorg. Biochem*. **2005**, *99*, 513.
15. Kumar, C. V.; Punzalan, E. H. A.; Tan, W. B. *Tetrahedron* **2000**, *56*, 7027.
16. Tyson, D. S.; Bialecki, J.; Castellano, F. N. *Chem. Commun*. **2000**, 2355.
17. Mondal, J. A.; Ramakrishna, G.; Singh, A. K.; Ghosh, H. N.; Mariappan, M.; Maiya, B. G.; Mukherjee, T.; Palit. D. K. *J. Phys. Chem. A.* **2004**, *108*, 7843.
18. Hartshorn, R. M.; Barton, J. K. *J. Am. Chem. Soc.* **1992**, *114*, 5919.
19. Juris, A.; Balzani, V.; Barigelletti, F.; Campagna, S.; Belser, P.; Zelewsky, A. V. *Coord. Chem. Rev*. **1988**, *84*, 85.
20. Nicholson, R. S.; Shain, I. *Anal. Chem*. **1964**, *36*, 706.
21. Rillema, D. P.; Allen, G.; Meyer, T. J.; Conrad, D. C. *Inorg. Chem*. **1983**, *22*, 1617.
22. Ghosh, B. K.; Chakravorty, A. *Coord. Chem. Rev.* **1989**, *95*, 239.

23. Delaney, S.; Pascaly, M.; Bhattacharya, P. K.; Han, K.; Barton, J. K. *Inorg. Chem*. **2002**, *41*, 1966.
24. Dupureur, C. M.; Barton, J. K. *J. Am. Chem. Soc.* **1994**, *116*, 10286.
25. Friedman, A. E.; Chambron, J-C.; Sauvage, J-P.; Turro, N. J.; Barton, J. K. *J. Am. Chem. Soc.* **1990**, *112*, 4960.
26. Patel, D. J. *Acc. Chem. Res.***1979**, *12*, 118.
27. Lehninger, A. L. *Biochemistry,* 2nd *ed.;* Worth Publishers: New York, **1975**; p 873.
28. Kumar, C. V.; Asuncion, E. H. *J. Am. Chem. Soc.* **1993**,*115*, 8547.
29. Satyanarayana, S.; Dabrowiak, J. C.; Chaires, J. B. *Biochemistry* **1992**, *31*, 9319.
30. Kelly, J. M.; Tossi, A. B.; McConnell, D. J.; OhUigin, C. *Nucl. Acid. Res*. **1985**, *13*, 6017.
31. Armitage, B. *Chem. Rev*. **1998**, *98*, 1171.

CHAPTER 5

A New Metallointercalator Containing Dipyridophenazine Ligand Endowed with an Acridine Subunit

5.1 Introduction

DNA metallointercalators of the type $[Ru(L)_2(dppz)]^{2+}$, (L = 2,2'-bipyridine (bpy) and 1,10-phenanthroline (phen), dppz = dipyrido[3,2-a:2',3'-c]phenazine) have shown strong binding affinity towards DNA and cause the "molecular light switch" effect, where the nearly undetectable emission from the triplet metal to ligand charge transfer (MLCT) excited state of $[Ru(L)_2(dppz)]^{2+}$ in H_2O is strongly enhanced due to the intercalation of the planar dppz ligand between the base pairs of DNA.[1-4] In our efforts to design metal complexes coordinated to ligands having planar, aromatic subunits, we have recently reported[5-8] a series of complexes containing modified phen/dppz ligands. These new ligands have been so designed that besides containing the expansively aromatic 'dppz' type of structure, they are also endowed with electroactive subunits that impart special properties of the complexes in the presence of DNA.

The interaction of small aromatic heterocyclic molecules such as acridine and its derivatives with DNA and RNA are well established. The possibilities of their various modes of action at both molecular and cellular level are expected to display different photochemical and pharmacological properties including antitumor activities.[9-12] Thus, we have focused on the construction of novel polypyridyl ligands containing both the dppz and acridine subunits in their architecture. This chapter presents synthesis, characterization, crystal structure, DNA binding and photocleavage properties of a novel mixed-ligand ruthenium(II) complex, $[Ru(phen)_2(acdppz)]^{2+}$ where acdppz is 11-(9-

acridinyl)dipyrido[3,2-a:2’,3’-c]phenazine - a dppz based ligand that incorporates an acridine chromophore in its architecture.

5.2 Experimental section

1,10-phenanthroline-5,6-dione, 9-(3,4-diaminophenyl)acridine (daa), $[Ru(phen)_3]^{2+}$ and $[Ru(phen)_2Cl_2]\cdot 2H_2O$ were synthesized by following the reported procedures as described in chapter 2. Syntheses of the new ligand acdppz and its corresponding mixed-ligand ruthenium(II) complex, $[Ru(phen)_2(acdppz)]^{2+}$, are described below.

5.2.1 11-(9-acridinyl)dipyrido[3,2-a:2’,3’-c]phenazine (acdppz)

A mixture of phen-dione (0.50 g, 2.40 mmol), 9-(3,4-diaminophenyl)acridine (0.82 g, 2.90 mmol) and C_2H_5OH (50 mL) were refluxed for 4 h. The solution was cooled to room temperature to yield the yellow solid of acdppz, which was suction filtered and recrystalized from $CHCl_3$ - acetone (7:3, v/v). Yield = 0.85 g (78%).

Analytical data: Found: C, 81.11; H, 3.84; N, 15.19; Calc. for $C_{31}H_{17}N_5$: C, 81.03; H, 3.73; N, 15.24; FAB-MS (m/z): 460 (M^+); IR (KBr): 3418, 3047, 1514, 1473, and 756 cm^{-1}. ^1H NMR ($CDCl_3$, 200 MHz, TMS) δ, ppm: 9.68(d, 1H), 9.56(d, 1H), 9.25(dd, 2H), 8.52(d, 1H), 8.46(s, 1H), 8.31(d, 2H), 7.78(d, 1H), 7.75(m, 6H), 7.69(q, 2H).

5.2.2 Bis-(1,10-phenanthroline)(11-(9-acridinyl)dipyrido[3,2-a:2,3c]phenazine)ruthenium(II) hexafluorophosphate dihydrate, $[Ru(phen)_2(acdppz)](PF_6)_2\cdot 2H_2O$

This complex was synthesized by refluxing acdppz (0.39 g, 0.85 mmol) with $[Ru(phen)_2Cl_2]\cdot 2H_2O$ (0.40 g, 0.71 mmol) in C_2H_5OH - H_2O (2:1, v/v)

mixture for 4 h. The crude complex was obtained on adding saturated solution of NH_4PF_6. It was purified by column chromatography (alumina, CH_3CN - toluene (3:2, v/v) mixture) and was further recrystallized from acetone-ether mixture (1:5, v/v). Yield = 0.41 g (47%).

Analytical data: Found: C, 52.86; H, 2.91; N, 10.26; Calc. for $C_{55}H_{37}N_9O_2F_{12}P_2Ru$: C, 52.95; H, 2.97; N, 10.11; FAB-MS (m/z): $[M - PF_6^-]^+$, 1067; $[M - 2PF_6^{2-}]^+$, 922; IR (KBr): 3638, 1626, 1427, 839, 557 cm^{-1}. ^1H NMR ($(CD_3)_2SO$, 200 MHz, TMS) δ, ppm: 9.66(d, 1H), 9.31(d, 1H), 8.84(m, 7H), 8.44(m, 7H), 8.27(d, 1H), 8.12(t, 3H), 7.92(m, 9H), 7.59(q, 2H), 7.50(q, 2H).

The chloride salt of $[Ru(phen)_2(acdppz)]^{2+}$ was obtained by dissolving the above hexafluorophosphate complex in minimum amount of acetone and by precipitating upon addition of a saturated solution of TBACl in acetone. The recovery was about 90% of theoretical yield.

All the spectroscopic, electrochemical and biochemical experiments were carried out as described in chapter 2.

5.3 Results and discussion

5.3.1 Synthesis

The scheme leading to the synthesis of acdppz and $[Ru(phen)_2(acdppz)]^{2+}$ is given in Fig. 5.1. The ligand acdppz was prepared by the condensation of 1,10-phenanthroline-5,6-dione and 9-(3,4-diaminophenyl)acridine in C_2H_5OH. $[Ru(phen)_2(acdppz)]^{2+}$ was prepared from the precursor $[Ru(phen)_2Cl_2]\cdot 2H_2O$ and acdppz in C_2H_5OH-H_2O. The ligand acdppz and its Ru(II) complex have been characterized by X-ray diffraction, CHN, IR, UV-visible, fluorescence, FAB-MS and ^1H NMR spectroscopic methods. The mass spectrum of acdppz showed the base peak at 460 (M^+). In the case of $[Ru(phen)_2(acdppz)]^{2+}$, peaks were seen at

1067 (M - PF_6^-) and at 922 (M - $2PF_6^{2-}$) corresponding to the removal of two PF_6^- counter anions.

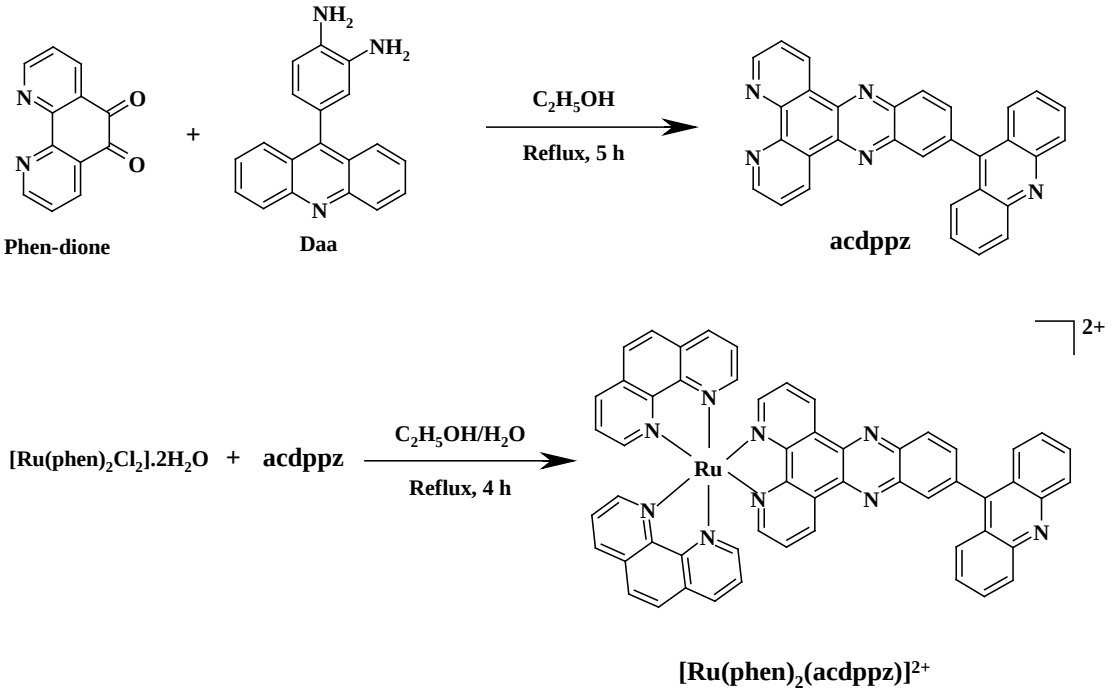

Fig. 5.1 Scheme leading to the synthesis of acdppz and $[Ru(phen)_2(acdppz)]^{2+}$.

5.3.2 Crystal structure

Slow evaporation of a DMF solution of acdppz and that of an CH_3CN/toluene (1:1) solution of $[Ru(phen)_2(acdppz)](PF_6)_2$ provided the single crystals of the respective compounds. Crystal parameters and details of the data collection and refinement for acdppz and $[Ru(phen)_2(acdppz)](PF_6)_2$ are given in Table 5.1. Selected bond lengths (Å) and bond angles (^{o}) for acdppz and $[Ru(phen)_2(acdppz)](PF_6)_2$ are given in the Appendix I, (Table 3) and Table 5.2 respectively. Atomic coordinates and equivalent isotropic displacement parameters for both acdppz and $[Ru(phen)_2(acdppz)](PF_6)_2$ are presented in

Appendix I(Table 2 and Table 4) respectively. The structures of acdppz and $[Ru(phen)_2(acdppz)]^{2+}$ are illustrated in Fig. 5.2 and Fig. 5.3, respectively.

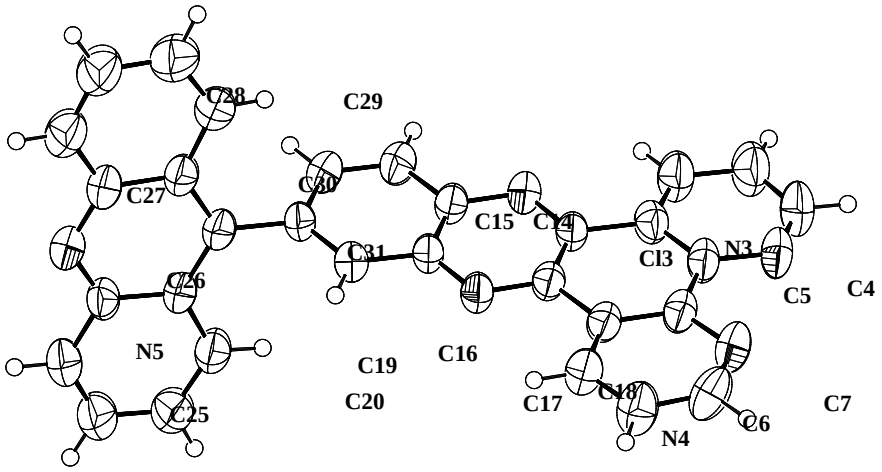

Fig. 5.2 Molecular structure of acdppz with the atom-labeling scheme. All non-hydrogen atoms are represented by their 50% probability thermal ellipsoids.

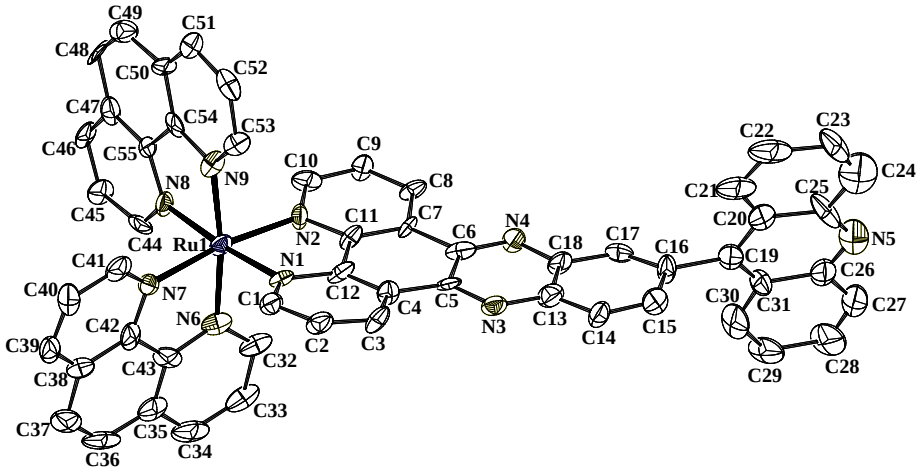

Fig. 5.3 The structure of one of the two $[Ru(phen)_2(acdppz)]^{2+}$ present in the asymmetric unit. The atoms are represented by their 50% probability thermal ellipsoids. Hydrogen atoms are omitted for clarity.

Table 5.1 Crystallographic data for acdppz and $[Ru(phen)_2(acdppz)](PF_6)_2 \cdot 2H_2O$

	acdppz	**$[Ru(phen)_2(acdppz)](PF_6)_2 \cdot 2H_2O$**
Chemical formula	C31 H17 N5	C55 H37 F12 N9 O2 P2 Ru
Formula weight	459.50	1246.96
Crystal system	Triclinic	Triclinic
Space group	$P\bar{1}$	$P\bar{1}$
a (Å)	8.5784(9)	11.8720(13)
b (Å)	8.9833(10)	21.470(2)
c (Å)	15.6576(17)	22.119(2)
α (°)	73.908(2)	89.991(2)
β (°)	78.427(2)	75.167(2)
γ (°)	77.002(2)	75.778(2)
V (Å^3)	1117.2(2)	5271.1(10)
Z	2	4
μ (mm^{-1})	0.083	0.453
F (000)	476	2512
Crystal size (mm^3)	0.21 x 0.19 x 0.12	0.35 x 0.31 x 0.04
Reflections collected	13118	61352
Reflections unique	5237[R(int) = 0.0471]	24580[R(int)=0.2900]
Parameters	325	1478
*R*1, *wR*2 [$I \geq 2\sigma(I)$]	0.0705, 0.1897	0.1344, 0.2410
*R*1, *wR*2 (all data)	0.1829, 0.2475	0.3744, 0.3401
Goodness-of-fit on F^2	0.986	0.954
Largest peak, hole [*e* Å^{-3}]	0.576, -0.185	1.179, -0.839

Table 5.2 Selected Bond lengths [Å] and angles [^{o}] for $[Ru(phen)_2(acdppz)]^{2+}$

Complex cation (1)		**Complex cation (2)**	
Ru(1)-N(1)	2.040(9)	Ru(2)-N(1A)	2.061(11)
Ru(1)-N(9)	2.040(10)	Ru(2)-N(9A)	2.060(11)
Ru(1)-N(7)	2.045(9)	Ru(2)-N(7A)	2.049(11)
Ru(1)-N(6)	2.048(10)	Ru(2)-N(6A)	2.050(10)
Ru(1)-N(8)	2.051(9)	Ru(2)-N(8A)	2.079(13)
Ru(1)-N(2)	2.065(9)	Ru(2)-N(2A)	2.079(11)
N(1)-Ru(1)-N(9)	92.1(4)	N(9A)-Ru(2)-N(1A)	92.6(4)
N(1)-Ru(1)-N(7)	174.7(4)	N(7A)-Ru(2)-N(9A)	93.7(4)
N(9)-Ru(1)-N(7)	92.2(4)	N(6A)-Ru(2)-N(9A)	171.3(4)
N(1)-Ru(1)-N(6)	95.5(4)	N(7A)-Ru(2)-N(1A)	172.2(4)
N(9)-Ru(1)-N(6)	171.5(4)	N(6A)-Ru(2)-N(1A)	93.9(4)
N(7)-Ru(1)-N(6)	80.5(4)	N(7A)-Ru(2)-N(6A)	80.3(4)
N(1)-Ru(1)-N(8)	94.3(4)	N(1A)-Ru(2)-N(8A)	94.2(5)
N(9)-Ru(1)-N(8)	79.0(4)	N(9A)-Ru(2)-N(8A)	78.5(5)
N(7)-Ru(1)-N(8)	89.5(3)	N(7A)-Ru(2)-N(8A)	91.5(4)
N(6)-Ru(1)-N(8)	96.5(4)	N(6A)-Ru(2)-N(8A)	95.3(4)
N(1)-Ru(1)-N(2)	80.5(4)	N(1A)-Ru(2)-N(2A)	80.3(5)
N(9)-Ru(1)-N(2)	95.2(4)	N(9A)-Ru(2)-N(2A)	93.9(5)
N(7)-Ru(1)-N(2)	96.1(4)	N(7A)-Ru(2)-N(2A)	94.7(4)
N(6)-Ru(1)-N(2)	89.9(4)	N(6A)-Ru(2)-N(2A)	92.8(4)
N(8)-Ru(1)-N(2)	172.1(4)	N(8A)-Ru(2)-N(2A)	170.5(4)

In the free acdppz, the intramolecular bond lengths and bond angles are found to be comparable to other structurally characterized similar molecules.[13] The dihedral angle between the planes containing the dppz moiety and the acridine fragment is 75.87(12)°. In the crystal lattice, acdppz forms a one-dimensional array through intermolecular C-H⋯N and π-π interactions (Fig. 5.4a). One of the C-H groups (C15-H15) of dppz moiety is involved in weak intermolecular hydrogen bonding with the nitrogen atom (N5) of the acridine

moiety. The C15····N5 distance and C15-H15····N5 angle are 3.396(4) Å and 168.9^{o}, respectively. The dppz moieties are involved in the π-π interactions. The inter-planar distance between the overlapping dppz planes is 3.403 Å. The C-H····N and π-π interactions are roughly orthogonal to each other (Fig. 5.4a).

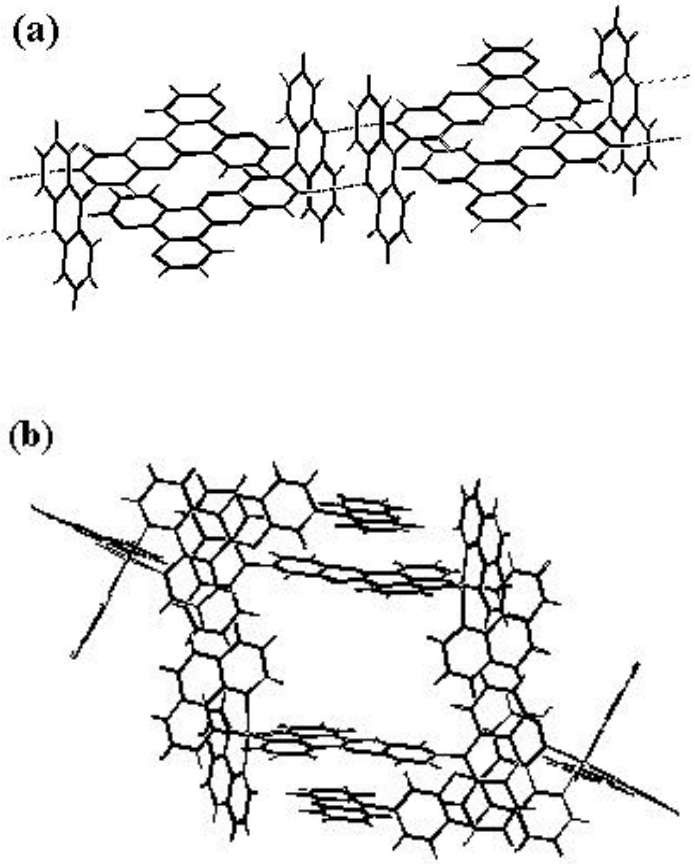

Fig. 5.4 Perspective view of the packing diagram of (a) acdppz and (b) $[Ru(phen)_2(acdppz)]^{2+}$

The crystal of the Ru(II) complex was very poorly diffracting. Despite our best efforts we could not grow a better crystal. However the diffraction data were

good enough to reveal the molecular structure. The unit cell contains two complex cations, four anions and four water molecules.

The bond parameters in the two complex cations are very similar (Table 5.3). In each of these two complex cations, the metal center is in distorted octahedral N_6 coordination sphere. The chelate bite angles are in the range 79.0(4)-80.5(4)°. The Ru-N bond lengths in the two cations are in the range 2.040(9)-2.079(13) Å. These are little smaller than those found in $[Ru(dmp)_2(dppz)]^{2+}$ (2.104 Å, dmp = 2, 9-dimethyl-1,10-phenanthroline)[14] and are comparable with the bond lengths in $[Ru(phen)_2(dpq)]^{2+}$ (2.064 Å, were dpq = dipyrido[3,2-*d*:2',3'-*f*]quinoxaline).[15] The dppz and phen ligands are essentially planar. The dihedral angles between the two phen planes in the two complex cations are 88.12(6)° and 82.47(6)°. The dihedral angles (86.13(4)° and 88.36(5)°) between the phen planes and the dppz moiety of acdppz in the first cation, are comparable with those angles (86.84(5)° and 83.37(6)°) observed in the second cation. These values are somewhat larger than the values (80.9(8)° and 50.2(9)^o) observed in $[Ru(dmp)_2(dppz)]^{2+}$.[14]

The acridine moiety of one cation is involved in π-π interaction with the dppz plane of the adjacent cation with an inter-planar distance of 3.365 Å (Fig. 5.4b) and forms a discrete dimer. This value is similar to the base-pair stacking distance in DNA[16] and to the intercalator-base pair stacking distance in oligonucleotide intercalator complexes.[17]

5.3.3 ^{1}H NMR Spectra

The proton assignments for both acdppz and $[Ru(phen)_2(acdppz)]^{2+}$ (Fig. 5.5) were made by utilizing the integrated intensity data in the ^{1}H spectra and proton connectivity patterns observed in the ^{1}H – ^{1}H COSY spectra (Fig 5.6). Salient features of the spectra are discussed here. In the ^{1}H NMR spectrum of

daa, a broad peak centered at 4.80 ppm corresponding to the resonance due to the NH_2 proton attached to the phenyl ring.[18] No such peak is observed in the spectrum of acdppz. For acdppz, two doublets centered at 9.68 and 9.56 ppm correspond to H_6 and H_3 protons of the phenanthroline subunit. A doublet of doublet occurs at 9.25 ppm which corresponds to H_1 and H_4 protons of the ligand. Two doublets and a singlet at 8.52, 7.78 and 8.46 ppm respectively, are due to the H_7, H_8 and H_9 protons of dppz moiety.

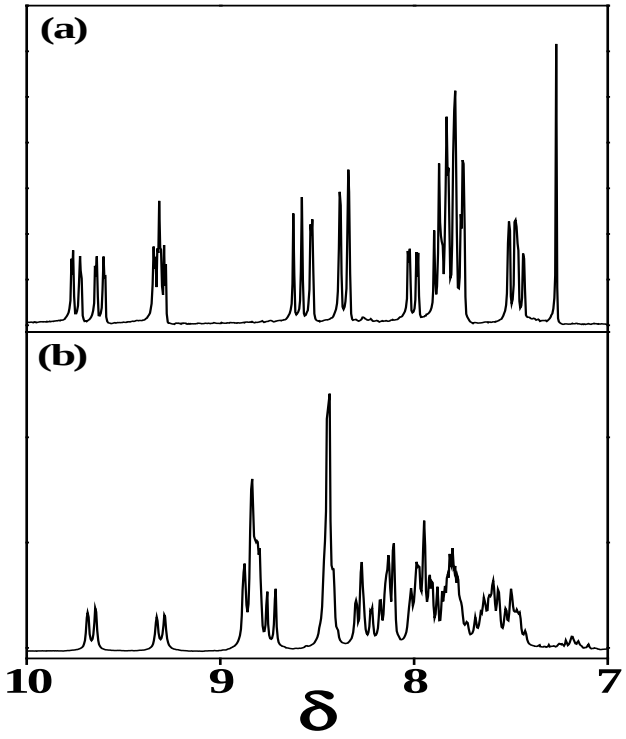

Fig. 5.5 ^1H NMR spectra of (a) acdppz (in $CDCl_3$) and (b) $[Ru(phen)_2(acdppz)]^{2+}$ (in $(CD_3)_2SO$).

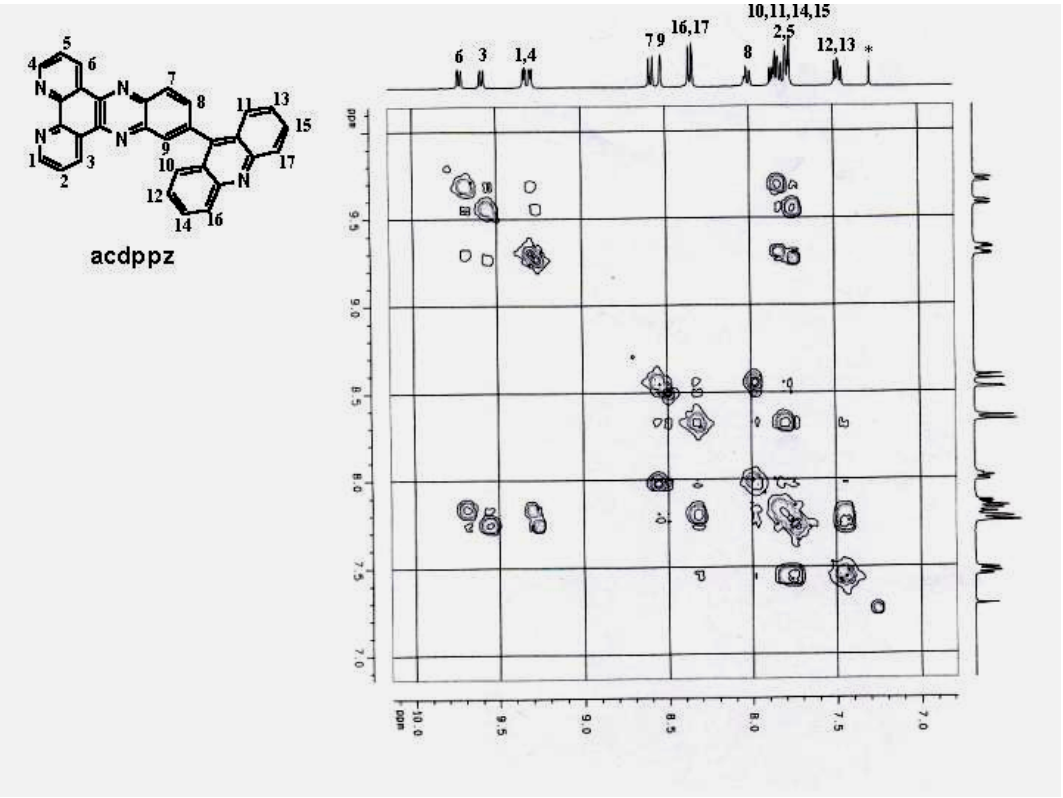

Fig. 5.6 $^{1}H - {}^{1}H$ COSY spectra of acdppz in $CDCl_3$

Doublet at 8.31 ppm is due to H_{16} and H_{17} protons of acridine ring. A multiplet centered at 7.75 ppm is due to the acridine (H_{10}, H_{11}, H_{14} and H_{15}) and the phenanthroline (H_2, H_5) protons. Protons H_{12} and H_{13} resonate as a triplet at 7.69 ppm. In the case of $[Ru(phen)_2(acdppz)]^{2+}$, resonances due to the protons of both phen and acdppz are seen to be considerably shifting to the downfield region compared to the free ligand indicating complexation. The well-defined ^{1}H NMR spectra observed permit unambiguous identification and assessment of purity to a satisfactory level.

5.3.4 Absorption and emission spectra

The overlay of electronic absorption and fluorescence spectra for acdppz and $[Ru(phen)_2(acdppz)]^{2+}$ are given in Fig. 5.7. The absorption spectrum of acdppz in acetonitrile displays low energy bands at 362 and 386 nm. These low intensity structured bands are assigned to $\pi \rightarrow \pi^*$ transitions of dppz and acridine chromophores.[19,20] The high-energy band at 251 nm, is attributed to the $\pi \rightarrow \pi^*$ transitions corresponding to the phenanthroline moiety of the ligand.

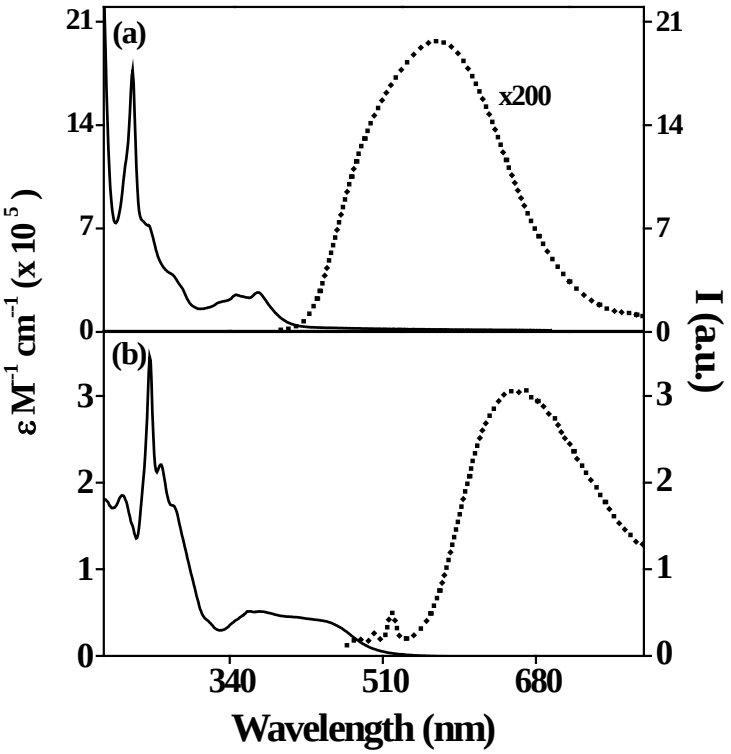

Fig. 5.7 UV-visible (——) and fluorescence (·····) spectra of (a) acdppz and (b) $[Ru(phen)_2(acdppz)]^{2+}$ in CH_3CN.

Dipyridophenazine complexes of ruthenium(II) are characterized by the intense absorption due to the metal to ligand charge transfer (MLCT) excited states in the visible region of the electromagnetic spectrum. Peak positions and extinction coefficients for both the compounds along with its corresponding starting materials are listed in Table 5.3. The low energy shoulder type band at 450 nm (ε = 19670 $M^{-1}cm^{-1}$) is assigned as MLCT Ru(dπ) $\rightarrow$ acdppz(π^*) transition for $[Ru(phen)_2(acdppz)]^{2+}$. The band in the 350–370 nm region arises from the $\pi \rightarrow \pi^*$ transitions of dppz and acridine. The $\pi \rightarrow \pi^*$ transition of the phen ligands, which is located in the upper 200 nm region, has a large absorbance. Overall, the spectral features are what we would expect for $[Ru(L)_2(dppz)]^{2+}$ - (where L is phen/bpy) type complexes.

When acdppz is excited at 330 nm in CH_3CN, the emission maxima appeared at 562 nm (ϕ = 0.83). Excitation of Ru(II) polypyridyl complexes at their MLCT wavelengths typically leads to visible light emission from the ruthenium excited state. The fluorescence of $[Ru(phen)_2(acdppz)]^{2+}$ has been examined in H_2O and in CH_3CN. It is intensively fluorescence in CH_3CN at 667 nm (ϕ = 0.002), but weakly fluorescence in H_2O at 610 nm (ϕ = 0.0003). The intensity in the former solvent is about 2 times larger than that in the latter solvent. The weak fluorescence of $[Ru(phen)_2(acdppz)]^{2+}$ in water may result from quenching by water. This can be interpreted by considering both the polarity and the proton-donating ability of the solvent.[21] The spectral shape and the λ_{em} values are quite similar to those of $[Ru(phen)_2(dppz)]^{2+}$, the ^{3}MLCT emission band maximum of which has been reported to be located at 618 nm.[3] The emission quantum yield of the complex investigated is lower than that of $[Ru(phen)_3]^{2+}$ (ϕ = 0.028 in CH_3CN).[22] A variety of excited state processes including enhanced internal conversion and intersystem crossing, ion-association, excitation energy transfer (EET), photoinduced electron transfer (PET) *etc.* are

likely to be operative in the emission quenching observed for this type of complexes in dry CH_3CN.[7] Fluorescence parameters for acdppz and its ruthenium(II) complex synthesized during this study along with the corresponding reference compounds are summarized in Table 5.3.

Table 5.3 UV-visible and emission spectral data in CH_3CN[a]

Compound	**Absorbance λ_{max}, (log ε)**		**Emission λ_{em}**
	Ligand Transitions	**MLCT**	
phen	226 (4.71), 264 (4.55)	--	--
acridine	249 (5.18), 340 (3.90), 356 (4.01)	--	428 (0.0004)
daa	219 (4.63), 251 (5.02), 300 (3.68), 359 (3.89)	---	---
dppz	269 (4.73), 295 (4.28), 359 (4.06), 378 (4.07)	---	---
acdppz	251 (5.25), 362 (4.40), 386 (4.43)	---	562 (0.83)
$[Ru(phen)_3](PF_6)_2$	223 (4.93), 263 (5.07), 422 (4.25)	446 (4.28)	596 (0.028)
$[Ru(phen)_2(dppz)](PF_6)_2$	265 (5.11), 360 (4.39), 369 (4.35)	439 (4.35)	607 (0.0073)
$[Ru(phen)_2(acdppz)](PF_6)_2$	220 (5.27), 252 (5.54), 264 (5.34), 361 (4.71)	450 (4.59)	667 (0.002)

a) Error limits: λ_{max} and $\lambda_{em,}$ ± 1 nm; log ε, ± 10%; ϕ, ± 10%

5.3.5 Electrochemistry

Uncomplexed acdppz shows one reversible (i_{pc}/i_{pa} = 0.9 - 1.0, ΔE_p = 60 - 70 mV; ΔE_p= 65 ± 3 mV for Fc^+/Fc couple)[23] reduction peak at –0.65 V and two irreversible reduction (i_{pc}/i_{pa} = 0.2 – 0.7 and ΔE_p = 90 - 200 mV) peaks at –1.05 and –1.29 V in DMF. The anodic scan was recorded in CH_2Cl_2. An irreversible oxidation is observed at +1.63 V. The cyclic and differential-pulse voltammograms of $[Ru(phen)_2(acdppz)]^{2+}$ are compared with that of $[Ru(phen)_2(dppz)]^{2+}$ and $[Ru(phen)_3]^{2+}$. The complex, $[Ru(phen)_2(acdppz)]^{2+}$, exhibits oxidation (in CH_3CN) and reduction (in DMF) waves in the sweep range –2.0 to + 1.6 V vs SCE (Fig. 5.8).

It exhibits a reversible oxidation wave at +1.43 V and two reversible and one quasi-reversible reduction waves at –0.81, –1.31 and –1.53 V. The redox potential data, as measured by the cyclic and differential-pulse voltammetric method for acdppz and $[Ru(phen)_2(acdppz)]^{2+}$ along with some of its reference compounds are summarized in Table 5.4. Oxidation of the complexes generally involves removal of an electron from the dπ orbital of Ru(II) while reduction involves transfer of an electron to the ligand (acdppz) centered orbitals.[24] As expected, the oxidation potential of $[Ru(phen)_2(acdppz)]^{2+}$ is 20 mV more positive when compared to $[Ru(phen)_2(dppz)]^{2+}$ and that is 60 mV more positive when compared to $[Ru(phen)_3]^{2+}$. The attachment of acridine chromophore to the dppz moiety expands the π delocalization and thus decreases the σ donor capacity of acdppz which leads to the decrease in the electron density on Ru(II) ion and in turn stabilizes the metal π (t_{2g}) orbital.[25] The same is true for $[Ru(phen)_2(dppz)]^{2+}$ and $[Ru(phen)_3]^{2+}$ when dppz and phen are compared.

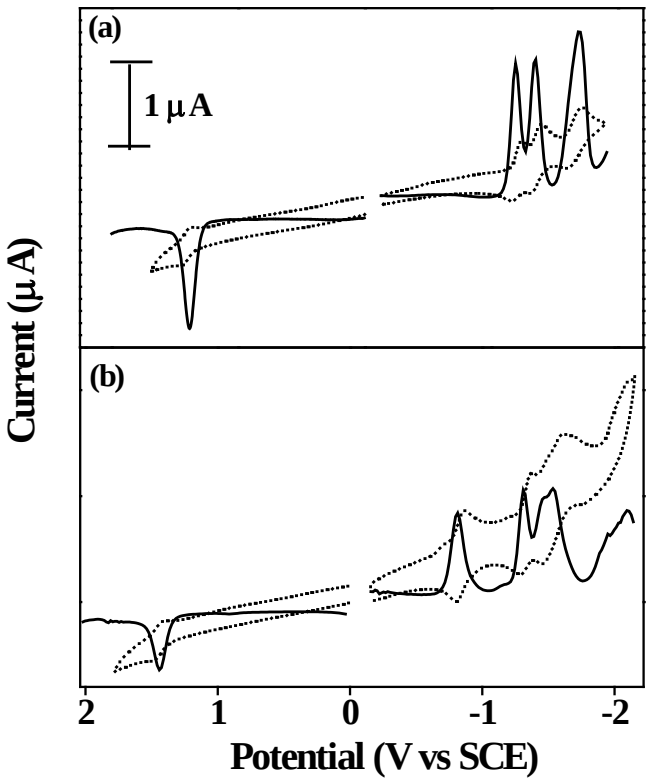

Fig. 5.8 Cyclic (·····) and differential pulse (——) voltammograms of (a) $[Ru(phen)_3]^{2+}$, (b) $[Ru(phen)_2(acdppz)]^{2+}$. CH_3CN and DMF containing 0.1 M TBAP were used as solvents for the anodic and cathodic runs, respectively. Scan rate: 100 mV s^{-1}.

As a result, the oxidation potential increases in the following order $[Ru(phen)_3]^{2+}$<$[Ru(phen)_2(dppz)]^{2+}$< $[Ru(phen)_2(acdppz)]^{2+}$. The first reduction wave (–0.81 V) is usually controlled by the ligand acdppz having the most stable LUMO[26] and the other two reduction waves for $[Ru(phen)_2(acdppz)]^{2+}$ are typical of the phen (–1.31 V) and dppz/ acridine (–1.52 V) chromophore of the ligands.[27,28]

Table 5.4 Redox potential data[a]

Compound	Oxidation $E_{1/2}$ (V vs SCE)	Reduction[d] $E_{1/2}$ (V vs SCE)
phen	---	-1.92
acridine	---	-1.46
daa	+0.88, +1.40	-0.77, -1.07
dppz	---	-1.48
acdppz	+1.63[b]	-0.65, -1.05, -1.29
$[Ru(phen)_3](PF_6)_2$	+1.37[c]	-1.19, -1.34, -1.69
$[Ru(phen)_2(dppz)](PF_6)_2$	+1.41[c]	-0.82, -1.25, -1.47
$[Ru(phen)_2(acdppz)](PF_6)_2$	+1.43[c]	-0.81, -1.31, -1.52

a) Obtained from the differential-pulse voltammetric measurements. Error limits: $E_{1/2,} \pm$ 0.03 V
b) CH_2Cl_2, 0.1 M TBAP
c) CH_3CN, 0.1 M TBAP
d) DMF, 0.1 M TBAP

5.3.6 DNA binding experiments

CT DNA was used for carrying out binding studies with the chloride salt of $[Ru(phen)_2(acdppz)]^{2+}$. The stock solution was made by dissolving CT DNA in appropriate buffers, kept overnight at 4 ^oC to ensure complete dissolution and used for the following different types of experiments to study the DNA binding features.

5.3.6.1 Absorption titration

Owing to the well resolved $\pi \rightarrow \pi^*$ transition on the phenazine portion of the dppz derivatives in this complex, one can delineate processes that are localized on the acdppz. The binding of $[Ru(phen)_2(acdppz)]^{2+}$ to CT DNA occurs by preferential intercalation of acdppz into the hydrophobic interior of the

DNA base stack. Moreover, it is accompanied by significant hypochromism in the $\pi \rightarrow \pi^*$ transition, extensive broadening, red shift of the vibronic bands and in turn increases the stability of the DNA double helix. The extent of hypochromism commonly parallels to the intercalative strength of the ligand. Generally higher planar area, extended π system, hydrophobicity and aromaticity of the ligand lead to the deep penetration and hence more stacking with the base pairs of DNA.[29] Fig. 5.9 shows the electronic spectral titration for the $[Ru(phen)_2(acdppz)]^{2+}$ with

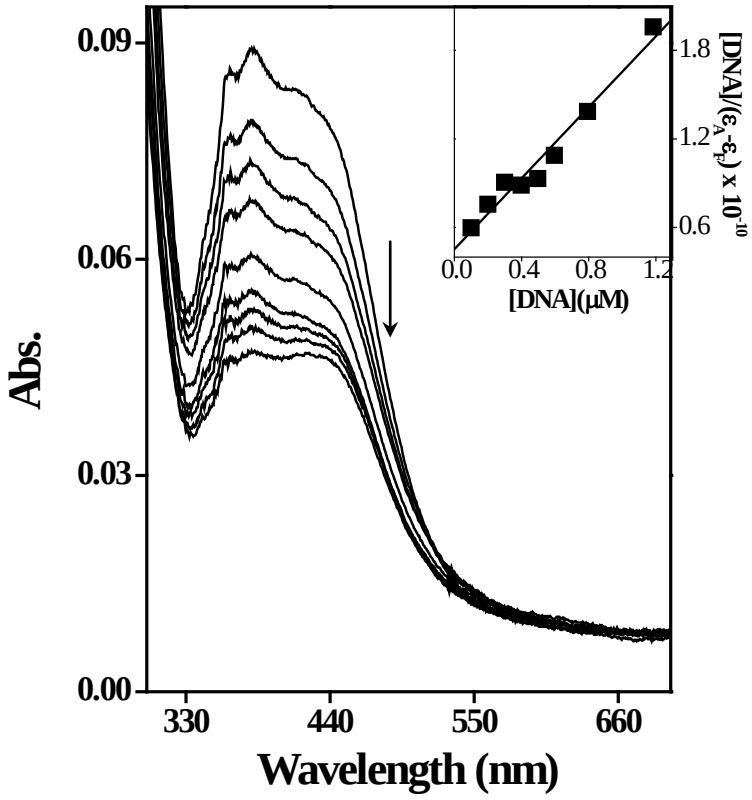

Fig. 5.9 UV-visible spectra of $[Ru(phen)_2(acdppz)]^{2+}$ (5 μM) in the absence (top curve) and presence (subsequent curves) of increasing concentrations (0 – 100 μM) of CT DNA in buffer A. The inset graph shows a fit of the absorbance data to equn. 2.2 to obtain K_b.

the increasing concentration of CT DNA. As the DNA concentration is increased, $[Ru(phen)_2(acdppz)]^{2+}$ showed hypochromicity (52%) along with the bathochromic shift of 3 nm during the absorption titration experiment. To compare quantitatively the affinity of $[Ru(phen)_2(acdppz)]^{2+}$ towards DNA, the intrinsic binding constant value (K_b) is determined by monitoring the absorbance at the MLCT using equn. 2.2 (Chapter 2) and is evaluated as high as 2.65×10^{6} M^{-1} (Table 5.5).

5.3.6.2 Fluorescence titration

Fluorescence spectra of 7 μM solution of $[Ru(phen)_2(acdppz)]^{2+}$ in tris buffer (5 mM Tris, 50 mM NaCl, pH 7.1) showed an increase in the emission intensity with successive addition of CT DNA. The emission maxima at 610 nm (in H_2O) due to the ^{3}MLCT ($d\pi(Ru) \rightarrow \pi^*(acdppz)$[20] state increases initially at low [DNA nucleotide phosphate]/[Ru] ratio but, reaches a plateau with the apparent enhancement factor of ~ 5 at higher [DNA nucleotide phosphate]/[Ru] ratio of 12 (Fig. 5.10). The complex has very weak emission in the aqueous medium in the absence of DNA, but on addition of increasing amount of DNA, the emission intensity increases with a bathochromic shift of about 4 nm. The increase in the emission intensity observed for $[Ru(phen)_2(acdppz)]^{2+}$ in the presence of DNA is due to the shielding of the nitrogens especially phenazine and acridine nitrogens of the intercalating ligand acdppz from protonation in the bulk solvent medium. This phenomenon has been extensively studied and described as the " molecular light switch" effect.[1,3,4] The mobility of the complex is restricted at the binding site and so the vibrational modes of relaxation (collision and energy discipation) decreases on intercalation.[24] The binding constant obtained utilizing the equn. 2.4 (Chapter 2) are reasonably well in agreement with the values from the absorption titration experiment. The binding site size in base pairs (n) is evaluated as 2. Thus

the intercalative strength follows the order, $[Ru(phen)_2(dppz)]^{2+} \geq [Ru(phen)_2(acdppz)]^{2+} > [Ru(phen)_3]^{2+}$.

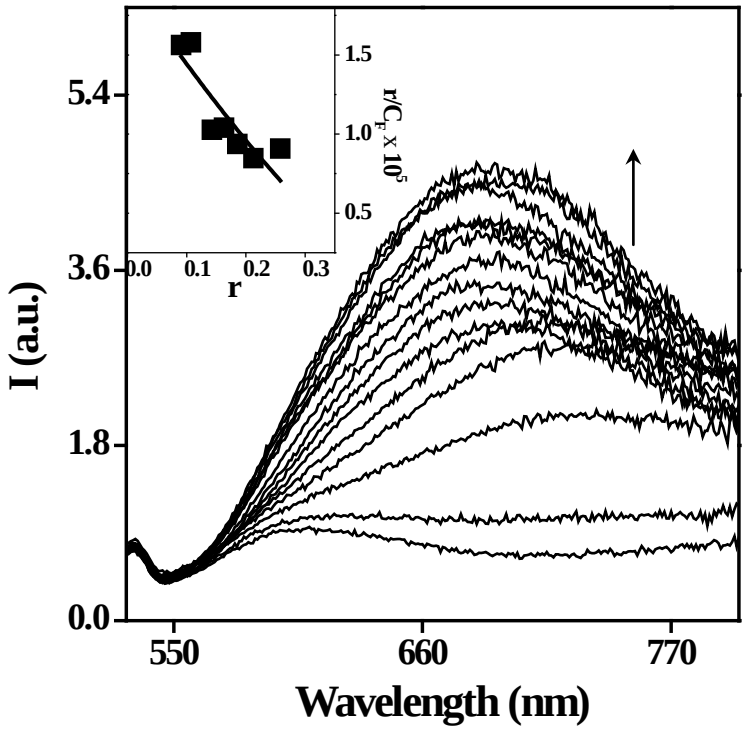

Fig. 5.10 Fluorescence spectra of $[Ru(phen)_2(acdppz)]^{2+}$ (7 μM) in the absence (bottom curve) and presence (subsequent curves) of increasing concentrations (0 – 200 μM) of CT DNA in buffer A (λ_{exc} = 450 nm). The inset graph shows a fit of the emission data to equn 2.4 to obtain $K_{b.}$

The lesser intrinsic binding constant (K_b) of $[Ru(phen)_2(acdppz)]^{2+}$ when compared to $[Ru(phen)_2(dppz)]^{2+}$ may be due to the fact that both the dppz and acridine moiety in acdppz are not coplanar as observed in the crystal structure.

5.3.6.3 DNA melting experiment

Intercalation of small molecules into the double helix is known to increase the helix melting temperature, the temperature at which the double helix denatures into single- stranded DNA.[30] The extinction coefficient of DNA bases at 260 nm in the double-helical form is much less than that in the single- stranded form; hence, melting of the helix leads to an increase in the absorption at this wavelength.[31] CT DNA was seen to melt at 61 ± 1° C (in buffer B) in the absence of any added complex.

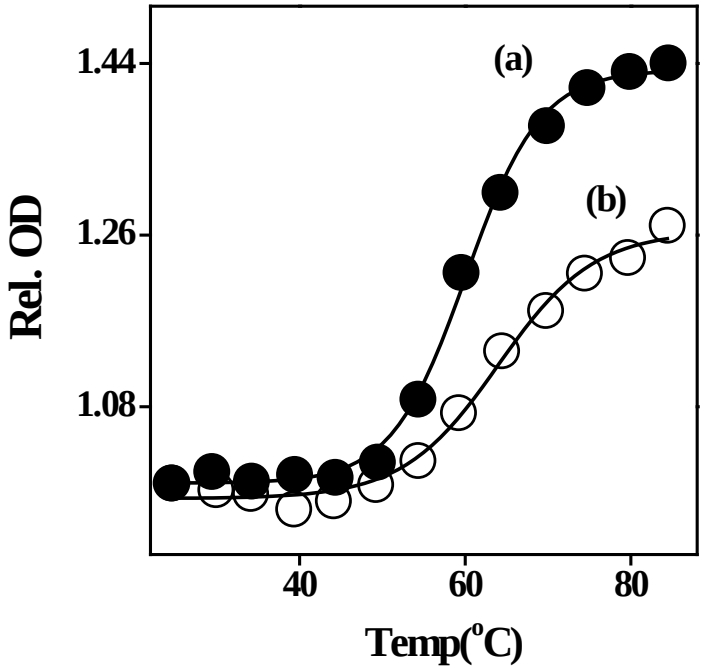

Fig. 5.11 Melting curves for CT DNA in the absence (●) and in the presence (○) of $[Ru(phen)_2(acdppz)]^{2+}$ in buffer B.

The T_m of DNA is increased by 4 °C in the presence of $[Ru(phen)_2(acdppz)]^{2+}$ (at [DNA nucleotide phosphate] /[complex] = 25). The DNA melting curves in the absence and presence of $[Ru(phen)_2(acdppz)]^{2+}$ are

presented in Fig. 5.11. This observation establishes the increased stability of the double helix when $[Ru(phen)_2(acdppz)]^{2+}$ binds to DNA. The T_m and the σ_T values of CT DNA in the absence and presence of the complex are tabulated in Table 5.5. The increase in the melting temperature is comparable to the value observed with the classical intercalator EtBr and lend strong support for the intercalation.[31,32]

Table 5.5 Absorption titration and Thermal melting data[a]

Compound	K_b (M^{-1})	T_m ^oC (σ_T ^{o})
DNA	--	61 (19)
acridine	8.9×10^4	63 (22)
$[Ru(phen)_3]^{2+}$	8.24×10^3	62 (21)
$[Ru(phen)_2(acdppz)]^{2+}$	2.65×10^6	64 (24)
$[Ru(phen)_2(dppz)]^{2+}$	$> 10^7$	65 (26)

a) Error limits: K_b, ± 10%; T_m, ± 1^{o}C; σ_T, ± 1^o

5.3.6.4 Viscometric titration

In order to further clarify the interaction of $[Ru(phen)_2(acdppz)]^{2+}$ with DNA, viscosity measurements were carried out. Optical probes provided essential, but insufficient, evidence to support a binding model. Hydrodynamic measurements, which are sensitive to changes in the molecular length (*i.e.* viscosity and sedimentation) are regarded as the least ambiguous and the most critical tests of a binding model in solution. A classical intercalator (e.g. EtBr) model demands that the DNA helix must lengthen the overall DNA molecular length (contour length) as base pairs are separated to accommodate the intercalated ligand, leading to an increase in DNA viscosity. In contrast, a partial and/or nonclassical intercalating ligand $[Ru(phen)_3]^{2+}$ could bend (or kink) the

DNA helix, reducing its effective length and concomitantly, its viscosity.[33] The effects of complex $[Ru(phen)_2(acdppz)]^{2+}$ on the viscosity of CT DNA are shown in Fig. 5.12 together with EtBr and $[Ru(phen)_3]^{2+}$.

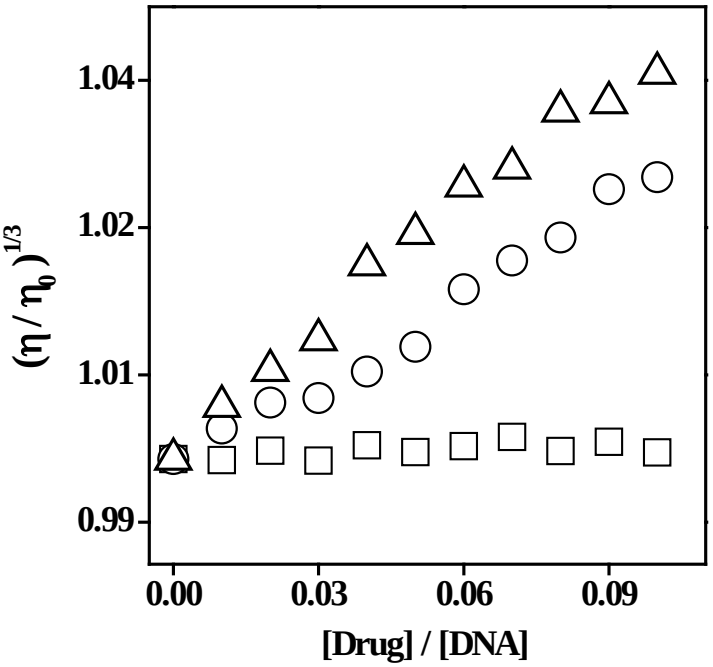

Fig. 5.12 Results of viscometric titrations carried out for CT DNA (300 μM) in the presence of $[Ru(phen)_3]^{2+}$ (□), $[Ru(phen)_2(acdppz)]^{2+}$ (○) and EtBr (△) in buffer C.

The experiments suggest that $[Ru(phen)_2(acdppz)]^{2+}$ binds to the polyanionic DNA *via* an intercalating mode that is similar to that of EtBr. From the above observation, obviously question arises about which part of acdppz intercalates between the base pairs of DNA. If we compare the binding constant of acridine ($K_b = 8.9 \times 10^4$)[10] with that of $[Ru(phen)_2(acdppz)]^{2+}$, one can easily

predict that besides acridine, phenazine portion of dppz also plays a major role in the intercalative process with CT DNA.

5.3.7 DNA photocleavage experiments

The single strand break of pBR 322 DNA (conversion of supercoiled (Form I) to open circular (Form II)) is generally studied by gel electrophoresis. In these experiments, relatively fast migration will be observed for the form I when compared to form II. Photocleavage experiments have been carried out for $[Ru(phen)_2(acdppz)]^{2+}$ along with $[Ru(phen)_3]^{2+}$ (for comparison) in presence of pBR 322 DNA and the results were summarized in Fig. 5.13. The pBR 322 DNA does not show any cleavage in the dark and even upon irradiation at 450 ± 5 nm for 60 min. (compare lanes 1 and 2). Considerably lesser activity was observed for pBR 322 treated with $[Ru(phen)_2(acdppz)]^{2+}$ and $[Ru(phen)_3]^{2+}$ in dark experiments (Lanes 3 and 5). Upon 60 min. irradiation at 450 ± 5 nm (Lanes 4 and 6), single-strand nicking is observed and the percentage of conversions (using equn. 2.5, chapter 2) from form I to form II are also calculated. Unexpectedly $[Ru(phen)_2(acdppz)]^{2+}$ shows low photocleaving efficiency (41% of form II) when compared to $[Ru(phen)_3]^{2+}$ (52% of form II). The same observation has been noted over various bp/Ru molar ratio. Furthermore, an enhancement in the photocleavage activity (59% of form II) is observed when the irradiation is carried out in D_2O instead of buffer, (Lane 7). These observations may be explained on the basis of singlet oxygen ($^1O_2$) cleaving mechanism given below.

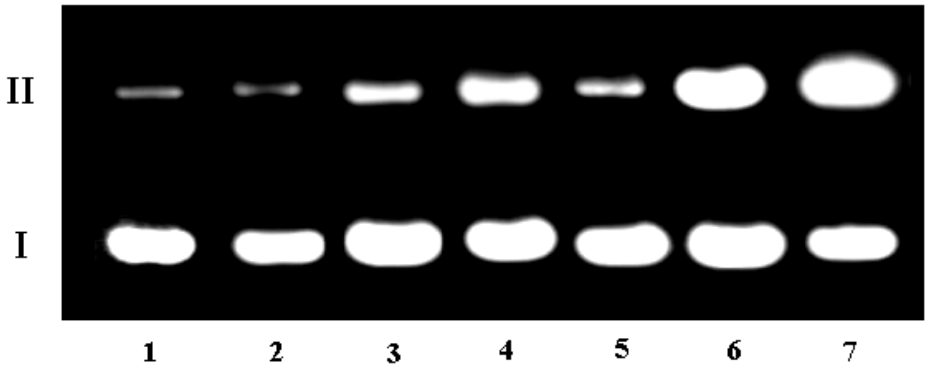

Fig. 5.13 Light-induced nuclease activities of $[Ru(phen)_2(acdppz)]^{2+}$. Dark and Light Experiments: Lanes 1 and 2: Untreated pBR 322 (100 μM) in the dark and upon irradiation. Lanes 3 and 5: pBR 322 + $[Ru(phen)_2(acdppz)]^{2+}$ (10 μM) and pBR 322 + $[Ru(phen)_3]^{2+}$ (10 μM) in dark. Lanes 4 and 6: pBR 322 + $[Ru(phen)_2(acdppz)]^{2+}$ and pBR 322 + $[Ru(phen)_3]^{2+}$ upon irradiation. Lane 7: pBR 322 +$[Ru(phen)_2(acdppz)]^{2+}$ + D_2O. $\lambda_{irrd.}$= 450 ± 5 nm (60 min.) in each case.

In order to establish the reactive species responsible for the photoinduced cleavage of the plasmid, the following experiments have been carried out in the presence of various 'inhibitors' (Fig. 5.14). Photocleavage by $[Ru(phen)_3]Cl_2$ has been reported to involve $^1O_2$ - based mechanism.[34] As mentioned before, the irradiation of pBR322 in the absence and presence of $[Ru(phen)_2(acdppz)]^{2+}$ at 450 ± 5 nm for 60 min. was done. Degassing of the solution with purified nitrogen for 30 min., decreased the efficiency of the cleavage by a factor of 2 (Fig. 5.14). It appears that oxygen is involved in the photolytic cleavage of DNA.

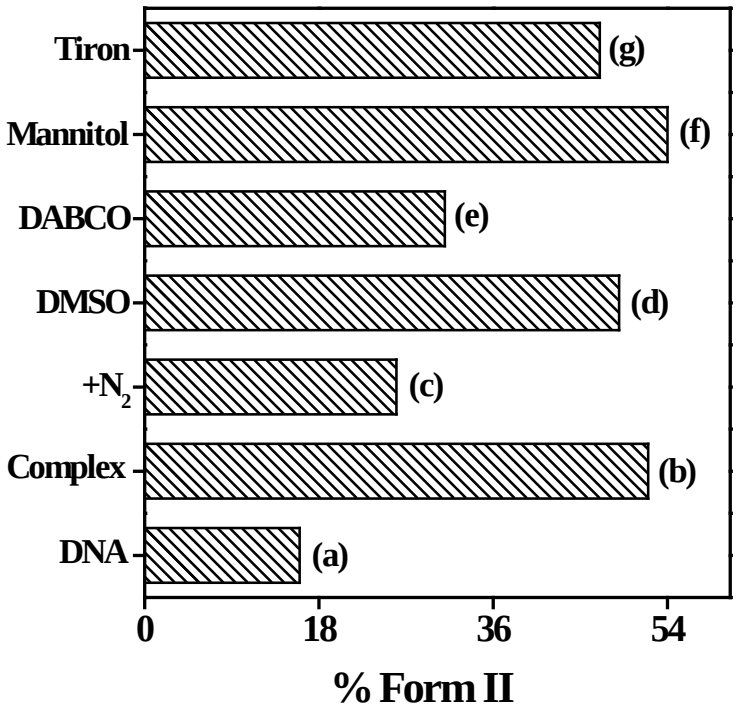

Fig. 5.14 Bar diagram representation of the effects of 'inhibitors' on the light-induced nuclease activity of $[Ru(phen)_2(acdppz)]^{2+}$. **(a)** DNA control; **(b)** pBR 322 + $[Ru(phen)_2(acdppz)]^{2+}$ (**c-g)**: pBR 322 + $[Ru(phen)_2(acdppz)]^{2+}$ in the presence of N_2, DMSO (200 mM), DABCO (10 mM), mannitol (100 mM) and tiron (10 mM) respectively, upon irradiation for 60 min. at 450 ± 5 nm in each case.

As can be seen in Fig. 5.14, the cleaving efficiency was not inhibited by the addition of DMSO (10 mM) and mannitol (100 mM). This observation suggests that hydroxyl radical ($OH^{\bullet}$) was not involved in the cleavage. In the presence of tiron (10 mM), the cleavage was not inhibited. Thus superoxide anion radical ($O_2^{\bullet -}$) was not involved in the cleavage. However, it was largely inhibited

by DABCO ($^1O_2$ quencher). Thus the singlet oxygen is likely to be the reactive species for the cleavage reaction as is the case with $[Ru(phen)_3]^{2+}$. This is also supported by the enhanced cleavage activity when the buffer is changed completely with D_2O (the life time of singlet oxygen is higher in D_2O than in H_2O).[35,36] A possible reason for the lower photocleavage activity of $[Ru(phen)_2(acdppz)]^{2+}$ is as follows. When the complex is intercalated, it is well protected from oxygen and so the yield of singlet oxygen and subsequently the cleavage efficiency of the complex would be lower than that of $[Ru(phen)_3]^{2+}$.[37,38]

5.4 Summary

Studies carried out so far have revealed that the modification of phen, especially extension of the planarity of the ligand and attaching the aromatic chromophore to it, increases the strength of interaction of the complex with DNA. Especially complexes with dppz and modified dppz are found to be better DNA binders and photocleaving agents than the other complexes with modified phenanthroline. These results suggest the importance of the phenazine functionality in the DNA interactions with the complexes containing this ligand. In this study, we have studied the interactions of DNA with a new mixed-ligand polypyridyl complex $[Ru(phen)_2(acdppz)]^{2+}$. It has been synthesized and fully characterized by crystal structure, spectroscopic and electrochemical methods. Based on absorption, fluorescence, thermal denaturation and viscometric experiments, an intercalative mode of DNA binding involving acdppz is suggested for this complex. The fluorescence of this complex (in buffer), shows moderate “molecular light switch” behaviour in the presence of DNA. The photonuclease activity is quite low for $[Ru(phen)_2(acdppz)]^{2+}$ than $[Ru(phen)_3)]^{2+}$. Moreover the reactive oxygen species ($^1O_2$) plays a significant role in the mechanism for the cleavage of DNA with $[Ru(phen)_2(acdppz)]Cl_2$.

5.5 References

1. Friedman, A. E.; Chambron, J-C.; Sauvage, J.-P.; Turro, N. J.; Barton, J. K. *J. Am. Chem. Soc.* **1990**, *112*, 4960.
2. Jenkins, Y.; Friedman, A. E.; Turro, N. J.; Barton, J. K. *Biochemistry* **1992**, *31*, 10809.
3. Hartshorn, R. M.; Barton, J. K. *J. Am. Chem. Soc.***1992**, *114*, 5919.
4. Dupureur, C. M.; Barton, J. K. *J. Am. Chem. Soc.* **1994**, *116*,10286.
5. Arounaguiri, S.; Maiya, B. G. *Inorg. Chem.* **1999**, *38*, 842.
6. Ambroise, A.; Maiya, B. G. *Inorg. Chem.* **2000**, *39*, 4256.
7. Ambroise, A.; Maiya, B. G. *Inorg. Chem.* **2000**, *39*, 4264.
8. Sastri, C. V.; Eswaramoorthy, D.; Giribabu, L.; Maiya, B. G. *J. Inorg. Biochem.* **2003**, *94*, 138.
9. Wadkins, R. M.; Graves, D. E. *Nucleic Acids Res.* **1989**, *17*, 9933.
10. McConnaughie, A. W.; Jenkins, T. C. *J. Med. Chem.* **1995**, *38*, 3488.
11. (a) Eldho, N. V.; Joseph, J.; Ramaiah, D. *Chem. Lett.* **2001**, 438. (b) Joseph, J.; Eldho, N. V.; Ramaiah, D. *Chem. Eur. J.* **2003**, *9*, 5926.
12. Takenaka, S.; Ihara T.; Takagi, M. *Chem. Commun.* **1990**, 1485.
13. Gupta, T.; Dhar, S.; Nethaji, M. Chakravarty, A. R. *J. Chem. Soc., Dalton Trans.* **2004**, 1896.
14. Liu, J-G.; Zhang, Q-L.; Shi, X-F. Ji, L-N. *Inorg. Chem.* **2001**, *40*, 5045.
15. Collins, J. G.; Sleeman, A. D.; Aldrich-Wright, J. R.; Greguric, I.; Hambley, T. W. *Inorg. Chem.* **1998**, *37*, 3133.
16. Stryer, L. *Biochemistry*, Freeman, New York, **1988**, p. 76.
17. Yam, V. W-W.; Lo, K. K-W.; Cheung, K-K.; Kong, R. Y-C. *J. Chem. Soc., Dalton Trans.* **1997**, 2067 and references therein.
18. Plater, M. J.; Greig, I.; Helfrich, M. H.; Ralston, S. H. *J. Chem. Soc., Perkin Trans.1* **2001**, 2553.

19. Amouyal, E.; Homsi, A.; Chambron, J-C.; Sauvage, J.-P. *J. Chem. Soc., Dalton Trans.* **1990**, 1841.
20. Werner, T.; Fahnrich, K.; Huber, C.; Wolfbeis, O. S. *Photochem. Photobiol.* **1999**, *70*, 585.
21. Olson, E. J.; Hu, D.; Hormann, A.; Johkman, A. M.; Arkin, M. R. Stemp, E. D. A.; Barton, J. K.; Babara, R. F. *J. Am. Chem. Soc.* **1997**, *119*, 11458.
22. Juris, A.; Balzani, V.; Barigelletti, F.; Campagna, S.; Belser, P.; Zelewsky, A. V. *Coord. Chem. Rev.* **1988**, *84*, 85.
23. Nicholson, R. S.; Shain, I. *Anal. Chem.* **1964**, *36*, 706.
24. Wu, J. Z.; Ye, B. H.; Wang, L.; Ji, L-N.; Zhou, J. Y.; Li, R. H. Zhou, Z. Y. *J. Chem. Soc., Dalton Trans.* **1997**, 1395.
25. Rillema, D. P.; Allen, G.; Meyer, T. J.; Conrad, D. C. *Inorg. Chem.* **1983**, *22*, 1617.
26. Ghosh, B. K.; Chakravorty, A. *Coord. Chem. Rev.* **1989**, *95*, 239.
27. Delaney, S.; Pascaly, M.; Bhattacharya, P. K.; Han, K.; Barton, J. K. *Inorg. Chem.* **2002**, *41*, 1966.
28. Joseph, J.; Eldho, N. V.; Ramaiah, D. *J. Phys. Chem. B.* **2003**, *107*, 4444.
29. Holmlin, R. E.; Barton, J. K. *Inorg. Chem.* **1995**, *34*, 7.
30. Patel, D. J. *Acc. Chem. Res.* **1979**, *12*, 118.
31. Lehninger, A. L. *Biochemistry,* 2nd *ed.;* Worth Publishers: New York, 1975; p 873.
32. Kumar, C. V.; Asuncion, E. H. *J. Am. Chem. Soc.***1993**,*115*, 8541.
33. Satyanarayana, S.; Dabrowiak, J. C.; Chaires, J. B. *Biochemistry* **1992**, *31*, 9319.
34. Kelly, J. M.; Tossi, A. B.; McConnell, D. J.; OhUigin, C.; *Nucl. Acid. Res.* **1985**, *13*, 6017.
35. Burrows, C. J.; Muller, J. G. *Chem. Rev.* **1998,** *98*, 1109.

36. Armitage, B. *Chem. Rev.* **1998**, *98*, 1171.
37. Sentagne, C.; Chambron, J-C.; sauvage, J-P.; Paillous, N. *J. Photochem. Photobiol. B Biol.* **1994**, *26*, 165.
38. Fleisher, M. B.; Waterman, K. C.; Turro, N. J.; Barton, J. K. *Inorg. Chem.* **1986**, *25*, 3549.

CHAPTER 6

DNA Binding and Photonuclease Activity of a Series of Metallointercalators with an Acridine Tethered Schiff base

6.1 Introduction

Design and synthesis of small synthetic systems that recognize specific sites of DNA is an important area of current research.[1-4] Earlier investigations have indicated that, while some metallosalen derivatives bind DNA avidly, few others induce effective DNA scission.[5-9] Variation in the structure of the $[salen]^{2-}$ unit and variation of the central metal ion influence the effect of the resulting complex on DNA in a widely interesting fashion. Griffin studied some of these aspects of DNA modification in detail with manganese(II)-salen complexes.[5] Burrows and Rokita synthesized some nickel(II)-salen derivatives which induced DNA cross-linking.[6] In addition to that, Routier *et al*. examined the interaction of DNA with a functionalized salen-copper(II) complex which induce DNA strand scission in the presence of a reducing agent.[7] Besides, Bhattacharya *et al.* examined the DNA cleavage processes induced by some bis-cationic salen analogues.[8] It is interesting to note from chapter 5 that the efficient fluorescence and DNA binding behaviour of complexes containing acridine attached ligands. In the present chapter, we have discussed the synthesis, characterization, DNA binding and DNA photocleavage properties of neutral Ni(II), Cu(II) and Zn(II) complexes with acridine fused H_2salen. Yu *et al*. have studied the effect of water-soluble Cu(II)-, Ni(II)-, Mn(II)- and Co(II)- salen complexes with DNA.[10,11] It reveals that Mn(II) and Co(II) complexes showed strong intercalative interactions with DNA than Cu(II) and Mn(II). Examination of the above reports have made it

clear that, still much has to be done to understand the role of salen structure and the central metal ion in the DNA binding/modification processes.

6.2 Experimental section

9-(3,4-diaminophenyl)acridine (daa) was synthesized according to the reported procedure[12] (Chapter 2). Its purity was checked by NMR analysis. Synthesis of H_2daasal and its corresponding complexes [Cu(daasal)], [Ni(daasal)] and [Zn(daasal)] are described below.

6.2.1 Synthesis of H_2daasal

9-(3,4-diaminophenyl)acridine (0.19g, 0.67mmol) and salicylaldehyde (1.68 mmol, 0.17 cm^3 of 99%) were dissolved in dry CH_3OH (40 mL) together with 5-8 drops of triethyl orthoformate. The mixture was heated under refluxion for 4 h and the yellow precipitate separated, was collected by filtration. The solid was washed with diethyl ether and dried under vacuum followed by recrystallization from DMF-diethyl ether (1:3, v/v) mixture. Yield = 0.26 g (78%).

Analytical data: Found: C, 80.18; H, 4.74; N, 8.42; Calculated for $C_{33}H_{23}N_3O_2$: C, 80.31; H, 4.67; N, 8.51; MALDI-TOF (m/z): 513.34; IR: ν_{max} (KBr, cm^{-1}): 3047 (C-H, aromatic), 1614 (C=N). ^{1}H NMR ($CDCl_3$, 400 MHz, TMS): 13.05 (s, 1H), 13.01 (s, 1H), 8.84 (s, 1H), 8.70 (s, 1H), 8.34 (d, 2H), 7.84 (t, 4H), 7.51 (m, 6H), 7.46 (s, 1H), 7.31 (d, 2H), 7.12 (dd, 2H), 6.96 (t, 1H), 6.90 (t, 1H).

6.2.2 Synthesis of [Ni(daasal)]

A mixture of $NiCl_2 \cdot 6H_2O$ (0.10 g, 0.42 mmol) and H_2daasal (0.31g, 0.63 mmol) in C_2H_5OH (35 mL) was refluxed with constant stirring for 2 h. The dark reddish-orange precipitate of [Ni(daasal)] was collected by filtration, washed with

cold C_2H_5OH and diethylether and dried under vacuum. It was recrystallized from DMF. Yield = 0.17 g (72%).

Analytical data: Found: C, 71.93; H, 3.74; N, 7.71; Calculated for $C_{33}H_{21}N_3O_2Ni$: C, 72.04; H, 3.82; N, 7.64; MALDI-TOF (m/z): 572.02 IR: ν_{max} (KBr, cm^{-1}): 3049 (C-H aromatic), 1608 (C=N). ^1H NMR ($(CD_3)_2SO$, 400 MHz, TMS): 9.35 (s, 1H), 9.08 (d, 1H), 8.91 (s, 1H), 8.41 (t, 2H), 8.38 (s, 1H), 8.26 (m, 3H), 7.89 (m, 3H), 7.65 (m, 5H), 7.04 (dd, 2H), 6.91 (t, 1H), 6.63 (t, 1H).

6.2.3 Synthesis of [Cu(daasal)]

$CuCl_2 \cdot 2H_2O$ (0.15 g, 0.88 mmol) and H_2daasal (0.65 g, 1.32 mmol) were taken in C_2H_5OH (40 mL). The resulting solution was refluxed for 2 h, allowed to cool and the precipitate separated was collected by filtration. The complex was washed with C_2H_5OH and diethylether and dried under vacuum. It was recrystallized from acetone - diethyl ether (1:5, v/v). Yield = 0.31 g (63%).

Analytical data: Found: C, 70.82; H, 3.74; N, 7.48; Calculated for $C_{33}H_{21}N_3O_2Cu$: C, 71.4; H, 3.79; N, 7.57; MALDI-TOF (m/z): 557.45 $(M+3H)^+$; IR: ν_{max} (KBr, cm^{-1}): 1608 (C=N). X band EPR with g_{11} =2.4267 (A_{11}= 123x10 $^{-4}$) and $g_{\perp}$=2.0363 ($A_{\perp}$= 3.4 $x10^{-3}$) in DMF glass at 110K; μ_{eff} = 2.70 $\mu_{B.}$

6.2.4 Synthesis of [Zn(daasal)]

$Zn(CH_3COO)_2 \cdot 2H_2O$ (0.10 g, 0.46 mmol) and H_2daasal (0.34 g, 0.68 mmol) were taken in C_2H_5OH (50 mL). The resulting solution was refluxed for 2 h, allowed to cool and the precipitate separated was collected by filtration. The complex was washed with C_2H_5OH, ether and dried under vacuum. It was recrystallized from DMF-diethyl ether (1:5, v/v). Yield = 0.21 g (81%).

Analytical data: Found: C, 70.85; H, 3.68; N, 7.63; Calculated for $C_{33}H_{21}N_3O_2Zn$: C, 71.17; H, 3.77; N, 7.55; MALDI-TOF (m/z): 555.36 $(M-H)^+$;

IR: ν_{max} (KBr, cm^{-1}): 1614 (C=N). ^1H NMR (C_5D_5N, 200 MHz, TMS): 9.28 (s, 1H), 8.70 (s, 4H), 8.53 (d, 1H), 8.02 (d, 1H), 8.01 (s, 1H), 7.80 (d, 2H), 7.55 (s, 3H), 7.41 (m, 4H), 6.71 (2, 1H), 6.62 (2, 1H).

All the complexes are highly soluble in DMF and moderately soluble in CH_3CN, CH_2Cl_2, CH_3OH and less soluble in H_2O. They are stable in the solid and as well as in the solution phase. Spectroscopic, electrochemical and biochemical experiments were carried out as described in chapter 2.

6.3 Results and discussion

6.3.1 Synthesis

Synthesis of H_2daasal and the corresponding Ni(II), Cu(II) and Zn(II) complexes are illustrated in Fig. 6.1. The CHN analyses, FAB-MS, infrared, ^1H NMR, EPR, and magnetic moments for all the new complexes are summarized in Section 6.2. H_2daasal was prepared by the reaction of daa and salicylaldehyde (1:2). The tetradentate N_2O_2 donor site of the dianionic ligand is capable of complexing easily with various metal ions and various complexes were prepared by reacting the appropriate precursors ($CuCl_2 \cdot 2H_2O$, $NiCl_2 \cdot 6H_2O$ and $Zn(CH_3COO)_2 \cdot 2H_2O$) with H_2daasal in 1:1.5 mole ratio. Each synthetic step involved here is straightforward and provided good-to-moderate yield of the desired product in pure form. All the above compounds showed expected fragmentation patterns in the MALDI-TOF mass spectra.

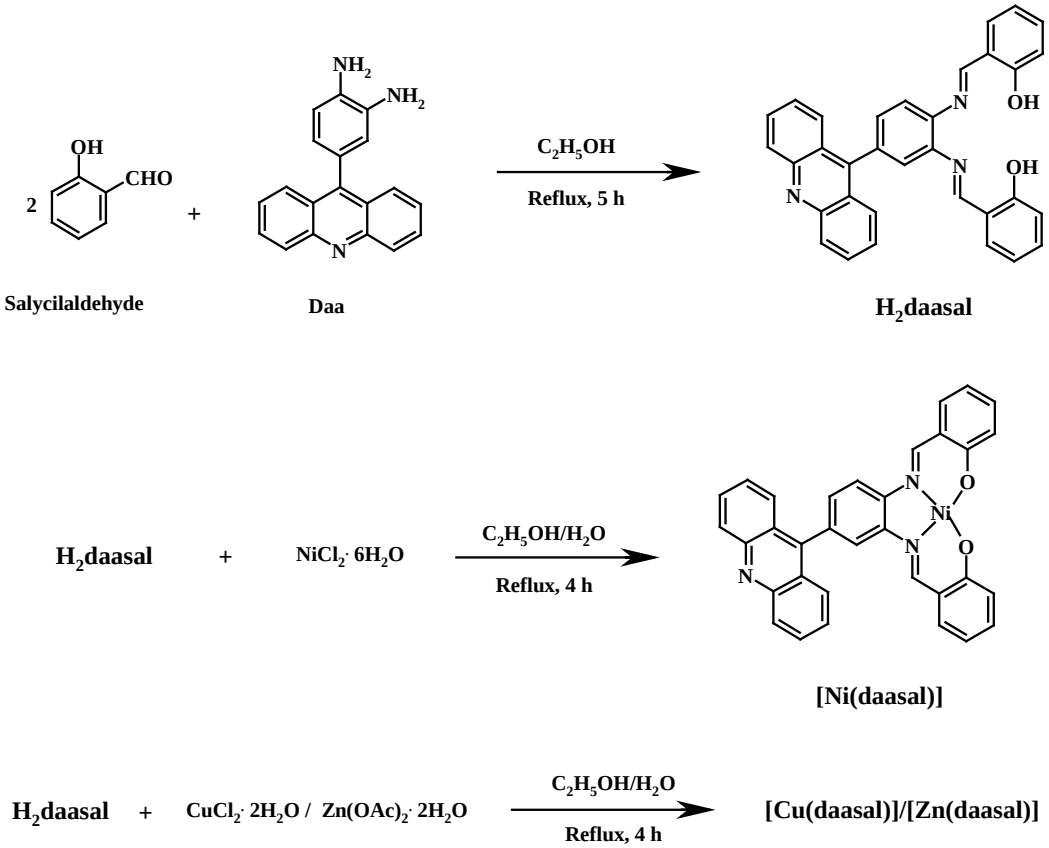

Fig. 6.1 Scheme leading to the synthesis of H_2daasal, [Ni(daasal)], [Cu(daasal)] and [Zn(daasal)].

6.3.2 Crystal structure

Slow evaporation of a DMF solution of H_2daasal and that of DMF-diethyl ether (1:3) solution of [Ni(daasal)] provided the single crystals of the respective compounds. Crystal parameters and details of the data collection and refinement, selected bond lengths (Å) and bond angles (^{o}) for H_2daasal and [Ni(daasal)] were given in Table 6.1, Table 6.2 and Table 6.3 respectively. Atomic coordinates and equivalent isotropic displacement parameters for both H_2daasal and [Ni(daasal)] were presented in Appendix I (Table 5 and Table 6).

Table 6.1 Crystallographic data for H_2daasal·$HCON(CH_3)_2$ and [Ni(daasal)]·$HCON(CH_3)_2$

	H_2daasal·$HCON(CH_3)_2$	**[Ni(daasal)]·$HCON(CH_3)_2$**
Chemical formula	C36 H30 N4 O3	C36 H28 N4 Ni O3
Formula weight	566.64	623.34
Crystal system	Monoclinic	Triclinic
Space group	$P2_1$ / c	P-1
a (Å)	9.0212(9)	17.9468(14)
b (Å)	13.0238(13)	13.4390(11)
c (Å)	13.7762(14)	12.8669(10)
α (°)	102.858(2)	90
β (°)	102.414(2)	108.1730(10)
γ (°)	103.829(2)	90
V ($Å^3$)	1469.5(3)	2948.5(4)
Z	2	4
μ (mm^{-1})	0.083	0.702
F (000)	596	1296
Crystal size (mm^3)	0.33 x 0.13 x 0.13	0.3 x 0.17 x 0.06
Reflections collected	17152	33697
Reflections unique	6831[R(int) = 0.0320]	7071[R(int)= 0.0542]
Parameters	392	487
*R*1, *wR*2 [$I \geq 2\sigma(I)$]	0.0736, 0.1782	0.0521, 0.1137
*R*1, *wR*2 (all data)	0.1342, 0.2124	0.0870, 0.1284
Goodness-of-fit on F^2	1.017	1.018
Largest peak, hole [*e* $Å^{-3}$]	0.302, -0.295	0.563, -0.257

The molecular structure of H_2daasal is shown in Fig. 6.2. The molecule as a whole is not planar primarily due to the twisting of acridine moiety along C18–C21 bond. The dihedral angle between the acridine and phenyl ring plane is 112^o. There are two intramolecular hydrogen bonds between the phenolic OH and imine – N atoms. The O1····N1 and O2····N2 distances are 2.587 (2) Å and 2.616 (3) Å, respectively. Both O1–H1····N1 and O2–H2····N2 angles are 147^o respectively.

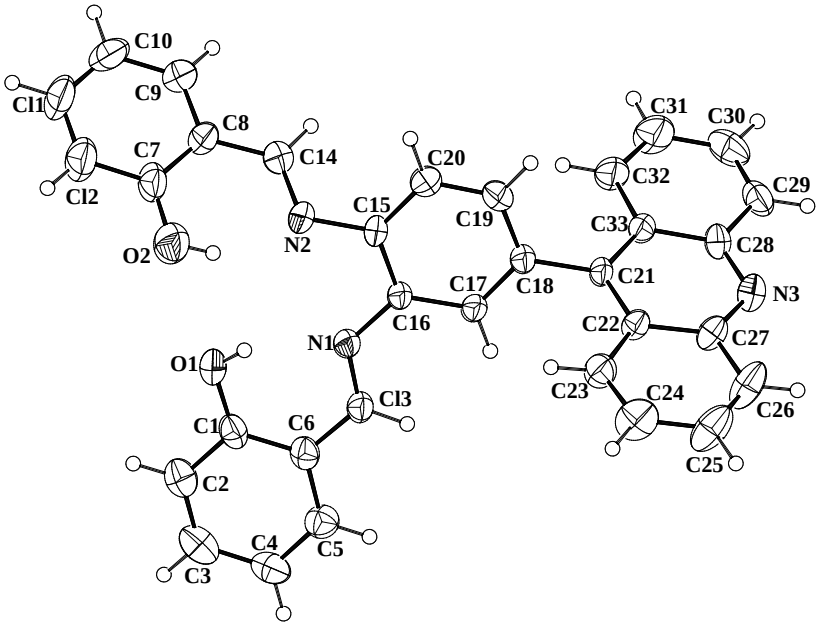

Fig. 6.2 Molecular structure of H_2daasal with atom-labeling scheme. All non-hydrogen atoms are represented by their 50 % probability thermal ellipsoids.

These hydrogen bonding parameters are comparable to those reported for H_2salen.[13] The hydrogen bond formation in the same salicylideneamine residue also prevents the planarity of the molecular fragment without acridine. The N=C and O-C bond lengths are 1.288(6) and 1.345(5) Å respectively. The latter value

is close to the values reported for salicylates and phenol derivatives [1.355(2)–1.377(4) Å].[14] The former is in the range [1.262(4)–1.281(9) Å] reported for N=C bond.[15] Another consequence of the different conformation of the two salicylideneamine fragments of the molecule is reflected in the N1-C16-C17 and N2-C15-C20 angles [124.6(2) and 121.2(2)^{o}]. The increase in the angle (3^{o}) in the former case alleviates steric interaction between atoms H13 and H17, which in the planar conformation is larger than that between the corresponding atoms H14 and H20 which are moved apart by the torsion around the N2-C15 bond.[13] Rest of the bond parameters in the molecule are unexceptional.

Table 6.2 Bond lengths [Å] and angles [^{o}] for H_2daasal·HCON(CH_3)$_2$

N(4)-C(36)	1.305(6)	C(17)-C(16)-N(1)	124.6(2)
N(4)-C(34)	1.398(5)	C(15)-C(16)-N(1)	116.54(19)
N(4)-C(35)	1.432(6)	C(28)-N(3)-C(27)	117.8(2)
O(3)-C(36)	1.199(6)	C(14)-N(2)-C(15)	118.6(2)
N(1)-C(13)	1.278(3)	N(1)-C(13)-C(6)z	121.5(2)
N(1)-C(16)	1.409(3)	C(22)-C(21)-C(18)	120.8(2)
C(16)-C(15)	1.396(3)	C(33)-C(21)-C(18)	120.35(19)
C(6)-C(13)	1.440(3)	C(17)-C(18)-C(21)	120.9(2)
N(3)-C(28)	1.338(3)	C(19)-C(18)-C(21)	120.4(2)
N(3)-C(27)	1.342(3)	N(3)-C(28)-C(29)	118.2(2)
N(2)-C(14)	1.284(3)	N(3)-C(28)-C(33)	123.6(2)
N(2)-C(15)	1.418(3)	C(20)-C(15)-C(16)	119.7(2)
C(21)-C(18)	1.488(3)	C(20)-C(15)-N(2)	121.2(2)
O(1)-C(1)	1.342(3)	C(16)-C(15)-N(2)	119.1(2)
O(2)-C(7)	1.346(3)	O(1)-C(1)-C(2)	118.9(2)
C(36)-N(4)-C(34)	122.8(6)	O(1)-C(1)-C(6)	121.4(2)
C(36)-N(4)-C(35)	117.4(5)	N(3)-C(27)-C(26)	118.3(2)
C(34)-N(4)-C(35)	119.8(6)	N(3)-C(27)-C(22)	123.5(2)
O(3)-C(36)-N(4)	126.8(6)	N(2)-C(14)-C(8)	121.9(3)
C(13)-N(1)-C(16)	122.92(19)	O(2)-C(7)-C(12)	117.9(3)
C(17)-C(16)-C(15)	118.8(2)	O(2)-C(7)-C(8)	122.1(2)

The molecular structure of [Ni(daasal)] is shown in Fig. 6.3. The dianionic ligand coordinates to the metal centre through the two phenolic –O and two imine-N atoms and forms a N_2O_2 square planar around the metal ion.[13,16] The azomethine (N=C) bond distances [1.301(3) and 1.303(3) Å] are slightly higher than that of H_2daasal while C-O bond lengths are [1.307(3) and 1.308 (3) Å] lower than the free ligand.

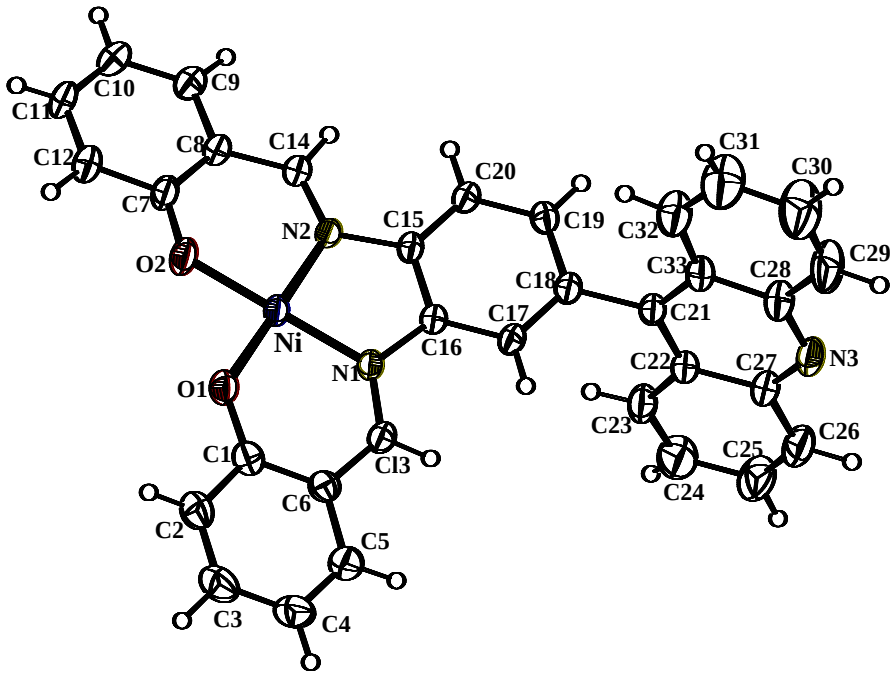

Fig. 6.3 Molecular structure of [Ni(daasal)] with atom-labeling scheme. All non-hydrogen atoms are represented by their 50 % probability thermal ellipsoids.

The planar NiN_2O_2 unit (0.0162 A^o) as bond lengths and bond angles typical of [Ni(salen)] type complexes.[17] The N1-C16-C17 (125.6(2)^o) and N2-C15-C20 (126.8(2)^o) angles are higher than that of H_2daasal. This indicates the change in the conformation compared to the free ligand due to chelation. The Ni-O bond lengths [1.8421(18) and 1.8365(18) Å] are shorter than Ni-N [1.854(2)

and 1.858(2) Å] bond distances. The dihedral angle between the acridine and phenyl ring in [Ni(daasal)] is about 103°. The sum of chelating angles around the nickel is 360.03(1)°.[17(a)] In both the cases, the presence of one DMF molecule was seen and this was removed for clarity in the ORTEP figures. In the crystal lattice, there is no significant intermolecular non-covalent interactions for both H_2daasal and [Ni(daasal)] compounds.

Table 6.3 Bond lengths [Å] and angles [°] for [Ni(daasal)]·$HCON(CH_3)_2$

O(3)-C(36)	1.328(9)	C(7)-O(2)-Ni(1)	127.24(17)
N(4)-C(36)	1.280(6)	C(13)-N(1)-C(16)	120.6(2)
N(4)-C(35)	1.385(7)	C(13)-N(1)-Ni(1)	126.60(17)
N(4)-C(34)	1.467(6)	C(16)-N(1)-Ni(1)	112.79(16)
Ni(1)-O(2)	1.8365(18)	C(14)-N(2)-C(15)	120.8(2)
Ni(1)-O(1)	1.8421(18)	C(14)-N(2)-Ni(1)	126.18(17)
Ni(1)-N(1)	1.854(2)	C(15)-N(2)-Ni(1)	113.03(15)
Ni(1)-N(2)	1.858(2)	C(16)-C(15)-N(2)	113.5(2)
O(2)-C(7)	1.308(3)	C(20)-C(15)-N(2)	126.8(2)
N(1)-C(13)	1.301(3)	C(1)-O(1)-Ni(1)	127.62(16)
N(1)-C(16)	1.422(3)	C(17)-C(18)-C(21)	118.9(2)
N(2)-C(14)	1.303(3)	C(19)-C(18)-C(21)	121.7(2)
N(2)-C(15)	1.421(3)	N(1)-C(13)-C(6)	124.9(2)
O(1)-C(1)	1.307(3)	C(22)-C(21)-C(18)	120.0(2)
C(18)-C(21)	1.492(3)	C(33)-C(21)-C(18)	121.0(2)
N(3)-C(27)	1.339(4)	N(2)-C(14)-C(8)	124.8(2)
N(3)-C(28)	1.346(4)	O(2)-C(7)-C(8)	124.2(2)
C(36)-N(4)-C(35)	124.5(7)	O(2)-C(7)-C(12)	118.6(3)
C(36)-N(4)-C(34)	119.2(6)	O(1)-C(1)-C(2)	118.9(3)
C(35)-N(4)-C(34)	116.2(5)	O(1)-C(1)-C(6)	124.0(2)
N(4)-C(36)-O(3)	117.6(8)	C(17)-C(16)-N(1)	125.6(2)
O(2)-Ni(1)-O(1)	84.88(8)	C(15)-C(16)-N(1)	113.9(2)
O(2)-Ni(1)-N(1)	178.17(9)	C(27)-N(3)-C(28)	117.7(2)
O(1)-Ni(1)-N(1)	94.43(8)	N(3)-C(27)-C(26)	118.3(3)
O(2)-Ni(1)-N(2)	94.71(8)	N(3)-C(27)-C(22)	123.4(3)
O(1)-Ni(1)-N(2)	179.43(9)	N(3)-C(28)-C(29)	117.9(3)
N(1)-Ni(1)-N(2)	86.00(8)	N(3)-C(28)-C(33)	123.6(3)
C(17)-C(16)-N(1)	125.6(2)	C(20)-C(15)-N(2)	126.8(2)

6.3.3 Characterisation of the compounds

6.3.3.1 Spectral characterization

^{1}H NMR spectrum of H_2daasal, Fig. 6.4a has been analyzed with the proton assignments being made on the basis of both integrated intensity and ^{1}H - ^{1}H coupling patterns observed in the ^{1}H – ^{1}H COSY spectra. The hydroxyl protons of the ligand appeared as two singlets at 13.03 and 12.99 ppm. These protons are not observed in the [Ni(daasal)] complex which confirms the deprotonation of the phenolic OH groups in the complex.[18,19]

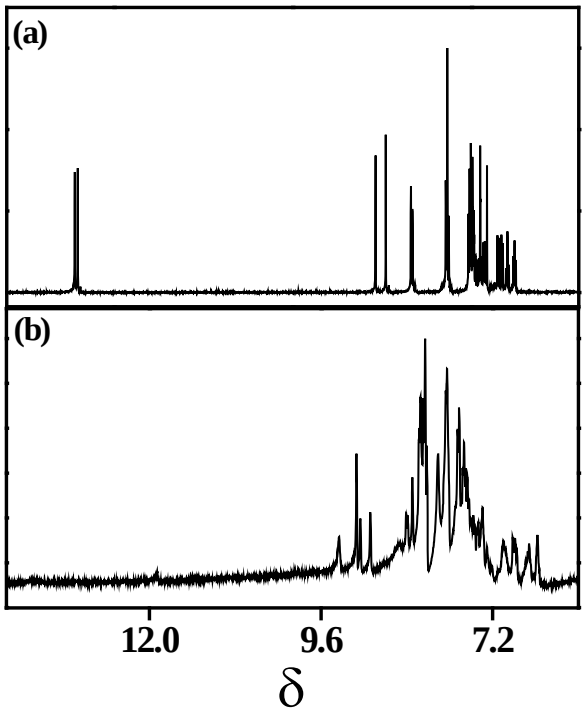

Fig. 6.4 ^{1}H NMR spectra of (a) H_2daasal (in $CDCl_3$) and (b) [Ni(daasal)] (in $(CD_3)_2SO$).

The –C(H)=N protons of H_2daasal appear as two sharp singlets at 8.84 and 8.69 ppm. Downfield shift of the azomethine protons in the case of [Ni(daasal)] (9.35 and 8.91ppm, Fig. 6.4b) when compared to free H_2daasal supports the coordination of the imine-N atoms. The acridine protons in both cases appear in the same region. Thus chelation has no effect on the acridine protons. Due to the paramagnetic nature of the [Cu(daasal)], we couldn't record the spectra. Due to the poor solubility of [Zn(daasal)] in DMSO, we recorded the 1H NMR spectrum in C_5D_5N. The hydroxyl protons are not observed in [Zn(daasal)] which confirms the deprotonation of the phenolic OH groups in the complex. The other protons of both [Ni(daasal)] and [Zn(daasal)] complexes and the ligand H_2daasal gave well-defined ^{1}H NMR spectra which permits unambiguous identification and assessment of purity. The COSY (^{1}H - ^{1}H) spectra for the ligand H_2daasal (in $CDCl_3$) is given in Fig. 6.5.

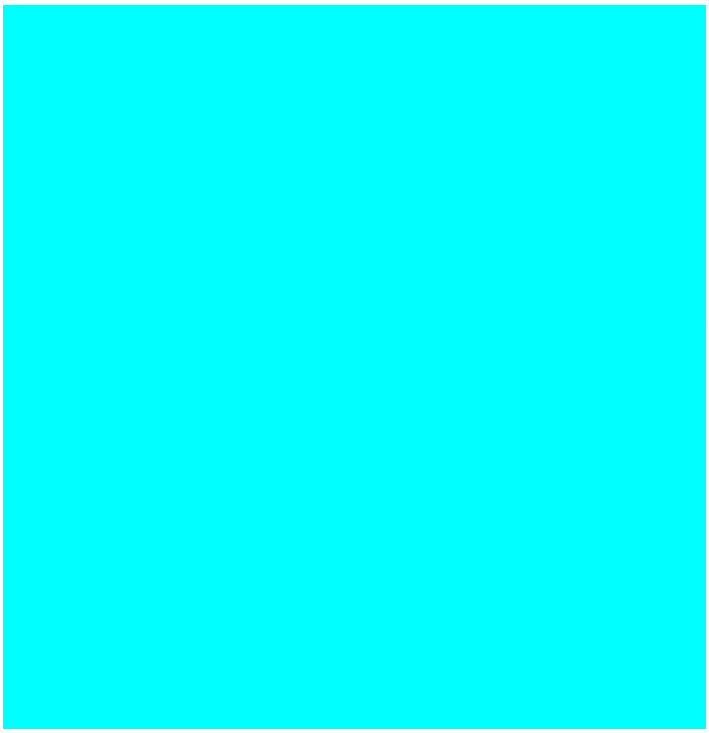

Fig. 6.5 ^{1}H – ^{1}H COSY spectrum of H_2daasal in $CDCl_3$

In the infrared spectrum of each of the three complexes, the characteristic intense absorption band corresponding to the imino C=N stretch is observed at ~ 1610 cm^{-1}. When compared to the free Schiff base, $\nu_{C=N}$ is shifted to lower wave number by 4 cm^{-1} due to the possible drift of the lone pair electron density towards the metal on coordination.[20] As expected, the Ni(II) and Zn(II) complexes [Ni(daasal)] and [Zn(daasal)] are diamagnetic. The Cu(II) complex, [Cu(Daasal)] is found to be paramagnetic and the μ_{eff} value (2.77 μ_B) suggests S=1/2 ground state.[21]

6.3.3.2 Absorption and emisssion

The absorption spectra of H_2daasal, and its metal complexes in DMF are shown in Fig. 6.6. The absorption maxima together with their extinction coefficients in various solvents are also recorded and given in Table 6.4, 6.5, 6.6 and Table 6.7 respectively. Fig. 6.6 shows the electronic perturbation that occurs upon metallation of the salen N_2O_2 cavity of H_2daasal with Ni(II), Cu(II) and Zn(II). Spectral modifications for the mononuclear metal complexes are noticed in both the high and low energy regions compared to the free H_2daasal. The bands in the range 355-390 nm are structurally characterized by low intensity.

These are assigned to the $\pi \rightarrow \pi^*$ transition of acridine chromophore[22] and the extended π -system of the daasalen skeleton. The absorption in the high energy region (270-330 nm) are attributed to the benzene $\pi \rightarrow \pi^*$ and imino $\pi \rightarrow \pi^*$ transitions. These bands are not significantly affected by chelation. In [Ni(daasal)], the prominent feature is the MLCT band at 482 nm typical of Ni(II)-salen complexes. The dissymmetric nature of this band may suggest the presence of $\pi \rightarrow \pi^*$ intra-ligand transition which undergoes a bathochromic shift relative to that of the free ligand. This shift can be attributed to a diminution of the HOMO-LUMO gap upon metallation.[18] The d-d band was not observed for both the Cu(II)

and Ni(II) complexes in DMF even at very high concentrations. The wavelength maxima (λ_{max}) and molar extinction coefficients (ε) of all the complexes change appreciably in different solvents due to physical intermolecular solute-solvent interaction forces (ion-dipole, dipole-dipole, H-bonding *etc*) which alter the energy difference between the ground and excited state of the absorping species containing the chromophore.[23]

The emission spectra of all the compounds were also recorded in various solvents. The emission maximum and the quantum yield values are evaluated by including refractive index corrections and tabulated in Tables 6.4, 6.5, 6.6 and 6.7. Fig. 6.6 shows the emission spectra of all the compounds in DMF. The presence of metal ions have little effect on the emission spectra is reflected by [Ni(daasal)] and [Cu(daasal)] complexes that includes fluorescence quenching and blue shift of 6 and 1 nm when compared to the free H_2daasal. But in the case of [Zn(daasal)], there is an enormous red shift (60 nm) when compared to the free H_2daasal. This may suggest a charge transfer character[24] that is highly solvent dependent.

In general, the fluorophore has a larger dipole moment in the excited state (μ_E) than in the ground state (μ_G) and on excitation in the presence of highly polar solvent, the dipoles can reorient or relax around μ_E which lowers the energy of the excited state and shifts the emission at longer wavelength.[25]

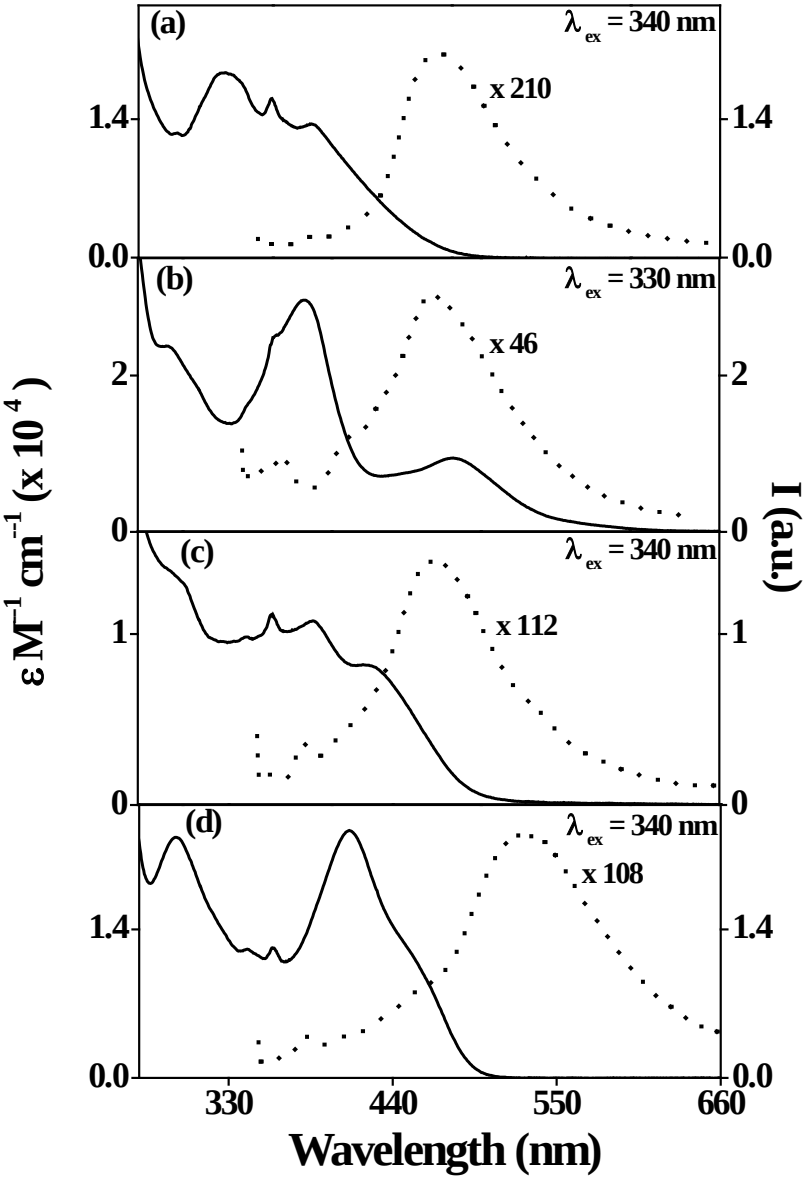

Fig. 6.6 UV-visible (——) and fluorescence (·····) spectra of (a) H_2daasal (b) [Ni(daasal)] (c) Cu(daasal)] and (d) [Zn(daasal)] in DMF.

Table 6.4 Absorption and fluorescence (λ_{exc} = 340 nm) data for **H_2daasal** in various solvents[a]

Solvent	**Absorption λ_{max} nm, (log ε)**	**Emission λ_{em} nm, (ϕ)**
	Ligand Transitions	
cyclohexane	246 (5.20), 253 (5.21), 273 (5.11), 328 (4.16), 359 (4.14)	463 (0.118)
toluene	221 (3.31), 253 (3.11), 286 (4.31), 338 (4.27), 359 (4.24)	468 (0.179)
CH_2Cl_2	252 (5.21), 335 (4.20), 360 (4.19)	467 (0.087)
THF	230 (4.68), 253 (3.37), 280 (4.36), 332 (4.25), 359 (4.21)	478 (0.223)
1,4-dioxane	257 (5.18), 334 (4.28), 359 (4.25), 384 (4.15)	476 (0.228)
CH_3CN	243 (5.21), 328 (4.27), 359 (4.25)	469 (0.051)
DMF	267 (4.39), 296 (4.10), 328 (4.27), 360 (4.21)	472 (0.087)
2-propanol	253 (5.20), 332 (4.24), 358 (4.24)	461 (0.092)
CH_3OH	242 (5.19), 325 (4.25), 358 (4.26), 389 (4.18)	452 (0.042)

a: Error limits: λ_{max}, ± 1 nm; log ε, ± 10%; ϕ, ± 10%

Table 6.5 Absorption and fluorescence (λ_{exc} = 330 nm) data for **[Ni(daasal)]** in various solvents[a]

Solvent	**Absorption λ_{max} nm, (log ε)**	**Emission λ_{em} nm, (ϕ)**
	Ligand Transitions	
cyclohexane	252 (5.14), 291 (4.38), 386 (4.47), 487 (3.95)	351, 367, 405 (0.029)
toluene	256 (3.31), 294 (4.39), 388 (4.50), 492 (3.99)	368, 477 (0.018)
CH_2Cl_2	204 (3.31), 253 (5.14), 292 (4.43)	369, 476 (0.015)
THF	230 (4.61), 253 (3.48), 281 (4.38), 291 (4.39), 386 (4.47), 488 (3.96)	367,475 (0.021)
1,4-dioxane	258 (5.11), 292 (4.45), 385 (4.54), 486 (4.03)	368, 477 (0.024)
CH_3CN	236 (5.14), 288 (4.42), 379 (4.50), 478 (4.00)	368, 471 (0.017)
DMF	213 (3.12), 269 (4.59), 381 (4.47), 482 (3.98)	349, 367, 466 (0.029)
2-propanol	210 (3.34), 217 (3.26), 254 (5.12), 291 (4.45), 362 (4.47), 381 (4.53), 482 (4.02)	368, 465 (0.018)
CH_3OH	242 (5.19), 325 (4.25), 358 (4.26), 389 (4.18)	368, 452 (0.042)

a: Error limits: λ_{max}, ± 1 nm; log ε, ± 10%; ϕ, ± 10%

Table 6.6 Absorption and fluorescence (λ_{exc} = 340 nm) data for **[Cu(daasal)]** in various solvents[a]

Solvent	**Absorption λ_{max} nm, (log ε)**	**Emission λ_{em} nm, (ϕ)**
	Ligand Transitions	
cyclohexane	246 (4.92), 340 (3.98), 359 (3.99), 385 (3.95), 429 (3.85)	380, 458 (0.068)
toluene	237 (3.10), 253 (3.11), 287 (4.18), 325 (4.12), 360 (4.06), 387 (3.98), 434 (3.91)	460 (0.129)
CH_2Cl_2	251 (4.93), 360 (4.03), 386 (3.96), 428 (3.85)	459 (0.031)
THF	231 (4.56), 281 (4.22), 359 (4.05), 385 (3.99), 430 (3.90)	477 (0.107)
1,4-dioxane	257 (4.90), 361 (4.06), 386 (4.01), 431 (3.90)	466 (0.063)
CH_3CN	243 (4.93), 343 (4.02), 360 (4.06), 383 (4.03), 420 (3.91)	462 (0.016)
DMF	228 (3.04), 248 (3.11), 269 (4.27), 361 (4.05), 388 (4.03), 421 (3.91)	381, 471 (0.039)
2-propanol	214 (3.14), 254 (4.88), 359 (4.09), 376 (4.03)	449 (0.014)
CH_3OH	209 (3.24), 245 (4.90), 291 (4.14), 359 (4.08), 373 (4.02)	350 (0.008)

a: Error limits: λ_{max}, ± 1 nm; log ε, ± 10%; ϕ, ± 10%

Table 6.7 Absorption and fluorescence (λ_{exc} = 340 nm) data for **[Zn(daasal)]** in various solvents[a]

Solvent	**Absorption λ_{max} nm, (log ε)**	**Emission**
	Ligand Transitions	**λ_{em} nm, (ϕ)**
cyclohexane	246 (5.10), 294 (4.35), 342 (4.08), 359 (4.08), 411 (4.32)	380, 517 (0.047)
toluene	222 (3.27), 235 (3.34), 255 (3.29), 298 (4.36), 344 (4.12), 361 (4.13), 415 (4.38)	522 (0.073)
CH_2Cl_2	252 (5.12), 295 (4.32), 344 (4.05), 361 (4.06), 410 (4.29)	520 (0.0503)
THF	230 (4.65), 254 (3.48), 296 (4.36), 360 (4.09), 414 (4.36)	521 (0.067)
1,4-dioxane	254 (5.09), 295 (4.39), 343 (4.14), 359 (4.14), 413 (4.38)	518 (0.098)
CH_3CN	235 (5.12), 293 (4.40), 342 (4.13), 360 (4.14), 405 (4.36)	517 (0.035)
DMF	214 (3.35), 221 (3.29), 235 (3.31), 267 (4.39), 295 (4.36), 343 (4.08), 360 (4.09), 411 (4.37)	381, 532 (0.059)
2-propanol	222 (3.43), 253 (5.08), 295 (4.39), 341 (4.13), 359 (4.14), 407 (4.36)	525 (0.064)
CH_3OH	245 (5.10), 294 (4.39), 341 (4.14), 359 (4.15), 401 (4.36)	447, 521 (0.024)

a: Error limits: λ_{max}, ± 1 nm; log ε, ± 10%; ϕ, ± 10%

6.3.3.3 ESR spectra

The ESR spectra of [Cu(daasal)] is recorded in solid state as well as in frozen (110 K) DMF-toluene (1:1) solution (Fig. 6.7).

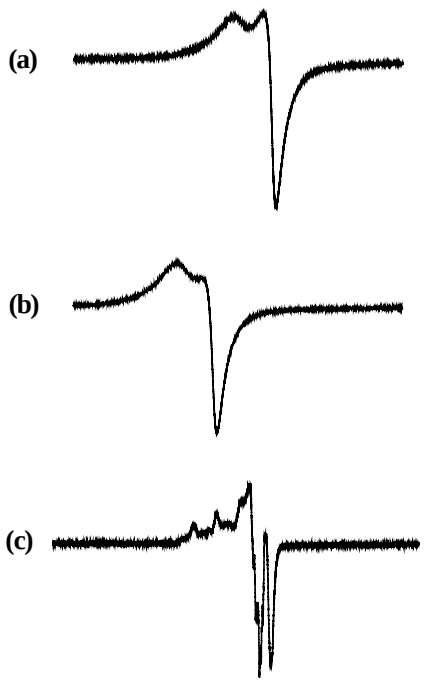

Fig. 6.7 ESR spectra of [Cu(daasal)] in (a) powder phase (298 K) (b) powder phase (110 K) and (c) frozen (110 K) DMF-toluene (1:1).

The spectral features are typical for a monomeric square planar or square pyramidal Cu(II) complex. The g_{11} and $g_{\perp}$ values are found to be in the range 2.18-2.16 and 2.06-2.02, respectively. The frozen solution spectrum displays the splitting of g_{11} signal to four lines (A_{11} = 20.8 G) due to ^{63}Cu nuclear spin (I=3/2).[26,27] The fine structure on the $g_{\perp}$ signal is most likely due to nitrogen super hyperfine splitting.

6.3.3.4 Cyclic voltammetry

Cyclic and differential-pulse voltammograms of H_2daasal, [Ni(daasal)], [Cu(daasal)] and [Zn(daasal)] are illustrated in Fig. 6.8 and the data are summarized in Table 6.8. For all the compounds, cathodic and anodic scans have been recorded in DMF and CH_3CN, respectively. During the cathodic scan in the cyclic voltammetric experiments containing 0.1 M TBAP, uncomplexed H_2daasal showed a poorly resolved reversible (i_{pc}/i_{pa} = 0.9 - 1.0) and diffusion controlled ($i_{pc}/\nu^{1/2}$ = constant in the scan rate (ν) range 50 - 500 mV s^{-1}) one–electron transfer (ΔE_p= 60 - 70 mV; ΔE_p = 65 ± 3 mV for Fc^+/Fc couple)[28] response at –1.44 V vs SCE. This potential is close to that for the one-electron reduction of acridine (-1.46 V).[29] No oxidation wave is observed for this ligand when scanned upto +1.9 V.

In the case of [Ni(daasal)], a reversible oxidation wave is observed at +1.03 V which is attributed to the formation of a nickel (III) complex. Such a potential is consistent with the $Ni^{III/II}$ redox couple of Ni-salen type complexes.[30] The first reduction wave at –1.21 V corresponds to the Ni(II) → Ni(I) reduction.[31] The second reduction response of [Ni(daasal)] is a reversible one which occurs at -1.48 V (acridine reduction). For [Cu(daasal)], an irreversible oxidation occurs at +0.96 V due to the Cu(II)→Cu(III) oxidative process.[32] The first reduction of [Cu(daasal)] at –1.35 V is attributed to the reduction of the metal center (Cu(II)→Cu(I)).[33]

The following quasi-reversible (i_{pc}/i_{pa} = 0.2 – 0.7 and ΔE_p = 90 - 200 mV in the scan rate (ν) range of 100 – 500 mV s^{-1}) reduction at –1.76 V is ascribed to the ligand reduction. In the case of [Zn(daasal)], two reduction waves are seen at –1.45 and –1.91V. The reversible reduction wave at –1.45 V is due to

the acridine chromophore and the second quasi-reversible reduction at –1.91 V probably corresponds to the salen reduction of the ligand.

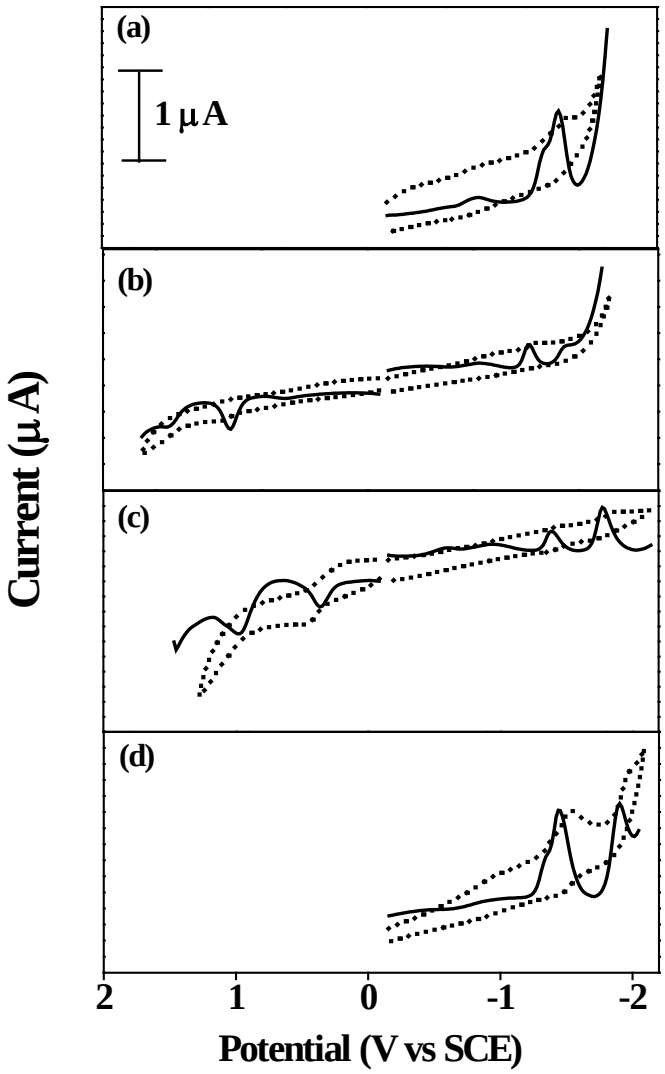

Fig. 6.8 Cyclic (·····) and differential pulse (——) voltammograms of (a) H_2daasal, (b) [Ni(daasal)], (c) [Cu(daasal)] and (d) [Zn(daasal)]. CH_3CN and DMF containing 0.1 M TBAP were used as solvents for the anodic and cathodic runs, respectively. Scan rate: 100 mV s^{-1}.

Table 6.8 Redox potential data[a] (recorded with 0.1 M TBAP)

Compound	Oxidation[b] $E_{1/2}$ (V vs SCE)	Reduction[c] $E_{1/2}$ (V vs SCE)
acridine	---	-1.46
daa	+ 0.88, +1.40[d]	-0.77, -1.07[d]
salicylaldehyde	---	-1.82
H_2daasal	---	- 1.44
[Ni(daasal)]	+1.03	-1.21, -1.48
[Cu(daasal)]	+0.96	-1.35, -1.76
[Zn(daasal)]	---	-1.45, -1.91

a) Obtained from the differential pulse voltammetri measurements. Error limits: $E_{1/2,} \pm 0.03$ V
b) CH_3CN
c) DMF
d) CH_2Cl_2

6.3.4 DNA binding

We set out to define the mode of interaction between the free ligand and all its complexes with the CT DNA using a combination of spectroscopic and hydrodynamic measurements. Attempts were made to convert all the compounds into its corresponding hydrochloride salts failed due to the cleavage of imine bond in the acidic medium. In order to make sure the complete solubility of the compounds in the buffer, DMF (10%) was added to the buffer solution while carrying out DNA studies.[34,35]

6.3.4.1 Absorption titration

The electronic absorption spectra in tris buffer (5 mM Tris, 50 mM NaCl, pH 7.1) of all the compounds are significantly perturbed on binding to CT DNA. In each instance, the addition of progressively increasing amounts of DNA

resulted in gradual hypochromism, decrease in the absorption intensities with a moderate red shift followed by saturation. Strong hypochromism and spectral broadening indicate intense interaction between the electronic states of the chromophore (acridine) in the complexes with that of the DNA bases.[10,36] Both H_2daasal and [Ni(daasal)] showed hypochromicity (14% and 39%) and red shift (by 2 and 3 nm) during the absorption titration experiments with CT DNA. Moreover, these compounds attain saturation at [DNA_{NP}]/[drug] ratio of 0.8 and 1.1 respectively. For [Cu(daasal)] and [Zn(daasal)], hypochromicity (42% and 17%) and red shift (by 3 and 2 nm) are observed. In these cases, the saturation is attained at [DNA_{NP}]/[drug] ratio of 1.4 and 0.5, respectively. The intrinsic binding constant values (K_b) which have been estimated for all the compounds (using equn. 2.2, chapter 2) are 1.16 x 10^5, 5.32 x 10^5, 7.43 x 10^5 and 8.21 x 10^4, M^{-1}, respectively for H_2daasal, [Ni(daasal)], [Cu(daasal)] and [Zn(daasal)] (Table 6.9). Representative titration figures for H_2daasal and [Zn(daasal)] are given in Figs. 6.9a and 6.9b.

6.3.4.2 Fluorescence titration

H_2daasal (λ_{em}, ϕ = 473, 0.034) and [Ni(daasal)] (λ_{em}, ϕ = 469, 0.062) are fairly good emitive species in comparison with [Cu(daasal)] (λ_{em}, ϕ = 473, 0.027) and [Zn(daasal)] (λ_{em}, ϕ = 512, 0.017) in buffer A in the absence of DNA under the similar experimental conditions. An excitation wavelength of 340 nm was used for all the compounds except [Ni(daasal)] where the wavelength used was 330 nm.

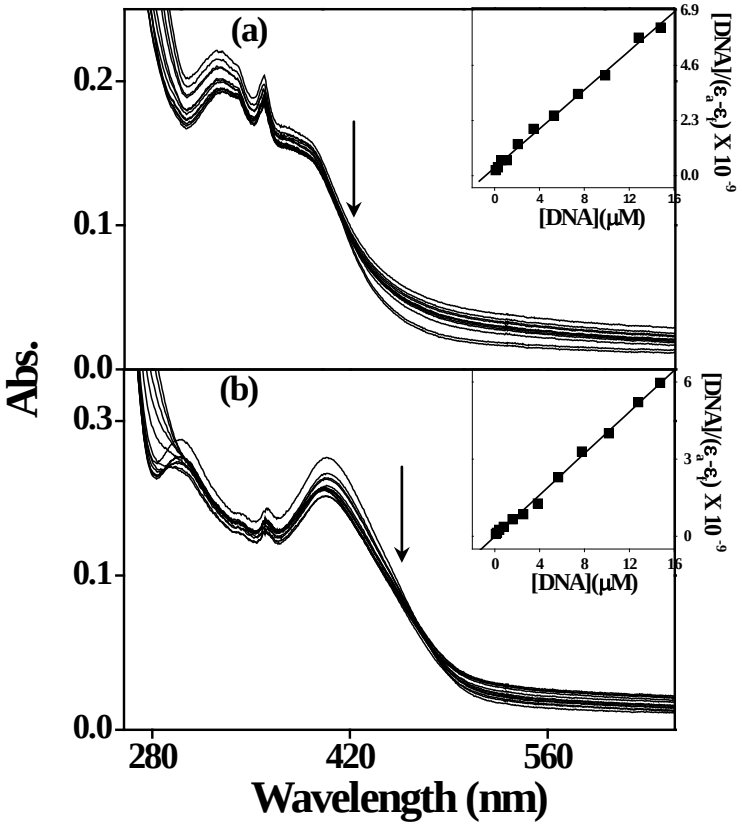

Fig. 6.9 UV-visible spectra of (a) H_2daasal (15 μM) and (b) [Zn(daasal)] (15 μM) in the absence (top curve) and presence (subsequent curves) of increasing concentrations (0 – 100 μM) of CT DNA in buffer A. The inset graphs show the fits of the absorbance data to obtain the binding constants.

The total emission intensity for all the compounds have been monitored in the range 390-640 nm. Steady state emission spectra of 8 μM solutions of all the compounds in tris buffer (5 mM Tris, 50 mM NaCl, pH 7.1) are titrated with the

increasing amounts of DNA over a range of concentration 0 - 200 μM. Upon addition of DNA to the compounds H_2daasal and [Ni(daasal), the emission intensity grows to 1.1 and 1.5 times larger than that in the absence of DNA. Both the compounds saturate at a [DNA_{NP}]/[drug] ratio of 4 and 8 with the bathochromic shift of 2 and 4 nm respectively.

Gradual addition of CT DNA (10 – 150 μM) to [Cu(daasal)] and [Zn(daasal)] have showed an increase in the emission intensity with an enhancement factor of ~ 2 and 1, respectively. The complexes attain saturation at the [DNA_{NP}]/[drug] ratio of ~ 8.6 and 1.2, respectively. The bathochromic shift of 2 nm is observed for [Zn(daasal)]. In the case of [Cu(daasal)], 7 nm blue shift of 7 nm is noted. The representative fluorescent titration curves for [Ni(daasal)] and [Cu(daasal)], are given in Fig. 6.10a and Fig. 6.10b. The shielding of the nitrogen on the intercalating acridine moiety from protonation in the bulk solvent medium causes emission enhancement on "molecular light switch" effect.[37-39] The mobility of these complexes is restricted at the binding site and so the vibrational modes of relaxation (collision and energy discipation) decreases on intercalation.[40] The data obtained from the emission spectra are fitted using the McGhee and Von Hippel equn. 2.4 (Chapter 2) to acquire the binding parameters including the binding constants (K_b). The K_b values obtained from McGhee and Von Hippel equn. are reasonably well in agreement with the values from the absorption titration experiments. The binding site sizes (n) for all the compounds are evaluated in the range 1-2. The emission enhancement and the very weak "molecular light switch" effect of all the compounds in the presence of DNA are comparable to that observed for dppz based Cu(II) and Ru(II) polypyridyl intercalators reported in the literature.[37-39,41]

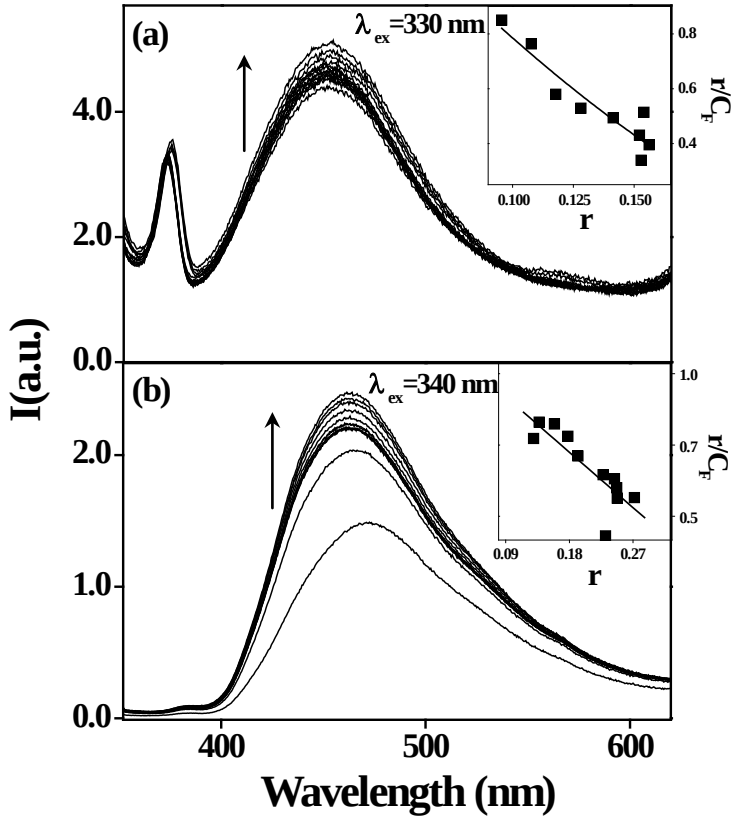

Fig. 6.10 Fluorescence spectra of (a) [Ni(daasal)] (8 μM) and (b) [Cu(daasal)] (8 μM) in the absence (bottom curve) and presence (subsequent curves) of increasing concentrations (0 – 200 μM) of CT DNA in buffer A. The inset graphs show the fits of the emission data to equn 2.4 (Chapter 2).

6.3.4.3 Thermal Denaturation

Interaction of small molecules with double helix is known to increase the melting temperature (T_m), the temperature at which the double helix denatures into single-stranded DNA.[42] The melting temperature for DNA in the absence

and presence of various complexes can be determined by monitoring the absorbance of the DNA at 260 nm as a function of temperature.[43] The OD at 260 nm are plotted against individual temperature in the presence of each metal complex and the mid point of the inflection regions in the temp. vs Rel. OD at 260 nm curves are taken as the corresponding T_m values. T_m for CT DNA in buffer B in the absence of any added complex is 60 ± 1°C under our experimental conditions. The T_m of DNA increased in the presence of the new compounds, at $[DNA_{NP}]/[complex] = 25$ in each case. Under the same set of conditions, addition of H_2daasal, [Ni(daasal)], [Cu(daasal)] and [Zn(daasal)] increased the T_m by 4, 6, 8, and 3°C, respectively (Table 6.9). The thermal denaturation curves for DNA in the absence and in the presence of all the compounds are shown in Fig. 6.11.

Table 6.9 Results of absorption titration and thermal melting experiments[a]

Compound	**K_b (M^{-1})**	**T_m °C (σ_T °)**
DNA	--	60 (21)
acridine	8.90×10^4	63 (22)
daasalH_2	1.16×10^5	64 (23)
daasalNi	5.32×10^5	66 (25)
daasalCu	7.43×10^5	68 (27)
daasalZn	8.21×10^4	63 (22)

a) Error limits: K_b, ± 10%; T_m, ±1 °C; σ_T, ±1°

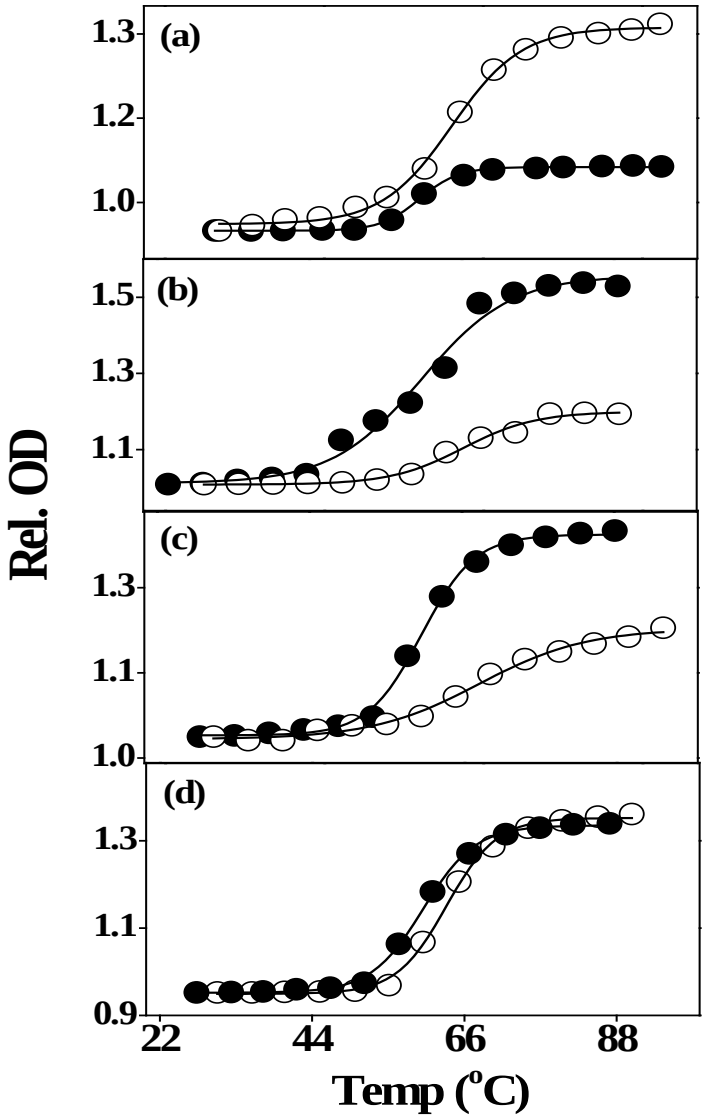

Fig. 6.11 Thermal melting curves of CT DNA (150 μM in NP) in the absence (●) and in the presence (○) of (a) H_2daasal (b) [Ni(daasal)], (c) [Cu(daasal)] and (d) [Zn(daasal)] ([(DNA)]/ [complex] = 25).

6.3.4.4 Viscometry experiments

The effects of H_2daasal, [Ni(daasal)], [Cu(daasal)] and [Zn(daasal)] on the viscosity of CT DNA solution have been investigated. The relative viscosity has been calculated for all the complexes studied at a complex to DNA ratio between 0.0 - 0.15 adopting the method described by Cohen and Eisenberg. Plots of $(\eta/\eta_o)^{1/3}$ vs [Drug]/[DNA] are shown in Fig. 6.12.

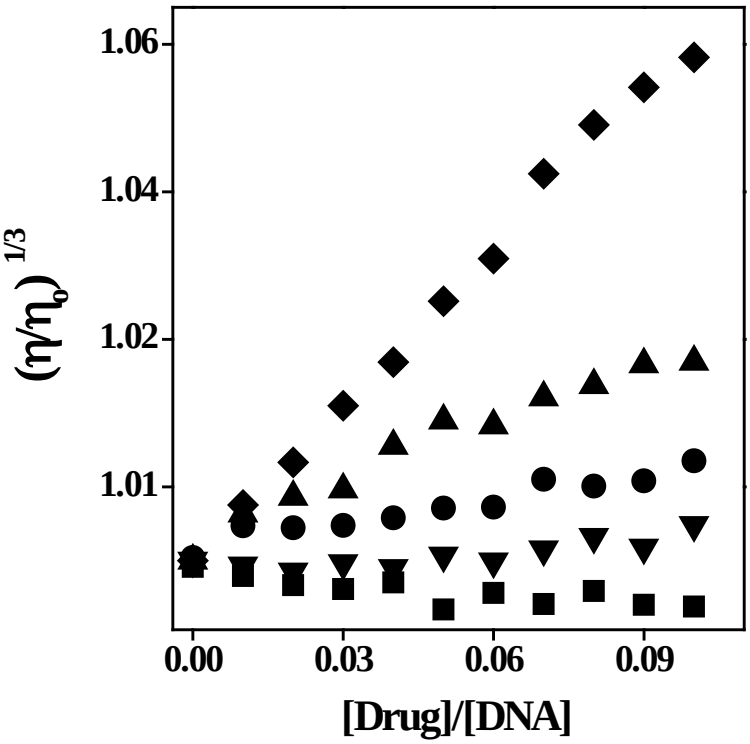

Fig. 6.12 Results of viscometric titrations carried out for CT DNA (300 μM, Buffer C) in the presence of H_2daasal (▼), [Ni(daasal)] (●), [Cu(daasal)] (▲), [Zn(daasal)] (■) and EtBr (◆) in buffer C.

Lerman observed a marked change in the viscosity of the DNA in solution when acridine, proflavin or acridine orange was added.[44] There is a reasonable change of viscosity with increasing addition of H_2daasal, [Ni(daasal)], [Cu(daasal)] and [Zn(daasal)] to the DNA solution. The EtBr acts as a classical intercalator and has stronger binding affinity when compared to all other compounds studied here. The reduction in peak intensities, bathochromic shifts in the absorption titration experiments, the increase in the T_m, σ_T values in the thermal denaturation experiments, the positive change of viscosity observed in the presence of DNA for these complexes and the free Schiff base are similar to those observed for various metallointercalator including the dppz-based complexes.[45-51]

Based on these similarities, it is proposed that acridine is involved in the intercalative interaction with DNA in the present set of complexes and moreover, the K_b values of all the complexes are higher than that of the free acridine (K_b = 8.9 x 10^4).[52] Thus the metal ion and the extended conjugation with salen moiety also contributes to a significant extent for the enhancement in the binding affinities with CT DNA. Overall the binding order sequence follows [Cu(daasal)] > [Ni(daasal)] > H_2daasal > [Zn(daasal)] ~ acridine.

6.3.5 DNA photocleavage

Fig. 6.13 summarizes the results of DNA photocleavage experiments carried out with the H_2daasal, [Ni(daasal)], [Cu(daasal)] and [Zn(daasal)]. The irradiation was done at 340 nm for 1 h and the cleavage has been monitored by the agarose gel electrophoresis method. Single-strand nicking is observed for each of these compounds and the percentage of conversions (using equn. 2.5, chapter 2) from form I (super coiled) to form II (nicked circular) are calculated. Control experiments suggested that untreated DNA does not show any cleavage

in the dark and even upon irradiation. (Lanes 1 and 2, Fig. 6.13). As reported in the literature, we also didn't observe any activity when pure Cu(II), Ni(II) and Zn(II) complexes and DNA were irradiated for about 1 h (data not shown). In the case of H_2daasal, there is a significant activity (30% of form II, lane 8, Fig. 6.13) are seen. [Cu(daasal)] complex is treated with 3-mercaptopropionic acid (3-MPA) (1.6 mM) in the dark as well as in the light experiments. It reveals that in the dark (8% of form II, lane 3, Fig. 6.13), there was very less activity as noticed in the case of DNA (12% of form II, lane 2, Fig. 6.13). However, in the case of light experiments with 3-MPA, it shows a noteworthy cleavage (72% of form II, lane 4, Fig. 6.13). The results indicate that the Cu(II) complex requires a reducing agent for its cleavage activity.[21,53-55]

Under light in the presence of $KHSO_5$ (oxone, 1 mM), [Ni(daasal)] cleaves DNA competently (32% of form II, lane 6, Fig. 6.13).[6(c),56,57] However no cleavage observed when the experiment was performed in dark in the presence of $KHSO_5$ (16% of form II, lane 5, Fig. 6.13). Similarly, no perceptible cleavage is observed for pBR 322 treated with [Zn(daasal)] in the dark and light experiments (Figures not shown). When this complex is treated with ascorbic acid (1mM)[58,59] nuclease activity (38% of form II, lane 7, Fig. 6.13) have been observed.

The active species responsible for the DNA cleavage mediated by the above compounds are described here. [Cu(daasal)] does not cleave DNA chemically. Addition of 3-MPA causes reduction of Cu(II) ($Cu^{II} \rightarrow Cu^{I}$) (72% of form II, (d), Fig. 6.13). The reduced complex presumably reacts with O_2 to give first $O_2^{\cdot -}$ and then hydrogen peroxide (H_2O_2). This *insitu* formed H_2O_2 would decompose upon reaction with DNA-bound Cu(I) to yield $OH^{\cdot}$ radicals which may react with deoxyribose residues in DNA leading to the cleavage of DNA.[7,60]

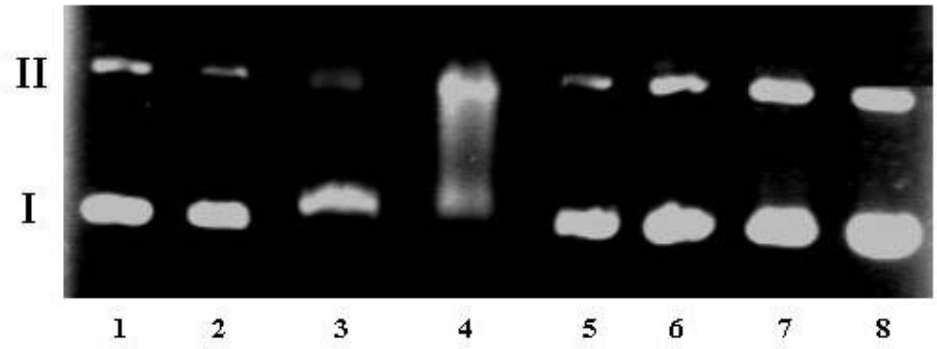

Fig. 6.13 Light-induced nuclease activity of H_2daasal, [Ni(daasal)], [Cu(daasal)] and [Zn(daasal)]. Dark and Light Experiments: Lanes 1 and 2: Untreated pBR 322 (100 μM) in the dark and upon irradiation ($\lambda_{irrd.}$= 340 nm, 60 min.). Lanes 3 and 4: pBR 322 + [Cu(daasal)] (10 μM) +3-MPA (1.6 mM) in the dark and light: Lanes 5 and 6: pBR 322 + [Ni(daasal)] (10 μM)+oxone (1 mM) in the dark and in light: Lane 7: pBR 322 + [Zn(daasal)] (10 μM) +ascorbic acid (1 mM) in light: Lane 8: pBR 322 + H_2daasal (10 μM) in presence of light respectively

This effect is also noticed in the inhibition experiments ((d), (f), Fig. 6.14). Inhibitors DMSO (49% of form II) and mannitol (42% of form II) act as hydroxyl radical quencher and inhibit the cleavage process. The other inhibiting reagents do not show any kind of activities. Moreover in the presence of tiron (superoxide anion radical quencher), inhibition (46% of form II, (g), Fig. 6.14) is observed. This supports the probability of the formation of superoxide anion radical ($O_2^{-\cdot}$) as a intermediate in the cleavage mechanism. For [Ni(daasal)], the active species involved is probably a Ni(III) species generated by the oxidizing agent (oxone) in the presence of light. On this basis, we anticipate the direct

involvement of an activated Ni(III) species for the observed DNA scission.[6b,61] The redox behaviour of the Ni(II) complex in cyclic voltammetry[57] (Ni(II)→Ni(III), +1.03 V) also supports our observations.

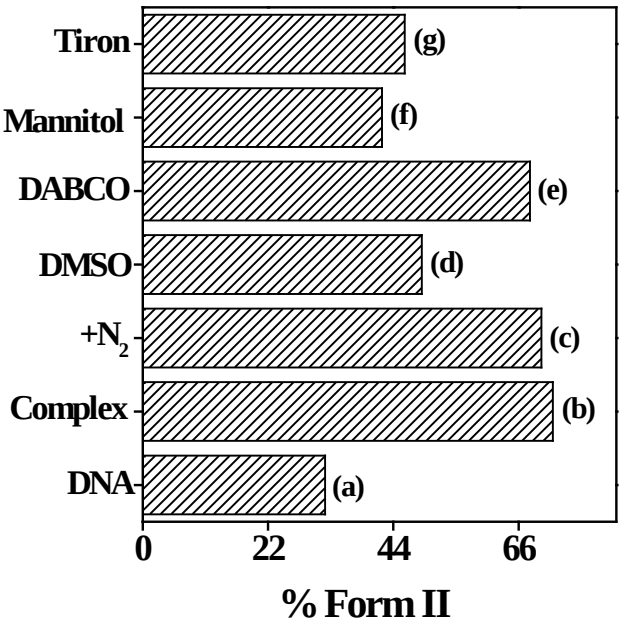

Fig. 6.14 Bar diagram representation of the effects of 'inhibitors' on the light-induced nuclease activity of [Cu(daasal)]. **(a)** DNA control: **(b)** pBR 322 + [Cu(daasal)] + 3-MPA(1.6 mM): **c-g**: pBR 322 + [Cu(daasal)] + 3-MPA (1.6 mM) in the presence of N_2, DMSO (200 mM), DABCO (10mM), mannitol (100 mM) and tiron (10mM), respectively, upon irradiation for 60 min. at 450 ± 5 nm in each case.

In the case of [Zn(daasal)], possibly DNA cleavage occurs *via* the same process as observed for the Cu(II) complex in presence of ascorbic acid.[58,59,62]

6.4 Summary

A series of Ni(II), Cu(II) and Zn(II) metal complexes with an acridine tethered Schiff base (H_2daasal) has been synthesized and characterized by FAB-MS, UV-visible, infrared, ^{1}H NMR, cyclic voltammetry and magnetic susceptibility methods. Solid structures of H_2daasal and [Ni(daasal)] have been determined by X-ray crystallography. The absorption and the emission spectra for all the compounds have been studied in various solvents. The ESR spectra of the Cu(II) complex shows typical monomeric copper(II) species. All the complexes are found to be square planar/square pyramidal on the basis of the above studies.

The absorption, fluorescence, thermal and viscometric experiments carried out to understand the DNA binding process by these compounds suggest an intercalative mode of DNA binding. The acridine moiety present in them plays a major role in the intercalative process. The apparent binding constants for all the compounds are in the range of 10^4 -10^5 M^{-1}. All the compounds are inactive for DNA cleaving in the dark experiments. In the presence of light (60 min. irradiation) free H_2daasal shows moderate activity with pBR 322. All the complexes treated with pBR 322 have been found to be inactive under the similar experimental conditions. When additives like 3-MPA(for [Cu(daasal)]), oxone (for [Ni(daasal)]) and ascorbic acid (for [Zn(daasal)]) were added cleaving of pBR 322 occurs to a noticeable extent. Especially Cu(II) complex cleaves DNA to a greater extent in presence of 3-MPA. The present findings demonstrate that modulation of the reactivities of the salen based reagents towards DNA is possible and provide a basis for sequence specific agents. This work can be extended by tethering suitable nucleic acid structural recognition matrices to the salen derivatives.

6.5 References

1. Topal, M. D.; Fresco, J. R. *Biochemistry* **1980**, *19*, 5531.
2. Wade, W. S.; Dervan, P. B. *J. Am. Chem. Soc.* **1987**, *109*, 1574.
3. Moser, H. E.; Dervan, P. B. *Science* **1987**, *238*, 645.
4. Kumar, C. V.; Asuncion, E. H. *Chem. Commun*. **1992**, 470.
5. (a) Gravert, D. J.; Griffin, J. H. *J. Org. Chem.* **1993**, *58*, 820. (b) Gravert, D. J.; Griffin, J. H. *Inor*g. *Che*m. **1996**, *35*, 4837.
6. (a) Woodson, S. A.; Muller, J. G.; Burrows, C. J.; Rokita, S. E. *Nucleic Acids Re*s. **1993**, *21*, 5524. (b) Muller, J. G.; Paikoff, S. J.; Rokita, S. E.; Burrows, C. J. *J. Inorg. Biochem.* **1994**, *54*, 199. (c) Burrows, C. J.; Rokita, S. E. *Acc. Chem. Res.* **1994**, *27*, 295.
7. Routier, S.; Bernier, J-L.; Waring, M. J.; Colson, P.; Houssier, C.; Baily, C. *J. Org. Chem*. **1996**, *61*, 2326.
8. (a) Mandal, S. S.; Vinaykumar, N.; Varshney, U.; Bhattacharya, S. *J. Inorg. Biochem.* **1996**, *63*, 265. (b) Bhattacharya, S.; Mandal, S. S. *Biochem. Biophys. Acta* **1997**, *132*3, 29. (c) Mandal, S. S.; Renuka, K.; Guru Row, T. N.; Bhattacharya, S. *J. Chem. Soc., Chem. Commun.* **1996**, 2725.
9. Sato, K.; Chikira, M.; Fujii, Y.; Komatsu, A. *J. Chem. Soc., Chem. Commun.* **1994**, 625.
10. Liu, G-D.; Yang, X.; Chen, Z-P.; Shen, G-L.; Yu, R-Q. *Anal. Sci.* **2000**, *16*, 1255.
11. Liu, G-D.; Liao, J-P.; Huang, S-S.; Shen, G-L.; Yu, R-Q. *Anal. Sci.* **2001**, *17*, 1031.
12. Plater, M. J.; Greig, I.; Helfrich, M. H.; Ralston, S. H. *J. Chem. Soc., Perkin Trans. 1* **2001**, 2553.

13. Pahor, N. B.; Calligaris, M.; Delise, P.; Dodic, G.; Nardin, G.; Randaccio, L. *J. Chem. Soc., Dalton Trans.* **1976**, 2478.

14. (a) Tsoucaris, D.; Rango, R. G.; Zelwer, C. H.; Parthasarathy, R.; Cole, F. E. *Cryst. Struct. Comm.* **1973**, *2*, 193. (b) Beale, J. P. *ibid*. P 125. (c) Cotrait, M.; Bideau, J. P. *ibid*. P 111. (d) Wozniak, K.; Grech, E.; Chelmieniecka, A. S. *Polish J. Chem.* **2000**, *74*, 717.

15. (a) Plana, F.; Miravitlles, C.; Brianse, J. L.; Foltalbana, M. *Cryst. Struct. Comm.* **1974**, *3*, 135. (b) Manotti, A. M.; Camellini, A. T. *ibid*. **1975**, *4*, 141.

16. (a) Averseng, F.; Lacroix, P. G.; Malfant, I.; Lenoble, G.; Cassoux, P.; Nakatani, K.; Fanton, I-M.; Delaire, J. A.; Aukauloo, A. *Chem. Mater.* **1999**, *11*, 995. (b) Haikarainen, A.; Sipila, J.; Pietikainen, P.; Pajunen, A.; Mutikainen, L. *J. Chem. Soc., Dalton Trans.* **2001**,991.

17. (a) Miller, H. A.; Laing, N.; Parsons, S.; Parkin, A.; Tasker, P. A.; White, D. J. *J. Chem. Soc., Dalton Trans.* **2000**, 3773. (b) A survey of the CCDC reveals huge number of square planar nickel(II)-salen complexes. Ni-N and Ni-O distances average 1.86 and 1.85 Å respectively. Fletcher, D. A.; McMeeking, R. F.; Parkin, D. J.; *J. Chem. Inf. Comput. Sci.* **1996**, *36*, 746.

18. Pellegrin, Y.; Berg, K. E.; Blondin, G.; Elodie, A-M.; Leibl, W.; Aukauloo, A. *Eur. J. Inorg. Chem.* **2003**, 1900.

19. Mokhles, M.; Elzaher, A. *J. Chin. Chem. Soc.* **2001**, *48*, 153.

20. Nejati, K.; Rezvani, Z. *New. J. Chem.* **2003**, *27*, 1665.

21. Dhar, S.; Senapati, D.; Das, P. K.; Chattopadhyay, P.; Nethaji, M.; Chakravarty, A. R. *J. Am. Chem. Soc*. **2003**, *125*, 12118.

22. Werner, T.; Fahnrich, K.; Huber, C.; Wolfbeis, O. S. *Photochem. Photobiol.* **1999**, *70*, 585.

23. Reichardt, C. *Solvents and Solvent Effects in Organic Chemistry*, 2nd ed.; VCH: Weinheim, 1988.
24. Wang, X-Y.; Guerzo, A. D.; Schmehl, R. H. *Chem. Commun.* **2002**, 2344.
25. Lackowicz, J. R. *Principles of Fluorescence Spectroscopy*; Plenum Press: New York, 1983**.**
26. (a) Sakaguchi, U.; Addison, A. W. *J. Chem. Soc., Dalton Trans.* **1979**, 600. (b) Nejati, K.; Rezvani, Z. *New J. Chem.* **2003**, *27*, 1665.
27. (a) Blake, A. B.; Chipperfield, J. R.; Hussain, W.; Paschke, R.; Sinn, E. *Inorg. Chem.* **1995**, *34*, 1125. (b) Shaffer, T. D.; Shet, K. A. *Mol. Cryst. Liq. Cryst.* **1989**, *172*, 27.
28. Nicholson, R. S.; Shain, I. *Anal. Chem*. **1964**, *36*, 706.
29. Joseph, J.; Eldho, N. V.; Ramaiah, D. *J. Phys. Chem. B.* **2003**, *107*, 4444.
30. Castro, B. D.; Freire, C. *Inorg. Chem.* **1990**, *29*, 5113.
31. (a) Lukes, P. J.; Mcgregor, A. C.; Clifford, T.; Crayston, J. A. *Inorg. Chem.* **1992**, *31*, 4697. (b) Fang, D. M.; Peters, D. G.; Mubarak, M. S. *Jour. Electrochem.Soc*. **2001**, *148*, 464.
32. Das, S.; Muthukumaragopal, G. P.; Pal, S. N.; Pal, S. *New J..Chem.* **2003**, *27*, 1102.
33. (a) Samide, M. J.; Peters, D. G.; *J. Electroanal. Chem.* **1998**, *443* 95. (b) Bhadbhade, M. M.; Srinivas, D. *Inorg. Chem.* **1993**, *32*, 6122.
34. Dhar, S.; Senapati, D.; Reddy, P. A. N.; Das, P. K.; Chakravarty, A. R. *Chem. Commun*. **2003**, 2452.
35. Sastri, C. V.; Eswaramoorthy, D.; Giribabu, L.; Maiya, B. G. *J. Inorg. Biochem*. **2003**, *94*, 138.
36. Kumar, C. V.; Asuncion, E. H. *J. Am. Chem. Soc.* **1993**,*115*, 8541.
37. Dupureur, C. M.; Barton, J. K. *J. Am. Chem. Soc.* **1994**, *116*, 10286.

38. Friedman, A. E.; Chambron, J-C.; Sauvage, J-P.; Turro, N. J.; Barton, J. K. *J. Am. Chem. Soc.* **1990**, *112*, 4960.
39. Hartshorn, R. M.; Barton, J. K. *J. Am. Chem. Soc.* **1992**, *114*, 5919
40. Wu, J-Z.; Ye, B-H.; Wang, L.; Ji, L-N.; Zhou, J-Y.; Li, R-H.; Zhou, Z-Y. *J. Chem. Soc., Dalton Trans.* **1997,** 1395.
41. Metcalfe, M.; Thomas, J. A. *Chem. Soc. Rev.* **2003**, *32*, 215.
42. Patel, D. J. *Acc. Chem. Res.***1979**, *12*, 118.
43. Lehninger, A. L. *Biochemistry*, 2nd *ed.;* Worth Publishers: New York, **1975**; p 873.
44. Lerman, L. S. *J. Mol. Biol.* **1961**, *3*, 18.
45. Holmlin, R. E.; Yao, J. A.; Barton, J. K. *Inorg. Chem*. **1999**, *38*, 174.
46. Stoeffler, H. D.; Thornton, N. B.; Temkin, S. L.; Schanze, K. S. *J. Am. Chem. Soc*. **1995**, *117*, 7119.
47. Olson, E. J. C.; Hu, D.; Hormann, A.; Jonkman, A. M.; Arkin, M. R.; Stemp, E. D. A.; Barton, J. K.; Barbara, P. F. *J. Am. Chem. Soc.* **1997**, *119*, 11458.
48. Murphy, C. J.; Barton, J. K. *Methods Enzymol.* **1993**, *226*, 576.
49. Holmlin, R. E.; Barton, J. K. *Inorg. Chem*. **1995**, *34*, 7.
50. Linncoln, B.; Broo, A.; Norden, B. *J. Am. Chem. Soc*. **1996**, *118*, 2644.
51. Schoch, K.; Hubbard, J. L.; Zoch, C. R.; Yi, G-B.; Sorlie, M. *Inorg. Chem.* **1996**, *35*, 4383.
52. McConnaughie, A. W.; Jenkins, T. C. *J. Med. Chem.* **1995**, *38*, 3488.
53. Dhar, S.; Chakravarty, A. R. *Inorg. Chem*. **2003**, *42*, 2483.
54. Gupta, T.; Dhar, S.; Nethaji, M.; Chakravarty, A. R. *Dalton Trans.* **2004**, 1896.
55. Pitie, M.; Boldron, C.; Gornitzka, H.; Hemmert, C.; Donnadieu, B.; Meunier, B. *Eur. J. Inorg. Chem.* **2003**, 528.

56. Sigman, D. S.; Mazumder, A.; Perrin, D. M. *Chem. Rev.* **1993**, *93*, 2295
57. Mandal, S. S.; Varshney, U.; Bhattacharya, S. *Bioconjugate Chem*. **1997,** *8*, 798.
58. Sigman, D. S. *Biochemistry* **1990**, *29*, 9097.
59. Santra, B. K.; Reddy, P. A. N.; Neelakanta, G.; Mahadevan, S.; Nethaji, M.; Chakravarty, A. R. *J. Inorg. Biochem*. **2002**, *89*, 191.
60. Sigman, D. S. *Acc. Chem. Res.* **1986**, *19*, 180.
61. Goldsby, K. A.; Blaho, J. K.; Hoferkamp, L. A. *Polyhedron* **1989** *8*, 113.
62. Hirohama, T.; Arii, H.; Chikira, M. *J. Inorg. Biochem.* **2004**, *98*, 1778.

CHAPTER 7

Conclusions

DNA binding and cleavage aspects of new mixed-ligand metallo-polypyridyl complexes that incorporate rationally designed electro- or photo-active ligands form the main theme of this study.

In chapter 1 of the thesis, recent literature related to DNA binding and photocleavage by organic molecules and metallointercalators in the light of their applicability as spectroscopic and structural probes, site specific agents, molecular light switches *etc* has been discussed. The literature survey presented in this chapter is not intended to be exhaustive, but is only representative, with emphasis being laid on those examples that bear relevance to the main theme of the present thesis. Chapter 2 describes the preparations of various precursor materials and a brief description of the physicochemical as well as biochemical techniques employed in this study while the synthesis of ppym, aip, pyip, acdppz, H_2daasal and its corresponding metal complexes are discussed in their respective chapters (Chapter 3, 4, 5 and 6 respectively). Chapters 3, 4, and 5 deal with the design, synthesis, structure, DNA binding and photocleavage properties of ruthenium(II) complexes containing modified 1,10-phenanthroline (phen) ligands. In chapter 6, synthesis, crystal structure, DNA binding and photocleavage properties of an acridine tethered H_2salen like Schiff base (H_2daasal) and its Ni(II), Cu(II) and Zn(II) complexes have been described. While CT DNA was used for binding studies, supercoiled pBR 322 DNA was used for the photocleavage experiments throughout this work.

7.1 Ruthenium(II) complexes of anthracene/pyrene/acridine-linked polypyridyl ligands

The effect of variation of the ligand architecture on the ability to bind and photocleave DNA by metal complexes by incorporating the polypyridyl family of ligands is of current interest. Here we synthesized some new ligands (*viz*. ppym, aip, pyip and acdppz) of this class (Fig. 7.1) and employed them to prepare mixed-ligand Ru(II) complexes. These complexes have been used to study the DNA binding and photocleavage properties.

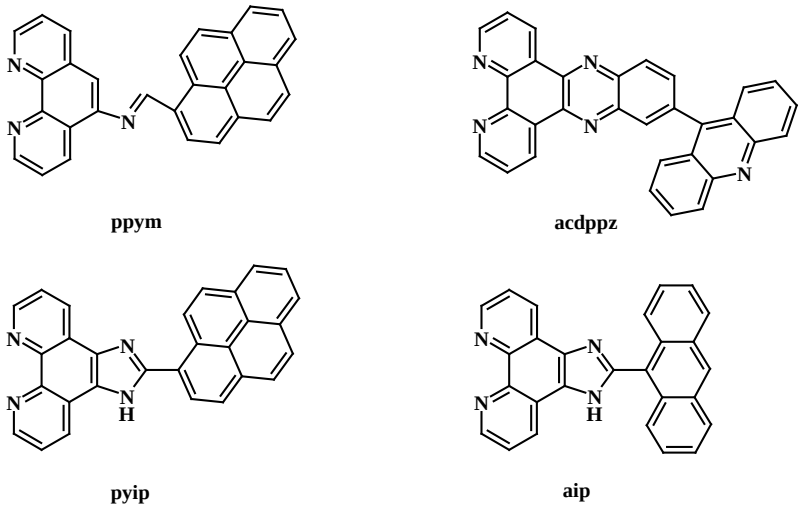

Fig. 7.1

In chapter 3, we have discussed the synthesis, spectral, photophysical and electrochemical characterization of N-[1,10]phenanthrolin-5-yl-pyrenylmethanimine (ppym) and its mixed-ligand ruthenium(II) complex $[Ru(phen)_2(ppym)]^{2+}$. The photophysical properties of the ligand ppym has been thoroughly studied. It shows dual emission characteristics and this has been interpreted by invoking an excimer mechanism. The crystal structure for the free ligand ppym is reported in this chapter. Complex $[Ru(phen)_2(ppym)]^{2+}$ shows a single emission characteristic of ^{3}MLCT. The results of DNA binding studies

carried out with $[Ru(phen)_2(ppym)]^{2+}$ are reminiscent of those reported earlier for various metallointercalators. This complex strongly binds with calf thymus (CT) DNA. The engagement of the ppym ligand of $[Ru(phen)_2(ppym)]^{2+}$ in the intercalative interaction is confirmed by absorption, fluorescence, thermal melting and viscometric titrations studies. The fluorescence studies have revealed that $[Ru(phen)_2(ppym)]^{2+}$ acts as moderate "molecular light switch" for DNA. The binding constant is in the order of 10^5 M^{-1}. This complex is an efficient photocleaving agent for the pBR 322 DNA and hydroxyl radical plays a key role in the photocleavage mechanism.

Chapter 4 of this thesis deals with the synthesis, characterization and DNA interactions of two new mixed-ligand complexes, *viz*: $[Ru(phen)_2(aip)]^{2+}$ and $[Ru(phen)_2(pyip)]^{2+}$ (aip = 2-(9-anthryl)-1H-imidazo[4,5-f][1,10]phenanthroline; pyip = 2-(1-pyrenyl)-1H-imidazo[4,5-f][1,10]phenanthroline) containing imidazole incorporated ligands aip and pyip. Results of absorption, emission, thermal melting and viscometric studies suggest that $[Ru(phen)_2(aip)]^{2+}$ and $[Ru(phen)_2(pyip)]^{2+}$ bind to DNA *via* an intercalative mode. DNA binding efficiencies roughly follow the trend: $[Ru(ip)_2(dppz)]Cl_2$ ~ $[Ru(phen)_2(dppz)]Cl_2$> $[Ru(phen)_2(pyip)]Cl_2$ > $[Ru(phen)_2(aip)]Cl_2$ > $[Ru(phen)_3]Cl_2$ (where, ip= imidazo[4,5-f][1,10]phenanthroline, dppz = dipyrido[3,2-a:2',3'-c]phenazine). Under the similar set of experimental conditions, $[Ru(phen)_2(aip)]^{2+}$ is found to be fairly good emitive species in aqueous buffer solutions in the absence of DNA in comparison with $[Ru(phen)_2(pyip)]^{2+}$. In the presence of excess DNA, these mixed-ligand ruthenium(II) complexes not only display fluorescence enhancements but also concomitant bathochromic shifts in their emission maxima. Emission enhancements observed for these mixed-ligand ruthenium(II) complexes on binding with DNA are interpreted in terms of a decrease in the non-radiative

deactivation process of each excited state due to the protection of aip/pyip by intercalation.[1]

DNA photocleavage experiments carried out with $[Ru(phen)_2(aip)]Cl_2$ and $[Ru(phen)_2(pyip)]Cl_2$ have been compared with those obtained for $[Ru(phen)_3]^{2+}$, $[Ru(phen)_2(dppz)]^{2+}$ and some compounds reported by L-N Ji ($[Ru(L)_2(L^1)]^{2+}$, where L is phen/bpy and L^1 is ip, pip and similar ligands).[2] Under the similar amount of drug dose and irradiation (60 min.) conditions, $[Ru(phen)_2(pyip)]^{2+}$ is seen to effectively photocleave the DNA compared to $[Ru(phen)_2(aip)]^{2+}$. The photocleaving abilities of both the complexes are comparable with that of other imidazole fused compounds reported by L-N. Ji and his co-workers.[2] DNA nicking efficiencies roughly follow the trend: $[Ru(phen)_2(pyip)]Cl_2$ > $[Ru(phen)_2(aip)]Cl_2$ > $[Ru(phen)_3]Cl_2$. This order can be explained on the basis of the differences in the π-aromatic character of the ligands in these complexes. The extended π- aromatic nature in the case of pyip is more when compared to aip and that of aip is more than phen. The results from 'inhibition' studies suggest that both the reactive oxygen species hydroxyl radical ($^{\bullet}OH$) and singlet oxygen ($^1O_2$, lesser extent) play a significant role in the cleavage mechanism for $[Ru(phen)_2(pyip)]Cl_2$ whereas for $[Ru(phen)_2(aip)]Cl_2$ only hydroxyl radical ($^{\bullet}OH$) plays a role.

As mentioned earlier, the new ligands employed in this study have been so designed that their architectures promote strong DNA intercalation and the electronic structures of the complexes derived out of these ligands assist efficient photocleavage of DNA. Dipyridophenazine, a near-planar, hetero-aromatic entity whose metal-complexes have found various applications,[3-6] has been chosen as the 'platform' for building more elaborate ligand systems. They have shown strong binding affinity towards DNA and cause the "molecular light switch" effect in the emission titration experiments. Eventhough acridine fluorophore and

its derivatives are well established DNA intercalators due to their mode of action at both molecular and cellular level. However, its binding affinity with DNA (K_b= 8.9 x 10^4)[7] is very weak when compared with dppz and its derivatives. Hence, we have planned to design a ligand that will have both the dppz and acridine moieties.

In chapter 5, we have discussed about the synthesis, crystal structure, DNA binding and photocleavage characteristics of $[Ru(phen)_2(acdppz)]^{2+}$ (where acdppz = 11-(9-acridinyl)dipyrido[3,2-a:2,3-c]phenazine (Fig. 7.1)). In the crystal lattice, acdppz forms a one-dimensional array through inter-molecular C-H⋯N and π-π interactions. The X-ray structure of the complex reveals that the acridine moiety of one complex cation is involved in π-π interaction with the dppz plane of the adjacent complex cation with an inter-planar distance of 3.365 Å and forms a discrete dimer. This value of inter-planar distance is similar to base pair stacking in DNA and for intercalator-base pair stacking in oligonucleotide intercalator complexes.

The interaction of this new complex with DNA has been monitored by absorption, fluorescence, thermal melting and viscometric methods. Results of the above experiments suggest that the molecule interacts with DNA through intercalative mode and the DNA binding constant, K_b, for $[Ru(phen)_2(acdppz)]^{2+}$ is 2.65 x 10^6 M^{-1}. Agarose gel electrophoresis experiments carried out with the above complex and the pBR 322 DNA suggest that this is an efficient photocleaving agent for the plasmid. Experiments carried out in the presence of various ‘inhibitors’ indicate that singlet oxygen ($^1O_2$) plays a significant role in the DNA photocleavage mechanism.

7.2 Cu(II), Ni(II) and Zn(II) complexes of acridine tethered Schiff base

It was noticed during the course of this work that, binding studies using complexes having a metal ion other than ruthenium have attracted much less attention. Earlier investigations have indicated that some metallo-salen [H_2salen = bis(salicylidene)ethylenediamine] derivatives bind DNA avidly and few others induce effective DNA scission. Therefore, subtle variation in the structure of the salen^{2-} unit and variation of the central metal ion may influence the effect of the resulting complex on DNA.[8-9]

Chapter 6 discusses the design, synthesis, crystal structure, DNA binding and photocleaving properties of a new H_2salen type Schiff base H_2daasal and its Ni(II), Cu(II) and Zn(II) complexes. The crystal structures of the H_2daasal and its Ni(II) complex have been determined. UV-visible and fluorescence spectra have been recorded for all the four compounds in various organic polar and nonpolar solvents. The results indicate that specific solvation effects such as ion-dipole, dipole-dipole, H-bonding etc. are operative and influence the spectral features. Room temperature magnetic moment and the EPR spectral characteristics of the Cu(II) complex are consistent with typical monomeric copper(II) species.

Results of absorption, fluorescence, thermal melting and viscometric studies carried out for all the compounds suggest that they all bind to DNA, probably, *via* an intercalative mode. For all the cases, acridine chromophore in the ligand moiety is engaged in the intercalative interaction with DNA. The intrinsic binding constants are evaluated and the values follow the order [Cu(daasal)] > [Ni(daasal)] > H_2daasal > [Zn(daasal)] ~ acridine. All the compounds except H_2daasal need to be activated by some oxidizing/reducing agents for effective DNA photocleavage in the presence of light. For [Cu(daasal)], 3-MPA was used as a reducing agent and effective cleaving of DNA is observed. The cleavage mechanism for this complex involves $OH^{\bullet}$

radical. This is proved by inhibition experiments. For [Ni(daasal)], the oxidizing agent oxone is used as an activator. The active species for DNA scission is like a Ni(III) generated by oxone in the presence of light. In the case of [Zn(daasal)] ascorbic acid is used as a reducing agent and possibly DNA cleavage occurs *via* the same process as observed for the Cu(II) complex.

7.3 Future scope

Overall, it has been demonstrated in this thesis that it is possible to design and synthesize potent photonucleases by suitably modifying the structures of visible light absorbing chromophores. A highlight of this approach is that the chromophore themselves can intercalate between the base pairs of DNA. The principal theme common to these new photonucleases is that (i) they all bind DNA with high affinity with K_b ranging from *ca*. 10^4 - 10^6 M^{-1}, (ii) they all absorb light in the 400-650 nm region and (iii) they generate cytotoxic species such as reactive oxygen intermediates ($^1O_2$ or $OH^{\bullet}$) and lead to DNA cleavage. The binding mode has been suggested to be base pair intercalation in all the cases. The photonucleases described here also have several practical applications. The 'dual wavelength-dual mechanism' theme as exemplified here in studies with ppym can be perceived to have immense application not only in photodynamic therapy but also in the design of photo-footprinting agents. The 'light-switching' abilities of most of the complexes in the presence of DNA permit the use of these complexes as 'fluorescence reporters' of DNA. The results from DNA binding studies also suggest that it is the modified phen ligand that is intercalating with DNA and that phen in each of these complexes acts only as a spectator ligand. Indeed, more elaborate mechanistic studies inquiring into the details of the photophysical properties of most of the free ligands and its corresponding complexes described in this study need to be carried out in near future. It should

be possible to take this study to the next higher level and to find out the site specificity involved in the DNA photocleavage by the metallointercalators including enantiomeric DNA binding of the complexes.

Structures of a few quinone-based ligands are known to be potent DNA cleaving agents capable of reacting with the duplex *via* various mechanisms including hydrogen abstraction, electron transfer *etc*.[5,6,10] Based on that we have designed some quinone incorporated ligands. These and some other new ligands are illustrated in Fig 7.2.

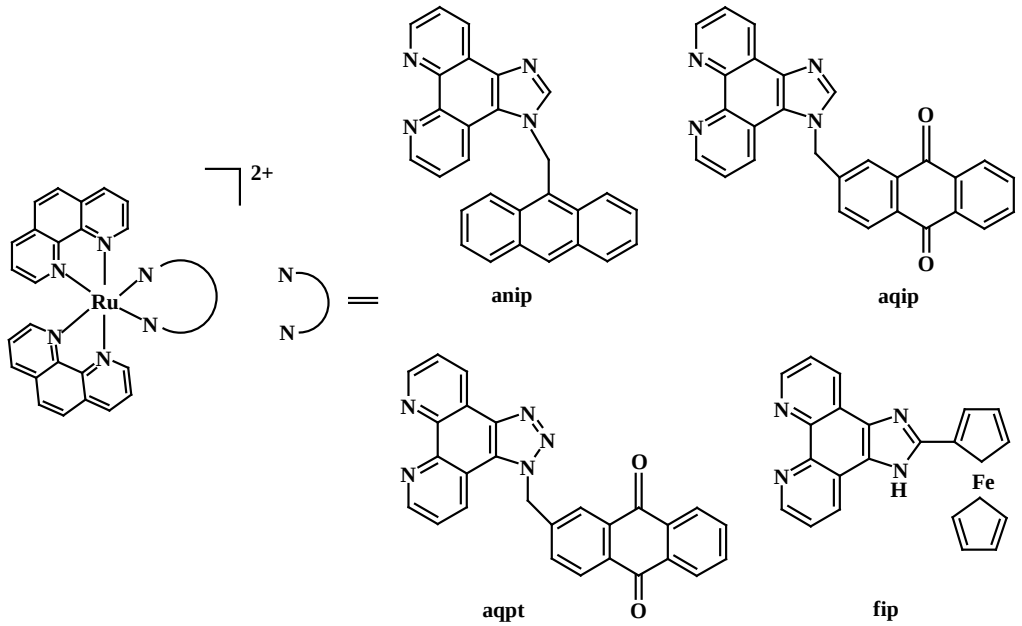

Fig. 7.2

It is also possible to link several other known intercalators, such as viologen/napthalimide,[11-13] to phen/dppz (Fig. 7.3). Complexes of such ligands are expected to not only accentuate DNA binding and photocleavage efficiencies but also may possess fascinating photophysical properties.

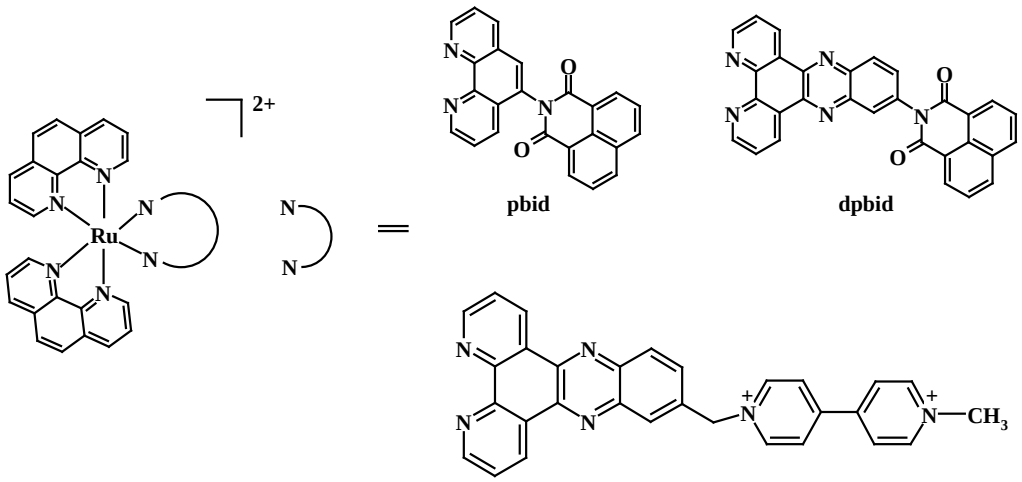

Fig. 7.3

7.4 References

1. Olson, E. J. C.; Hu, D.; Hormann, A.; Jonkman, A. M.; Arkin, M. R.; Stemp, E. D. A.; Barton, J. K.; Barbara, P. F. *J. Am. Chem. Soc.* **1997**, *119*, 11458 (and references therein).
2. Wu, J-Z.; Ye, B-H.; Wang, L.; Ji, L-N.; Zhou, J-Y.; Li, R-H.; Zhou, Z-Y. *J. Chem. Soc., Dalton Trans.* **1997,** 1395.
3. Friedman, A. E.; Chambron, J-C.; Sauvage, J-P.; Turro, N. J.; Barton, J. K. *J. Am. Chem. Soc.* **1990**, *112*, 4960.
4. Jenkins, Y.; Friedman, A. E.; Turro, N. J.; Barton, J. K. *Biochemistry* **1992**, *31*, 10809.
5. Arounaguiri, S.; Maiya, B. G. *Inorg. Chem.* **1999**, *38*, 842.
6. Ambroise, A.; Maiya, B. G. *Inorg. Chem.* **2000**, *39*, 4256.
7. McConnaughie, A. W.; Jenkins, T. C. *J. Med. Chem.* **1995**, *38*, 3488.
8. (a) Gravert, D. J.; Griffin, J. H. *J. Org. Chem.* **1993**, *5*8, 820. (b) Burrows, C. J.; Rokita, S. E. *Acc. Chem. Res.* **1994**, *27*, 295. (c) Woodson, S. S.;

Muller, J. G.; Burrows, C. J.; Rokita, S. E. *Nucleic Acids Res.* **1993**, *21*, 5524. (d) Bhattacharya, S.; Mandal, S. S. *J. Chem. Soc., Chem. Commun.* **1995**, 2489.

9. (a) Muller, J. G.; Paikoff, S. J.; Rokita, S. E.; Burrows, C. J. *J. Inorg. Biochem.* **1994** *54*, 199. (b) Mandal, S. S.; Renuka, K.; Guru Row, T. N.; Bhattacharya, S. *J. Chem. Soc., Chem. Commun.* **1996,** 2725.
10. (a) Armitage, B.; Yu, C. J.; Devadoss, C.; Schuster, G. B. *J. Am. Chem. Soc*. **1994**, *116*, 9847. (b) Breslin, D. T.; Coury, J. E.; Anderson, J. R.; McFail-Isom, L.; Kan, Y.; Williams, L. D.; Bottomley, L. A.; Schuster, G. B. *J. Am. Chem. Soc*. **1997**, *119*, 5043. (c) Armitage, B. *Chem. Rev*. **1998**, *98*, 1171. (d) Plater, M. J.; Greig, I.; Helfrich, M. H.; Ralston, S. H. *J. Chem. Soc., Perkin Trans.1* **2001**, 2553.
11. (a) Tyson, D. S.; Luman, C. R.; Zhou, X.; Castellano, F. N. *Inorg. Chem.* **2001**, *40*, 4063. (b) Tyson, D. S.; Castellano, F. N. *Inorg. Chem.* **1999**, *38*, 4382. (c) Tyson, D. S.; Gryczynski, I.; Castellano, F. N. *J. Phys. Chem. A.* **2000**, *104*, 2919. (d) Tyson, D. S.; Castellano, F. N., unpublished results.
12. (a) Takenaka, S.; Ihara, T.; Takagi, M. *J. Chem. Soc., Chem. Commun*. **1990**, *21*, 1485. (b) Takenaka, S.; Ihara, T.; Takagi, M. *Chem. Lett*. **1992**, 1.
13. (a) Eldho, N. V.; Joseph, J.; Ramaiah, D. *Chem. Lett*. **2001**, *5*, 438. (b) Joseph, J.; Eldho, N. V.; Ramaiah, D. *J. Phys. Chem. B* **2003,** *107*, 4444. (c) Joseph, J.; Eldho, N. V.; Ramaiah, D. *Chem. Eur. J.* **2003**, *9*, 5926.

APPENDIX I

X-ray Crystallographic Data

Table 1 Atomic coordinates (x 10^4) and equivalent isotropic displacement parameters (A^2 x 10^3) for **ppym·CHCl$_3$**. U(eq) is defined as one third of the trace of the orthogonalized Uij tensor.

atom	x	y	z	U(eq)
Cl(1)	12436(1)	834(2)	4848(1)	81(1)
Cl(2)	12889(1)	79(2)	13682(1)	109(1)
Cl(3)	12823(1)	3835(2)	14142(1)	110(1)
C(12)	10067(2)	1838(5)	12375(2)	43(1)
N(1)	10544(2)	1738(4)	13155(2)	52(1)
N(2)	11189(2)	1746(4)	12186(2)	53(1)
C(7)	9925(2)	2037(5)	11048(2)	46(1)
C(15)	6834(2)	896(5)	8257(2)	43(1)
C(11)	10406(2)	1880(5)	11860(2)	43(1)
C(14)	7456(2)	2094(5)	8728(2)	45(1)
N(3)	8648(2)	2477(4)	9924(2)	52(1)
C(4)	9253(2)	1922(5)	12047(2)	45(1)
C(3)	8938(3)	1905(6)	12558(2)	54(1)
C(27)	5695(2)	234(6)	6976(2)	49(1)
C(26)	6316(2)	1430(5)	7470(2)	45(1)
C(8)	10281(2)	2093(6)	10577(2)	57(1)
C(6)	9096(2)	2145(5)	10734(2)	45(1)
C(13)	7998(2)	1646(6)	9544(2)	50(1)
C(29)	7542(2)	3750(6)	8412(2)	55(1)
C(17)	6112(2)	1973(6)	8051(2)	58(1)
C(18)	5587(2)	-1491(6)	7256(2)	55(1)
C(2)	9427(3)	1785(6)	13340(2)	61(1)
C(9)	11071(3)	1972(6)	10911(2)	60(1)
C(28)	7042(2)	4291(6)	7662(2)	56(1)
C(5)	8789(2)	2068(5)	11221(2)	49(1)
C(16)	6693(2)	-841(6)	8519(2)	53(1)
C(24)	5876(3)	3681(7)	6389(2)	64(1)
C(22)	5182(2)	786(7)	6196(2)	60(1)
C(1)	10214(3)	1709(6)	13613(2)	57(1)

C(25)	6425(2)	3160(5)	7180(2)	49(1)
C(10)	11495(3)	1778(6)	11715(2)	60(1)
C(19)	4977(3)	-2648(8)	6757(3)	75(1)
C(23)	5295(3)	2548(7)	5929(3)	69(1)
C(30)	12401(3)	1615(7)	13985(2)	64(1)
C(21)	4588(3)	-420(9)	5729(3)	78(2)
C(20)	4480(3)	-2082(9)	5992(3)	84(2)

Table 2 Atomic coordinates (x 10^4) and equivalent isotropic displacement parameters (A^2 x 10^3) for **acdppz**. U(eq) is defined as one third of the trace of the orthogonalized Uij tensor.

atom	**x**	**y**	**z**	**U(eq)**
N(4)	7478(3)	4667(3)	4024(2)	52(1)
C(7)	6367(4)	788(3)	5293(2)	50(1)
C(5)	5087(4)	3810(4)	3888(2)	49(1)
C(18)	7391(4)	5566(3)	3177(2)	50(1)
C(13)	6177(4)	5569(4)	2691(2)	53(1)
C(17)	8577(4)	6512(4)	2755(2)	56(1)
N(3)	5009(3)	4676(3)	3058(2)	55(1)
C(19)	9841(4)	8371(4)	1441(2)	55(1)
C(6)	6322(4)	3795(3)	4372(2)	48(1)
C(11)	5172(4)	1845(4)	5682(2)	53(1)
C(4)	3839(4)	2842(4)	4314(2)	55(1)
C(12)	3897(4)	1884(4)	5180(2)	54(1)
C(20)	9829(4)	9790(4)	1667(2)	53(1)
N(1)	2794(4)	957(3)	5595(2)	69(1)
C(14)	6173(4)	6501(4)	1809(2)	61(1)
C(16)	8569(4)	7401(4)	1886(2)	55(1)
N(2)	5145(4)	908(3)	6518(2)	67(1)
C(31)	11103(4)	7862(4)	803(2)	58(1)
C(25)	11138(4)	10623(4)	1248(2)	54(1)
C(26)	12364(4)	8786(4)	430(2)	57(1)
N(5)	12367(3)	10120(3)	659(2)	61(1)
C(15)	7335(4)	7391(4)	1418(2)	62(1)
C(24)	11139(5)	12029(4)	1484(2)	71(1)

C(3)	2574(4)	2884(4)	3873(3)	71(1)
C(21)	8608(5)	10410(4)	2299(2)	66(1)
C(2)	1427(5)	1961(5)	4293(3)	83(1)
C(8)	7540(4)	2747(4)	5794(2)	63(1)
C(22)	8689(5)	11759(4)	2497(3)	79(1)
C(29)	12464(6)	6061(5)	-114(3)	94(1)
C(9)	7518(5)	1799(5)	6645(3)	77(1)
C(10)	6296(5)	917(5)	6963(3)	79(1)
C(30)	11211(5)	6479(4)	508(2)	81(1)
C(27)	13647(5)	8282(5)	-205(3)	78(1)
C(1)	1613(5)	1041(5)	5145(3)	80(1)
C(23)	9972(5)	12570(5)	2083(3)	81(1)
C(28)	13702(5)	6969(5)	-475(3)	91(1)

Table 3 Selected bond lengths [A^o] and angles [deg] for **acdppz**

N(4)-C(6)	1.338(4)
N(4)-C(18)	1.356(4)
C(5)-N(3)	1.322(4)
C(13)-N(3)	1.361(4)
C(19)-C(16)	1.491(4)
C(11)-N(2)	1.346(4)
C(12)-N(1)	1.349(4)
N(1)-C(1)	1.323(5)
N(2)-C(10)	1.319(5)
C(25)-N(5)	1.339(4)
C(26)-N(5)	1.344(4)
C(6)-N(4)-C(18)	115.6(3)
N(3)-C(5)-C(6)	122.2(3)
N(3)-C(5)-C(4)	118.2(3)
N(4)-C(18)-C(13)	122.2(3)
N(4)-C(18)-C(17)	119.2(3)
N(3)-C(13)-C(14)	119.2(3)
N(3)-C(13)-C(18)	121.3(3)
C(5)-N(3)-C(13)	116.4(3)
C(31)-C(19)-C(16)	120.3(3)
C(20)-C(19)-C(16)	120.9(3)
N(4)-C(6)-C(5)	122.3(3)
N(4)-C(6)-C(7)	117.7(3)
N(2)-C(11)-C(7)	122.2(3)

N(2)-C(11)-C(12)	117.7(3)
N(1)-C(12)-C(4)	122.3(3)
N(1)-C(12)-C(11)	116.8(3)
C(1)-N(1)-C(12)	116.3(3)
C(17)-C(16)-C(19)	120.8(3)
C(15)-C(16)-C(19)	120.1(3)
C(10)-N(2)-C(11)	116.5(3)
N(5)-C(25)-C(24)	118.5(3)
N(5)-C(25)-C(20)	123.4(3)
N(5)-C(26)-C(27)	118.2(3)
N(5)-C(26)-C(31)	122.6(3)
C(25)-N(5)-C(26)	118.6(3)
C(14)-C(15)-C(16)	120.9(3)
C(14)-C(15)-H(15)	119.5
N(2)-C(10)-C(9)	125.9(4)
N(2)-C(10)-H(10)	117.0
N(1)-C(1)-C(2)	126.2(4)
N(1)-C(1)-H(1)	116.9

Table 4 Atomic coordinates (x 10^4) and equivalent isotropic displacement parameters (A^2 x 10^3) for **$[Ru(phen)_2(acdppz)](PF_6)_2 \cdot 2H_2O$**. U(eq) is defined as one third of the trace of the orthogonalized Uij tensor.

atom	**x**	**y**	**z**	**U(eq)**
Ru(1)	2907(1)	2115(1)	10057(1)	34(1)
N(1)	1341(8)	2824(4)	10261(4)	32(2)
N(2)	3173(9)	2589(4)	9240(4)	36(3)
N(3)	-552(9)	4765(5)	9446(4)	37(3)
N(4)	1397(9)	4524(5)	8360(4)	39(3)
N(5)	-1130(12)	7319(6)	6580(5)	69(4)
N(6)	2265(8)	1474(4)	9641(4)	35(3)
N(7)	4447(9)	1388(4)	9775(4)	33(3)
N(8)	2583(8)	1767(4)	10931(4)	31(2)
N(9)	3717(8)	2635(5)	10503(5)	40(3)
C(1)	350(11)	2888(6)	10752(5)	35(3)
C(2)	-670(12)	3407(6)	10803(5)	44(4)
C(3)	-684(11)	3872(5)	10383(6)	41(3)

C(4)	343(10)	3799(6)	9866(5)	33(3)
C(5)	364(11)	4249(5)	9380(5)	33(3)
C(6)	1346(12)	4148(6)	8815(6)	43(4)
C(7)	2349(11)	3557(5)	8767(6)	34(3)
C(8)	3292(10)	3367(5)	8228(5)	35(3)
C(9)	4148(11)	2803(5)	8208(5)	38(3)
C(10)	4068(11)	2423(6)	8709(5)	42(4)
C(11)	2273(10)	3148(5)	9250(6)	33(3)
C(12)	1291(11)	3282(5)	9814(6)	40(3)
C(13)	-553(12)	5172(6)	8980(6)	44(4)
C(14)	-1550(12)	5690(5)	9021(6)	42(4)
C(15)	-1555(12)	6074(6)	8538(6)	50(4)
C(16)	-566(12)	5970(6)	7983(5)	48(4)
C(17)	399(13)	5481(6)	7960(6)	49(4)
C(18)	457(12)	5049(6)	8435(5)	43(4)
C(19)	-704(14)	6426(6)	7481(6)	55(4)
C(20)	-1638(15)	6397(7)	7177(6)	64(5)
C(21)	-2354(15)	5963(8)	7299(7)	80(6)
C(22)	-3277(14)	5980(8)	6996(7)	82(6)
C(23)	-3360(15)	6479(8)	6528(7)	86(7)
C(24)	-2655(17)	6885(9)	6415(8)	99(8)
C(25)	-1746(13)	6888(9)	6717(6)	73(6)
C(26)	-308(14)	7322(7)	6874(6)	56
C(27)	305(16)	7798(7)	6732(6)	80
C(28)	1159(17)	7858(8)	7016(7)	85
C(29)	1499(16)	7416(8)	7446(6)	75
C(30)	881(15)	6942(8)	7578(6)	73
C(31)	-64(14)	6872(7)	7324(6)	53
C(32)	1198(11)	1518(6)	9565(5)	36
C(33)	915(12)	1036(7)	9235(6)	49
C(34)	1767(12)	469(6)	8991(6)	45
C(35)	2890(11)	406(6)	9080(5)	36
C(36)	3875(12)	-153(6)	8860(6)	44
C(37)	4961(13)	-205(5)	8951(6)	48
C(38)	5227(12)	309(6)	9250(5)	42
C(39)	6367(12)	291(6)	9343(5)	45
C(40)	6504(11)	810(6)	9648(6)	40
C(41)	5528(11)	1351(6)	9847(5)	39
C(42)	4308(10)	853(5)	9487(5)	26
C(43)	3137(11)	905(6)	9398(5)	36
C(44)	1886(11)	1389(6)	11178(6)	46

C(45)	1753(12)	1178(6)	11784(6)	51
C(46)	2370(12)	1375(6)	12158(6)	48
C(47)	3078(13)	1774(6)	11926(6)	51
C(48)	3775(13)	2032(7)	12270(7)	61
C(49)	4376(12)	2476(7)	12037(7)	59
C(50)	4386(11)	2693(6)	11443(7)	46
C(51)	4913(13)	3178(7)	11236(7)	65
C(52)	4849(11)	3389(6)	10636(7)	51
C(53)	4237(11)	3122(6)	10277(7)	47
C(54)	3802(11)	2454(6)	11080(5)	43
C(55)	3145(12)	1981(6)	11323(6)	45
Ru(2)	989(1)	7676(1)	4500(1)	46(1)
N(1A)	-65(10)	7029(5)	4622(4)	43(3)
N(2A)	1676(10)	7117(5)	5153(4)	46(3)
N(3A)	-748(9)	5224(5)	5801(5)	42(3)
N(4A)	1201(9)	5235(5)	6308(5)	44(3)
N(5A)	571(13)	2539(7)	8500(6)	74(4)
N(6A)	-218(9)	8334(5)	5178(4)	39(3)
N(7A)	1970(10)	8338(4)	4509(4)	43(3)
N(8A)	370(12)	8093(5)	3759(5)	60(4)
N(9A)	2234(11)	7134(5)	3741(5)	57(4)
C(1A)	-1026(13)	7031(7)	4409(6)	55(4)
C(2A)	-1714(13)	6598(7)	4561(5)	52(4)
C(3A)	-1420(12)	6136(6)	4960(5)	44(4)
C(4A)	-474(12)	6122(6)	5201(5)	36(3)
C(5A)	-117(12)	5641(6)	5640(6)	39(3)
C(6A)	856(12)	5672(6)	5896(6)	44(4)
C(7A)	1526(11)	6170(6)	5739(5)	37(3)
C(8A)	2411(13)	6246(6)	5990(7)	55(4)
C(9A)	2926(12)	6745(6)	5814(7)	56(4)
C(10A)	2567(11)	7182(6)	5403(6)	45(4)
C(11A)	1144(11)	6616(5)	5313(5)	35(3)
C(12A)	214(12)	6570(6)	5040(5)	43(4)
C(13A)	-452(12)	4817(6)	6242(5)	41(4)
C(14A)	-1176(12)	4373(6)	6447(6)	48(4)
C(15A)	-890(13)	3964(6)	6895(5)	47(4)
C(16A)	93(13)	3965(6)	7120(6)	50(4)
C(17A)	806(12)	4366(6)	6916(6)	44(4)
C(18A)	524(11)	4810(6)	6471(6)	39(3)
C(19A)	338(13)	3472(7)	7605(6)	49(4)
C(20A)	-556(14)	3539(7)	8179(6)	59(4)

C(21A)	-1585(14)	4061(7)	8343(6)	67(5)
C(22A)	-2456(16)	4119(8)	8908(7)	89(6)
C(23A)	-2266(19)	3602(11)	9333(7)	108(9)
C(24A)	-1304(18)	3099(10)	9197(8)	91(7)
C(25A)	-384(17)	3031(9)	8609(6)	70(6)
C(26A)	1447(15)	2460(8)	7940(7)	65(5)
C(27A)	2417(14)	1916(7)	7824(8)	64(5)
C(28A)	3230(15)	1832(8)	7262(8)	77(5)
C(29A)	3175(14)	2297(7)	6827(7)	61(4)
C(30A)	2288(13)	2840(7)	6933(7)	62(4)
C(31A)	1307(14)	2949(7)	7491(6)	58(4)
C(32A)	-1332(14)	8354(7)	5489(6)	61(5)
C(33A)	-2092(13)	8854(7)	5948(6)	56(4)
C(34A)	-1623(14)	9333(7)	6083(6)	60(5)
C(35A)	-451(14)	9351(6)	5767(6)	56(4)
C(36A)	117(14)	9842(7)	5867(6)	60(4)
C(37A)	1212(14)	9854(6)	5540(6)	53(4)
C(38A)	1905(13)	9349(6)	5049(6)	47(4)
C(39A)	3062(14)	9317(7)	4670(6)	64(5)
C(40A)	3594(13)	8846(7)	4221(7)	66(5)
C(41A)	3056(12)	8361(6)	4155(6)	56(5)
C(42A)	1360(13)	8854(6)	4956(6)	45(4)
C(43A)	208(14)	8837(6)	5317(6)	49(4)
C(44A)	-622(15)	8570(6)	3789(7)	67(5)
C(45A)	-900(19)	8823(8)	3251(8)	92(7)
C(46A)	-186(19)	8578(9)	2675(7)	91(7)
C(47A)	868(18)	8095(9)	2632(7)	86(7)
C(48A)	1700(2)	7800(12)	2066(7)	142(15)
C(49A)	2640(2)	7301(11)	2020(8)	132(14)
C(50A)	2911(18)	7030(10)	2606(7)	98(8)
C(51A)	3778(18)	6494(10)	2614(10)	111(10)
C(52A)	3949(15)	6272(9)	3171(9)	92(7)
C(53A)	3131(13)	6617(7)	3769(8)	81(6)
C(54A)	2117(15)	7355(8)	3183(6)	68(5)
C(55A)	1100(16)	7877(7)	3181(6)	65
P(1)	6580(3)	858(2)	7555(2)	47
P(2)	4827(8)	1992(4)	4523(4)	164
P(3)	7992(4)	1665(2)	908(2)	54
P(4)	5848(8)	4715(4)	1956(4)	70(3)
P(5)	5705(7)	5157(4)	960(4)	64(3)
F(1)	6975(7)	147(3)	7784(3)	62(2)

F(2)	7007(8)	1137(4)	8093(4)	72(3)
F(3)	5257(6)	951(3)	8012(3)	54(2)
F(4)	6201(7)	1569(3)	7322(3)	61(2)
F(5)	6168(7)	565(4)	7004(3)	61(2)
F(6)	7883(7)	767(4)	7087(4)	76(3)
F(7)	5083(18)	1196(8)	4606(12)	283(12)
F(8)	5056(16)	2194(9)	5190(8)	219(7)
F(9)	3467(12)	2073(8)	4900(11)	240(9)
F(10)	4636(19)	2701(9)	4358(12)	122(9)
F(11)	4730(2)	1701(8)	3863(7)	227(9)
F(12)	6232(15)	1779(10)	4115(9)	235(9)
F(13)	7828(12)	1291(6)	1511(5)	139(5)
F(14)	9311(8)	1643(5)	941(5)	109(4)
F(15)	7511(8)	2331(5)	1289(5)	112(4)
F(16)	8244(11)	1961(6)	265(5)	138(5)
F(17)	6700(7)	1651(4)	865(4)	80(3)
F(18)	8490(8)	979(4)	524(5)	101(3)
F(19)	6120(2)	4963(9)	2549(8)	114(8)
F(20)	7111(18)	4457(7)	1581(11)	144(12)
F(21)	5813(17)	4028(9)	2208(9)	94(6)
F(23)	4470(16)	4973(10)	2219(15)	163(13)
F(24)	5932(9)	5357(4)	1632(5)	103(3)
F(25)	4567(12)	4990(7)	1368(7)	60(5)
F(26)	5022(15)	5902(7)	1002(8)	73(5)
F(27)	6640(2)	5415(10)	499(9)	164(13)
F(28)	6050(2)	4446(6)	1085(11)	293(14)
F(29)	5340(2)	5035(10)	362(9)	117(8)
O(2)	9279(12)	9818(6)	9452(6)	121(5)
O(4)	5432(17)	5208(10)	5170(2)	440(3)
O(3)	9326(13)	352(7)	8335(7)	136(5)
O(1)	6579(17)	9263(9)	4585(9)	194(8)

Table 5 Atomic coordinates (x 10^4) and equivalent isotropic displacement parameters (A^2 x 10^3) for **H_2daasal·HCON(CH_3)$_2$**. U(eq) is defined as one third of the trace of the orthogonalized Uij tensor.

atom	x	y	z	U(eq)
N(4)	4000(4)	2412(3)	3872(2)	101(1)
C(34)	5020(7)	3053(6)	3452(4)	214(4)
C(35)	2961(8)	2871(6)	4361(5)	196(3)
O(3)	3124(6)	798(3)	4196(3)	190(2)
C(36)	3945(7)	1394(6)	3842(3)	137(2)
N(1)	5149(2)	7026(2)	1001(2)	44(1)
C(16)	6363(3)	7967(2)	1681(2)	41(1)
C(17)	7546(3)	8628(2)	1387(2)	41(1)
C(6)	3858(3)	5650(2)	-614(2)	47(1)
C(33)	9820(3)	11357(2)	1749(2)	45(1)
C(22)	11078(3)	9920(2)	1432(2)	43(1)
N(3)	12199(2)	11693(2)	1148(2)	53(1)
N(2)	5090(3)	7619(2)	3007(2)	56(1)
C(13)	5128(3)	6605(2)	65(2)	47(1)
C(21)	9873(3)	10285(2)	1750(2)	41(1)
C(18)	8670(3)	9559(2)	2088(2)	45(1)
O(1)	2532(2)	5494(2)	703(2)	67(1)
C(28)	11031(3)	12030(2)	1440(2)	48(1)
C(15)	6309(3)	8273(2)	2707(2)	49(1)
C(2)	1403(3)	4220(2)	-950(2)	63(1)
C(1)	2600(3)	5127(2)	-272(2)	50(1)
C(27)	12223(3)	10665(2)	1140(2)	50(1)
C(5)	3860(3)	5214(2)	-1636(2)	59(1)
O(2)	3599(3)	5785(2)	3313(2)	87(1)
C(20)	7475(3)	9185(2)	3423(2)	68(1)
C(19)	8643(3)	9819(2)	3118(2)	64(1)
C(8)	3023(3)	7494(2)	3850(2)	60(1)
C(29)	11000(4)	13122(2)	1457(2)	66(1)
C(32)	8635(3)	11801(2)	2035(2)	66(1)
C(23)	11231(3)	8850(2)	1394(2)	59(1)
C(3)	1425(4)	3827(2)	-1956(2)	68(1)
C(14)	4244(3)	8097(2)	3477(2)	59(1)
C(26)	13472(4)	10304(3)	844(2)	76(1)

C(24)	12429(4)	8546(3)	1092(2)	76(1)
C(7)	2757(3)	6373(2)	3761(2)	63(1)
C(4)	2656(4)	4317(2)	-2305(2)	67(1)
C(12)	1594(4)	5828(3)	4145(3)	83(1)
C(30)	9864(4)	13513(2)	1745(3)	79(1)
C(25)	13560(4)	9284(3)	822(3)	88(1)
C(31)	8669(4)	12846(3)	2033(3)	81(1)
C(9)	2110(4)	8046(3)	4319(3)	87(1)
C(11)	722(4)	6407(4)	4612(3)	101(1)
C(10)	957(5)	7505(4)	4702(3)	109(1)

Table 6 Atomic coordinates (x 10^4) and equivalent isotropic displacement parameters (A^2 x 10^3) for **[Ni(daasal)]·HCON(CH$_3$)$_2$.** U(eq) is defined as one third of the trace of the orthogonalized Uij tensor.

atom	**x**	**y**	**z**	**U(eq)**
C(30)	6408(3)	10144(3)	8195(4)	95(2)
O(3)	7508(2)	6284(4)	10525(3)	170(2)
N(4)	6207(2)	6265(4)	9770(3)	98(1)
C(36)	6839(4)	6776(7)	10112(4)	118(2)
C(34)	5452(3)	6782(6)	9365(5)	139(2)
C(35)	6177(5)	5235(6)	9773(8)	200(4)
Ni(1)	10926(1)	6335(1)	11080(1)	33(1)
O(2)	11987(1)	6565(2)	11566(2)	47(1)
N(1)	9850(1)	6130(2)	10623(2)	31(1)
N(2)	10768(1)	6959(2)	9740(2)	31(1)
C(15)	9961(1)	7077(2)	9138(2)	30(1)
O(1)	11092(1)	5710(2)	12407(1)	43(1)
C(18)	8347(1)	7300(2)	8243(2)	36(1)
C(6)	9787(2)	5085(2)	12119(2)	36(1)
C(13)	9460(2)	5571(2)	11098(2)	35(1)
C(33)	7148(2)	8375(2)	7947(2)	40(1)
C(17)	8656(1)	6753(2)	9194(2)	36(1)
C(21)	7482(1)	7457(2)	7818(2)	36(1)
C(14)	11312(2)	7269(2)	9345(2)	36(1)
C(7)	12424(2)	6891(2)	10993(2)	41(1)
C(20)	9653(2)	7590(2)	8160(2)	39(1)

C(1)	10589(2)	5189(2)	12729(2)	39(1)
C(22)	6988(2)	6677(2)	7302(2)	39(1)
C(16)	9459(1)	6640(2)	9636(2)	31(1)
N(3)	5830(1)	7704(2)	7095(2)	49(1)
C(8)	12130(1)	7216(2)	9901(2)	37(1)
C(19)	8850(2)	7704(2)	7722(2)	41(1)
C(27)	6159(2)	6843(2)	6948(2)	45(1)
C(5)	9283(2)	4530(2)	12550(2)	45(1)
C(10)	13446(2)	7517(3)	9845(3)	58(1)
C(11)	13735(2)	7223(3)	10926(3)	57(1)
C(28)	6310(2)	8452(2)	7583(2)	48(1)
C(12)	13249(2)	6925(3)	11495(3)	54(1)
C(4)	9557(2)	4081(3)	13547(3)	56(1)
C(23)	7273(2)	5740(2)	7082(3)	53(1)
C(25)	5953(2)	5186(3)	6201(4)	77(1)
C(3)	10349(2)	4181(3)	14148(3)	59(1)
C(29)	5964(2)	9365(3)	7742(3)	73(1)
C(2)	10847(2)	4712(2)	13759(3)	53(1)
C(26)	5659(2)	6053(3)	6399(3)	65(1)
C(9)	12653(2)	7521(2)	9336(3)	52(1)
C(24)	6772(2)	5024(3)	6553(4)	72(1)
C(32)	7587(2)	9220(3)	8438(3)	60(1)
C(31)	7231(3)	10080(3)	8548(4)	86(1)

Appendix II

List of Publications

1. Ultrafast Intramolecular Electronic Energy-Transfer Dynamics in a Bichromophoric Molecule. Mondal, J. A.; Ramakrishna, G.; Singh, Ajay K.; Ghosh, H. N.; **Mariappan, M**.; Maiya, B. G.; Mukherjee, T.; Palit, D. K. *J. Phys. Chem. A.* **2004**, *108*, 7843.
2. Structure-Property Correlations in DNA Binding and Photocleavage Characteristics of metallointercalators. Sastri, C. V.; **Mariappan, M**.; Ghosh, T.; Maiya, B. G. *Proc. Indian Natn. Sci. Acad.* **2004**, *70A*, 2343.
3. Effects of Anthracene and Pyrene Units on the Interactions of Novel Polypyridyl Ru(II) Mixed-ligand Complexes with DNA. **Mariappan, M**..; Maiya, B. G. *Eur. J. Inorg. Chem.* **2005**, 0000.
4. $[Ru(phen)_2(acdppz)]^{2+}$: A Novel Singlet Oxygen Mediated photocleaving agent that Incorporates Dipyridophenazine Ligand Endowed with an Acridine Subunit. **Mariappan, M**.; Mukhopadhyay, P.; Raghavaiah, P.; Maiya, Bhaskar G. (Submitted).
5. Ruthenium(II) Complexes of modified Polypyridyl Ligands bearing photoactive subunits: Synthesis, Characterization, and DNA interactions. Sastri, C. V.; **Mariappan, M**.; Maiya, B. G. (to be submitted).
6. New generation of photoactive ligands containing phenanthroline appended with anthracene/pyrene chromophore. Sastri, C. V.; **Mariappan, M**.; Maiya, B. G. (to be communicated).
7. Design, Synthesis, Structure, DNA Binding and Photonuclease Activity of a New Ni(II), Cu(II) and Zn(II) Metallointercalators Containing Modified Salen Ligands. **Mariappan, M**.; Maiya, B. G. (manuscript under preparation).